# Investigations into Zika virus-host interactions:

# A Neurological Perspective

**Stephanie Louise Cumberworth BSc (Hons)**


Submitted in part-fulfilment for the degree of Doctor of Philosophy in

Infection and Immunology

MRC-University of Glasgow Centre for Virus Research

Institute of Infection Immunity and Inflammation

College of Medical, Veterinary and Life Sciences

Oilthigh Ghlaschu – University of Glasgow

September 2019



# Abstract

Zika virus (ZIKV) is a member of the *Flavivirus* genus of the family *Flaviviridae*. Members of this genus possess a single-stranded positive-sense RNA genome which are flanked by 5' and 3' untranslated regions. Previously, ZIKV infection was thought to cause symptomatic infection in 20% of patients, characterised by a non-purulent rash and a mild fever. However, recent ZIKV outbreaks have seen the emergence of novel neurological sequelae associated with ZIKV infection. These symptoms affected the central and peripheral nervous systems (CNS and PNS, respectively) of neonates and adults (congenital ZIKV syndrome and Guillain-Barré syndrome, respectively). Consequently, prior to commencement of this thesis, the knowledge of ZIKV interactions within the CNS and PNS was limited. Therefore, the primary aim of this thesis was to expand the current knowledgebase of ZIKV infection within cells of the CNS and PNS.

The work presented herein assessed available tools to study ZIKV infection *in vitro*, including testing previously uncharacterised commercial antibodies targeting the ZIKV envelope (ZIKV E) and NS1 proteins. Subsequently, a suitable antibody raised against the ZIKV E was identified and used in downstream analyses.

A model system of ZIKV infection of the CNS and PNS using mixed-cell co-cultures derived from mouse spinal cord (CNS) or dorsal root ganglion (PNS) was used to determined cell-type specific susceptibility to ZIKV infection. It was found that cells of the PNS are refractory to ZIKV infection, whereas cells of the CNS are permissive to ZIKV infection. In the CNS, oligodendrocytes and their precursors were the most susceptible cell type to ZIKV infection. Moreover, when infecting CNS co-cultures at a time point which reflects prenatal life through to post-natal life, white matter structures (myelin sheath and axons) are injured. However, neuronal cell bodies remained healthy. Using purified primary neuronal cultures derived from mouse spinal cord, it was determined that neurons were refractory to ZIKV infection in the absence of accompanying glial cells. This suggests axonal damage may not be a result of direct infection of neurons themselves and may be a consequence of oligodendrocyte infection and injury.

Transcriptomic analyses of ZIKV-infected CNS co-cultures revealed that ZIKV infection induces the upregulation of genes involved in antiviral responses and inflammatory pathways, including TNF and ROS/NO pathway components; these pathways may be involved in exacerbating injury to white matter structures within ZIKV-infected CNS-co-cultures.

In summary, the results described in this thesis show that ZIKV can infect the early post-natal CNS. Furthermore, ZIKV-infection of this murine model demonstrates that infection induces the injury and depletion of myelin and axons. This is likely to be due to a combination of effects such as direct viral infection, cell death of oligodendrocytes, and secreted inflammatory factors. Myelination occurs late in foetal development and carries on into early adulthood. These data, in combination with precedent pathological findings, suggest that ZIKV-infected children born absent of microcephaly may develop other, more subtle, neurological sequelae later in life.

# Table of Contents

# List of Tables

# List of Figures

# Acknowledgements

A body of work is rarely the efforts of a sole individual. Chapter specific acknowledgements highlight the important work of others who contributed directly to these findings. This space is dedicated to the people who were invaluable to my professional and personal development; my village.

Firstly, I would like to thank **Prof Alain Kohl**, the 'accidental' supervisor. Thank you for picking me up as an orphaned PhD student, and giving me a study subject which challenged and inspired me. This project has led me to meet and work with inspiring scientists. Your generosity* (*need to promote our work) has given me the opportunity to build confidence and a love for communicating science, which ultimately has led to my new career in medical writing. It has also led to some memorable drinking sessions across the globe!

To **Ben**, my other unintentional supervisor. Thank you for putting up with the numerous delays in writing this thesis, and indeed this thesis itself! Your feedback has been invaluable. The coffee breaks, the lunch breaks, the bar breaks with you are all sorely missed.

I would also like to thank the late **Prof Richard Elliott**, my original intended supervisor – without whom my Scottish adventure would never had happened.

To the best floor in CVR, HWB L3 (members old and new…er), thank you for being so supportive; each one of you made my time at the CVR unforgettable. **Jodie** – I will forever be thankful for you inviting this newbie to your engagement party. You are a ray of sunshine in shiny silver boots, and I am lucky to have you as a friend. With great kindness and generosity, you and Sam gave me a home from home, for which I will always be grateful. My time in Glasgow was made all the better having met you P.B & J'S. **Mel** – my lab 'mum' (I fully acknowledge you are nowhere near old enough for that title, but it's what I call you so…). Thank you for being my sounding board and always checking in on my emotional wellbeing. **Claire** – Zika Woman. Thank you for being the best conference companion and listening to my various frustrations over the years. **Margus** – YESSS. Your intellect knows no bounds, and I will forever be in awe of your

‘machine’-like capabilities. Thank you for being a willing contributor of ideas, when my idea fountain was dry. **Jordan** – sorry for taking out my mental instability on you, you put up with so much from my end, so thank you. All the joking, dancing and hissing will not be forgotten. **Tim –** messy boy. Thank you for being my main work ceilidh partner. You and Jordan made ‘bits and pieces’ of lab-life more fun. **Steph, Christie and Mavi** – thank you for your friendship and for letting me vent to each of you. All of you are so wonderful, kind and patient. Lest I forget **James, Jamie and Rommel** – thank you for the laughter.

To **Yas**, my PhD pal - I am so grateful to have met you. Thank you for the many motivational pep talks, tea breaks and thoughtful surprise presents. I doubt any of this could have happened without you helping me through and being my personal cheerleader. I’m glad I got to take this journey with you.

**Mairi**, your abundance of compassion and wisdom has been an anchor for me since we met – I frequently question ‘what would Mairi do’ to help me make better choices. No matter the problem, you were always there to help me navigate it. Thank you.

Lastly, to my family. The struggle was real. I haven’t always been present during this process, and I thank you for persevering and supporting me through my changing locations, moods, career goals etc. I love you very much and am lucky to have you.

# Author's Declaration

I, Stephanie Louise Cumberworth, declare that, except where explicit reference is made to the contribution of others, that this thesis is the result of my own work and has not been submitted for any other degree at the University of Glasgow or any other institution.

Printed Name: _____

Signature: _____

# Definitions/Abbreviations

**Ab** – antibody

***Ae.*** – Aedes species mosquito

**C** – capsid protein

cDNA – complementary DNA (deoxyribonucleic acid)

**CNS** – central nervous system

**CZV** – congenital Zika virus syndrome

**DC-SIGN** – dendritic cell-specific intercellular adhesion molecule 3-grabbing non-integrin

**DENV** – dengue virus

**$dH_20$** – deuterated $H_20$

**DIV** – days *in-vitro*

**DMSO** - dimethyl sulfoxide

**DNA** – deoxyribonucleic acid

**DRG** – dorsal root ganglion

**dsRNA**- double stranded RNA

**DTT** - dithiothreitol

**E** – envelope protein

**E13** – embryonic day 13

**EDTA** - ethylenediaminetetraacetic acid

**ELISA** – enzyme-linked immunosorbent assay

**ER**- endoplasmic reticulum

**FBS** – foetal bovine serum

**FUDR** - 5-fluoro- 2'deoxyuridine

**GAPDH** - Glyceraldehyde 3-phosphate dehydrogenase

**GBS** - Guillain-Barré syndrome

**GFAP** – glial fibrillary acidic protein

**gRNA** – genomic RNA

**HCL** – hydrochloric acid

**HCMV** – human cytomegalovirus

**HCV** – hepatitis C virus

**h p.i.** – hours post-infection

**IFN** - interferon

**IFN-I** – type I interferon

**IFN-ß**- interferon ß

***Ifnar1*** – IFN α/ß receptor subunit 1

**JEV** – Japanese encephalitis virus

**KCl** – potassium chloride

**kDa** – kilo daltons

**KO** – knockout

**KUNV** – Kunjin virus

**Log2FC** – Log2 fold change

**Mab** – monoclonal antibody

**MBP** – myelin basic protein

**MOI** – multiplicity of infection

**MRI** – magnetic resonance imaging

**MSI1/2** – mushashi 1/2 protein

**MTase** – methytransferase

**NBM** – neurobasal medium

**NS** – non-structural protein

**OPC** – oligodendrocyte precursor cell

**ORF**- open reading frame

**PE243** – zika virus strain: ZIKV/H.sapiens/Brazil/PE243/2015

**PCR**- polymerase chain reaction

**PFU** – plaque-forming units

**PHEIC** – public health emergency of international concern

**PLP** – proteolipid protein

**PNS** – peripheral nervous system

**prM** – pre-membrane protein

**PRNT** – plaque reduction neutralisation test

**RdRp** – RNA dependant RNA polymerase

**RNA** – ribonucleic acid

**RNP** – ribonucleoprotein

**SDS-PAGE** – sodium dodecyl sulphate – polyacrylamide gel electrophoresis

**sfRNA** – subgenomic flavivirus RNA

**sNS1** – secreted NS1 protein

**TBEV** – tick-borne encephalitis virus

**UTR** – untranslated region

**UV** – ultra-violet

**WHO** – World Health Organisation

**WNV** – West Nile virus

**WT** – wild type

**YFV** – yellow fever virus

**ZIKV** – zika virus

# 1 Introduction

## *1.1* Molecular biology of the *Flaviviridae*

### 1.1.1 Classification

The *Flaviviridae* is a family of small, enveloped viruses which possess a single-stranded, positive-sense RNA genome between 9-13 kb in length. The family comprises over 100 species which are further categorised into 4 genera: *Flavivirus, Pestivirus, Hepacivirus,* and *Pegivirus* (Simmonds et al., 2017).

Pestiviruses are important pathogens of animals, infecting pigs and ruminants; they are transmitted through direct and indirect contact with infected bodily fluids. A notable member of this genus is bovine viral diarrhoea virus (BVDV), associated with respiratory, reproductive and gastrointestinal disease of cattle (Smith et al., 2017).

Pegiviruses have been detected in a wide range of mammals in addition to bats and rodents and are categorised into species (*Pegivirus A-K*; *Pegivirus C* possesses 6 genotypes which infect humans) (Adams et al., 1998, Simmonds et al., 2017). *Pegivirus* frequently cause persistent infections with rare disease consequence in humans, whereas Theiler's disease in horses has been associated with *Pegivirus* infection (Chandriani et al., 2013) .

Hepaciviruses have a broad host range, infecting a variety of mammals, rodents and bats. The most well characterised virus of the genus is hepatitis C virus, of the species *Hepacivirus C*. Members of this genus cause acute and chronic disease of the liver (Smith et al., 2016).

Members of the *Flavivirus* genus are predominantly arthropod-borne viruses (arboviruses), spread via infection of mosquitoes or ticks which subsequently transmit the virus to the primary host, mammals and birds, when taking a bloodmeal (Section 1.3.2). Many important human pathogens belong to the genus *Flavivirus*, for instance yellow fever virus (YFV), Japanese encephalitis (JEV), West Nile virus (WNV), dengue virus (DENV), and the recently emerged, Zika virus (ZIKV). Human *Flavivirus* infection results in a range of pathological

outcomes from asymptomatic infection to severe haemorrhagic or neurological manifestations (Maximova and Pletnev, 2018). Other members of this family, such as louping ill virus (LIV) and Tembusu virus (TMUV), cause disease of socio-economic consequence within animals (Zhang et al., 2017, Dagleish et al., 2018).

### 1.1.2 Genome organisation

Flaviviruses have a single-stranded, positive-sense RNA genome of around 11 kb in length. The genome comprises a single open reading frame (ORF) flanked by 5' and 3' untranslated regions (UTR's) (Figure 1–1). Furthermore, flavivirus genomes possess a 5' cap, but lack a poly(A) tail. The genome encodes three structural genes: Capsid (C), Pre-membrane/membrane (PrM), Envelope (E), in addition to seven non-structural genes: NS1, NS2A, NS2B, NS3, NS4A, NS4B and NS5 (Figure 1–1). As flaviviruses contain a positive-sense RNA genome, these genomes can be translated directly by host cell machinery (membrane-associated ribosomes of the rough endoplasmic reticulum [ER]). The ORF is translated as a single polyprotein which is cleaved by host and viral proteases, subsequently producing ten viral proteins – their namesake corresponds to their gene name. The structural proteins are implicated in the assembly of progeny virions, whereas the non-structural proteins, which are pleiotropic in nature, are involved in numerous aspects of the virus life cycle. Non-structural proteins potentiate viral replication and virion assembly through interactions with host and viral proteins to render the host cell conducive to viral reproduction; combat host antiviral responses; act as scaffolds for viral replication; catalyse viral replication processes.

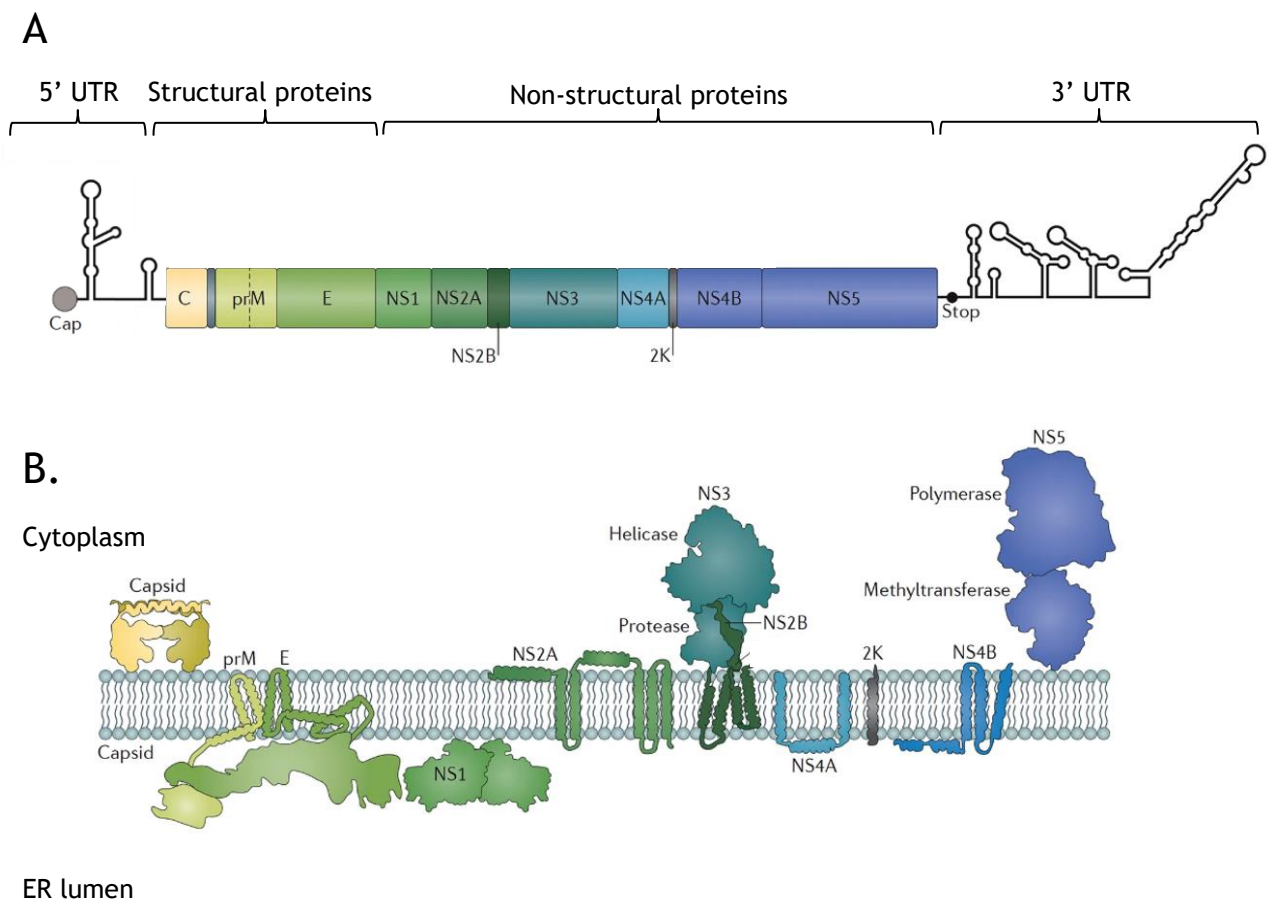


**Figure 1–1 *Flavivirus* genus genome organisation and membrane topology of proteins in the ER**

**A.** Schematic representation of the *Flavivirus* genome structure. Flaviviruses comprise a single open reading frame which is flanked by 5' and 3' untranslated regions (UTRs), shown as stem loop structures on the diagram. The genome is capped but lacks a poly(A) tail. Structural proteins are organised closer to the 5' region, and non-structural proteins towards the 3' region. **B.** A simplified schematic of flavivirus protein topology across the ER membrane. The genome is translated as single polyprotein, which is cleaved by viral and host proteases within the ER. Figure adapted from (Neufeldt et al., 2018).

### 1.1.3 *Flavivirus* genus genome: gene products

### 1.1.4 Capsid

The capsid (C) protein is largely considered a structural protein which is implicated in virus assembly. It is a small protein of approximately 14 kDa that possesses an affinity for both nucleic acids and lipid membranes. The primary, and most critical function of the C protein is to encapsidate nascent viral RNA, forming the nucleocapsid, and to aid its incorporation into progeny virions. Structural data of the DENV C protein, obtained by NMR, revealed each C protein monomer is composed of four α-helices (α1-4), with a flexible N terminal region (Ma et al., 2004). Upon dimerization, the C protein forms structures which facilitate association with lipid bilayers, via a hydrophobic cleft formed by α2 helices, and the viral genome via positively charged, arginine-rich regions formed by α4 helices (Markoff et al., 1997, Kiermayr et al., 2004). The 3D structures of WNV C and ZIKV C protein possess similar gross topologies to DENV C protein (Shang et al., 2018). However, ZIKV C protein possesses a larger flexible N terminal domain, and shorter α1 helix compared to either WNV or DENV (Shang et al., 2018). It is thought that the pre-α1 region of ZIKV C acts to further stabilise dimer interactions, in addition to specific residues contributing to association with lipid droplets (Shang et al., 2018). The structure of the nucleocapsid, i.e. viral RNA encapsidated with C protein, is yet to be determined.

The C protein retains the ability to package RNA *in-vitro* despite deletions made to various α-helical structures in WNV or TBEV (Kofler et al., 2002, Schlick et al., 2009). Furthermore, the C protein localises to discrete cellular organelles including lipid droplets, the ER membrane in addition to the nucleus (Roby et al., 2015); this suggests alternative roles for C protein functionality.

It has been found that the nuclear trafficking of C is mediated by the presence of a nuclear localisation signal (NLS) within the protein; in DENV and WNV this is a bi-partite NLS which enables C to interact with importin-α to facilitate nuclear translocation (Mori et al., 2005, Bhuvanakantham et al., 2010, Colpitts et al., 2011). The role of C in the nucleus is ill-defined, though some interactions have been identified: DENV C has been shown to interact with four histone proteins

(H2A, H2B, H3 and H4) in addition to heterogenous nuclear ribonucleoprotein K (hnRNP K), all of which are implicated in the regulation of host gene expression (Colpitts et al., 2011).

It has also been demonstrated that the C proteins of both YFV and ZIKV possess the capability to bind dsRNA, suggesting a role for C protein in the suppression of RNA silencing, though no mechanistic data is available to support this claim yet (Samuel et al., 2016, Shang et al., 2018).

### 1.1.5 Pre-membrane/membrane (prM)

prM is a membrane glycoprotein of approximately 19-21 kDa. Through associations with the E protein, prM is an integral component of the *Flavivirus* virion. An N-terminal signal sequence at the C/prM junction enables the translocation of prM into the ER lumen during polyprotein translation (Lobigs et al., 2010). Host cell signalase cleaves prM from this signal sequence in the ER lumen – a process which is dependent on prior cleavage of C by the NS2B/3 protease (Lobigs et al., 2010). prM is anchored to the ER lumen via two C-terminal transmembrane helices. The protein exists in an immature (prM) and mature form (M); prM maturation is mediated by furin cleavage of the pr peptide in the trans-Golgi network, generating the mature M protein which is approximately 10 kDa in size (Stadler et al., 1997, Yu et al., 2008).

In addition to its structural role, prM has several other proposed roles in including: assisting chaperone-mediated folding of the E protein (Lorenz et al., 2002, Konishi and Mason, 1993), contributing to pH-dependent conformation rearrangements of trimeric prM/E heterodimer spikes in immature virions (Zhang et al., 2012), and preventing premature fusion during virion egress by concealing the fusion loop of E (Yu et al., 2009). The interactions between prM/E and its role in virus particle formation is explored further in section 1.1.6.

### 1.1.6 Envelope

The envelope (E) protein constitutes the major component of the virus envelope. It is a large (approximately 53 kDa), membrane-bound glycoprotein which is responsible for binding cell surface receptors to facilitate virus entry. The E

protein decorates the outer surface of the virus particle, and as such, it is a major antigenic target for the development of neutralising antibodies.

Each E protein monomer comprises three ß-barrel domains: DI, DII and DIII (Figure 1–2). The three domains are connected by flexible hinges which mediate conformational changes essential for virus infectivity (Zhang et al., 2004). DI constitutes the central domain, which harbours the N terminus and acts as an anchor for the hinge point of DII. DII is a large distal domain, containing the loop peptide which is involved in virus fusion during cell entry (Allison et al., 2001). The C-terminal DIII domain is an immunoglobulin-like domain containing the receptor binding motif, which is critical for virus entry.

The E protein undergoes major conformational changes during the virus life cycle. Initially, the immature virus particle is composed of 60 trimeric surface spikes; each spike is composed of a trimer of prM-E heterodimers (Zhang et al., 2003, Prasad et al., 2017) (Figure 1–2A). The fusion loop of each E protein is concealed by prM proteins at the tip of each spike, thereby preventing early fusion events (Yu et al., 2009, Heinz et al., 1994). The first major conformational change occurs within the trans-Golgi network, resulting in the furin cleavage of the pr peptide (Yu et al., 2008). Subsequently, the 60 trimers rearrange into 90 E homodimers which are in an anti-parallel configuration (Plevka et al., 2014) (Figure 1–2B). The 90 E dimers are arranged in a ‘herringbone’ pattern, formed of three adjacent homodimers, which lie flat on the virion surface (Kuhn et al., 2002, Mukhopadhyay et al., 2003) (Figure 1–2D). prM remains associated with E in mature intracellular virions, and its release coincides with virus egress (Zhang et al., 2012, Zhang et al., 2013) (Figure 1–2C). In the mature virion, the fusion loop is buried within DI and DII of the opposing monomer (Allison et al., 2001). The second major conformational change occurs during virus entry. Upon internalisation, the virus particle enters the endosomal pathway, progression through which results in pH mediated exposure of the fusion loop. The fusion loop penetrates the endosomal membrane, causing the fusion of virus and endosomal membranes, liberating the viral genome into the cytoplasm (Bressanelli et al., 2004, Modis et al., 2004).

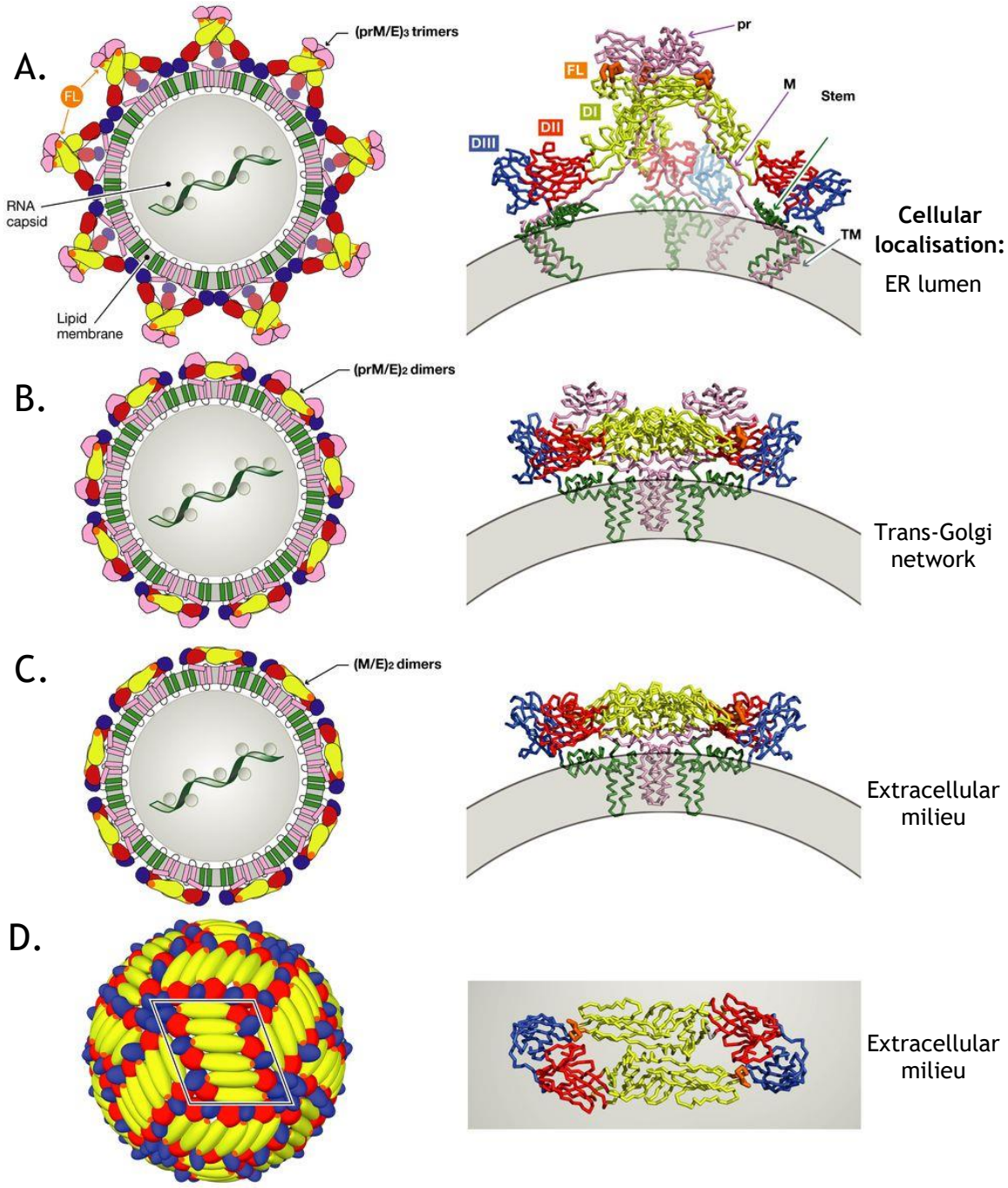


**Figure 1–2 The structural rearrangements of the envelope protein during *Flavivirus* particle maturation.**
*Flavivirus* virions are first generated as immature particles. Envelope/prM heterodimers assemble to form trimeric spikes on the ER membrane (the envelope protein has been coloured according to its domains: red, blue, yellow, correspond to DI, DII and DIII respectively. Green denotes the transmembrane region). **A.** The nucleocapsid interacts with the trimeric spikes, causing the particle to bud into the ER lumen. **B.** The virion is transported through the trans-Golgi network, where changes in pH and furin cleavage of prM result in a major conformational change in the envelope protein, causing it to form dimers which lie flat on the surface of the virion. PrM is still associated with E at this stage. **C/D**. Following exocytosis, prM disassociates from E, producing the mature, infectious progeny virion. The E dimers form a herringbone pattern on the surface of the virion, as shown in **D**. The fusion peptide is coloured in orange and is concealed until virus entry. Figure from (Rey et al., 2018).

### 1.1.7 NS1

NS1, like many of the *Flavivirus* genus non-structural proteins, is a multifaceted protein. Dependent upon glycosylation status, the molecular weight of NS1 ranges from 46-55 kDa. Furthermore, NS1 can associate to form higher order structures, which also dictate functionality; NS1 can exist as a monomer, dimer (membrane-bound, mNS1) or a hexamer (secreted, sNS1).

The extent of glycosylation influences virulence, viral replication and determines whether NS1 is secreted (sNS1). Monomeric NS1 initially undergoes N-linked glycosylation at sites Asn-130 and Asn-207, which is performed by glycosidase within the ER (Pryor and Wright, 1994). Further modifications carried out by glycosidases and glycosyltransferases takes place in the trans-Golgi network, enabling NS1 to form a soluble hexamer which is secreted from the cell (Somnuke et al., 2011). The sNS1 hexamer is composed of three dimers associating to form a barrel with a hydrophobic core; sNS1 forms a lipoprotein particle, carrying lipid cargo within its core (Gutsche et al., 2011). sNS1 plays a crucial, yet widely mechanistically debated, role in DENV pathogenesis, contributing to haemorrhagic manifestations observed severe DENV infections. Furthermore, sNS1 is found circulating in the sera of patients infected with DENV, and as such is used as an early diagnostic biomarker (Young et al., 2000, Rastogi et al., 2016).

### 1.1.8 NS2A

NS2A is a hydrophobic, membrane-associated protein approximately 22 kDa in size. Like the other non-structural proteins, NS2A is pleiotropic in nature; as such it is implicated in various aspects of the virus life cycle. As demonstrated by experiments with Kunjin virus (KUNV), NS2A interacts with high specificity to the 3'UTR of viral RNA in addition to other components of the replication complex, including NS3 and NS5 (Mackenzie et al., 1998). More recently, an A175V substitution in the ZIKV NS2A protein attenuated the virus *in vitro* and *in vivo* (Márquez-Jurado et al., 2018).

Mutagenesis studies found a K190S mutation in YFV NS2A inhibited the production of virus particles (Kümmerer and Rice, 2002). Further studies using a

KUNV replicon demonstrated that the single amino acid substitution in NS2A, I59N, blocked virus production (Liu et al., 2003). It was later found that this substitution ablates the generation of virus-induced membranous structures (Leung et al., 2008). Interestingly, compensatory mutations, namely T149P or substitutions with hydrophobic residues at position 59, rescued virus-induced membrane rearrangements and the production of virus particles (Leung et al., 2008). Furthermore, the introduction of an R84A mutation in DENV-2 NS2A blocked the intracellular formation of virions (Xie et al., 2013). Together these studies implicate NS2A in virus assembly, in addition to the generation of virus-induced membranous structures - the site of *Flavivirus* replication (discussed further in section 1.1.11). However, further studies are required to provide mechanistic insight into these processes.

NS2A is also involved in the modulation of host immunity. The expression of DENV NS2A was sufficient to enable the replication of GFP tagged Newcastle disease virus (NDV), an IFN sensitive virus (Muñoz-Jordan et al., 2003). Additionally, when acting in combination with NS4A and 4B, DENV-2 NS2A inhibits STAT1 phosphorylation, thereby blocking the IFN signalling cascade and subsequent IFN response (Muñoz-Jordan et al., 2003). JEV NS2A modulates host immunity via an alternative mechanism, involving the blockade of dsRNA-activated protein kinase PKR (Tu et al., 2012).

### 1.1.9 NS2B

NS2B acts as a cofactor, supporting the enzymatic activity of NS3. It is a small, integral membrane protein of ~14kDa in size. It contains a conserved central hydrophilic region which is flanked by three hydrophobic transmembrane domains, two reside within the N-terminus and one at the C-terminus (Falgout et al., 1993). The central region has been demonstrated to be necessary and sufficient for NS3 protease function (Chambers et al., 1993, Falgout et al., 1993). Whilst the transmembrane domains are not essential for NS3 protease activity, studies show that mutagenesis of the predicted transmembrane regions negatively impacts virus replication and virion assembly (Li et al., 2016b, Chambers et al., 1993, Li et al., 2014). A genome-wide CRISPR/Cas9-based screen identified that the loss of signal peptidase complex subunit 1 (SPCS1) reduced the yield of a range of flaviruses including: WNV, DENV, ZIKV, YFV, JEV

and HCV (Zhang et al., 2016). Ma et al (2018) demonstrated that SPCS1 interacts with the transmembrane domains of the NS2B protein from JEV and is implicated in post-translational protein processing and virus assembly. SPCS1 was also found to interact with WNV and ZIKV NS2B, suggesting this interaction is conserved amongst flaviviruses (Ma et al., 2018b).

### 1.1.10 NS3

After NS5, NS3 is the second largest non-structural protein produced by flaviviruses (~69kDa). NS3 comprises two functional domains: an N-terminal protease and a C-terminal helicase domain (Cui et al., 1998, Wengler, 1991, Li et al., 1999). The protease domain, in complex with NS2B which acts as a co-factor, is critical in viral polyprotein processing. The helicase domain functions cooperatively with NS5 (an RNA dependent RNA polymerase; RdRp) to replicate viral RNA. The NS3 helicase domain unwinds dsRNA, a replicative intermediate molecule, to facilitate the production of positive sense viral RNA genomes (carried out by the action of NS5) (Cui et al., 1998, Xu et al., 2019). NS3 also exhibits RNA 5' triphosphatase activity, which is vital in producing capped RNA genomes. Progeny genomes possess a terminal 5' triphosphate, the triphosphatase activity of NS3 catalyses the removal of the terminal phosphate, which facilitates capping by the action of NS5 (Issur et al., 2009).

### 1.1.11 NS4A

NS4A is a small, integral membrane protein of approximately 16 kDa. NS4A and NS4B are connected by the conserved 2K peptide region. Cleavage at the C-terminus of NS4A by the NS2B/NS3 helicase is a prerequisite for the subsequent cleavage event at the N-terminus of NS2B by a host signalase, which liberates NS2B from the 2K leader peptide (Lin et al., 1993). Structural data of DENV4 NS4A in micelles, obtained by solution NMR spectroscopy, revealed six helices: three amphipathic N-terminal helices which interact with the membrane, in addition to three C-terminal transmembrane helices (Li et al., 2018). The N-terminus contains regions of hydrophobicity, allowing the amphipathic helices to interact with the cytosolic face of the ER membrane (Li et al., 2018, Hung et al., 2015). Introducing mutations in this region which interferes with its amphipathic

nature decreases homo-oligomerisation of NS4A, and abolishes viral replication (Stern et al., 2013).

NS4A is involved in forming virus-induced membranous structures, called vesicle packets, which are the site of flavivirus replication and particle formation (Miller et al., 2007). The formation of vesicle packets is thought to be a result of NS4A homo-oligomerisation which induce membrane curvature (Stern et al., 2013, Lee et al., 2015, Hung et al., 2015). The membrane remodelling capabilities of flaviviruses have also been ascribed to interactions with host proteins. DENV NS4A interacts with the intermediate filament protein, vimentin (Teo and Chu, 2014). The role of this interaction in membrane remodelling is yet to be determined; however, it has been suggested that vimentin may perform a structural role in replication complex formation (Teo and Chu, 2014). The host protein RTN3.1A (Reticulon 3.1) has also been found to contribute to membrane remodelling, possibly via interacting with NS4A; silencing this protein results in impaired vesicle packet formation in KUNV, DENV-2 and ZIKV infection and decreases replication and particle release (Aktepe et al., 2017).

Further to its role in membrane remodelling, NS4A also contributes to inhibition of type I IFN responses (Dalrymple et al., 2015, Ma et al., 2018a), induces autophagy (McLean et al., 2011) and modulate the host stress response to benefit viral replication (Hou et al., 2017).

### 1.1.12 NS4B

Once liberated from the viral polyprotein by the action of the NS2B/NS3 protease, NS4B exists in a ‘pro’ form with an N-terminal leader peptide, 2K-NS4B. This 30 kDa protein is further processed by a host cell signalase which cleaves the 2K region, resulting in mature NS4B production (Lin et al., 1993). The 2K peptide forms a transmembrane domain that enables the translocation of NS4B into the ER lumen (Miller et al., 2007). However, the 2K peptide is not essential for NS4B function.

NS4B is an integral membrane protein, localising to the ER and ER-derived structures (Miller et al., 2006). Its function is implicated in the *Flavivirus* replication complex, though the exact role of NS4B in viral replication remains

elusive. A range of mutagenesis and co-localisation studies highlight the capacity for NS4B to interact with viral dsRNA (Miller et al., 2006) in addition to other *Flavivirus* non-structural proteins including NS1 (Youn et al., 2012), NS2B (Yu et al., 2013), NS3 (Umareddy et al., 2006, Zou et al., 2015a) and NS4A (Zou et al., 2015b). It has also been demonstrated that NS4B plays a role in *Flavivirus* immune evasion via blockade of type I IFN signalling cascade at the level of STAT1 phosphorylation (Liu et al., 2005, Muñoz-Jordán et al., 2005). An engineered mutation in WNV NS4B, P38G, was found to be associated with small-plaque phenotype and temperature sensitivity (Wicker et al., 2012). Furthermore, this mutation conferred attenuated neuroinvasive capabilities in mice compared to the neurovirulent strain WNV NY-99 (Wicker et al., 2012) - further demonstrating the range of biological functionality of NS4B.

### 1.1.13 NS5

NS5 is the largest and most conserved protein of the *Flaviviridae* family (approximately 900 amino acids). It comprises two domains which confer enzymatic activity; a N-terminal methlytransferase domain (MTase) which is connected to a C-terminal RNA-dependent RNA polymerase (RdRp) via a flexible linker (Grun and Brinton, 1987). The RdRp domain replicates viral RNA, whereas the MTase activity (cooperatively with NS3) produces and methylates the 5’ cap on viral progeny RNA molecules (Egloff et al., 2002, Ray et al., 2006, Zhou et al., 2007).

The *Flavivirus* NS5 protein adopts a structure resembling a right-hand palm, fingers and thumb domains which surround an active site (Yap et al., 2007, Malet et al., 2007). To date, no structure of an NS5 RdRdp:RNA complex from a flavivirus has been solved.

In addition to its role in viral replication, NS5 is a potent antagonist of the type I IFN response (Best, 2017, Cumberworth et al., 2017b). Absent of any other interactions with host proteins, NS5 aids the immune evasion strategies of flaviviruses by producing a 5’ cap which mimics host RNA structures. The 5’ cap of the *Flavivirus* genome is methylated (N7 and nucleoside-2’-O sites), disguising the viral RNA from cytoplasmic pathogen recognition receptors that recognise RNA possessing a terminal 5’trisphosphate, in addition to preventing degradation

by exoribonucleases. NS5 antagonises the type I IFN response at the level of STAT inhibition – the mechanisms of which vary between flaviviruses. NS5 inhibition of STAT1/2 activation or translocation prevents the upregulation of ISGs and the establishment of an antiviral state.

### 1.1.14 3'UTR and subgenomic flavivirus RNA

Flaviviruses produce a non-coding RNA product called sfRNA which is derived from the 3' untranslated region (3'UTR) (Pijlman et al., 2008, Donald et al., 2016, Göertz et al., 2018, Slonchak and Khromykh, 2018). sfRNA production is a result of incomplete degradation of viral genomic RNA (gRNA), facilitated by the stalling of cellular 5'-3' exoribonuclease XRN1 at complex RNA structures located in the 3'UTR of flaviviruses (Figure 1–3), thus protecting downstream RNA from degradation (MacFadden et al., 2018, Chapman et al., 2014a, Chapman et al., 2014b). Resultant RNA species are subsequently formed with an average length of ~500 nucleotides; some viruses such as WNV, DENV and YFV generate multiple truncated species of sfRNA during infection (Liu et al., 2010, Funk et al., 2010, Pijlman et al., 2008). XRN1-resistant RNA (xrRNA) elements in sfRNA also have the capacity to halt other exoribonucleases unrelated to XRN1, indicating that these structures function as a general block to degradation as opposed to halting degradation via specific RNA-protein interactions (MacFadden et al., 2018).

The 3'UTR of flaviviruses form interactions with viral proteins during infection. Ribonucleoprotein co-immunoprecipitation of JEV 3'UTR found that the 3'UTR interacts with viral NS5 protein (Chang et al., 2013). Furthermore, interactions between the 3'UTR of KUNV with capsid (Khromykh and Westaway, 1996) and NS2A proteins (Mackenzie et al., 1998) and DENV and JEV with the NS3 protein (Chang et al., 2013, Cui et al., 1998) have been demonstrated using various *in vitro* assays. Whether this reflects interactions of viral proteins with the genomic 3'UTR RNA or the sfRNA itself remains to be determined. Given that most of the aforementioned viral proteins are involved in replication complex formation, it would seem likely that these interactions exist with genomic RNA. However, as the sequences are conserved between the two RNA molecules, these interactions could also exist with sfRNA.

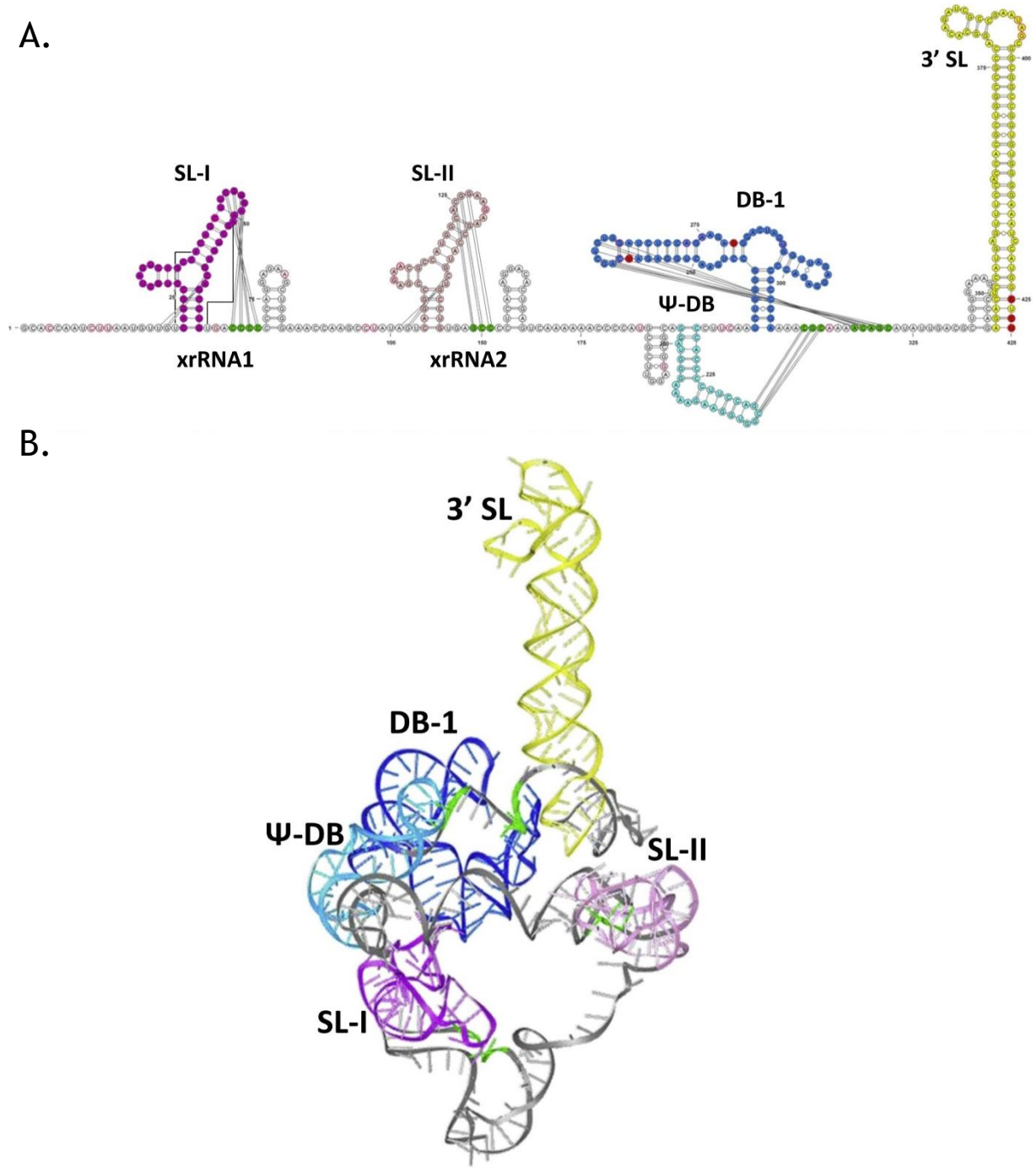


**Figure 1–3 Schematic representation of the *Flavivirus* 3'UTR (based upon ZIKV 3'UTR)**
The 3'UTR of flaviviruses is composed of highly structured RNA. sfRNA is produced as a result of incomplete degradation of the viral genome by host cellular ribonuclease XRN1. The structure of sfRNA varies between flaviviruses; however, they share similar motifs. All sfRNA contain stem loop (SL) and dumbbell (DB) structures, which are capable of forming pseudoknots. Pseudoknot interactions are indicated in **A** by lines joining nucleotides with other nucleotides highlighted in green (**A**) Secondary structure of ZIKV 3'UTR (Natal strain). The sfRNA of ZIKV produces two sfRNAs of differing lengths which can be ascribed to the stalling of XRN1 at different positions of the genome. xrRNA1 is produced by stalling at SL-I, and xrRNA2 at SL-II. Here the full length sfRNA molecule is shown (**B**) Predicted tertiary structure of ZIVK 3'UTR RNA/sfRNA containing both SL-I and SL-II. Figure adapted from .(Göertz et al., 2018).

In regards to 3'UTR interactions with host proteins, numerous candidate interaction partners have been identified for a range of flaviviruses - summarised elsewhere (Roby et al., 2014). These candidates have varying roles in translation, RNA processing and stability, and immune modulation. Again, these findings reflect interactions with the 3'UTR of the gRNA and not specifically the sfRNA, though it is likely sfRNA retains the capacity to interact with the suggested proteins.

Considering the roles of these candidate interaction partners, it would seem sfRNA serves to (1) to prevent the degradation of genomic viral RNA; (2) to prevent the elicitation of type I IFN responses; and (3) to promote viral translation.

## 1.2 *Flavivirus* life cycle

### 1.2.1 Cell entry

Flaviviruses enter cells through receptor-mediated endocytosis, followed by fusion of viral and endosomal membranes, resulting in the release of viral genomic RNA into the host cytoplasm (Figure 1–4). The binding of the virus to its associated receptor, via interactions with the E protein, triggers the internalisation of the receptor-virus complex via the formation of clathrin coated pits (Chu and Ng, 2004a). The receptors used by flaviviruses to gain entrance to the host cell are poorly characterised; numerous candidate molecules have been proposed including $\alpha_v\beta_3$ integrins (Chu and Ng, 2004b), C-type lectin receptors (Davis et al., 2006), TAM receptors such as Axl (identified as a ZIKV entry receptor) and phosphatidylserine receptors (Meertens et al., 2012, Nowakowski et al., 2016, Laureti et al., 2018). Following receptor binding, the clathrin coated pit buds into the host cell from the plasma membrane, entering the endocytic trafficking cycle, whereby the endosomal pH lowers throughout its progression. The change in endosomal pH triggers conformational changes in the *Flavivirus* E protein, which exposes a fusion loop and subsequently causes the formation of a fusion pore. Viral components are released from the endosomal compartment into the host cell cytoplasm through the newly formed fusion pore. Viral genome replication can then take place within the cytoplasm.

### 1.2.2 Translation and Genome Replication

Positive sense RNA has one of two fates in the *Flavivirus* life cycle; it can either be translated directly by host cell translational machinery to produce viral proteins to assist in replication and packaging of progeny virions, or it can be used to generate template RNA for genome replication (Figure 1–4). Prior to replication, translation must occur to generate proteins involved in viral replication. *Flavivirus* genomes possess a 5'cap, which facilitates direct translation of the virus genome by host cell machinery via cap-dependant RNA translation. Viral proteins are translated as a single polyprotein which traverses the ER membrane via numerous transmembrane domains.

The polyprotein is processed by the host signal peptidase and further proteases, in addition to the viral protease, NS2B/NS3, to yield 10 individual proteins. The non-structural proteins have broad functionality, as described previously, in immune evasion, remodelling of intracellular membranes and replication complex formation, whereas structural proteins are required to assemble progeny virions.

*Flavivirus* replication takes place in virus-induced ER-derived membranous structures (Welsch et al., 2009, Westaway et al., 1997). It is thought that the role of these structures is three-fold: to increase the local concentration of molecules required for virus replication thereby increasing the efficiency of the process, compartmentalisation to spatially coordinate translation and genome replication, and to evade immune detection by concealing foreign molecules such as dsRNA. The main structures induced by, and involved in, *Flavivirus* replication are membrane vesicles, vesicle packets and convoluted membranes. Membrane vesicles are derived from invaginations of the rough ER membrane, clusters of which are collectively termed vesicle packets; membrane vesicles possess a small pore linking to the cytoplasm, allowing the exchange of small molecules and viral RNA (Welsch et al., 2009).

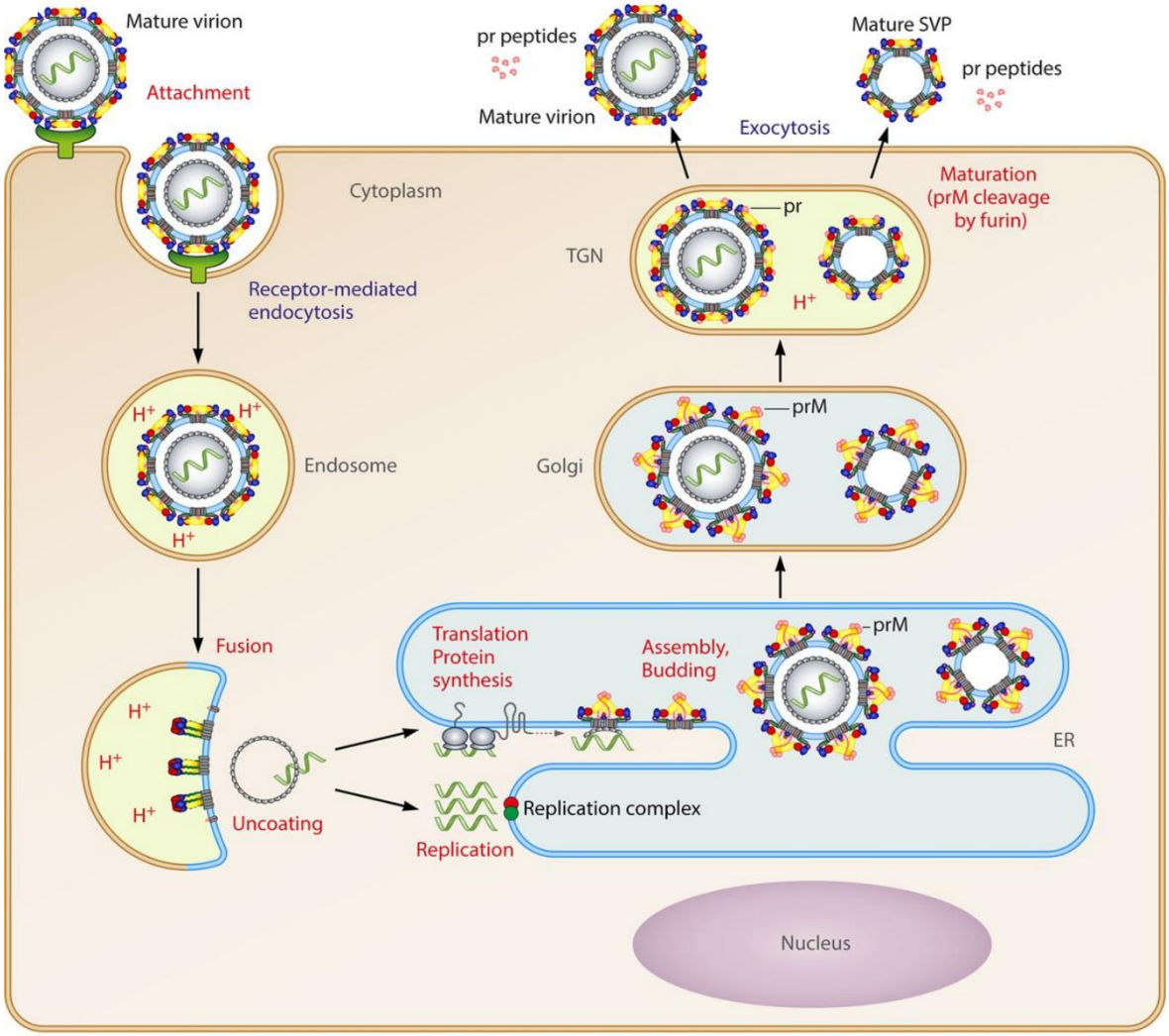


**Figure 1–4 The *Flavivirus* life cycle.**
The virus enters the host cell by receptor-mediated endocytosis and progresses through the endocytic pathway. Fusion of the viral and endosomal membranes is facilitated by pH-mediated conformational changes in the virus envelope protein. This fusion event releases viral RNA into the cytoplasm where it is transported to the ER. Viral RNA is translated to produce viral proteins which aid viral replication. The virus replicates its genome and forms particles within ER-derived membranous structures. Immature virus particles are transported through the trans-Golgi network whereby pH-mediated conformational changes of prM/E occur, producing a mature virus particle which can be released from the cell by exocytosis. prM is shed in the extracellular milieu. Particles which do not possess nucleocapsid structures can also be produced and are non-infectious – these are called sub-viral particles (SVPs). Figure from (Heinz and Stiasny, 2017)

NS5 and NS3 act cooperatively to provide the enzymatic activity required for RNA replication and 5' capping. First, the positive sense RNA genome forms a cyclic structure via complementary sequences in the 5' and 3' UTRs, termed the cyclisation sequence (Khromykh et al., 2001). *Flavivirus* RNA (positive sense) acts as a template for minus strand synthesis (negative sense RNA); minus strand synthesis is required to provide templates for genome replication (Figure 1–5). NS5 recognition of a conserved stem loop in the 5' UTR initiates RdRp activity, which generates dsRNA composed of both positive and negative sense RNA (Weber et al., 2006). The helicase activity of NS3 unwinds the dsRNA, liberating negative sense RNA to act as a template for the production of progeny viral RNA.

Progeny viral RNA (positive sense) is capped and methylated prior to packaging. The triphosphatase activity of NS3 removes the terminal phosphate from the 5' triphosphate, which is replaced with a guanosine monophosphate moiety by the action of the NS5 guanylyltransferase (Cui et al., 1998). The methyltransferase domain of NS5, using S-adenosyl-L-methionine as a methyl donor, methylates the cap structure at position N7, and the 2'-O position of the ribose of the first RNA nucleotide (Egloff et al., 2002, Issur et al., 2009). This results in a 5' type 1 cap structure (m7GpppNm-RNA) on progeny viral genomes.

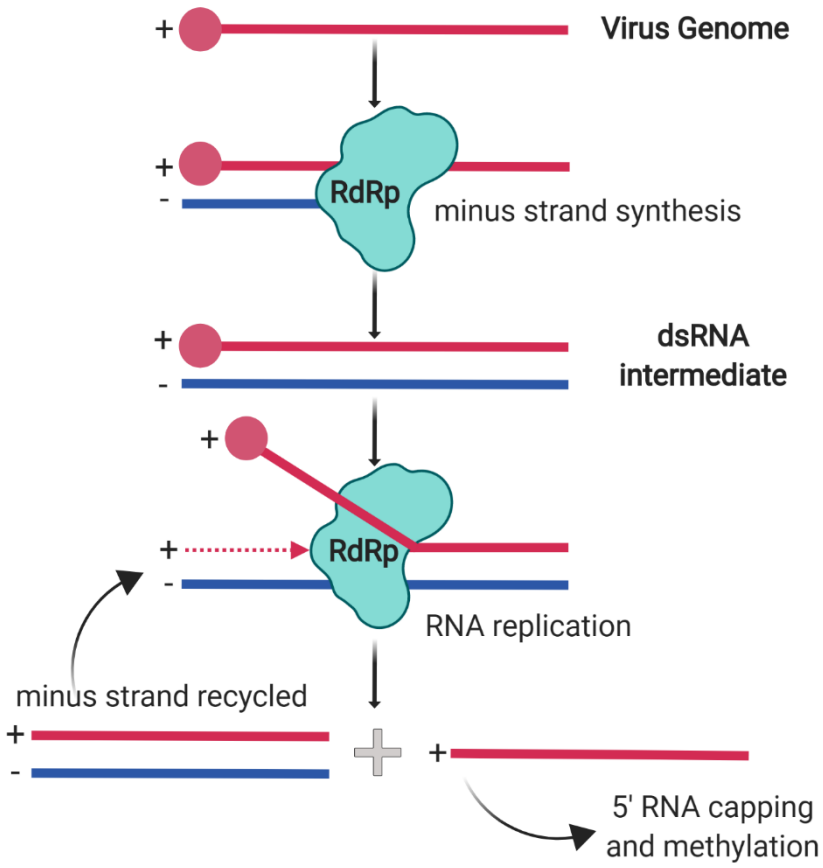


**Figure 1–5 *Flavivirus* genome replication strategy**
The virus genome is released into the cytoplasm after fusion of the virus and endosomal membranes. The RdRp function of NS5 transcribes an anti-sense genome (minus strand synthesis) using the genome as a template; this produces a dsRNA intermediate. The helicase function of NS3 unwinds this intermediate structure so that the NS5 protein can transcribe positive sense RNA, this time using the negative strand as the template. This results in the formation of dsRNA composed of positive and negative sense RNA, in addition to a further copy of the positive sense RNA. The positive sense RNA can then be capped and methylated by the enzymatic action of NS3/NS5, and subsequently packaged into progeny virions. Created with BioRender.

### 1.2.3 Packaging and egress

Nascent viral RNA exits the site of replication via a pore in the vesicle packet, allowing it to be packaged into budding virions which are formed at the opposing ER-derived membrane (Welsch et al., 2009). In order to generate the virus envelope, prM and E must form heterodimers, which further multimerise into heterotrimeric prM/E spikes at the ER membrane. This induces membrane curvature and facilitates the budding of immature virions into the ER lumen. To generate infectious virus particles, prior to budding, the nucleocapsid (capsid proteins associated with viral genomic RNA) must associate with prM/E – this process is poorly characterised. Once virions bud into the ER lumen, they enter the host cell secretory pathway, progressing through the trans-Golgi network. A series of post-translational modifications and conformational changes (section 1.1.6) occur which generate the mature virus particle. Once released into the extracellular space by exocytosis, the pr portion of prM is shed, resulting in infectious progeny virions.

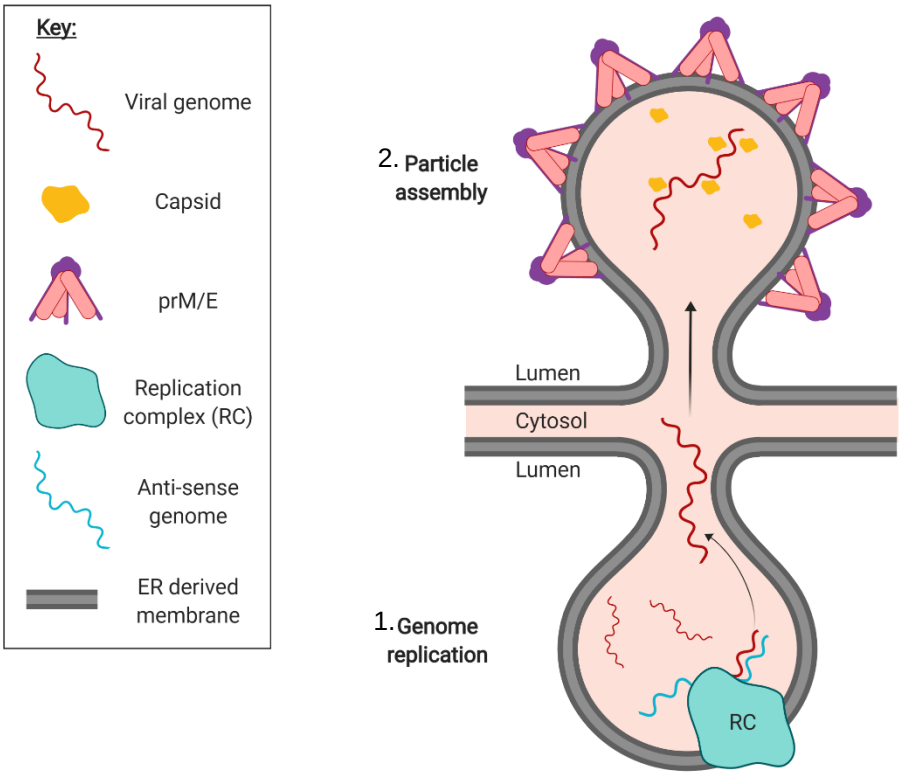


**Figure 1–6 Schematic representation of RNA replication and packaging**
*Flavivirus* replication and particle formation occurs within virus-induced ER-derived membranous structures. 1. Virus replication takes place within vesicle packets by the replication complex (RC). Nascent viral RNA is transported through a pore in the vesicle packet to the site of virus assembly. 2. Progeny virus particles assembly on the cytosolic face of the ER membrane, and bud into the ER lumen to be transported through the exocytic pathway. Created with BioRender.

## 1.3 Zika virus

### 1.3.1 The epidemiological history of ZIKV

Zika virus (ZIKV) is a member of the *Flavivirus* genus of the family *Flaviviridae*. It was first isolated in 1947 from the serum of sentinel rhesus monkey enrolled in a YFV study, caged in a canopy of the Ziika forest (the namesake of the virus), Uganda (DICK et al., 1952). It was isolated again the following year in the same forest from a pool of *A. africanus* mosquitoes (DICK et al., 1952); the first human case was detected in Nigeria in 1954 (MACNAMARA, 1954, SIMPSON, 1964). In subsequent years, serological and entomological data indicated sporadic ZIKV infections occurred over West and Central Africa (Figure 1–7), and South-East Asia (Figure 1–8) (HADDOW et al., 1964, Marchette et al., 1969, Robin and Mouchet, 1975, Jan et al., 1978, Fagbami, 1979, Olson et al., 1981, Saluzzo et al., 1981, McCrae and Kirya, 1982, Darwish et al., 1983, Monlun et al., 1993, Lanciotti et al., 2008, Duffy et al., 2009, Heang et al., 2012, Haddow et al., 2012).

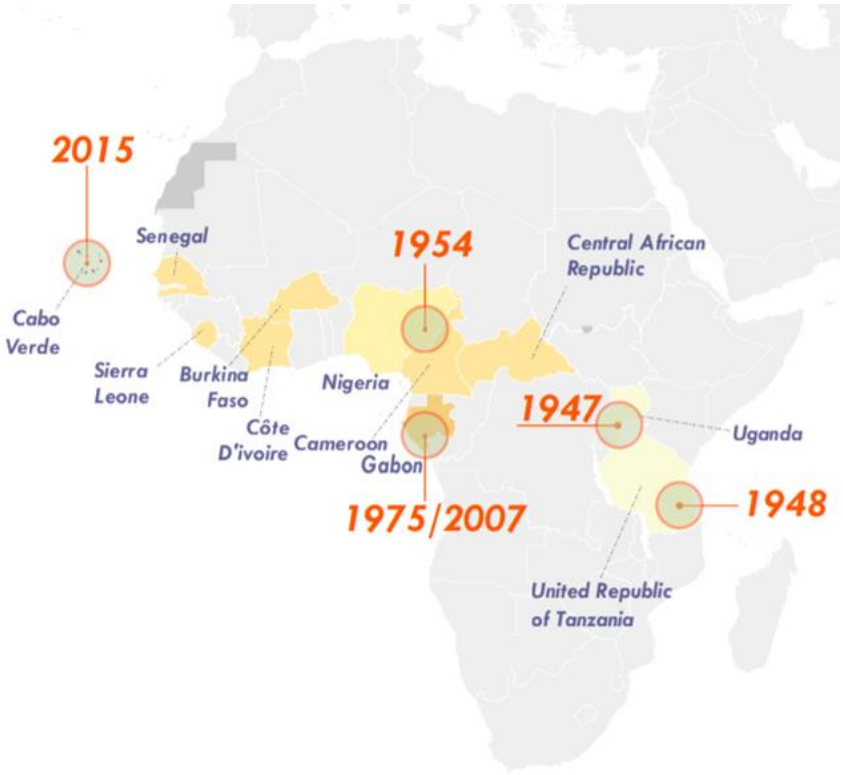


**Figure 1–7 Geographical distribution of documented evidence of ZIKV infection in Africa**
Evidence of ZIKV infection was either in the form of serological and entomological data or by virus isolation. The darker shading of orange represents more recent data was documented. Where two dates are shown for the same location, is indicative of two independent data points. This is a rendering demonstrating geographical distribution of ZIKV infection until February 2016. Figure from (Kindhauser et al., 2016).

The first documented epidemic occurred in 2007 in Yap island, Micronesia, where 49 residents had confirmed ZIKV infection and 73% had serological evidence of a recent ZIKV infection (Lanciotti et al., 2008, Duffy et al., 2009). Thereafter, outbreaks occurred in French Polynesia (2013), New Caledonia (2014), the Cook Islands (2014) and Easter Island (2014) (Figure 1–8 and Figure 1–9) (Cao-Lormeau et al., 2014, Dupont-Rouzeyrol et al., 2015, Pyke et al., 2014, Tognarelli et al., 2016). Phylogenetic studies highlighted that the ZIKV sequences from the French Polynesian outbreak are more related to the strains from South-East Asia than those from the Yap island outbreak, which is indicative of independent introductions into Polynesia from Asia (Faye et al., 2014).


**Figure 1–8 Geographical distribution of documented evidence of ZIKV infection across Asia and the Pacific**
Evidence of ZIKV infection was either in the form of serological and entomological data or by virus isolation. The darker shading of orange represents more recently acquired data. Two dates shown for the same location is indicative of two independent data points. This is a rendering demonstrating geographical distribution of ZIKV infection until February 2016. Figure from (Kindhauser et al., 2016).

The largest ZIKV outbreak to date originated in the State of Bahia, Brazil in 2015 which rapidly spread neighbouring states such as Pernambuco, then throughout Brazil and central America, with reports of ZIKV transmission reaching Florida, and further afield via travel imported cases (Figure 1–9) (Campos et al., 2015, Zanluca et al., 2015). By October 2015, Bahia reported 56,318 suspected cases of ZIKV infection; owing to the scale of the subsequent outbreak, Brazil ceased counting cases of ZIKV (WHO, 2015). The 2014 World Cup football tournament

and the Va'a canoe event (2014), both held in Rio de Janeiro, have been implicated in the introduction of ZIKV into Brazil. Conversely, one molecular clock analysis suggests that the introduction of ZIKV into Brazil predates both these events (Faria et al., 2016). The subsequent outbreak was declared a Public Health Emergency of International Concern (PHEIC) in February 2016 (WHO, 2015). Symptomatic ZIKV infection is thought to occur in 1/5 patients, establishing a mild-febrile illness with a maculopapular rash (further details of ZIKV disease are explored in section 1.3.3). A curiosity of the 2015-2016 outbreak was the unprecedented increase in the incidence of neurological disease complications, which were spatiotemporally associated with ZIKV infection. The aetiology of such conditions at the time were unknown, and as such was the precipitating factor for the declaration of ZIKV as a PHEIC. As of March 2017, the World Health Organisation (WHO) reported 61 areas with ongoing ZIKV transmission since its first introduction or reintroduction from 2015 onwards (WHO, 2017). More recently a large, previously unreported outbreak in Cuba was identified retrospectively via a genomics approach; the outbreak in Cuba peaked in 2017, as ZIKV cases in the Americas were reported to be waning (Grubaugh et al., 2019).

The ZIKV outbreak 2015-2016 was infamous due to the unprecedented increase in the number cases of neurological disorders, namely microcephaly and Guillain-Barré syndrome (discussed further in sections 1.3.3.3 and 1.3.4). Retrospective analyses of the 2013 ZIKV outbreak in French Polynesia, identified a 20-fold increase in the number of cases of Guillain-Barré syndrome, found to be associated with ZIKV infection (Cao-Lormeau et al., 2016). Evidence for a causal link between ZIKV infection and microcephaly was established through a series of case studies performed on post-mortem new-borns with microcephaly and suspected ZIKV infection (Martines et al., 2016, Mlakar et al., 2016, Driggers et al., 2016). Specimens, including tissue from the central nervous system, tested positive for ZIKV by RT-PCR and histopathologic methods; in one case, the virus was successfully isolated from the tissue (Mlakar et al., 2016). Since 2015, 31 countries or territories have reported microcephaly or other central nervous system disorders potentially associated with ZIKV infection, and 23 countries or territories have reported ZIKV-related GBS (WHO, 2017).


**Figure 1–9 Geographical distribution of documented evidence of ZIKV infection across Central and South America**

Evidence of ZIKV infection was either in the form of serological and entomological data or by virus isolation. The darker shading of brown represents more recently acquired data. Two dates shown for the same location is indicative of two independent data points. This is a rendering demonstrating geographical distribution of ZIKV infection until February 2016. Figure from (Kindhauser et al., 2016).

### 1.3.2 ZIKV transmission

ZIKV is an arthropod-borne virus (arbovirus). Arboviruses are maintained in nature through transmission cycles between a vertebrate host and a hematophagous arthropod e.g. mosquitoes, ticks, midges and sandflies. ZIKV is primarily transmitted by *Aedes* species (*Ae*.) mosquitoes, in particular *Ae. aegypti* and *Ae. Albopictus* mosquitoes, which are prevalent in tropical and subtropical regions (Figure 1–10).

The *Ae. aegypti* mosquito is predominantly active during the day and has a propensity to feed on human blood – though it will feed on other non-human vertebrates (Christophers, 1960). This mosquito has adapted to survive in close proximity to humans and breeds in artificial containers of fresh water e.g. pools of water collected in tyres, flower pots, water storage tanks etc (Christophers, 1960). In addition to ZIKV, *Ae. aegypti* also transmit other arboviruses such as DENV, YFV and chikungunya virus.*Ae. albopictus* originated in tropical forests of South-East Asia; trade and travel practices have perpetuated the global dispersion of this mosquito species (ECDC, 2016). Ae. albopictus are more tolerant of milder temperatures than Ae. aegypti, as such Ae. albopictus can be found in abundance in southern regions of Europe (Figure 1–10) (Caminade et al., 2012, Ding et al., 2018). Adult females are day biters, preferably feeding outdoors on a range of blood hosts including humans, mammals, birds, reptiles and amphibians. Ae. albopictus can breed in natural habitats such as bodies of fresh water held by terrestrial plants, and rock pools, in addition to artificial habitats such as tyres (ECDC, 2016). Like Ae. aegypti, Ae. albopictus can also transmit DENV and chikungunya virus; in experimental conditions Ae. albopictus serves as a competent vector of 22 other arboviruses of medical and veterinary concern including YFV, JEV and Rift Valley fever virus (Schaffner et al., 2013).

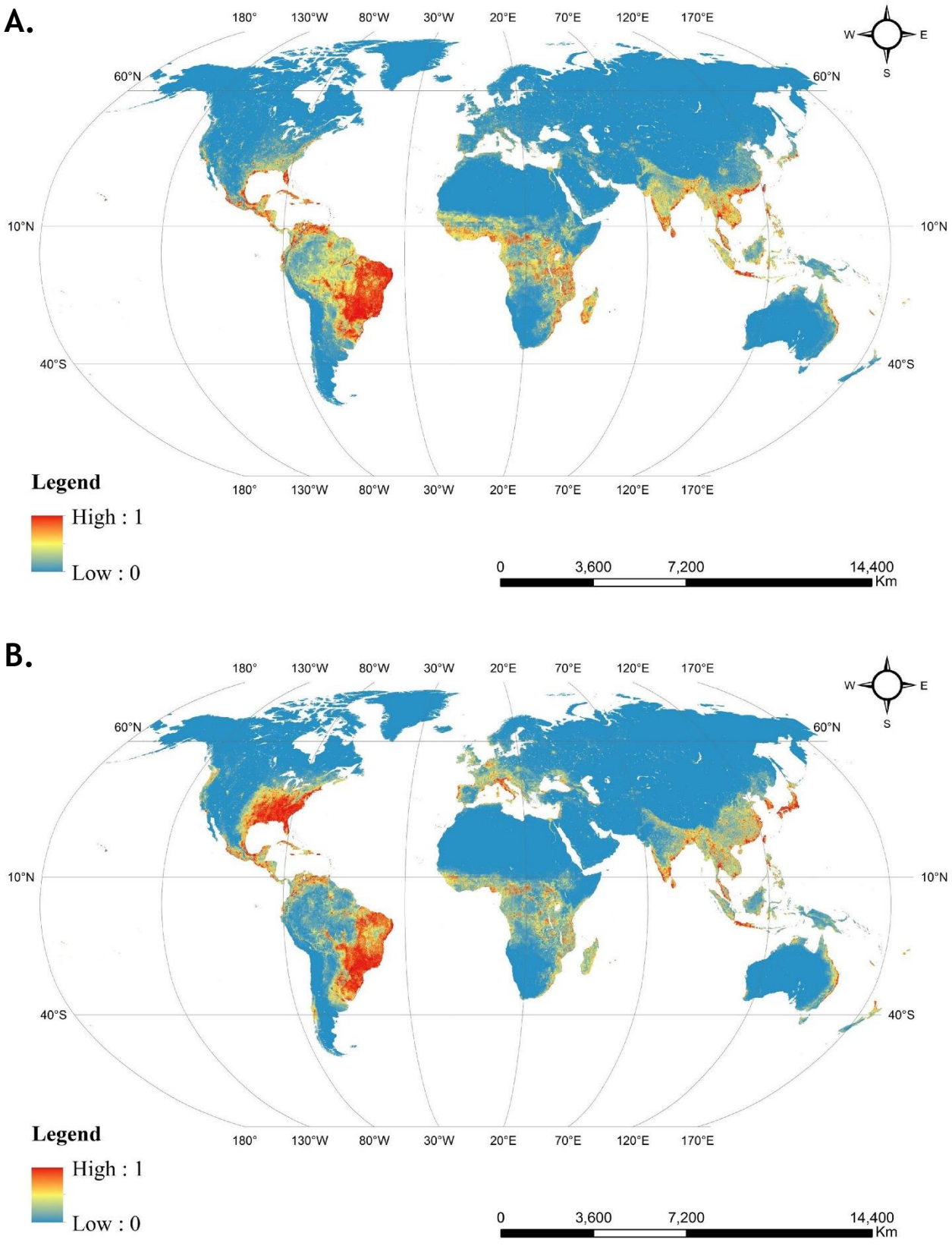


**Figure 1–10 Predicted global distribution of *Aedes species* mosquitoes**
The probability of occurrence of *Aedes aegypti* (***A***) *and Aedes albopictus* (***B***) mosquitoes across the world (0-1). Red indicates regions highly suitable for growth (1), and blue regions which are less suitable (0). *Aedes species* mosquitoes are prevalent in tropical and sub-tropical regions. *Aedes albopictus* mosquitoes are more prevalent in Europe and Northern America, than *Aedes aegypti*. Some areas in Europe such as Italy and Spain may also provide suitable habitats for *Aedes aegypti* growth and survival. Figure from (Ding et al., 2018).

Transmission occurs when the mosquito ingests a viraemic blood meal taken from a vertebrate host; the virus then replicates within the mosquito, disseminating throughout the tissues via the arthropod haemolymph until it reaches the salivary glands. The virus can then be transmitted to a vertebrate through salivary secretions when ingesting the next bloodmeal (Figure 1–11). This cycle maintains many arboviruses in nature, and is usually dependent upon non-human vertebrates, with humans generally being considered a 'dead-end host'. However, urban transmission cycles can be established whereby transmission is reliant solely upon human-mosquito transmission, as is the case for DENV and Chikungunya virus (Weaver and Reisen, 2010); this route of transmission can potentiate epidemics, and maintain a virus population within urban areas (Figure 1–11). Between 2015 and September 2019, there were no reports of autochthonous transmission of ZIKV amongst mosquitos in Europe, despite an estimated 2130 travel imported cases being recorded since the outbreak in 2015 (ECDC, 2017). In October 2019, three cases of locally acquired ZIKV infection were confirmed in southern France (Hyères, Var department) (Giron et al., 2019). Investigations suggest that these cases provide the first evidence of mosquito (Ae. albopictus) transmitted ZIKV infection in Europe.

In addition to mosquito-borne transmission, several other routes have been identified for the transmission of ZIKV including intrauterine transmission from mother to foetus, sexual transmission (male-female, female-male, male-male), and via contaminated blood products (Grischott et al., 2016). Furthermore, ZIKV RNA has been detected in several bodily fluids including saliva (Musso et al., 2015a), breast milk (infective viral particles have also detected) (Dupont-Rouzeyrol et al., 2016, Besnard et al., 2014), urine (Gourinat et al., 2015) and semen (Musso et al., 2015b). These fluids may be exploited for diagnostic purposes e.g. urine and saliva (see Section 1.3.3.2 for more information relating to ZIKV diagnostics).

Maternal-foetal transmission of ZIKV is an important transmission route of serious biological consequence. This was highlighted by the 2015-2016 outbreak, whereby a rise in ZIKV-associated neurodevelopmental disorders was documented in neonates born to mothers who had been infected with ZIKV during pregnancy. ZIKV exhibits broad cellular tropism within the human

placenta including placental trophoblasts, fibroblasts, endothelial cells and Hoffbauer cells (foetal macrophages), in addition to umbilical cord tissue (El Costa et al., 2016, Miner and Diamond, 2017). It has been postulated that the breach of the maternal-foetal barrier is multifactorial and may involve a combination of: viral cytopathic effects, soluble factors which regulate immune trafficking, and antibody-virus complex formation (Pereira, 2018). However, the mechanisms underlying ZIKV maternal-foetal transmission remain to be determined.

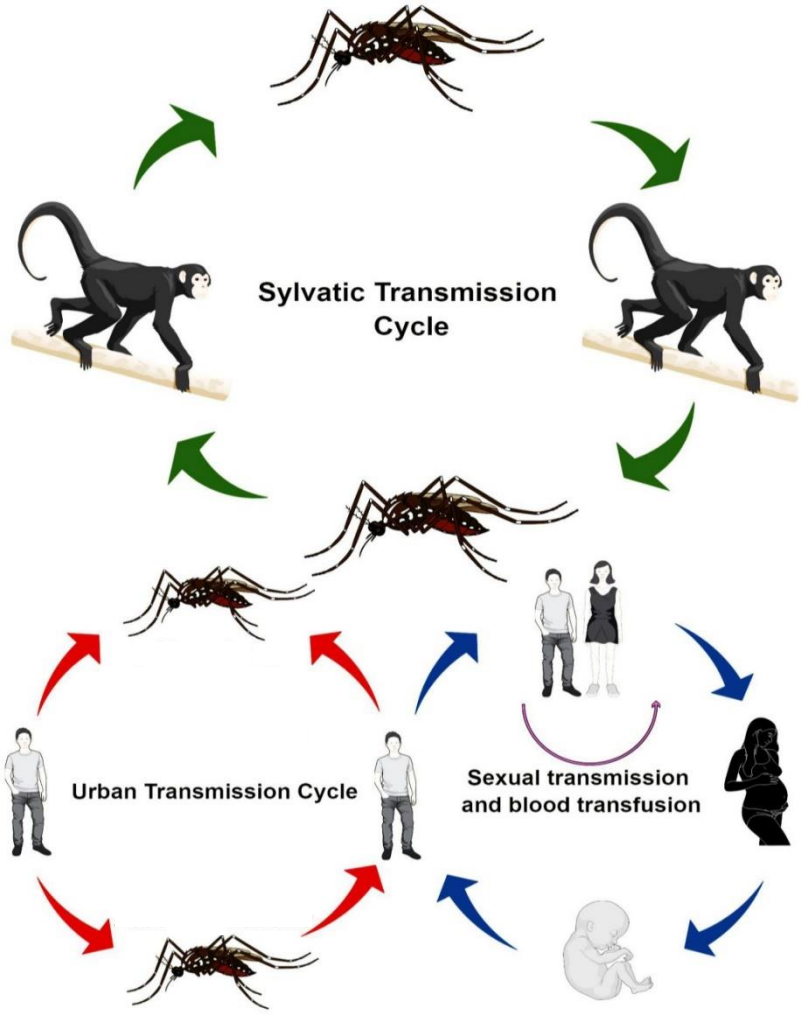


**Figure 1–11Transmission cycles of the Zika virus**
It has been postulated that a sylvatic cycle exists for ZIKV, though this may be a historical feature of ZIKV transmission. Sylvatic cycles of arbovirus transmission occur between primates and the arthropod host. The arthropod (in the case of ZIKV, the *Aedes aegypti* mosquito) takes a bloodmeal from a viraemic primate, the virus replicates in the mosquito and is transmitted via salivary secretions upon subsequent bloodmeals from a ZIKV-naïve primate. Urban transmission cycles remain the main form of transmission for ZIKV. Like in the sylvatic cycle, the virus is transmitted between humans by the *Aedes aegypti* mosquito during blood feeds. An infected individual can also transmit the virus via other routes, including contaminated blood products during blood transfusions, sexual transmission and vertical transmission *in utero*. Figure adapted from (Rather et al., 2017).

## 1.3.3 ZIKV Disease and Diagnosis

### 1.3.3.1 Symptomatic ZIKV infection

ZIKV typically establishes an asymptomatic infection, causing symptoms in roughly 20% of patients, resolving within a week of onset (SIMPSON, 1964, Filipe et al., 1973). Symptomatic ZIKV infection is characterised by a maculopapular rash, mild fever, malaise, pruritus (itching), arthralgia (joint pain), retro-orbital pain/headache, myalgia (muscle pain/weakness), conjunctivitis, and/or oedema of the extremities (SIMPSON, 1964, Olson et al., 1981, Lanciotti et al., 2008, Duffy et al., 2009). In rare cases, severe clinical sequalae can occur, highlighted by recent ZIKV outbreaks (Cao-Lormeau et al., 2016, Mlakar et al., 2016). Guillain-Barré syndrome, a peripheral neuropathy, and congenital ZIKV syndrome are notable severe conditions associated with ZIKV infection (detailed further in section 1.3.3.3 and 1.3.4, respectively).

### 1.3.3.2 Diagnosing ZIKV infection

The diagnosis of suspected ZIKV infection requires the collection of specimens, and obtaining a detailed patient history including: symptoms, date of onset, duration of symptoms, contact with known ZIKV cases, travel history and vaccination history (e.g. YFV, JEV, DENV) (WHO, 2016). At the time of the Brazil outbreak, the recommended specimens to be collected for nucleic acid testing (by RT-PCR) included whole blood, serum and/or urine (if symptom onset ≤ 7 days prior) (WHO, 2016). For the diagnosis of patients who presented with symptom onset ≥ 7 days, serological testing of whole blood and serum (IgM and IgG enzyme linked immunosorbent assays; ELISAs) or plaque reduction neutralisation test (PRNT) was recommended (WHO, 2016). Serological diagnostic testing is particularly useful in diagnosing prior ZIKV infections, as the resultant viraemia is short-lived; however, serology cannot confirm active ZIKV infection (Fagbami, 1979, Shan et al., 2017, Lanciotti et al., 2008).

Conventional molecular and serological diagnostic tests are performed in a laboratory setting, often requiring processing of specimens prior to the chosen diagnostic test. Furthermore, in some cases cross-reactivity with other related viruses, such as DENV, can occur (Singh et al., 2017). New methodologies which can be performed at point of care are being developed for rapid ZIKV

diagnostics, for example loop-mediated isothermal amplification (LAMP) based assays to detect ZIKV RNA (Silva et al., 2019). Reverse-transcription (RT) LAMP is a one-step method used to rapidly amplify and detect target RNA. Firstly, RNA is reverse transcribed into complementary DNA (cDNA). Target cDNA is then amplified using four specific primers which allow for the formation of loop structures, which drive the amplification of concatemer cDNA via a self-priming mechanism (Notomi et al., 2015). Unlike conventional PCR, target amplification doesn't require thermocycling and instead occurs at one constant temperature (between 60-65 °C); furthermore RT-LAMP can be completed in under 1 hour. Detection of the amplified product can be performed by observing the turbidity and/or colour of the sample, either produced from magnesium pyrophosphate (a by-product of the reaction), or from inclusion of a fluorescent dye which reacts specifically with double-stranded DNA (Notomi et al., 2015). Moreover, this method is compatible with liquid specimens without the need for RNA extraction (Silva et al., 2019). However, further development is required prior to commercialisation.

A combination of foetal ultrasound and neuroimaging techniques such as computed tomography (CT) and magnetic resonance imaging (MRI) scans can be used to detect some neurodevelopmental abnormalities associated with congenital ZIKV syndrome (de Fatima Vasco Aragao et al., 2016) (see section 1.3.4 for more information of congenital ZIKV infection).

#### 1.3.3.3 **ZIKV-associated Guillain-Barré Syndrome (GBS)**

GBS is characterised by a rapidly progressive symmetrical weakness of muscles in the arms and legs, reduced tendon reflexes and sensory symptoms (Willison et al., 2016). However, disease progression and clinical presentation is variable between patients and can result in facial palsy, an inability to walk and respiratory distress, requiring hospitalisation (Leonhard et al., 2018). Patients recovering from GBS may need extensive physiotherapy, placing not only a substantial burden on the quality of life of the patient, but also a socio-economic burden through loss of work.

GBS is considered to be a post-infectious immune disorder, with two-thirds of patients reporting having had an infectious disease one month prior to the

clinical onset of GBS (Willison et al., 2016). Several pathogens have been associated with the development of GBS such as: C*ampylobacter jejuni, Mycoplasma pneumoniae, Haemophilus influenzae,* cytomegalovirus, hepatitis E virus, and Epstein-Barr virus (Jacobs et al., 1998, Mori et al., 2000). More recently, ZIKV infection has been associated with GBS (Cao-Lormeau et al., 2016). The current model underpinning the development of GBS is that an infectious agent triggers an inappropriate immune response which subsequently injures nerve components. Such is the case in GBS related to infection with *C. jejuni (Yuki et al., 2004)*. The lipo-oligosaccharides of *C.jejuni* mimic gangliosides found on peripheral nerves, resulting in autoreactive antibody production – nerve components are injured as a consequence (Yuki et al., 2004). In ZIKV-associated GBS, some cases report the onset of GBS occurs in quick succession of, or even concurrent with symptomatic infection, challenging the post-infectious auto-immune paradigm of GBS development (Parra et al., 2016). Further investigation is required to understand whether ZIKV-associated GBS is a result of direct viral infection, or the elicitation of an aberrant immune response.

### 1.3.4 Congenital ZIKV syndrome

Microcephaly is the most striking physical phenotype associated with congenital ZIKV infection; microcephaly is a congenital disorder whereby the head circumference is smaller than the norm for the age and sex (below the 3$^{rd}$ percentile) (Figure 1–12). However, an expanding spectrum of neurodevelopmental disorders can occur in neonates as a result of ZIKV infection – collectively termed 'congenital ZIKV syndrome' (CZS). CZS is defined by the CDC as a proven, *in utero* ZIKV infection associated with severe microcephaly in which the skull has partially collapsed, decreased brain tissue with a specific pattern of brain damage (including subcortical calcifications), damage to the back of the eye, congenital contractures and hypertonia which restrict body movement soon after birth (CDC, 2019, Moore et al., 2017). However, this definition is still debated; other abnormalities are associated with ZIKV infection, including: brain asymmetry, craniofacial disproportion, hydrocephalus, neuronal migration disorders, excessive scalp skin, tremors, seizures in addition to ocular and hearing impairments (Culjat et al., 2016, de Fatima Vasco Aragao et al., 2016, Aragao et al., 2017, Leal et al., 2016, Moura da Silva et al., 2016,

Pessoa et al., 2018). Moreover, neonates who are born with a head circumference within the normal range display evidence of brain-abnormalities when assessed using neuroimaging methods (Aragao et al., 2017).

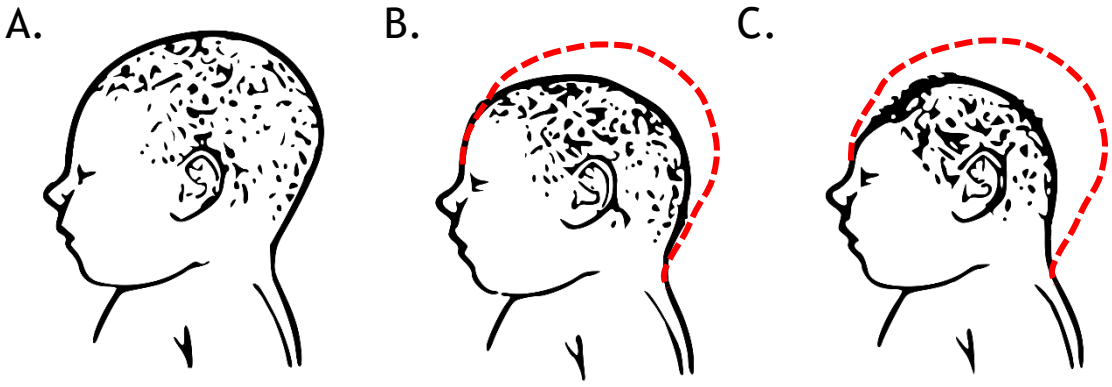


**Figure 1–12 Illustrative representation of a neonate with microcephaly**
A. Healthy human baby B. Human baby with microcephaly C. Human baby with severe microcephaly. Figure was redrawn from (CDC, 2019).

Post-natal CT and MRI scans have identified numerous anomalies within the CNS of infants with presumed or laboratory confirmed ZIKV infection. These include: cortical thinning with abnormal gyral patterns, calcifications (primarily subcortical), increased fluid spaces, hypoplasia (underdeveloped or incomplete development of tissue) or absence of corpus callosum, cerebellar hypoplasia and decreased myelination (Aragao et al., 2017, de Fatima Vasco Aragao et al., 2016, Chimelli et al., 2017). The gross morphological features of the brain which are affected by CZS, are shown in Figure 1–13.

Even in the absence of CNS morphological anomalies, the potential for slow-progressing, delayed-onset, chronic neurocognitive disorders remain. Studies in a non-human primate model of maternal-foetal ZIKV transmission demonstrate ZIKV infection depleted neural stem cells within late foetal neurogenic zones of the brain; this led to deficits in neuron maturation and patterning in the hippocampus (Adams Waldorf et al., 2018). Moreover, no foetal abnormalities were detected by ultrasound. However, foetal brain MRI scans did detect abnormalities in 4/5 foetuses which were infected with ZIKV (Adams Waldorf et al., 2018). Nonetheless, the damage to hippocampal neural stem cells should not be ignored. The hippocampus is involved in learning and memory; neurogenesis occurs within the hippocampus occurs in the human through to adolescence

(Gonçalves et al., 2016). If the findings of Adams Waldorf et al, 2018 are replicated in congenital ZIKV infection in humans, the affected individual could be at an increased risk of developing neurocognitive and psychiatric disorders later in life (Adams Waldorf et al., 2018, Walker et al., 2019).

CZS is an expanding spectrum of neurodevelopmental disorders. Current antenatal ultrasound methodologies are unable to detect subtle neural pathologies associated with ZIKV and requires access to MRI imaging, which isn't always feasible (Walker et al., 2019). Furthermore, some ZIKV-associated neurological injury may evolve over time. Therefore, non-microcephalic neonates which were exposed to ZIKV in gestation should be monitored in accordance with current guidelines (Adebanjo et al., 2017).

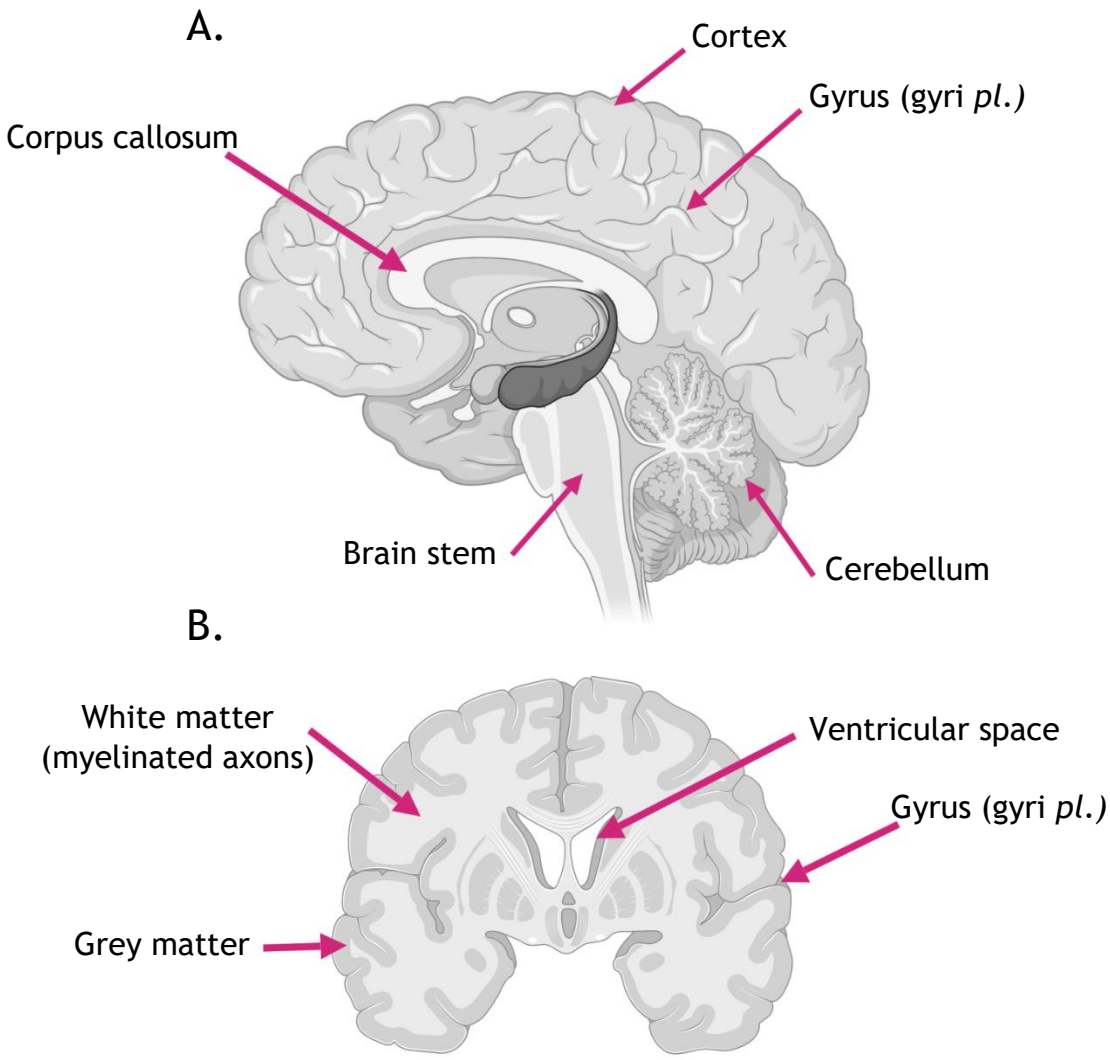


**Figure 1–13 Key morphological features of the brain which are altered in congenital zika virus syndrome**

A schematic of the human brain in the sagittal plane (A) and axial plane (B), highlighting key structures implicated in congenital zika virus syndrome (CZS). In CZS, in addition to overall gross reduction in brain matter, the following morphological anomalies can occur: cortical thinning with abnormal gyral patterns, calcifications (primarily subcortical), increased ventricular spaces, hypoplasia or absence of corpus callosum, cerebellar hypoplasia and decreased myelination. Created using BioRender.

### 1.3.5 Teratogenic infections

Teratogens are agents which disturb foetal development; toxoplasmosis (To), rubella (R), cytomegalovirus (C) and herpes simplex virus (H) are collectively termed 'TORCH' pathogens, which can cause congenital malformations and foetal/neonatal mortality. Since the term was coined, the O in TORCH has been replaced with 'other' to encompass an expanding spectrum of teratogenic infections caused by pathogens such as syphilis, varicella-zoster virus, parvovirus B19, hepatitis viruses, listeria, enteroviruses, Rift Valley fever virus and human immunodeficiency virus. ZIKV is the most recent addition to the group of TORCH infections.

Cytomegalovirus (CMV) is the most common congenital viral infection in the USA and affects 5-7/100 live births in developed countries (Lanzieri et al., 2014). CMV is a member of the *Herpesviridae* family of viruses, classified further by the subfamily *Betaherpesvirinae* and genus, *Cytomegalovirus (*species: *Human betaherpesvirus 5)* (Davison et al., 2003). In terms of their virology, ZIKV and CMV are very distant. ZIKV possesses a single stranded positive sense RNA genome approximately 11 kb in length, which expresses 12 different gene products encoded on a single ORF. Whereas CMV possesses a linear dsDNA genome approximately 235 kb in length, comprising over 170 ORFs (Davison et al., 2003, Hage et al., 2017). Remarkably, despite their fundamental differences, ZIKV and CMV elicit similar clinical manifestations during congenital infection.

CMV infection is asymptomatic in 85-90% of neonates; neurological sequelae occurs in >50% of symptomatic CMV-infected neonates at birth (Dollard et al., 2007). CNS involvement may manifest as white matter abnormalities, calcifications, ventriculomegaly, cortical atrophy, cerebellar hypoplasia, cortical malformations (e.g. polymicrogyria or lissencephaly [smooth brain]) and periventricular cysts (Barkovich and Lindan, 1994, Lucignani et al., 2019). Other developmental disorders may be present, for example seizures, cognitive dysfunction, sensorineural hearing loss, learning disorders and microcephaly. Furthermore, delayed-onset sensorineural hearing loss has been documented in patients with asymptomatic congenital-CMV infection, indicating that neurological sequelae may continue to develop during childhood development

(Lanzieri et al., 2017). All of the aforementioned symptoms have been documented in CZS. The molecular mechanisms unpinning these events in both CMV and ZIKV infection are unknown and require further investigation.

## 1.4 Project aims

The 2015 ZIKV outbreak was characterised by an unprecedented upsurge in neurological disease in adults and neonates; namely Guillain-Barré syndrome and congenital ZIKV syndrome, which affect the peripheral and central nervous systems, respectively. Prior to this outbreak, ZIKV was associated with sporadic, small scale infections in man causing a mild self-limiting febrile illness in 20% of patients. Consequently, precedent studies of neurological disease complications associated with ZIKV infection were limited.

The overarching aim of works undertaken in this thesis, was to advance the understanding of ZIKV interactions within cells of the central and peripheral nervous system.

Objectives included:

I. To develop and assess methods to study ZIKV *in vitro*.

II. To characterise cell types of the central and peripheral nervous system which are permissive to ZIKV infection.

III. To identify a relevant cell type and analyse changes in the transcriptomic profile of ZIKV infected cells compared with uninfected cells.

# 2 Materials and Methods

## 2.1 Cell maintenance and passage

### 2.1.1 Mammalian cell lines

The cell line A549, was originally derived from human lung adenocarcinoma tissue, and are transformed alveolar basal epithelial cells. This cell line, and its derivatives were used to propagate 'mammalian' ZIKV PE243 virus stocks and used to titrate virus. A549 cells were grown in Dulbecco's modified Eagles medium (DMEM) supplemented with 10% v/v heat inactivated foetal bovine serum (FBS; Gibco), 100 U/mL penicillin and 100 µg/mL streptomycin (10% DMEM). A549 cells expressing the bovine viral diarrhoea virus N terminal protease fragment protein (herein referred to as A549 Npro) render the cells type-I IFN incompetent by targeting IRF-3 for proteasomal degradation (Hilton et al., 2006). A549 Npro cells were maintained in A549 media supplemented with 10 µg/mL puromycin. A549 Npro cells were kindly provided by R.E. Randall. Cells were maintained in 5% $CO_2$ at 37 °C.

The cell line, Vero E6 (provided by the lab of R.M. Elliott), was originally derived from kidney epithelial cells extracted from an African green monkey. This cell line was used to characterise a panel of previously untested antibodies raised against the ZIKV E and NS1 proteins (Section 3.3.1). Vero E6 cells were maintained in 10% DMEM, in 5% $CO_2$ at 37 °C.

SVGp12 (ATCC® CRL-8621™) is a cell line derived from human foetal astrocytes, transformed by the simian virus SV40 T-antigen. SVGp12 cells were maintained in 10% DMEM, in 5% $CO_2$ at 37 °C.

The cell line SFT-R was originally derived from foetal sheep thymus cells.SFT-R cells were maintained by Jordan Clark using Iscove's Modified Dulbecco's Media (Gibco) supplemented with 10% (v/v) heat-inactivated FBS,in 5% $CO_2$ at 37 °C. Lysate derived from SFT-R cells was used as a negative control when testing for the expression of GFAP by western blot.

When cells were approximately 80-90% confluent, old growth media was discarded, and cells were washed once with 5 mL of Versene in phosphate buffered saline (PBS; Versene in PBS, EDTA in PBS; E&O Laboratories Ltd). After washing, cells were incubated with 1x trypsin solution using a volume sufficient to cover the cell monolayer ([Merck] 10x diluted to 1x in Versene/PBS). Cells were incubated at 37 °C until the monolayer had detached from the plastic. The cells were resuspended in 10% DMEM, which inhibited the action of the trypsin. The cells were then pelleted by centrifugation at 1000 rpm for 5 minutes (ThermoScientific Heraeus Megafuge 16R, Rotor 75003181 [TX-400 swinging bucket rotor]). The supernatant was discarded, and cells were resuspended in an appropriate volume of fresh media until homogenous. A fraction of these cells were transferred to a fresh flask of appropriate size and fresh growth media was applied to cover the surface of plastic. Routine passaging of mammalian cells was typically performed using a 1:10 splitting ratio from resuspended cells. When a specific number of cells were required, cells were counted using a Bio Rad TC20™ automated cell counter (verified by manual cell count with a glass haemocytometer with each new cell line), the cells were then diluted as appropriate in their respective growth media and transferred to the desired plasticware and incubated at 37 °C until required.

### 2.1.2 Primary mammalian cells

Myelinating CNS and PNS cultures, and neuronal cultures were derived from the embryos of Ifnar1 knockout (KO; type I interferon incompetent) and wild type (WT) mice (A129 mice; 129S7/SvEvBrdBkl-Hprtb-m2 background [B&K Universal]) and were kindly provided by V Schultz and J Barrie. Myelinating CNS cultures were maintained in serum free differentiation medium (DMEM [4.5 mg/mL glucose], 100 U/mL penicillin, 100 µg/mL streptomycin, 10 ng/mL biotin, 1% N1, 50 nM hydrocortisone, and 10 µg/mL insulin) (Cumberworth et al., 2017a). Myelinating PNS cultures were maintained in Minimal Essential Media [MEM 4 mg/ml glucose], 100 U/ml penicillin, 100 µg/ml streptomycin, 5% horse serum, 50 ng/ml nerve growth factor, 1% N2, 20 µg/ml bovine pituitary extract, 0.5 µM forskolin, 50 µg/ml ascorbic acid). Neuronal cultures were maintained in serum free neurobasal medium (NBM) either supplemented with or without 5-Fluoro-2'-deoxyuridine. Cells were maintained in 5% $CO_2$ at 37 °C. Growth media was replenished every 2-3 days by removing 40% of the old media and replacing with

60% of fresh growth media (to account for evaporation and prevent drying of cells).

### 2.1.3 Invertebrate cell lines

The cell line C6/36 was originally derived from whole larvae of the species Ae. albopictus. C6/36 cells were maintained in Schneider's drosophila media supplemented with 10% FBS and 1% penicillin and streptomycin. Cells were incubated without $CO_2$ at 28 °C in non-vented tissue culture flasks.

At approximately 80% confluency, the growth media was removed from the cells and a volume of fresh media was applied to the cells. The cells were removed from the plastic using a cell scraper (Falcon) and resuspended by pipetting. A fraction of these cells was then transferred to a fresh flask containing the appropriate volume of growth media (1:15 ratio of resuspended cells:fresh media). Routine passaging took place in a non-vented T80 flask.

## 2.2 Virus techniques

### 2.2.1 Virus origin & propagation

#### 2.2.1.1 **Virus propagation of mammalian cell origin**

ZIKV isolates, ZIKV/H.sapiens/Brazil/PE243/2015 (abbreviated to ZIKV PE243, Gen Bank accession: KX197192 (Donald et al., 2016)) and MR766 (Gen Bank accession: AY632535), was propagated in A549 Npro cells.

The culture media of a confluent T225 vented flask of A549 Npro cells was discarded and the monolayer was washed 1x with PBS. The PBS wash was discarded prior to incubation with virus diluted in 10 mL of 2% FBS/PBS to achieve a MOI of 0.1 (see section 2.2.3 for MOI calculation). The cells were incubated for 1 hour at 37 °C and gently rocked after 30 minutes. The virus was discarded, and the cell monolayer washed 1x with PBS prior to the addition of complete growth media (section 2.1.1) supplemented with 25 mM HEPES buffer (4-(2-hydroxyethyl)-1-piperazineethanesulfonic acid). The cells were incubated at 37 °C until substantial cytopathic effect (CPE) was observed, typically 3-5 days post infection. The cell supernatant was harvested and clarified of debris

by centrifugation at 4000 rpm for 10 minutes (ThermoScientific Heraeus Megafuge 16R, Rotor 75003181 [TX-400]). Aliquots of clarified supernatant was stored at -80 °C until required. See section 2.2.2 for details of virus titration.

#### 2.2.1.2 Virus propagation of invertebrate cell origin

ZIKV isolate ZIKV/H.sapiens/Brazil/PE243/2015 was also propagated in mosquito cell line C6/36. The procedure follows that of section 2.2.1.1 with minor amendments to growth media and incubation conditions. C6/36 cells were maintained in Schneider's drosophila media supplemented with 10% FBS, 1% PenStrep and 25 mM HEPES buffer. The cells were incubated in T80 non-vented tissue culture flasks at 28 °C without $CO_2$. Cytopathic effect could not be used as an indicator of virus infection in invertebrate cells; therefore, cell culture supernatant was harvested 3-4 days post infection. The supernatant was clarified by centrifugation at 4000 rpm for 10 minutes (ThermoScientific Heraeus Megafuge 16R, Rotor 75003181 [TX-400]) and stored at -80 °C until required.

### 2.2.2 Titration of virus by plaque assay

ZIKV titres were determined by standard plaque assay using A549 Npro cells. Approximately 1 mL of cells were seeded at a density of 2.5 x $10^5$ cells per well of a 12 well plate and incubated overnight at 37 °C (see section 2.1.1 for details of cell passage). 10-fold serial dilutions of the virus were performed using PBS supplemented with 2% v/v FBS. Growth media was discarded from each well and replaced with 200 µL of each dilution. Cells were incubated with virus dilutions for 1 hour at 37 °C with gentle agitation after 30 minutes. After incubation, virus was aspirated and discarded and replaced with 2 mL of overlay media per well (1.2% w/v Avicel [FMC Biopolymer]:2x MEM [Life technologies] supplemented with 4% FBS, in 50:50 ratio). The cells were incubated for a further 5 days at 37 °C prior to fixation with 8% formaldehyde/PBS at room temperature for 1 hour. The overlay and fixative were then discarded and replaced with 0.1% w/v toluidine blue stain (Sigma Aldrich). The cells were incubated in stain with agitation for 1 hour before the stain was gently washed away with tap water. Circular clearings in the stained cell monolayer were considered to be plaques and were subsequently counted. Virus plaque forming units (PFU)/mL was calculated by the following formula:

*Plaque forming units (PFU)/mL* $= \left(\frac{average\ number\ of\ plaques}{amount\ of\ innoculum\ (mL)}\right) x\ dilution\ factor$

### 2.2.3 Infection of cells with virus

The appropriate volume of virus required for infection was determined using the following equation:

$$\frac{number\ of\ cells\ x\ MOI}{virus\ titre} = volume\ of\ virus\ (mL)$$

Virus was diluted in a suitable amount of infection media (2% FBS/PBS) to achieve the desired MOI and volume of inoculum. The total infectious volume used for a 12 or 24 well plate was 200 µL, and 600 µL for 30 mm dish containing 3x coverslips of myelinating CNS cultures. Cellular growth media was aspirated from vessels and replaced with virus. Cells were incubated at 37 °C for 1 hour and gently rocked after 30 minutes to prevent monolayers from drying. Control mock infections were treated in parallel with infection medium only (2% FBS/PBS). Following incubation, infection medium (with or without virus) was aspirated and the cultures returned to the appropriate media for cell maintenance until required (as described in section 2.1).

## 2.3 Nucleic acid methods

### 2.3.1 Polymerase chain reaction (PCR)

PCR amplification was performed using KOD Hot Start mastermix (ThermoFisher Scientific) using primers detailed in Table 2–1. The reaction mixture was set up as follows:

25 µL of KOD hotstart mastermix

1.5 µL of forward primer (at 10 µM)

1.5 µL of reverse primer (at 10 µM)

10 ng of template

$H_2O$ to total reaction volume of 50 µL

| Name | Sequence |
|---|---|
| **SP6 3'UTR FWD** | ATTTAGGTGACACTATAGAGCACCAATCTTAATGTTGTCAGGCCTG |
| **3'UTR REV** | CCATGGATTTCCCCACACCGGC |
| **qGSF** | CGCTACTTGGGTGAAGAAGG |
| **qREV** | GCGTTCTCGGCCTGACTATAG |

**Table 2–1 Primer sequences used to amplify the 3'UTR region of ZIKV**

The cycling conditions were as follows:

Initial melting period, 2 minutes at 95 °C

20 seconds at 95 °C (melting)

10 seconds annealing time (70 °C for SP6 3'UTR FWD/3'UTR REV, 58 °C for qGSF/qREV – Table 2–1)

10 second extension period at 70 °C

Final 5-minute extension period at 70°C

Steps 2-4 were repeated for 30 cycles.

PCR products were separated by agarose gel electrophoresis (section 2.3.2) prior to gel purification (2.3.3) and a further round of PCR amplification using the sample primer pairs as the primary amplification. PCR products in solution were purified by ethanol precipitation (2.3.4) to remove reaction components and a sample of precipitated products were analysed by agarose gel electrophoresis to assess purity.

## 2.3.2 Agarose gel electrophoresis of DNA

Separation of DNA fragments was achieved using agarose gel electrophoresis. Agarose gels were prepared by adding agarose to Tris-acetate-EDTA (TAE; 1x TAE, 40 mM Tris, 10 mM acetic acid, 1mM EDTA; ThermoFisher Scientific) buffer to a final concentration between 1-2% w/v (depending on fragment sizes to be resolved). The agarose/buffer mix was heated until the agarose had completely

dissolved, then allowed to cool before the addition of 0.5 µg/mL ethidium bromide (EtBr). The solution was poured into a gel sled, a well forming comb added at the top of the gel and the gel was allowed to set at room temperature. The sled was submerged in TAE buffer inside a horizontal gel electrophoresis tank (Bio-Rad) and the well-forming comb was removed. Samples were mixed with 6x loading dye (New England Biolabs) and loaded into the gel alongside either a 100 bp or 1 kb DNA ladder (New England Biolabs) to facilitate the measurement of DNA fragments. Gels were run at 100 V for 40 minutes. Nucleic acids were visualised by UV transillumination (Bio-Rad).

### 2.3.3 DNA extraction and purification from agarose gel

DNA products were first separated and visualised as described in section 2.3.2. The band of interest was excised from the gel using a scalpel and transferred to a fresh 1.5 mL tube. The tube was weighed and the weight of the gel slice calculated. The DNA was extracted from agarose gel slices using the Illustra GFX PCR DNA and Gel band purification Kit (GE Healthcare) in accordance to the manufacturer's suggested protocol. Briefly, 10 µL of capture buffer was added to the tube per 10 mg of gel. The sample was heated to 60 °C for up to 30 minutes, until the gel slice had melted. The sample was then transferred to a microspin column placed inside a collection tube and centrifuged at 13,500 rpm for 1 minute (Eppendorf Centrifuge 5418, Rotor FA-45-18-11). The flow through was discarded and filter was washed 2x with wash buffer with 1 minute centrifugation at 13,500 rpm (Eppendorf Centrifuge 5418, Rotor FA-45-18-11) between washes. Following the last wash step, the column was subjected to a further 2 minute centrifugation step. The spin column was transferred to a fresh tube and the DNA products were eluted by applying 25 µL of nuclease free water which had been preheated to 60 °C. The water was allowed to incubate on the filter for 5 minutes prior to centrifugation at 13,500 rpm (Eppendorf Centrifuge 5418, Rotor FA-45-18-11) for 2 minutes. Eluted products were quantified and stored at -20 °C until required.

### 2.3.4 Ethanol precipitation of nucleic acid products in solution

0.1 volumes of 3 M sodium acetate pH 5.2 and 2.5 volumes of ice-cold 100% ethanol was added to DNA samples in 1.5 mL microcentrifuge tubes. For RNA

samples, 2.5 volumes of ice-cold 100% ethanol and ammonium acetate to a final concentration of 2.5 M was added. The sample was mixed briefly by inversion. Samples were stored at -80 °C overnight to precipitate the nucleic acid. Nucleic acid was recovered by centrifugation at 16,000x rpm for 30 minutes at 4 °C (Eppendorf Centrifuge 5418, Rotor FA-45-18-11). The supernatant was discarded and the DNA/RNA pellet was washed 2x with 70% ethanol with 5 minutes centrifugation at 16,000 x rpm (Eppendorf Centrifuge 5418, Rotor FA-45-18-11) at 4 °C in between washes. The DNA/RNA pellet was allowed to air dry for 5-10 minutes before resuspending in an appropriate volume of distilled water (or RNase free water for RNA samples). Samples were quantified as per section 2.3.5. DNA samples were stored at -20 °C and RNA samples were stored at -80 °C until required.

### 2.3.5 Quantification of nucleic acids

Nucleic acid yields were quantified using a NanoDrop ND-1,000 spectrophotometer (Thermo Fisher Scientific). In addition to concentration, sample purity was assessed by observing the 260/280 and 260/230 ratios. For DNA, samples possessing a 260/280 ratio ~1.8 is considered 'pure'. The 260/280 ratio is ~2.0 for 'pure' RNA samples. The 260/230 ratio is an additional measure of nucleic acid purity. Ratio's lower than 2.0-2.2 may be an indicator of contaminants which absorb and 230 nm, such as TRIzol® reagent.

### 2.3.6 Sequencing of PCR products

To verify the successful amplification/modification of products of interest, samples were sent for sequencing at Source Biosciences alongside the appropriate primers. Resulting sequences were analysed using Geneious version 7.0 (http://www.geneious.com, (Kearse et al., 2012)).

### 2.3.7 *In vitro* RNA transcription of ZIKV 3'UTR from SP6 promoter

The template for transcription was generated by PCR amplification of the 3'UTR region from the plasmid pCCl-SP6-ZIKV* WT (donated from Prof A. Merits, University of Tartu; contains 5' and 3' UTRs from ZIKV PE243) using primer pairs found in section 2.3.1 (SP6 3'UTR FWD and 3'UTR REV). The reaction generated PCR products of the ZIKV PE243 3' UTR possessing an SP6 promoter immediately

upstream of the start of the 3'UTR. PCR products were separated by agarose gel electrophoresis and was subsequently purified (section 2.3.2-2.3.3). The purified PCR products underwent a further round of PCR amplification using the same primer pair as previously described, prior to purification by ethanol precipitation (section 2.3.4). A sample of purified PCR products was analysed by agarose gel electrophoresis to check the product quality.

The ZIKV 3'UTR was transcribed using the MEGAscript™ SP6 Transcription Kit (Thermo Fisher Scientific). The reaction was set up as described in Table 2–2. The reaction was incubated in a PCR cycler overnight at 37 °C. To digest the DNA template, 1 µL of TURBO DNase (Thermo Fisher Scientific) per 20 µL reaction was added, the samples were briefly mixed and collected by centrifugation prior to a further 15 minute incubation at 37 °C. The RNA was purified by ethanol precipitation as described in section 2.3.4.

| Component | Amount per 20 µL reaction |
|---|---|
| **Biotin-16-UTP (Jena Biosciences)** | 0.7 mM |
| **UTP** | 1.3 mM |
| **ATP** | 5 mM |
| **CTP** | 5 mM |
| **GTP** | 8 mM |
| **10 x Reaction buffer** | 2 µL |
| **SP6-3'UTR template** | 1 µg |
| **SP6 enzyme** | 2 µL |
| **H2O** | Total to 20 µL |

**Table 2–2 Components of in vitro transcription reaction to produce biotinylated 3'UTR RNA**
In vitro transcription was performed suing the MEGAscript™ SP6 Transcription Kit (Thermo Fisher Scientific), and the protocol modified to include biotin-16-UTP, and varying amounts of nucleotides, as described in (Chavali et al., 2017).

## 2.3.8 Denaturing agarose gel electrophoresis of RNA

The quality of *in vitro* transcribed RNA was assessed by denaturing agarose gel electrophoresis. To make a 1% gel, 1 g of agarose was dissolved in 72 mL of distilled water by boiling. Once dissolved, 18 mL of 37% formaldehyde and 10 mL

of 10 x MOPS (3-(N-morpholino)propanesulfonic acid) running buffer (1X MOPS buffer, 50 mM MOPS, 50 mM Tris Base, 0.1% SDS, 1mM EDTA, pH 7.7; ThermoFisher Scientific) was added to the solution inside a fume cupboard and mixed. An appropriate amount of the gel solution was poured into a gel sled with a well forming comb, both of which had been treated with RNaseZAP (Sigma Aldrich) prior to the addition of the gel. The gel was allowed to set at room temperature.

Once the gel had set and samples were prepared, the gel sled was submerged in 1 x MOPS running buffer, the well forming comb was removed and appropriate volumes of the samples were added. Samples were run at 100V for 1.5-2 hours. The samples were visualised by UV transillumination.

### 2.3.9 Isolation of total cellular RNA – TRIzol ®

To extract total cellular RNA from cell culture, cell culture supernatant was discarded and the appropriate volume of TRIzol ® (Thermo Fischer Scientific) was added to the cells for harvest (1 mL per well of a 12 well plate or CNS culture dish, 333 µL for PNS samples in 24 well plate [3x wells were pooled to give 1 sample]). Cells were incubated with TRIzol ® for 5 minutes prior to resuspension and transfer to a fresh RNase-free tube. Samples were stored at -80 °C until required.

Samples for RNA extraction were defrosted and 200 µL of chloroform was added per 1 mL of TRIzol ®. Samples were vortexed for 15 seconds prior to centrifugation at 10,500 rpm at 4 °C (Eppendorf Centrifuge 5418, Rotor FA-45-18-11). The upper phase (water phase) was carefully removed and transferred to a fresh RNase free tube. 0.5 µL of RNase free glycogen (10 mg/mL) and 500 µL of isopropanol per 1 mL of TRIzol ® was added to the upper phase, mixed briefly and incubated for 10 minutes at room temperature. The sample was subjected to centrifugation for 10 minutes at 10,500 rpm at 4 °C to pellet the RNA (Eppendorf Centrifuge 5418, Rotor FA-45-18-11). The RNA pellet was washed 2 x with 500 µL of 70% ethanol with a 10 minutes centrifugation at 4 °C in between washes. The pellet was then air dried prior to resuspension 35 µL of nuclease-free water. RNA samples were stored at -80 °C until required.

## 2.3.10 Reverse transcription PCR (RT-PCR)

cDNA synthesis was performed using the SuperScript™ III First-Strand Synthesis System (Invitrogen). Reactions were performed in 0.2 µL thin walled PCR tubes. Briefly, 1 µg of total cellular RNA was incubated with 1 µL random hexamer primers, µL dNTPs and water to total 10 µL. Samples were mixed and incubated at 65 °C in a PCR thermocycler for 5 minutes and returned to ice for 1 minute. 4 µL of 5 x buffer, 3 µL of $H_2O$, 1 µL of DTT, RNaseOUT and SuperScript™ III were added to the sample to total 20 µL. The reaction was incubated at 50 °C for 1 hour followed by a 10-minute incubation at 70 °C to terminate the reaction. cDNA samples were stored at -20 °C until required.

## 2.3.11 Quantitative PCR (qPCR)

### 2.3.11.1 General qPCR methodology

qPCR protocols were performed using the standard curve method. qPCR standard were generated by PCR amplification (Section 2.3.1) of the pCCl-SP6-ZIKV* WT plasmid using primers qGSF and qREV, and purified as described in sections 2.3.2-2.3.4. The PCR product was quantified as described in section 2.3.5 and 10-fold serial dilutions were performed.

A qPCR master mix was prepared inside a PCR cabinet (Sartorius) and contained the following per well:

10 µL SYBR™ Green PCR Master Mix (Thermo Fisher Scientific)
1 µL forward primer (from 10 µM stock)
1 µL reverse primer (from 10 µM stock)
7 µL RNase free $H_2O$

1 µL of cDNA sample or PCR standard was added to the master mix outside of the PCR cabinet, in a different room. The reaction mixture was then applied to a 96 well qPCR plate in triplicate.

#### 2.3.11.2 **Absolute quantitation of sfRNA vs genomic RNA (gRNA)**

ZIKV sfRNA and gRNA levels were quantified using a differential qPCR assay based upon that described in (Bidet et al., 2014). Samples were prepared as per section 2.3.11.1. Each qPCR plate contained a range of standards from 0.000927 ng/µL – 0.927 ng/µL and cDNA samples prepared with primer pairs qGSF/qREV and qSF/qREV, cDNA samples prepared with internal control primers GAPDH FWD/GAPDH REV, in addition to water only negative controls (primers detailed in Table 2–3). One primer specifically recognises gRNA only (qG) by annealing upstream of the stop codon of ZIKV PE243, in the NS5 coding region. The other primer recognises a region downstream of the stop codon, within the 3'UTR, which is shared by both sfRNA and gRNA (qGSF). The reverse primer is shared by both forward primers (qREV). To determine the amount of sfRNA, the following equation was used:

$$concentration\ of\ sfRNA = \ concentration\ of\ GSF - concentration\ of\ G$$

| Name | Sequence |
|---|---|
| **qG** | CGCTACTTGGGTGAAGAAGG |
| **qGSF** | GTTGTCAGGCCTGCTAGTCAG |
| **qREV** | GCGTTCTCGGCCTGACTATAG |
| **GAPDH FWD (donated by C.Donald)** | TGCACCACCAACTGCTTAGC |
| **GAPDH REV (donated by C.Donald)** | GGCATGGACTGTGGTCATGAG |

**Table 2–3 Primers used to determine quantity of genomic and sfRNA, including internal control primer pairs**

## 2.4 Cellular protein composition analysis

### 2.4.1 Cell lysis & preparation for western blot

Cell culture supernatant was discarded, and cells washed 1x in sterile PBS. The cells were lysed in an appropriate volume of ice-cold lysis buffer (25 mM Tris HCl pH 7.6, 150 mM KCl, 5mM EDTA pH 8. 5 mM $MgCl_2$, 1% NP40, 0.1% mM dithiothreitol [DTT] (Chavali et al., 2017)) supplemented with cOmplete™ mini protease inhibitor cocktail (Roche) and 100 U/ml RNAse OUT (Thermo Fisher Scientific) prior to use. The lysate was clarified of insoluble cellular debris by

centrifugation at 16,000 rpm (Eppendorf Centrifuge 5418, Rotor FA-45-18-11) for 5 minutes. The cell lysate was then transferred to a fresh 1.5mL tube and 10x Bolt™ Sample Reducing Agent and 4X Bolt™ LDS Sample Buffer (both Thermo Fisher Scientific) were added to equal 1X solutions. Protein samples were heated at 90 °C for 10 minutes to denature the sample and stored at -20 °C until required.

### 2.4.2 Sodium Dodecyl Sulphate – Polyacrylamide Gel Electrophoresis (SDS-PAGE)

Samples were prepared as described in section 2.4.1.1 and loaded into Bolt™ 4-12% Bis-Tris Plus gels (Invitrogen) whilst submerged in 1x Bolt™ MES SDS running buffer (Invitrogen). Protein samples were run alongside a sample of SeeBlue™ Plus2 Pre-stained Protein Standard (Thermo Fisher Scientific) to aid in size determination in downstream applications. Gels were run at 100V for approximately 45 minutes, or until the loading dye appeared 2/3's down the length of the gel. Protein gels were either analysed by western blot (sections 2.4.1.3-2.4.1.4) or stained for total protein composition (section 2.3.1.5).

### 2.4.3 Protein transfer

Proteins were transferred onto a 0.45 µm nitrocellulose membrane (Thermo Fisher Scientific) using a Tran-Blot SD semi-dry transfer cell (RioRad) and semi-dry transfer buffer (48 mM Tris, 39 mM glycine, 0.0375% (w/v) SDS, 20% (v/v) methanol) at 15 V for 30 min. The following was assembled and placed into the semi dry transfer machine in the following order (1 being closest to the top, 4 being closest to the bottom):

1. Whatman 2mm filter paper (soaked in 1x semi-dry transfer buffer)

2. SDS-PAGE gel (released from original cassette)

3. Nitrocellulose membrane (soaked in $dH_2O$)

4. Whatman 2mm filter paper (soaked in 1x semi-dry transfer buffer)

Protein transfer was carried out at 15V for 35 minutes.

### 2.4.4 Immuno-detection

Protein samples were transferred to a nitrocellulose membrane as described in section 2.4.1.3. The membrane was incubated with agitation in blocking buffer (1x PBS, 0.1% v/v Tween-20, 5% w/v non-fat dried milk [Marvel]) for 1 hour at room temperature. Following blocking, the membrane was incubated overnight at 4 °C with agitation, in the appropriate primary antibody diluted in blocking buffer (see table Table 2–4 for primary antibodies). The membrane was washed5 times for 2 minutes in PBST solution (1x PBS, 0.1% v/v Tween-20). The membrane was then incubated with the appropriate secondary antibody (Table 2–4) diluted in blocking buffer for 45 minutes (secondary antibody with fluorescent conjugate) or 1.5 hours (horseradish peroxidase conjugated secondary antibody) at room temperature. A further five 2-minute washes in PBST solution was performed prior to protein band visualisation.

Membranes probed with a secondary antibody conjugated with horseradish peroxidase were incubated with Pierce™ ECL (enhanced chemiluminescence) Western Blotting Substrate (ThermoFisher Scientific) in accordance with manufacturer protocols. Protein bands were visualised by exposing X-ray film to the western blot membrane. Western blot membranes processed in this way can be found in Chapter 3 only. Western blot membranes probed with a secondary antibody conjugated with a fluorescent marker were visualised using a Li-cor Odyssey imaging system (Li-cor Biosciences).

| Antibody name | Species | Working dilution |
|---|---|---|
| **Anti-ZIKV E (clone 0402166, Aalto Bio Reagents)** | Mouse | 1:5000 |
| **Anti- β-Actin (Sigma-Aldrich)** | Rabbit | 1:2000 |
| **Anti- β-tubulin (Abcam)** | Mouse | 1:5000 |
| **Anti- Musashi-1 (Abcam)** | Rabbit | 1:2000 |
| **Goat anti-mouse IgG conjugated with horseradish peroxidase (Abcam)** | Goat | 1:2000 |
| **Goat anti-mouse IgG (H+L) cross-adsorbed secondary antibody, Alexa Fluor ® 700 (ThermoFischer Scientific)** | Goat | 1:10,000 |
| **Goat anti-rabbit IgG (H+L) cross-adsorbed secondary ntibody, Alexa Fluor ® 800 (ThermoFischer Scientific)** | Goat | 1:10,000 |

**Table 2–4 Antibodies used in Western blot protocols**
Secondary antibodies are highlighted grey. Secondary antibodies conjugated with horseradish peroxidase were used to visualise western blot membranes by film exposure. Secondary antibodies conjugated with a fluorescent marker (Alexa Fluor ®) were used to visualise western blot membranes using the Li-cor Odyssey imaging system (Li-cor Biosciences).

## 2.5 Total protein composition analysis

Cell lysates were prepared as per section 2.4.1.1 and run on a SDS-PAGE as described in section 2.4.1.2. The protein gel was washed in $dH_2O$ for 5 minutes, then removed and replaced with SYPRO® orange protein gel stain (SYPRO® [Thermo Fisher Scientific] diluted 1:5000 in 7.5% acetic acid in $H_2O$) for total protein composition. The gel was incubated in staining solution for 30 minutes with agitation whilst wrapped in tin foil as the reagent was light sensitive. Following incubation, the stain was removed, and the gel was washed 3x with $H_2O$ for 5 minutes a time. The gel was visualised by UV transillumination.

## 2.6 Immunostaining

CNS and PNS co-cultures were cultured in dishes containing glass coverslips (section 2.1.2). Coverslips possessing fixed cells were permeabilised in 1 mL of PBS containing 0.5% v/v Triton X-100 for 15 minutes. Coverslips were then incubated with blocking buffer (PBS supplemented with 5% FBS) for 1 hour. The blocking buffer was then aspirated and discarded prior to incubation with the appropriate primary antibody (as detailed in Table 2–5) for 2 hours at room temperature. Coverslips were then washed 3x with PBS prior to incubation with

the appropriate secondary antibody (detailed in Table 2–5) for 1 hour at room temperature. Coverslips were then washed 3x with PBS followed by 2x washes with distilled water. Coverslips were then mounted onto glass slides using VECTORSHEILD® with DAPI mounting media (Vector Laboratories) and sealed with nail enamel. Immunofluorescence images were taken using EVOS Fl cell imaging system.

| Antibody name | Molecular/Cellular target | Working dilution |
|---|---|---|
| **Mouse anti-ZIKV E (clone 0402166, Aalto Bio Reagents )** | ZIKV envelope protein | 1:500 |
| **Rabbit anti-NeuN (Millipore)** | Neuronal nuclei, NeuN (Fox-3) | 1:750 |
| **Rabbit anti-SMI31 (Biolegend)** | Phosphorylated neurofilament (axons) | 1:1500 |
| **Rat anti-MBP (AbD serotec)** | Myelin basic protein (myelin sheath) | 1:500 |
| **Rat anti-PLP/DM20 (clone AA3, donated by Dr.Steven Pfeiffer)** | PLP/DM20 (myelin components and oligodendrocyte cell bodies) | 1:400 |
| **Rabbit anti-GFAP (Dako)** | Glial fibrillary acidic protein (astrocytes) | 1:400 |
| **Rat anti- F480 (AbD serotec)** | F4/80, an adhesion G protein coupled receptor (microglia) | 1:600 |
| **Rabbit anti-NG2 (Millipore)** | NG2 – an integral membrane proteoglycan (oligodendrocyte precursor cells) | 1:200 |
| **Mouse anti- Olig2 (Abcam)** | Olig2 – oligodendrocyte transcription factor 2 (immature and mature oligodendroglia) | 1:200 |
| **Goat anti-mouse IgG Alexa Fluor ® 488 (Invitrogen)** | Mouse IgG | 1:10,000 |
| **Goat anti-rabbit IgG Alexa Fluor ® 594 (Invitrogen)** | Rabbit IgG | 1:10,000 |
| **Goat anti-rat IgG Alexa Fluor ® 594 (Invitrogen)** | Rat IgG | 1:10,000 |

**Table 2–5 Primary and secondary antibodies used in immunofluorescence protocols**
Secondary antibodies are highlighted grey. All primary antibodies were incubated at room temperature for 2 hours; all secondary antibodies were incubated at room temperature for 1 hour.

## 2.7 3'UTR RNA pull down

### 2.7.1 Cell lysate preparation

Two confluent T225 flasks of A549 cells were infected at MOI 2 as per section 2.2.3. At 24 hours post infection (h p.i.) the cell culture supernatant was discarded and the monolayer washed 2x with ice cold PBS. Per each T225 flask, Cells were lysed in 5 mL of ice-cold lysis buffer (as described in section 2.4.1.1). Prior to use, the lysis buffer was supplemented with cOmplete™ mini protease inhibitor cocktail (Roche), 100 U/mL RNAse OUT (Thermo Fisher Scientific). Lysates from 2x T225 flasks were pooled for each replicate to give 10 mL of lysate. The lysate was then clarified and stored as described in section 2.4.1.1.

### 2.7.2 Bead preparation

MyOne Streptavidin c1 Beads (Thermo Fisher Scientific) were transferred to a fresh RNase free tube and placed in a magnetic tube rack. The storage buffer was discarded and beads were washed 2x by resuspending in an equal volume of wash buffer (lysis buffer containing 300 mM KCl (Chavali et al., 2017)). The beads were then separated from wash buffer in the magnetic stand and beads were resuspended in an equal volume of lysis buffer.

### 2.7.3 Pull down assay

Cell lysates (prepared as per section 2.4.3.1) were defrosted and precleared by incubating with 50 µL of prepared MyOne Streptavidin T1 Beads (as detailed in 2.4.3.2) for 30 minutes at 4 °C, with rotation. The lysate was separated from the beads using a magnetic rack and 5 mL of lysate was transferred to 2x fresh 15 mL tubes. To one of the tubes, 50 pmol of biotinylated ZIKV 3' UTR was added. The lysate was then left to incubate with or without RNA for 2 hours at 4 °C, with rotation. RNA:protein interactions were precipitated by incubating with 50 µL of prepared MyOne Streptavidin T1 Beads (Thermo Fisher Scientific) for a further 1 hour at 4 °C, with rotation. RNA:protein:bead complexes were separated from lysate using a magnetic rack. The beads were then washed 3x by resuspending the beads with washing buffer (detailed in section 2.4.3.1) to reduce non-specific binding to beads. The beads were separated from the wash buffer using a magnetic rack and the buffer was discarded. The beads were then

resuspended in 40 µL of sample buffer (10x Bolt™ Sample Reducing Agent and 4X Bolt™ LDS Sample Buffer, diluted to 1x in nuclease free $H_2O$ [both Thermo Fisher Scientific]). The samples were then denatured by heating to 90 °C for 10 minutes, cooled by centrifugation at 13,500 rpm (Eppendorf Centrifuge 5418, Rotor FA-45-18-11) for 1 minute and analysed by SDS PAGE and western blot (section 2.4.1).

## 2.8 Methods involving CNS and PNS co-cultures

CNS and PNS co-cultures were prepared as previously described in Section 2.1.2.

### 2.8.1 Analysis of cell-type specific infection levels in CNS and PNS cultures

CNS and PNS co-cultures were infected on DIV24 with ZIKV (MOI either 0.3 or 3 PFU/cell) and fixed at 24- or 72 h p.i by incubating with 4% formaldehyde (diluted in PBS) for 1 hour at room temperature. The cells were immunolabelled as per Section 2.6. For cell quantification, fluorescence microscopy and image capture were performed using an Olympus IX70 microscope using Image Pro Plus 6 software. Ten images per coverslip (minimum of 2 coverslips per cell type/infection condition) were taken using the 20x objective. To avoid bias, fields of view were selected in the blue (DAPI) channel, following the pattern below:

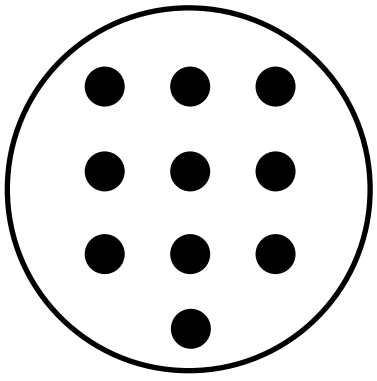

Rectangular areas of interest (AOI) of 148,427 $\mu m^2$ (to enumerate cell type specific and ZIKV cells) and 20,000 $\mu m^2$ (to enumerate DAPI positive cells) were placed on each image; cells within and touching west and north borders were quantified. Cells were defined as immunopositive structures with a DAPI positive nucleus. Pyknotic nuclei were identified based on size, and homogeneity and intensity of DAPI staining; pyknotic nuclei being small, condensed and intensely labelled. The average cell density per AOI was converted to cells/$mm^2$ using the formula:

Cells/mm2 = cell density per AOI/area of AOI $\mu m^2$ x 1,000,000

Representative images for illustration were obtained using a Zeiss LSM 710 inverted confocal microscope and Zen Black software.

## 2.8.2 Extended ZIKV infection in CNS co-cultures

CNS co-cultures were infected on DIV18 with ZIKV using a MOI of 0.3 PFU/cell. Media replenishments occurred every 2 days (detailed in section 2.1.2). At 6 d p.i cells were fixed by incubating in 4% formaldehyde at room temperature for 1 hour. Cells were immunolabelled using antibodies targeting axon and myelin structures, detailed in Section 2.6. Imaging was performed as per Section 2.8.1.

### 2.8.2.1 Assessing the role of soluble factors in inducing white matter structure injury

Cell culture supernatant was harvested from cells in Section 2.8.2, at 6 d p.i and infectious virus particles inactivated by exposure to UV-C light (8 W; 254 nm at a distance of 2 cm for 4 minutes, with shaking after 2 minutes) (Rezelj et al., 2017). UV-treated supernatant was mixed with fresh media (75% UV-supernatant, 25% fresh media). The mixture was transferred onto fresh DIV18 CNS co-cultures; cells were incubated with UV-supernatant for 6 days with media replenishments taking place on days 2 and 4 (media replenishment mixture contained both UV-supernatant and fresh media in a ratio of 1:1). On day 6, cells were fixed by incubating in 4% formaldehyde at room temperature for 1 hour. Cells were immunolabelled using antibodies targeting axon and myelin structure, as well as ZIKV E to confirm the absence of active viral infection

(immunolabelling details can be found in Section 2.6. Imaging was performed as per Section 2.8.1.

## 2.8.3 Transcriptomic analysis of mixed cell CNS cultures

### 2.8.3.1 **Sample preparation**

### 2.8.3.2 **Infection of CNS cells**

Primary murine CNS cultures (described in Sections 2.1.2 and 4.2.2, kindly provided by V Schultz and J Barrie) were infected with ZIKV PE243 at MOI 1 (as described in section 2.2.3) on culture day 28 *in vitro* (DIV28). At 48- and 96-hours post infection, cell culture supernatant was removed and discarded, and 1 mL of Trizol reagent was applied to per 35 mm dish. Cells were incubated with Trizol reagent for 5 minutes at room temperature prior to resuspension and placement into a fresh 1.8mL cryotube and stored at -80 °C until required.

### 2.8.3.3 **RNA extraction for RNAseq**

Trizol samples were defrosted at room temperature. Once thawed, 200 uL of chloroform was added per 1 mL of Trizol sample and vortexed for 15 seconds until thoroughly mixed. Samples were allowed to rest for 2 minutes at room temperature prior to centrifugation at 12,500 rpm (Eppendorf Centrifuge 5418, Rotor FA-45-18-11) at 4 °C . The upper water phase was then transferred to a sterile RNase free tube. RNA was further purified using the RNeasy Minkit (Qiagen) with on column DNase I digestion, according to the manufacturers protocol. The RNA was stored at -80 °C until required. Prior to library preparation, the quality and quantity of RNA was analysed using a High Sensitivity RNA ScreenTape ® (Agilent), and was performed by Natasha Johnson.

### 2.8.3.4 **Library preparation and RNAseq**

Library preparation and sequencing (RNAseq) was performed using the TruSeq stranded mRNA library prep workflow (illumina), in accordance with manufacturers protocols. Library preparation and RNAseq was performed by Natasha Johnson of the Viral Genomics and Bioinformatic team of the MRC University of Glasgow Centre for Virus Research.

#### 2.8.3.5 **Analysis of RNAseq data**

Read assembly, alignment, and identification of differentially expressed genes were performed by Dr Quan Gu. RNAseq read quality was assessed using FastQC software (http://www.bioinformatics.babraham.ac.uk/projects/fastqc). Sequence adaptors were then removed using TrimGalore (https://www.bioinformatics.babraham.ac.uk/projects/trim_galore/). Sequence reads were aligned to the *Mus musculus* genome (GRCm38.p6), which was downloaded via Ensembl (Ensembl genome browser 93) using HISAT2.

After the alignment of sequencing reads, FeatureCount was used to count reads mapping to gene annotation files. The edgeR package was used to calculate the gene expression level and to analyse differentially expressed genes. False discovery rate (FDR) values were calculated using the Benjamini–Hochberg method using edgeR. The significant differential expression genes were selected based on FDR adjusted p-value (Q-value) < 0.05.

The Ingenuity Pathway Analysis (IPA) tool (Qiagen) was used to interpret RNAseq data (analysis performed by Stephanie Cumberworth). RNAseq data were imported into IPA, which included: the list of identified DEGs at a given timepoint and their associated Log2 fold change (Log2FC) in expression value and Q-value (adjusted p-value which takes into account false discovery rate). A core expression analysis was performed by IPA using information from the uploaded dataset using the following conditions: reference set used was the Ingenuity Knowledge Base (genes only), species was defined as *Mus musculus*, initial analyses were conducted with 'all' tissues and cell lines and where indicated disease and function pathway analyses were restricted to only include tissues and cell lines of the central nervous system. All other values in the expression analysis wizard were set as default. IPA was used to predict the top canonical signalling pathways, in addition to disease and function pathways affected during ZIKV infection of CNS co-cultures at 96 h p.i. using input RNAseq data.

## 2.9 Software

All figures were assembled using Inkscape software, unless stated otherwise. Where stated, some illustrations were created using BioRender. Graphs and statistical analyses were generated using GraphPad Prism version 6.07 for Windows, GraphPad Software, La Jolla California USA, www.graphpad.com. Geneious 7.0 (https://www.geneious.com) software was used to perform multiple sequence alignments and verify Sanger sequencing results.

# 3 Results chapter 1: Establishing methods for ZIKV investigations

## 3.1 Chapter specific acknowledgements

The author would like to thank the following for their contributions which enabled investigations within this chapter to take place.

Lindomar Pena and Rafael Freitas de Oliveira França (Fundação Oswaldo Cruz-PE) for the initial isolation of the ZIKV strain PE243 used in this thesis and providing the Kohl group with this virus.

Benjamin Brennan (MRC University of Glasgow Centre for Virus Research) for the preparation of master ZIKV PE243 stocks.

Claire Donald (MRC University of Glasgow Centre for Virus Research) for establishing routine protocols for ZIKV propagation and titration.

Jennifer Barrie and Verena Schultz (University of Glasgow) for the preparation of CNS and PNS co-cultures.

## 3.2 Introduction

Upon commencement of this thesis, limited studies of ZIKV had been undertaken. Information such as propagation and detection methods, complete genome sequence information (with complete UTRs) and cellular tropism were not established and ill-defined.

### 3.2.1 Host cell species origin in the study of arboviruses

Following the 2015 ZIKV outbreak there was a rapid increase in the number of publications pertaining to ZIKV. As ZIKV study was in its infancy such investigations lacked methodical continuity. This made comparing investigative findings increasingly difficult. A range of virus propagation techniques were used to generate ZIKV stocks, including passage in a variety of mammalian and invertebrate cell lines. Depending on the nature of downstream experimentation, inappropriate virus propagation techniques may result in artefactual findings.

Arboviruses, such as ZIKV, replicate in both their mammalian and invertebrate hosts. In the case of mosquito-borne viruses like ZIKV, the mosquito ingests the virus when taking a blood meal. The ingested virus must then infect cells of the mosquito midgut, replicate and disseminate throughout the mosquito, eventually reaching the salivary glands where it can then be transmitted through salivary secretions when the mosquito next takes a blood meal.

Progeny virions adopt the membrane and protein glycosylation patterns of its host cell. Early studies of insect and mammalian glycosylation noted the heterogeneity of carbohydrate moieties which adorn DENV (Hsieh and Robbins, 1984, Johnson et al., 1994). More recent studies of DENV originating from either mosquito or mammalian cells reveal that the E protein of progeny virions are differentially glycosylated dependent upon its host cell (Lei et al., 2015). The E protein of DENV originating from mosquito cells possesses high mannose type, complex type and fucosylated and sialylated N-glycans (Lei et al., 2015); high mannose type is the dominant moiety. Whereas in mammalian cells, it has been reported that complex type N-glycan is the dominant moiety, with some high mannose and hybrid structures detected (Lei et al., 2015).

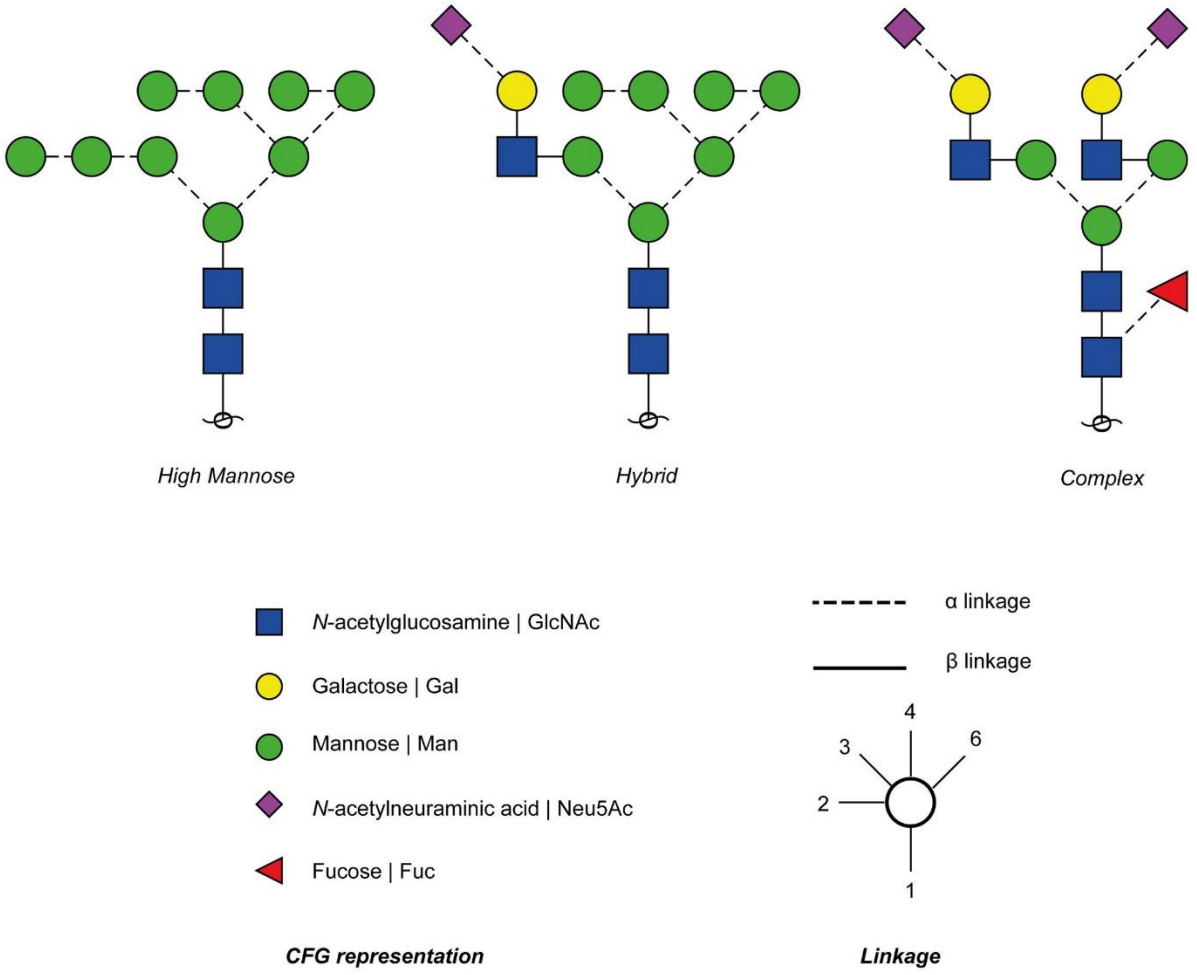


**Figure 3–1 N-linked glycan structures**
Examples of high mannose, hybrid and complex N-linked glycans. The dominant moiety in insect cells is high mannose-type N-linked glycans, whereas in mammalian cells complex-type moieties are dominant. Different carbohydrate structures are represented by coloured symbols, the direction of the connecting line indicates the position of the linkage between the backbones of differing carbohydrate molecules. Dashed lines indicate α glycosidic bonds, and solid lines indicate β glycosidic bonds.

If one were to investigate arbovirus interactions with cells present at a bite-site, invertebrate propagated virus stocks would be appropriate, as this represents virus transmission from invertebrate to mammal. However, in principle, studies involving cells/tissue matter not implicated at the bite-site should adopt mammalian propagated virus stocks, as the virus in nature would have undergone several rounds of replication in mammalian host tissue during dissemination.

In the case of ZIKV investigations, some researchers have adopted invertebrate propagated virus stocks to study ZIKV interactions with the central and peripheral nervous system. Glycosylation of the *Flavivirus* envelope protein has been shown to affect virus entry, egress and pathogenicity (Shirato et al., 2004, Lee et al., 2010, Alen et al., 2012). In the interest of artefact prevention, it would seem prudent to study whether host cell species origin influences ZIKV infection.

### 3.2.2 Protein interactions with 3'UTR-derived sfRNA

Flaviviruses, including ZIKV, produce a highly structured, non-coding RNA product called sfRNA which is derived from the 3' untranslated region (3'UTR) (Slonchak and Khromykh, 2018, Göertz et al., 2018). As detailed in Section 1.1.14, numerous candidate interaction partners have been identified for the 3'UTR of a range of flaviviruses, as summarised elsewhere (Roby et al., 2014). These candidates have varying roles in cellular translation, RNA processing and stability, and immune modulation. To date, only one protein, Musashi 1(MSI1), has been identified as an interaction partner with the ZIKV 3'UTR (Chavali et al., 2017).

MSI1 is a neural RNA binding protein implicated in the self-renewal of stem cells (Fox et al., 2015, Sakakibara et al., 1996). In the study by Chavali *et al* (2017), three consensus MSI binding sites were identified in stem loop structures within the ZIKV PE243 3'UTR, two of which were conserved in African lineage ZIKV strain, MR766. A combination of RNA pulldowns and UV cross-linking immunoprecipitation (CLIP) assays demonstrated that MSI1 but not MSI2 binds the ZIKV 3'UTR. Immunofluorescence analyses using confocal and super resolution microscopy illustrate that MSI1 co-localises with double stranded RNA (dsRNA; a replicative intermediate of positive sense virus replication) in ZIKV infected cells. Furthermore, infection of MSI1 KO cells resulted in a marked reduction of viral load in comparison to control cells. Additionally, a 'dose dependent' effect was observed between expression levels of MSI1 and the amount of viral RNA in infected cells Together these findings suggest an interaction between MSI1 and ZIKV, which is in part mediated by the ZIKV 3'UTR.

The sfRNA of DENV is produced in excess of genomic RNA during infection. It would therefore be interesting to have a robust understanding of the range of proteins that the 3'UTR RNA can interact with within the host cell, using ZIKV as a model virus.

### 3.2.3 Chapter Aims

- Characterise commercially available antibodies using western blot and immunofluorescence techniques

- Identify biologically relevant cells and to study ZIKV infection in the central nervous system

- Develop methods to study ZIKV 3' UTR interactions with host proteins

- Determine if the species of cell line used to propagate ZIKV influences viral fitness

## 3.3 Tools for ZIKV study

### 3.3.1 Testing methods of molecular detection

At the time of this investigation, there were limited tools available for the study of ZIKV. A repertoire of uncharacterised anti-ZIKV antibodies which targeted either the envelope or NS1 protein were obtained from Aalto Bio Reagents Ltd (Table 3–1 and Table 3–2). To assess the suitability of these antibodies, each was employed in the detection of ZIKV by western blot and immunofluorescence analysis. Vero E6 cells were infected with ZIKV at a MOI of 3.0 PFU/cell. After 48 h p.i., cells were either fixed with 4% formaldehyde for immunofluorescence study, or cell lysates were harvested for western blot analysis. A starting antibody concentration of 10 µg/ mL was used to probe immunofluorescence coverslips and western blot membranes (Table 3–2).

| Antigen | Product code | Clone number | Chosen Ab name | Ig subclass | (ug/ml) |
|---|---|---|---|---|---|
| Zika envelope protein | AZ1176 | 0302156 | E_1 | IgG1κ | 5555.556 |
| Zika envelope protein | AZ1176 | 0402166 | E_2 | IgG1κ | 3846.154 |
| Zika envelope protein | AZ1176 | 0502176 | E_3 | IgG1κ | 10000 |
| | | | | | |
| Zika NS1 protein | AZ1225 | 2701106 | NS1_1 | IgG1κ | 2000 |
| Zika NS1 protein | AZ1225 | 2801116 | NS1_2 | IgG1κ | 2500 |
| Zika NS1 protein | AZ1225 | 2901126 | NS1_3 | IgG1κ | 3571.429 |
| Zika NS1 protein | AZ1225 | 0102136 | NS1_4 | IgG2a | 1515.152 |
| Zika NS1 protein | AZ1225 | 0202146 | NS1_5 | IgG1κ | 5000 |

**Table 3–1 Details of uncharacterised ZIKV antibodies targeting the envelope or NS1 protein (Aalto Bio Reagents).**

| z | | Estimated ratio of Ab:buffer | |
|---|---|---|---|
| Ab Name | Clone No. | 10 ug/mL | 100 ug/mL |
| E_1 | 0302156 | 1:600 | 1:60 |
| E_2 | 0402166 | 1:400 | 1:40 |
| E_3 | 0502176 | 1:1000 | 1:100 |
| | | | |
| NS1_1 | 2701106 | 1:200 | 1:20 |
| NS1_2 | 2801116 | 1:250 | 1:25 |
| NS1_3 | 2901126 | 1:350 | 1:35 |
| NS1_4 | 0102136 | 1:150 | 1:15 |
| NS1_5 | 0202146 | 1:500 | 1:50 |

**Table 3–2 Table of estimated antibody:buffer ratios used for each antibody testing when used at a concentration of either 10 µg/mL or 100 µg/mL**

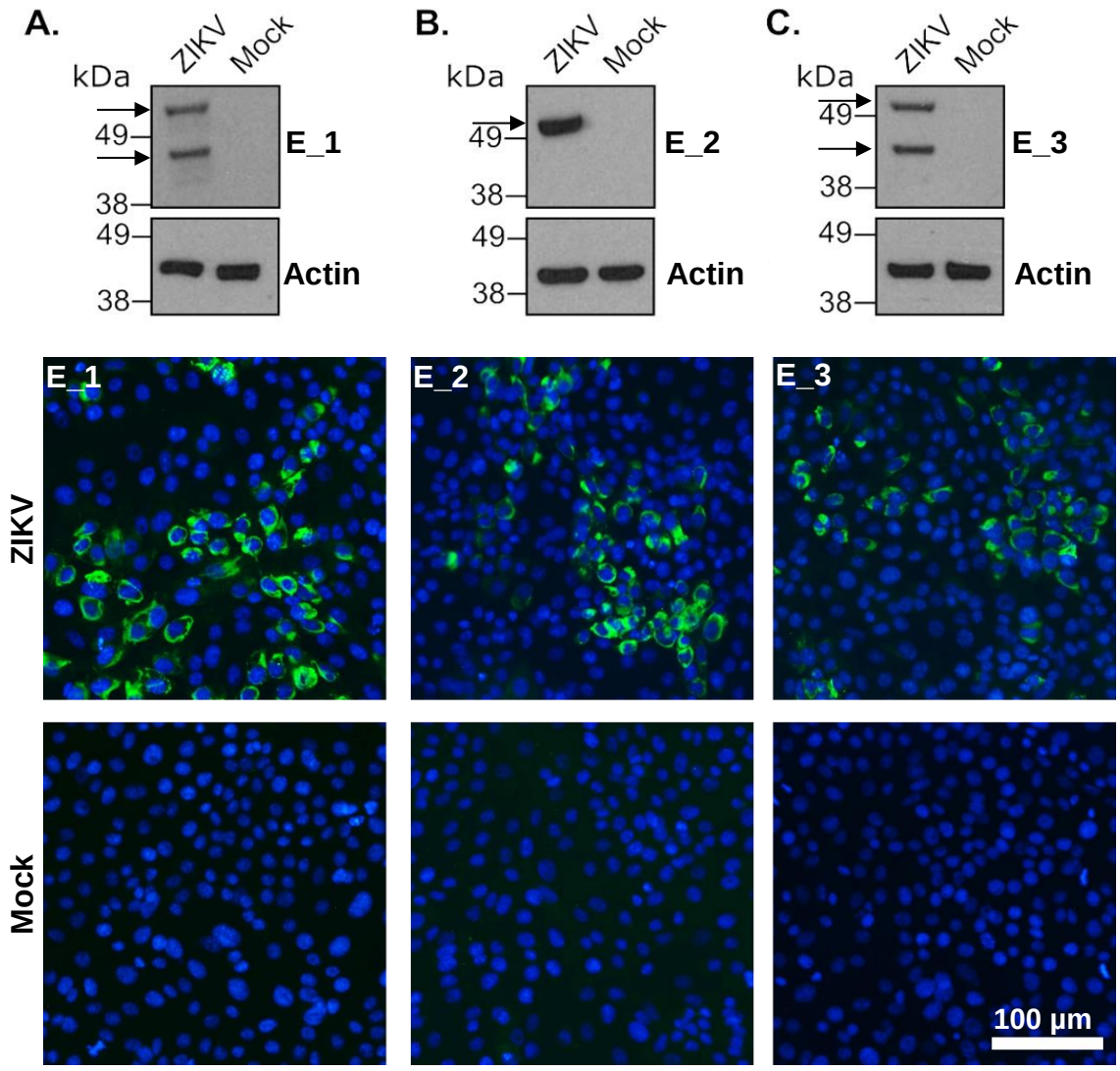


**Figure 3–2 Testing uncharacterised commercially available antibodies targeting the ZIKV envelope protein (ZIKV E) by western blot and immunofluorescence analysis.**
(**A-C**) Vero E6 cells were infected with ZIKV at a MOI of 1 PFU/cell. Cell lysates were harvested at 48 h p.i. and subjected to western blot analysis. Membranes were probed with one of three antibodies targeting the ZIKV E protein (E_1, E_2 or E_3; mouse anti-ZIKV E protein).The membrane was also probed with an antibody raised against actin (rabbit anti- α-actin), which was used as a loading control. Secondary antibodies raised against mouse or rabbit IgG, conjugated to horseradish peroxidase, and ECL substrate were used to visualise protein bands on X-ray film. Arrows indicate positive ZIKV staining. (**D**) Vero E6 cells were infected with ZIKV at a MOI of 1 PFU/cell and fixed at 48 h p.i. with 4% formaldehyde. Cells were reacted with one of three antibodies targeting the ZIKV E protein (mouse- anti ZIKV-E primary antibodies E_1, E_2 or E_3), followed by incubation with goat anti-mouse Alexa Fluor ® 488 secondary antibody. Nuclei were counterstained with DAPI. Cells were visualised using an EVOS Fl fluorescent microscope using the 20x objective. ZIKV E can be seen in green, and nuclei in blue.

All the anti-ZIKV envelope (ZIKV E) antibodies tested gave a specific signal for infected material compared to mock when tested by western blot and immunofluorescence analysis (Figure 3–2). In immunofluorescence images (Figure 3–2B), the detected signal showed cytoplasmic, perinuclear distribution; as envelope protein is synthesised by the virus in the endoplasmic reticulum of infected cells, this staining pattern is consistent with envelope protein localisation during infection.

By western blot analysis, in addition to a discreet band ~50 kDa in size (corresponding with the ZIKV E protein estimated size of ~52 kDa, predicted by ProtParam, ExPASY based upon sequence information based upon ZIKV PE243), the membranes probed with antibodies E_1 and E_3 displayed a second band ~45 kDa in size (Figure 3–2A).

The anti-NS1 antibodies also demonstrated specificity when used in immunofluorescence analysis, generating a signal only in infected cells (Figure 3–3). The signal for NS1 was diffuse in the cytoplasm. The NS1_3 antibody had some non-specific speckles appearing both in the infected and uninfected samples. However, the presence of these speckles is more likely reflective of an insufficient washing protocol following the staining with a fluorescently labelled secondary antibody for this specific sample.

Testing the anti-NS1 antibodies by western blot did yield some non-specific signals in mock infected lanes; this band was most prominent in membranes probed by NS1_1,2 and 5 antibodies. This band appeared in the mock infected lysate lane and is ~55 kDa in size. In the ZIKV infected lysate lane, all of the membranes displayed multiple bands; bands typically appeared ~62 kDa, ~55 kDa and <49 kDa (Figure 3–3, indicated by red arrows). The appearance of multiple signals in ZIKV lysate (and non-specific binding in mock infected lysate) was least prominent in the membrane probed with 10 µg/mL NS1_3.

The flavivirus NS1 protein is between 41-55 kDa in its monomeric state; NS1 proteins are post-translationally modified by glycosylation. Perhaps the range of signals detected by membranes probed by the anti-NS1 antibodies reflect the range of glycosylated NS1 proteins present in infected cells. To test this theory, lysate samples could be incubated with an enzyme to remove N-linked glycans,

such as PNGase F. These samples could be assayed by western blot probing the membrane with an antibody targeting NS1, alongside a sample which has been untreated; if a singular band appears in the enzyme treated sample and multiple appear in the untreated sample – it can be assumed that the multiple forms represent alternatively glycosylated forms.

Owing to the lack of clarity when probing Western blot membranes with antibodies targeting NS1 (i.e. multiple band staining pattern), it was decided that such antibodies not be employed in the detection of ZIKV infection *in vitro*. Given the specificity of the envelope protein antibody E_2 by western blot and immunofluorescence analysis, this will be the chosen antibody for ZIKV detection in downstream analysis and shall simply be referred to herein as α-ZIKV-E.

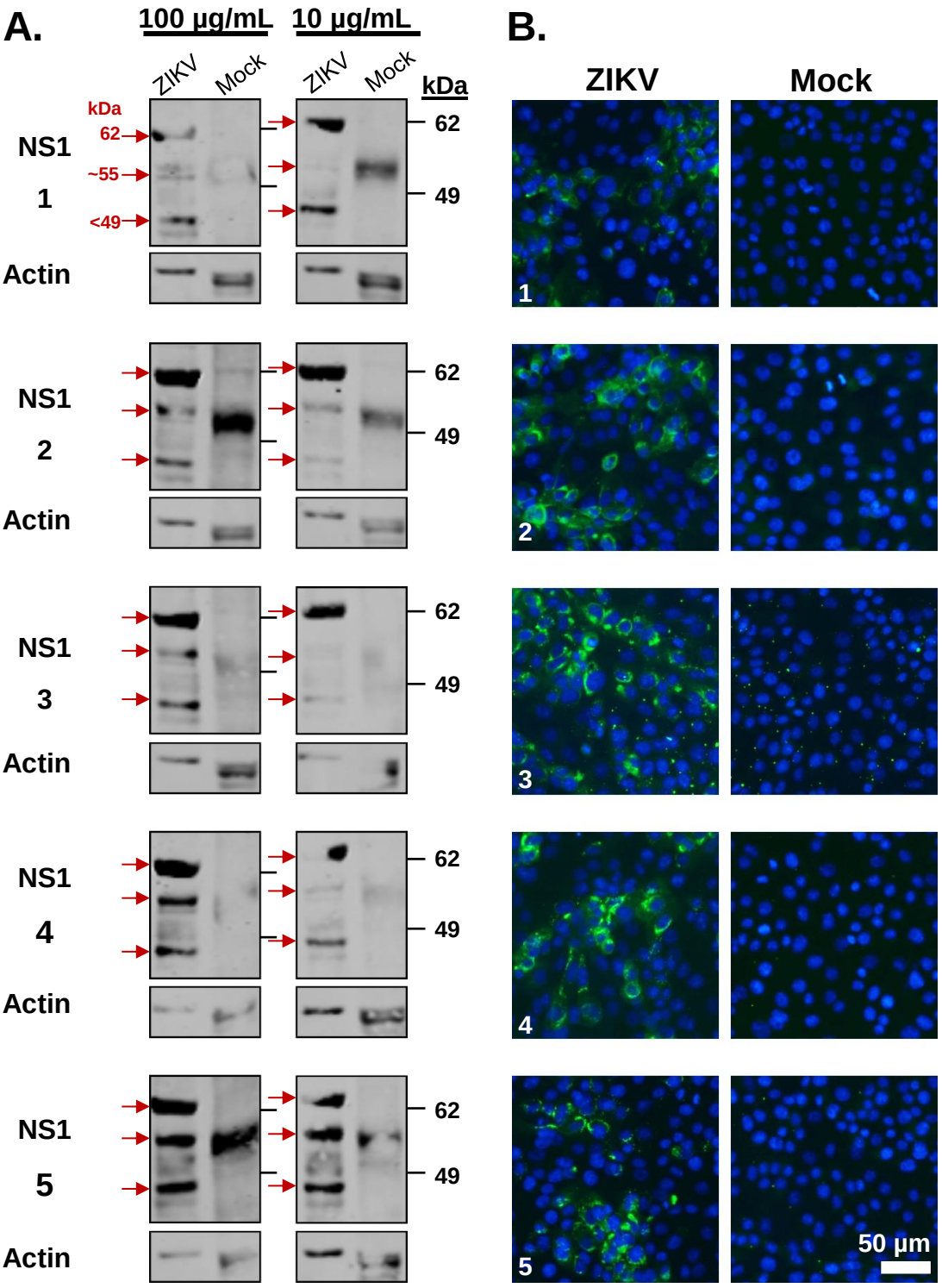


**Figure 3–3 Testing uncharacterised commercially available antibodies targeting the ZIKV NS1 protein by western blot and immunofluorescence analysis**

Each row corresponds to a different antibody clone which targets the ZIKV NS1 protein, labelled 1-5. (**A**) Vero E6 cells were infected with ZIKV at a of MOI 1 PFU/cell. Cell lysates were harvested at 48 h p.i. and subjected to western blot analysis. Membranes were probed with one of five antibodies targeting the ZIKV NS1 protein (mouse anti-ZIKV NS1 protein).The membrane was also probed with rabbit anti- α-actin antibodies, which was used as a loading control. Secondary antibodies raised against mouse or rabbit IgG, conjugated to horseradish peroxidase, and ECL substrate were used to visualise protein bands on X-ray film. Red arrows indicate bands of interest. (**B**) Vero E6 cells were infected with ZIKV at a MOI of 1 PFU/cell and fixed at 48 h p.i. with 4% formaldehyde. Cells were immunolabelled with one of five antibodies (10 µg/mL) targeting the ZIKV NS1 protein (mouse-anti NS1 primary antibody), followed by incubation with goat anti-mouse Alexa Fluor ® 488 secondary antibody. Nuclei were counterstained with DAPI. Cells were visualised using an EVOS Fl fluorescent microscope (20x objective). ZIKV NS1 protein can be seen in green, and nuclei in blue.

## 3.3.2 Establishing neural cellular systems for ZIKV study

One of the original intentions of this thesis was to conduct a transcriptomic analysis of ZIKV infection in a biologically relevant, CNS cell line at an 'early' and 'late' infectious timepoint. The aim of this approach was to decipher if the development of neurological complications could possibly be attributed to alterations in gene expression levels. Chapter 5 discusses an investigation by transcriptomics. Herein are some preliminary studies which were performed in order to try and assess the suitability of astrocyte cells for downstream investigations.

Astrocytes are a highly prevalent cell type within the brain which exhibit diverse functionality including (but not limited to) blood-brain barrier function, CNS homeostasis and synapse formation (Miller, 2018). Astrocytes can be infected by other neurotropic flaviviruses such as Japanese encephalitis virus (JEV) and dengue virus (DENV). Upon infection, astrocytes become activated and a potent type I IFN response is elicited (van Marle et al., 2007, Lee et al., 2016, Lindqvist et al., 2016). Given that astrocytes are susceptible to infection with other related viruses, and may contribute to neurologic disease outcomes in JEV patients, they may represent an interesting cell type for the study of ZIKV infection (German et al., 2006).

### 3.3.2.1 Establishing SVGp12 seeding densities

The astrocytic cell line SVGp12 (ATCC® CRL-8621™) is an immortal cell line derived from first trimester foetal brain tissue, as such it was selected as a candidate cell line for downstream experimentation. SVGp12 cells were new to the laboratory and required basic characterisation, including determining appropriate seeding densities, prior to experiments.

Initially SVGp12 cells were seeded into 6 well tissue culture plates at either 0.5, 1.0, 1.5 or 2.0 x $10^5$ cells/mL. The cells were maintained at 37 °C overnight and observed the following day, in addition to 48 hours post-seeding (Figure 3–4). At one day post-seeding, wells containing 0.5 x $10^5$ cells/mL were sparsely populated. Morphologically the cells appeared needle-like, which may be an indicator of ill health. At day 2 post-seeding, these cells displayed a marginal

increase in count, and still appeared spindle-like, indicating this density is too low for experiments. Wells seeded at a density of 2.0 x $10^5$ cells/mL were almost confluent one day post-seeding and were overcrowded at day two. Wells seeded at 1.5 x $10^5$ cells/mL were neither too sparse or dense at day one, yet densely populated at day two. Given that during infection of mammalian cells, ZIKV causes cytopathic effect by 48 h p.i., the seeding density of 1.5 x $10^5$ cells/mL seems dense enough to withstand infection, without becoming too sparse or overcrowding. Therefore, 1.5 x $10^5$ cells/mL was chosen as the appropriate seeding density for infection studies.

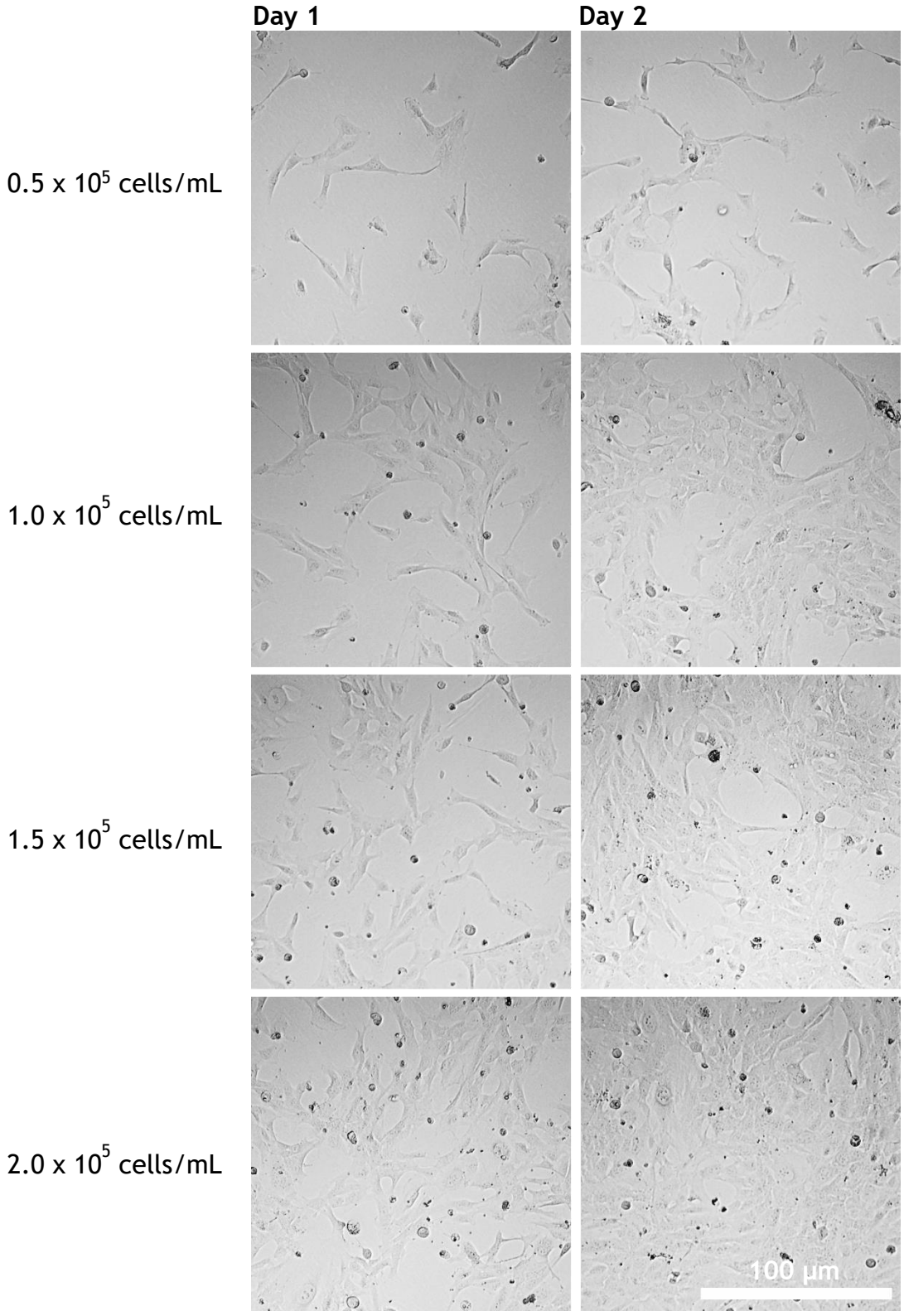


**Figure 3–4 Seeding density test of SVGp12 cells in 6 well tissue culture plate**
The concentration of a homogenous cell suspension of SVGp12 cells was determined using a haemocytometer. The suspension was diluted in culture media to produce varying defined concentrations of SVGp12 cells. The cells were seeded into 6 well tissue culture plates and incubated overnight at 37 °C, after which they were imaged using an EVOS Fl microscope on the transmitted light setting using the 20x objective (day 1). Cells were maintained at 37 °C and imaged once more after a further 24 hours (day 2).

#### 3.3.2.2 **Infection of SVGp12 cells**

SVGp12 cells were infected with ZIKV at two different MOIs, a low MOI (0.5 PFU/cell) and a high MOI (5 PFU/cell), to increase the likelihood of establishing infection. Cell lysates were harvested at 24, 48 and 72 h p.i. and were subjected to analysis by western blot, using an α-ZIKV E antibody to detect infection (Figure 3–5A). ZIKV E could be detected at all timepoints in infected cell lysates pertaining to both MOI 0.5 and MOI 5, indicating SVGp12 cells are susceptible to infection with ZIKV. The 24 h p.i./MOI 0.5 lysate sample showed a faint band in comparison to the others, indicating that infection has progressed to a lesser degree than at other timepoints. By increasing the initial viral input to a MOI of 5 PFU/cell, the band intensity at 24 h p.i. too increases.

The positive control (lysate from Vero E6 cells infected with ZIKV at a MOI of 3 PFU/cell) was faint at the band corresponding to ZIKV ~50 kDa but has two stronger bands both <17 kDa in size. As this lysate sample had previously been freeze-thawed, this may represent degraded ZIKV E protein. Furthermore, the actin bands for this sample was weaker in comparison to other timepoints; similarly, infected lysate (both MOI 0.5 and MOI 5) display weaker actin staining.

In addition to western blot analysis, SVGp12 infected cells were fixed at 48 h p.i. and processed for immunofluorescence analysis. Cells were probed again with α-ZIKV E and nuclei were counterstained with DAPI (Figure 3–5B). The nuclei of ZIKV infected cells at both MOI 0.5 and MOI 5 displayed morphological changes. Cells infected with ZIKV at MOI 0.5 have misshapen nuclei, some of which appeared to be blebbing and/or sickling. Whereas at MOI 5, cell nuclei appeared much more sickled in appearance. This is in contrast with mock infected samples whereby nuclei appeared healthy in nature (oval/kidney shaped [reniform] and absent of condensed chromatin in non-dividing cells).

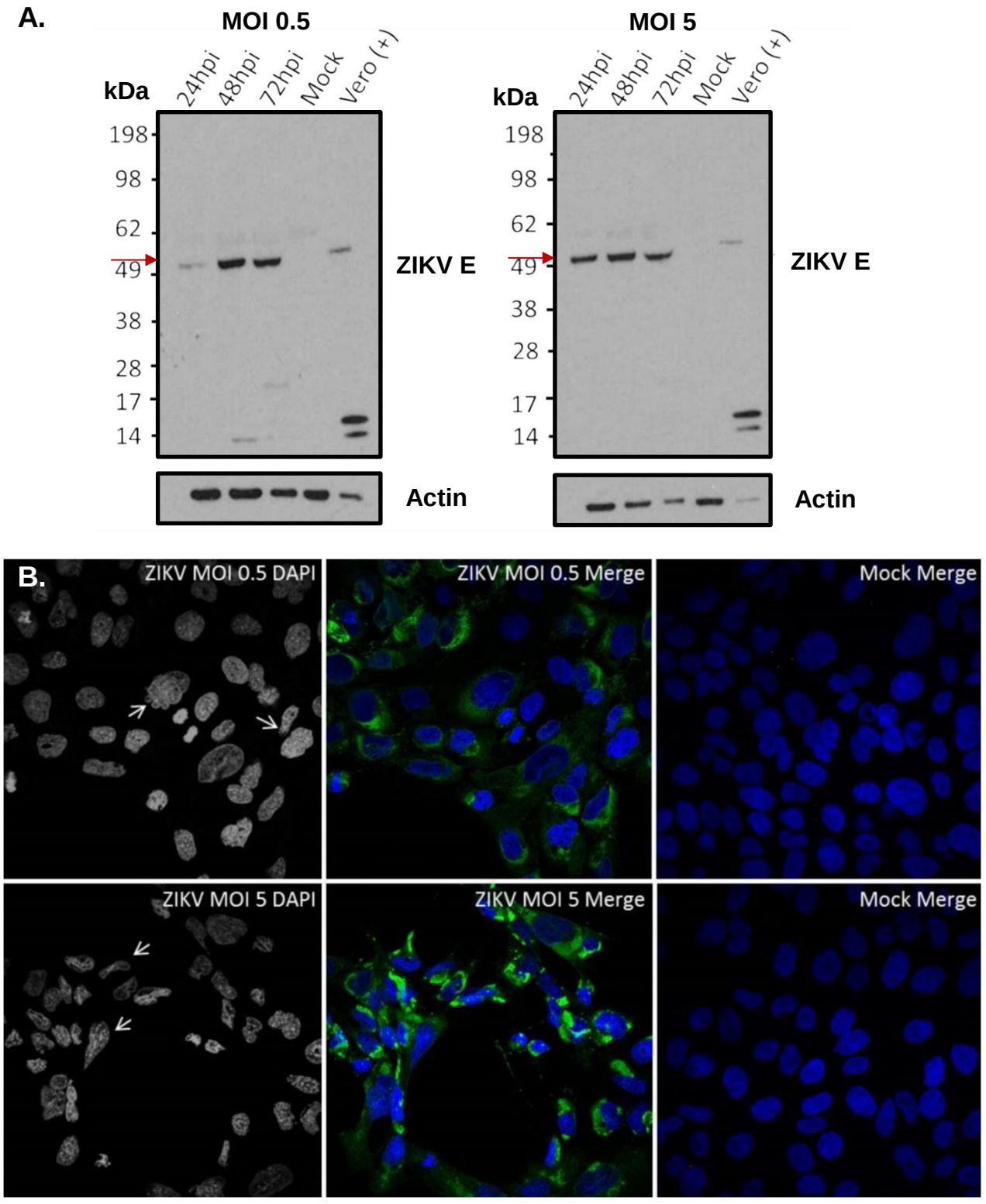


**Figure 3–5 SVGp12 cells can be infected with the ZIKV**
(**A**) SVGp12 cells were infected with ZIKV at either a MOI 0.5 or 5 PFU/cell. At 24, 48 and 72 h p.i., cell lysates were harvested and subjected to analysis by western blot to detect the expression of the ZIKV envelope protein (ZIKV E [E_2]; indicated by red arrow). (**B**) SVp12 cells were infected with ZIKV with a MOI 0.5 or 5 PFU/cell. At 48 h p.i. cells were fixed in 4% formaldehyde for one hour prior to immunolabelling with an antibody targeting ZIKV E (green). Nuclei were counterstained with DAPI. Representative images from 2 biological replicates with 2 coverslips per condition, per replicate. Images were taken using a Zeiss LSM 710 confocal microscope using the 50x objective (with oil immersion).

#### 3.3.2.3 GFAP expression in SVGp12 cells

Upon further characterisation of this cells line it was apparent that SVGp12 cells do not express the astrocytic marker glial fibrillary acidic protein (GFAP) (Figure 3–6), as tested by western blot and immunofluorescence analysis. GFAP is an intermediate filament expressed in astrocytes; GFAP expression is used as a differential marker of astrocytes from other glial cell types present in the central nervous system (Eng et al., 2000). The lack of GFAP expression in SVGp12 cells may indicate that the expression of other proteins may be altered in this cell line, raising the question of their relevance as a cell type for investigation by transcriptomics. It was therefore concluded that alternative cells be sought out for further investigation.

#### 3.3.2.4 GFAP expression in primary Normal Human Astrocytes (NHA)

The next cell line to be investigated were primary human astrocyte cells – normal human astrocytes (NHA; Lonza). As determined by western blot and immunofluorescence analysis, these cells do express the astrocytic marker GFAP (Figure 3–6). The calculated molecular weight of GFAP as determined using the ProtParam tool (ExPASY) is ~49.9 kDa. The antibody used to probe the western blot membrane was a polyclonal antibody (Rabbit anti-GFAP; Agilent, Dako). The GFAP positive band on the western blot which pertains to NHA cell lysate appears at ~40 kDa, with less prominent smear staining ranging between 38-49 kDa. Whereas lysate from a mixed cell co-culture of central nervous system origin displays a discrete band ~49 kDa surrounded by a faint smear, with further faint discrete bands appearing at ~38 and ~40 kDa. The range in observed estimated molecular weights between NHA and CNS co-culture cells may be attributed to the fact that several isoforms of GFAP exist. The predominant splice form in CNS white matter is GFAP-α; CNS co-cultures are derived from murine spinal cord tissue (white matter) (Eng et al., 2000). Therefore, the discrete band ~50 kDa in CNS co-culture lysate may represent the GFAP-α isoform and the smear in NHA lysate representative of alternative isoforms. Both mouse and human GFAP has an estimated molecular weight of ~49.9 kDa. However, species-specific differences in splice variant expression may contribute to the differed staining patterns by western blot (Eng et al., 2000, Kamphuis et al., 2012).

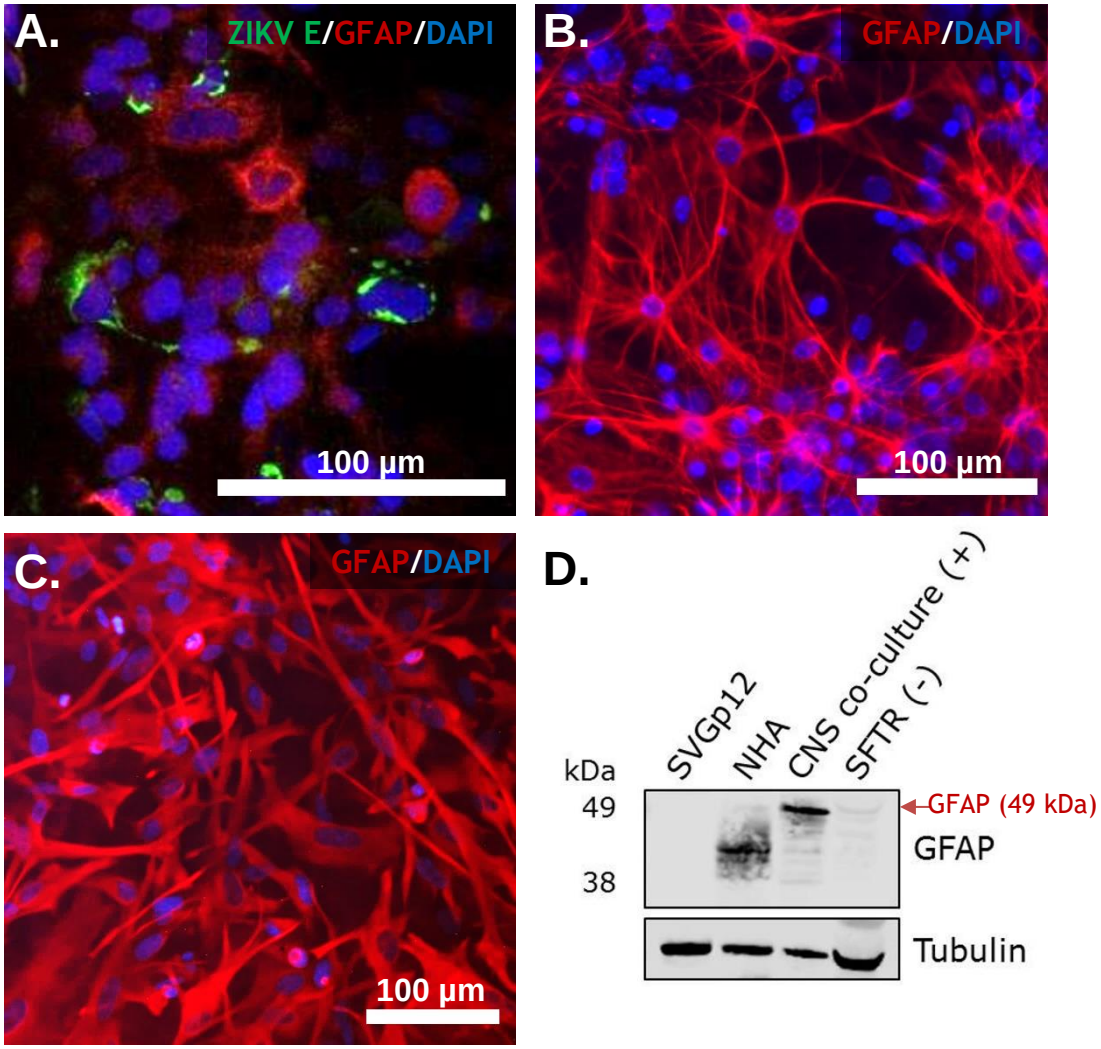


**Figure 3–6 The astrocytic cell line SVGp12 does has limited expression of the astrocyte marker glial fibrillary acidic protein (GFAP).**
Cell lines (**A**) SVGp12, (**B**) murine central nervous system co-cultures or (**C**) Primary human astrocyte cells, normal human astrocytes (NHA) were plated onto cover slips. (**A**) Cells were infected at a MOI of 5 PFU/cell for 24 h p.i (**B&C**) cells were uninfected. Samples were fixed in 4% formaldehyde and slides assayed for GFAP (Red) or ZIKV E (Green) and Nuclei were counterstained with DAPI (Blue). (**D**) Western blot testing for the expression of GFAP in cell cultures. SFTR cells are a cell line derived from sheep foetal thymus and were used as a negative control for GFAP expression.

### 3.3.2.5 **ZIKV infection in NHA cells**

As NHA cells were deemed GFAP positive, these cells were subsequently used in infection studies. Firstly, NHA cells were infected with ZIKV at a MOI of 0.1 PFU/cell; cell culture supernatant and cellular lysates were harvested at 5, 10, 24, 48 and 72 h p.i. Western blot analysis of NHA lysate probing for the expression of ZIKV E indicates that NHA cells are susceptible to ZIKV infection (Figure 3–7A). ZIKV E expression was detected from 48 h p.i onwards. Plaque assays were performed using the cell lysate to determine if infection was productive i.e. results in the creation of infectious progeny virions (Figure 3–7B). No virus replication was detected at 10 h p.i. with a 1-log increase detected by 24 h p.i. At 48 h p.i. the virus titre 1.3 x$10^4$ PFU/ml. At 72 h p.i. the virus titre started to plateau at around 6 x$10^4$ PFU/ml. The limit of detection by western blot when probing for expression of E appeared to be $10^4$ PFU/mL (the virus titre at 48 h.p.i). These data indicate that ZIKV can establish a productive infection in NHA cells.

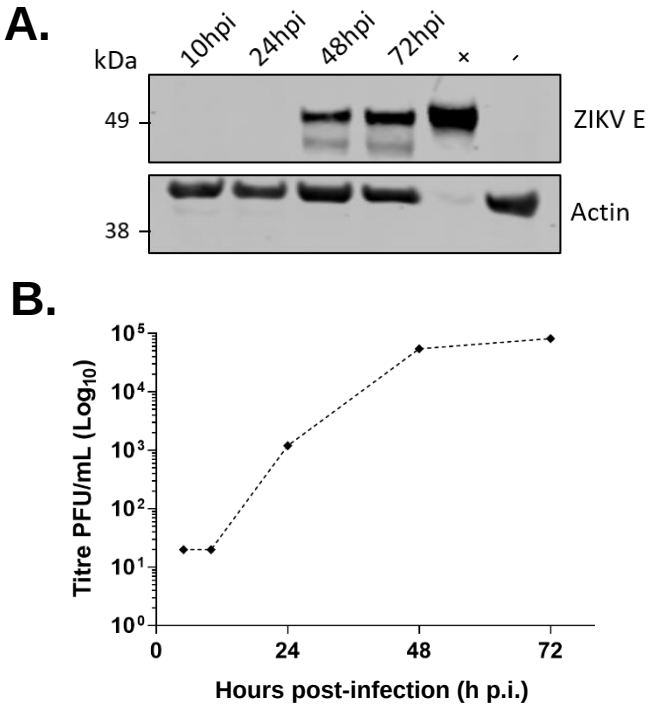


**Figure 3–7 ZIKV can establish infection in primary normal human astrocytes (NHAs)**
NHA cells were infected with ZIKV using a MOI of 0.1 PFU/cell. At 5, 10, 24, 48 and 72 h p.i., cell culture supernatants were harvested and lysates of cell monolayers prepared. (**A**) Cell lysates were subjected to western blot analysis to test for the expression of the ZIKV envelope protein (ZIKV E; E_2). The membrane was also probed with an antibody raised against actin (rabbit anti- α-actin), which was used as a loading control. Secondary antibodies raised against mouse or rabbit IgG, conjugated to horseradish peroxidase, and ECL substrate were used to visualise protein bands on X-ray film (**B**) The infectious titres of cell culture supernatants were determined by plaque assay to produce a virus growth curve, n= 1.

As it was now established that ZIKV could infect NHA cells (Figure 3–7), the appropriate MOI and timepoints needed to be determined for transcriptomic analysis. The initial aim for transcriptomics experiments was to compare gene expression profiles of ‘early’ and ‘late’ infectious timepoints. For transcriptomics experiments it is ideal to have as many cells infected as possible. Therefore, to determine which MOI was appropriate to achieve this at an ‘early’ timepoint, immunofluorescence analyses were performed. As ZIKV E expression occured late in the virus infectious replicative cycle and failed to be detected by western blot at 10 h p.i. and 24 h p.i. (Figure 3–7), it was decided that an antibody targeting double stranded RNA (dsRNA; a replicative intermediate of virus infection) would be used to detect infection levels. NHA cells were infected at a MOI of either 3 or 5 PFU/cell and fixed with 4% formaldehyde at 10 and 24 h p.i. and immunostained with antibodies against dsRNA and GFAP (Figure 3–8). At 10 h p.i., detection of dsRNA was achieved only in cells infected at a MOI of 5 PFU/cell (Figure 3–8C inset image). However, at 24 h p.i. dsRNA was detected in cells infected at a MOI of 3 PFU/cell, as well as in cells infected at a MOI of 5 PFU/cell (Figure 3–8B/C).

At 24 h p.i. the morphology of the NHA cells had changed from larger cell bodies reminiscent of fibroblasts into cells with condensed GFAP, giving the appearance of smaller cell bodies, with long, thin projections emanating from the cell body (compare Figure 3–8A with Figure 3–8B/C). The morphology change was most striking in cells infected at a MOI of 5 PFU/cell. Furthermore cells infected at a MOI of 5 PFU/cell did not display these morphological changes at 12 h p.i., indicating this may be a viral load dependent effect (compare Figure 3–8B with 1-7C and 1-7C with inset image). However, this experiment could only be performed once owing to culturing difficulties and further study would be required to confirm this finding. Owing to cell culturing difficulties such as failure to obtain high cell counts within the recommended passage timeframe (NHA cells were guaranteed for 10 population doublings per manufacturer guidelines; Lonza), NHA cells were therefore disregarded for future studies.

Fortunately, a collaboration opportunity arose with neuroimmunology researchers at the University of Glasgow capable of culturing murine mixed cell, central and peripheral nervous system cultures (CNS and PNS respectively). Use

of these CNS and PNS cultures to model cell-cell interactions was well established within this research group, and could be tailored to reflect different developmental stages of human neural development (Thomson et al., 2006, Thomson et al., 2008). Furthermore, these cultures had also been used to study Semliki Forest virus interactions in the CNS (Unpublished, Dr Clive McKimmie, University of Leeds & Dr Julia Edgar, University of Glasgow). Therefore, the culture system seemed ideal to study ZIKV interactions within the CNS and PNS, and all future investigations were performed using these cells. More in depth introduction to these culture systems can be found in Chapter 4, Section 4.2.2.

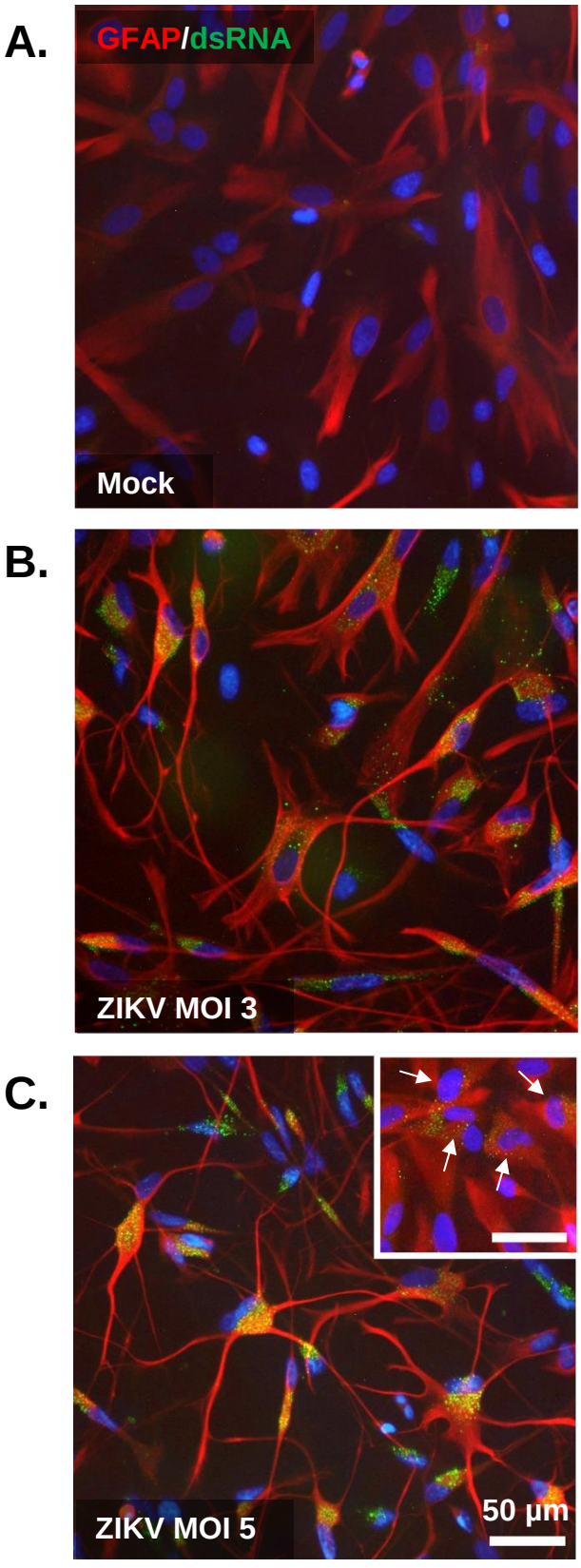


**Figure 3–8 Detection of ZIKV infection in NHA cells at early time points using double stranded RNA (dsRNA) as a marker of infection**

NHA cells were either mock infected (**A**) or infected with ZIKV at a MOI of either 3 (**B**) or 5 (**C**) PFU/cell. At 24 h p.i., cell monolayers were fixed with formaldehyde and immunolabelled for GFAP (red; goat anti-rabbit IgG Alexa Fluor ® 594 secondary antibody), dsRNA ( green; goat anti-mouse IgG Alexa Fluor ® 488) and DAPI (blue). The inset image in C displays NHA cells infected at a MOI of 5 PFU/cell fixed with formaldehyde at 10 h p.i., arrows indicate cells with positive staining for dsRNA. Images were taken using an EVOS Fl microscope using the 20x objective. Images are representative of 2 coverslips for one biological replicate. Scale bar: 50 µm.

### 3.3.3 ZIKV 3' UTR: protein interactions

Given the capacity of the 3'UTR of related flaviviruses to interact with a range of host proteins, these candidate interaction partners may also function in the ZIKV life cycle. The only protein known to interact with the 3'UTR of ZIKV is MSI1. This was identified through a target study which primarily identified putative binding sites prior to downstream experimental studies which did not involve proteomic analysis (Chavali et al., 2017). It was therefore my aim to build upon this RNA pulldown protocol and develop methodology to conduct a proteomic study to assess a breadth of potential interaction partners of the ZIKV PE243 3'UTR.

#### 3.3.3.1 **Absolute quantitation of ZIKV genomic- and sfRNA by qPCR**

It has previously been found that DENV sfRNA is produced in higher amounts during infection in comparison to genomic RNA (gRNA) (Bidet et al., 2014). To quantify the amount of ZIKV sfRNA versus gRNA produced during infection, an infection time course was conducted to assay the levels of gRNA and sfRNA produced during infection by differential RT-qPCR. This protocol is based upon a previously described assay used to quantify DENV sfRNA (Bidet et al., 2014). The determination of a growth curve for sfRNA production was to inform timepoints for any downstream analyses. Briefly, forward qPCR primers were designed to specifically amplify regions of the ZIKV genome which pertained to either only the genome, or a region found in both the genome and the sfRNA (schematic representation can be found in Figure 3–9A). The same reverse primer was used for both reactions. The molar amounts of gRNA and gRNA+sfRNA were determined using the standard curve method (Figure 3–9B). By subtracting the molar amount of gRNA from the gRNA+sfRNA, the molar amount of sfRNA could be inferred.

A549 cells were infected with ZIKV at a MOI of 0.1 PFU/mL. Cell culture supernatant and total cellular RNA was harvested at 8, 10, 24, 48 and 72 h.p.i. After extraction, total cellular RNA was reverse transcribed into cDNA and analysed by qPCR to determine the amount of gRNA and sfRNA. The results from the qPCR indicated that sfRNA was produced in excess of genomic RNA by 1 log (Figure 3–9C). At 24 hours post infection, the amount of genomic RNA increased

substantially, indicating that genome replication was active at this timepoint. However, the exponential phase of genome production appeared to plateau at 48 h p.i.

By comparing this data to a growth curve obtained by viral plaque assay, a comparison between genome replication (as determined by qPCR data) and virus release (plaque assay) was performed (Figure 3–9C). In comparison to the growth curve, at 24 h p.i. virus replication exceeded that of virus release, whereby the inverse occured after 48 h p.i. Therefore, the 48 h p.i. timepoint was too late a timepoint to capture the profile of infected cells undergoing virus genome replication.

These data will inform the time point required to harvest infected cellular lysate to be used in a pulldown assay; this pulldown assay will employ ZIKV 3'UTR RNA as bait to explore 3'UTR-protein interactions. The intention to use infected cell lysate to perform the pulldown assay is two-fold. Firstly, the proteomic profile of the host cell alters during infection, and secondly, because prior studies indicate that the 3'UTR of flaviviruses can interact with viral proteins. Therefore, by using infected cell lysate the proteome is relevant to infection, in addition to being able to determine if any interactions occur with viral proteins.

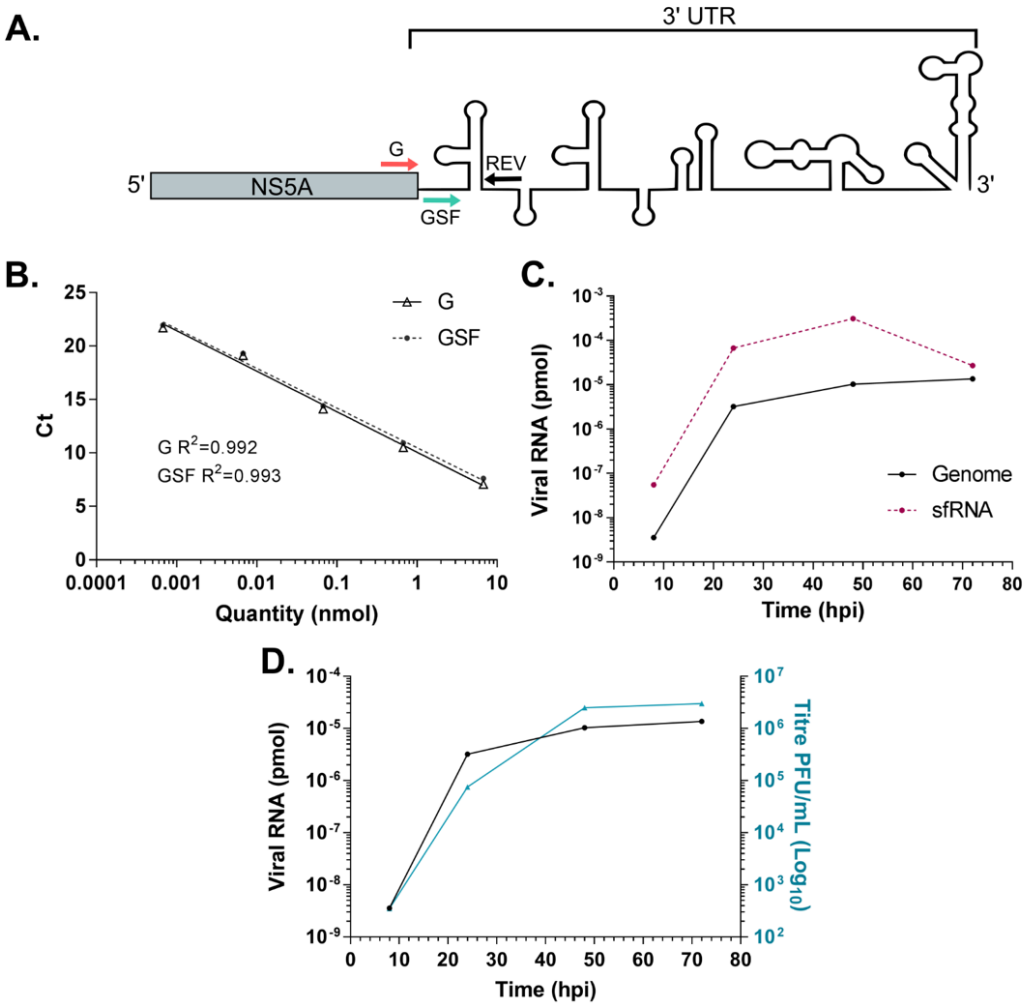


**Figure 3–9 Quantification of ZIKV gRNA and sfRNA**

(**A**) Schematic representation the NS5/3UTR region of the ZIKV genome which is amplified during the differential qPCR reaction for the absolute quantification of ZIKV sfRNA and gRNA. The red arrow (labelled G) indicates the position of the forward primer. G specifically amplifies a region in the NS5 coding region, therefore will only be found in genomic RNA. The blue arrow (labelled GSF) indicates the position of the forward primer which is used to amplify a region of RNA which can be found both in genomic RNA and sfRNA. By subtracting the molar amount of product amplified (G) from the molar amount of products amplified from GSF; the molar amount of sfRNA can be determined (n(GSF)-n(G)=n(SF). (**B**) The standard curve generated from qPCR of serial 10-fold dilutions of PCR products amplified from the pCCI-SP6-ZIKV* WT plasmid using the G/REV primers. (**C**) A growth curve of the production of sfRNA and genomic RNA generated from differential qPCR data. (**D**) A direct comparison of virus titre determined by plaque assay and gRNA production determined by qPCR of total cell RNA. Both sets of data were obtained from the same growth curve to allow direct comparisons to be made n=1.

#### 3.3.3.2 **Production of biotinylated ZIKV 3'UTR RNA**

To elucidate potential 3'UTR:protein interactions, a pulldown assay was developed based upon a previously described protocol (Chavali et al., 2017). Briefly, the 3'UTR of ZIKV PE243 was cloned from the plasmid pCCl-SP6-ZIKV* WT (donated from Prof A. Merits, University of Tartu; contains 5' and 3' UTRs from ZIKV PE243) using a primer which inserted the SP6 promoter directly upstream of the 3'UTR start position (Figure 3–10). 3'UTR RNA was produced by *in vitro* transcription using the SP6 polymerase (Figure 3–10). Initially, exhaustive efforts were made to end label ZIKV 3'UTR RNA with desthiobiotin using the Pierce™ Magnetic RNA-Protein Pull-Down Kit (Thermo Fisher Scientific). After numerous attempts to optimise this protocol, this direction was no longer pursued. Instead, biotinylated UTP was incorporated into ZIKV 3'UTR RNA during *in vitro* transcription as per (Chavali et al., 2017) (Figure 3–10). Figure 3–10 demonstrates the successful production of RNA in addition to incorporation of biotinylated UTP, visible by the slightly higher position on the gel relative to the unlabelled equivalent.

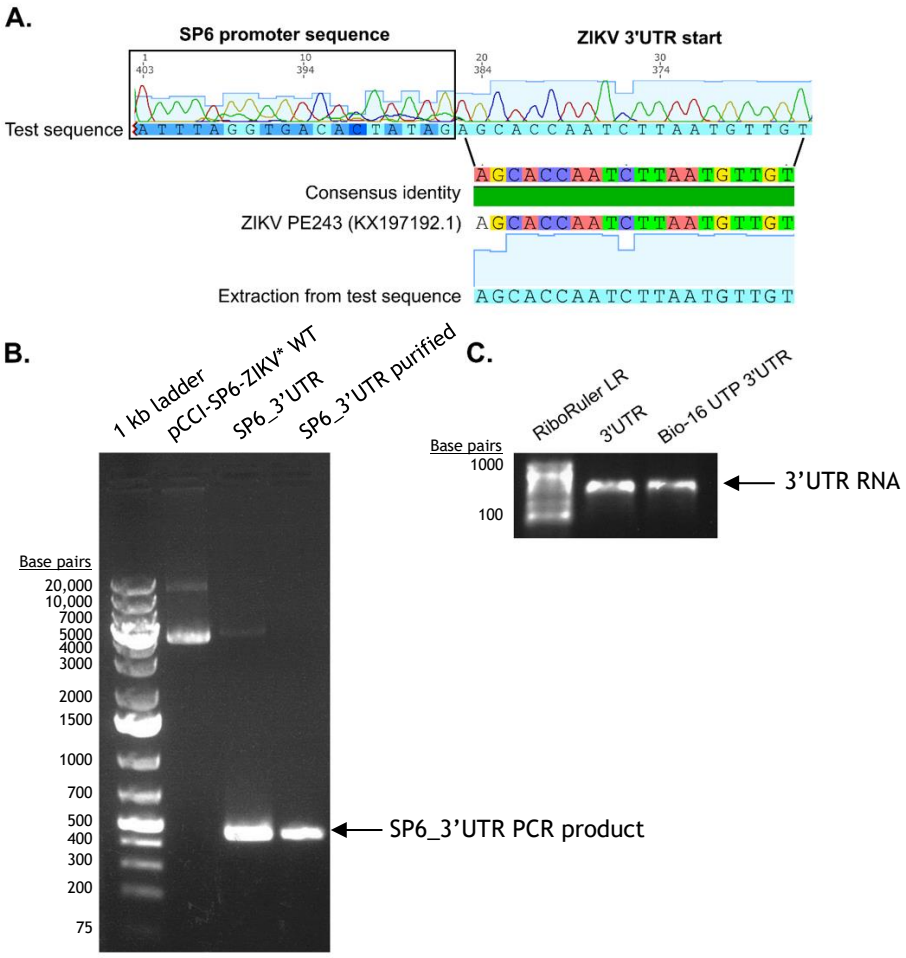


**Figure 3–10 Generation of biotinylated 3'UTR ZIKV RNA**
The ZIKV 3'UTR was cloned from the plasmid pCCI-SP6-ZIKV* WT (donated from Prof A. Merits, University of Tartu; contains 5' and 3' UTRs from ZIKV PE243), using a primer pair which inserted the SP6 promoter sequence immediately upstream of the 3'UTR start site. (**A**) Sanger sequencing demonstrating the successful insertion of the SP6 promoter sequence upstream of the ZIKV 3'UTR start site. (**B**) Agarose gel electrophoresis of template plasmid and subsequent products of cloning SP6-3'UTR. Lane 1: GeneRuler 1kb Plus DNA ladder. Lane 2: Template plasmid pCCI-SP6-ZIKV* WT. Lane 3: 3'UTR-SP6 product after insertion of SP6 site upstream of 3'UTR Lane 4: Products from lane 2 underwent a second round of amplification by PCR was subsequently purified by ethanol precipitation. (**C**). Agarose-formaldehyde gel of ZIKV 3'UTR RNA *in vitro* transcribed from SP6 promoter either in the absence or presence of biotinylated UTP (lanes 2 and 3 respectively). Lane 1: RiboRuler LR, RNA ladder. Lane 2: 3'UTR RNA. Lane 3: Bio-16 UTP 3'UTR RNA.

#### 3.3.3.3 **3'UTR RNA pulldown**

Two T250 flasks of A549 cells were infected with ZIKV at a MOI of 2 PFU/cell; cells were lysed at 24 h p.i and protein lysate pooled. ZIKV 3'UTR RNA was incubated with lysate at 4 °C. After 2 hours, 50 µL of MyOne Dynabeads conjugated with streptavidin were added to the RNA:protein mixture and incubated for a further 1 hour at 4 °C. RNA:protein complexes were then precipitated using a magnetic rack, washed and analysed staining for total protein composition (Figure 3–11A) and western blot for MSI1 (Figure 3–11B).

The total protein composition of both lysate and RNA:protein:bead complexes were analysed by SDS-PAGE followed by staining with sypro orange (Figure 3–11A). Whilst no visible differences appeared between lysates which had been incubated with or without 3'UTR RNA, the bead bound samples demonstrated some visible differences of protein composition as determined by protein molecular weight and density (indicated by * in Figure 3–11). These visible differences suggest that the pulldown assay functioned.

To further validate if the assay functioned, these samples were analysed by western blot, whereby membranes were probed using the Musashi-1 (MSI1) antibody as a positive control for the pulldown (Figure 3–11). MSI1 is an RNA binding protein which can be found in a range of tissues, predominantly the brain and testis (Fagerberg et al., 2014); expression of MSI1 has also been detected in lungs, which is the origin of A549 cells used in these experiments. The interaction of ZIKV 3'UTR and MSI1 has previously been described (Chavali et al., 2017). Briefly, MSI1 binding sites were identified in the secondary structure of the 3'UTR of ZIKV PE243, and the protein interaction was confirmed using a similar method, with minor changes in RNA concentration used (20pmol) and lysate samples (uninfected human glioblastoma cell line U251) (Chavali et al., 2017). Unfortunately, Figure 3–11 demonstrates that the 3'UTR was unable to pulldown MSI1, at least to sufficient quantities to be detected by Western blot.

As determined by qPCR (section 823.3.3.1), sfRNA was expressed in higher quantities than genomic RNA during infection by almost 1-log difference (Figure 3–9C). The excess of sfRNA produced during infection could be acting as a molecular sponge, sequestering endogenous MSI1 and therefore preventing

efficient pull down in this assay. To determine if this was a possibility, the pulldown assay was performed in tandem with uninfected A549 lysate. However, the staining pattern was the same for both infected and uninfected bead bound lysate samples (Figure 3–11B).

An extremely faint staining the equivalent size of MSI1 was present in both infected and uninfected bead bound protein samples, which may be a positive band. The assay would require further optimisation to determine if this is the case. Consequently, this line of investigation was no longer pursued.

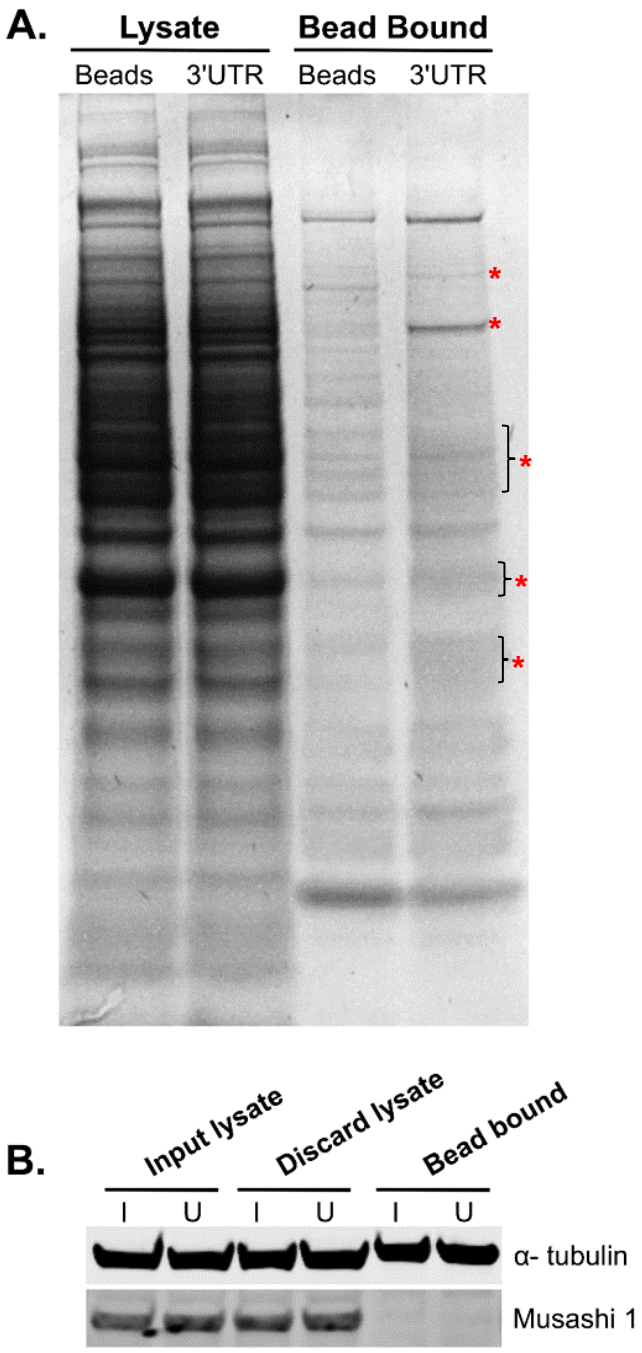


**Figure 3–11 ZIKV 3'UTR RNA pulldown**
Cell lysate was harvested at 24 h.p.i from A549 cells that had been infected with ZIKV at a MOI of 2 PFU/cell. The cell lysate was incubated either with ZIKV 3'UTR or alone for 2 hours at 4 °C, then with 50 µL of MyOne Dynabeads conjugated with streptavidin for a further hour. RNA:protein:bead complexes were precipitated using a magnetic rack, washed and subjected to SDS-PAGE. (**A**) The SDS-PAGE gel was stained using sypro orange to visualise the total protein composition of samples. Lysate: indicates samples of protein lysate taken after precipitation of RNA:protein:bead complexes. Bead bound: indicates samples which were precipitated using MyOne Dynabeads. Beads: indicates samples incubated only with MyOne Dynabeads. 3'UTR: indicates samples incubated first with ZIKV 3'UTR RNA, then MyOne Dynabeads. (**B**) Lysates from both infected (I) and uninfected (U) cell lysate was used in the pulldown protocol and were run on an SDS-PAGE gel. The proteins were transferred from the SDS-PAGE gel by western blot, and the subsequent membrane probed with antibodies against α-tubulin (loading control), and Musashi-1 (positive control for the pulldown). In this instance labelled 3'UTR did not pull down Musashi 1. α-tubulin was used as a loading control for the lysate samples but also appears to bind MyOne Stepvavidin beads. Input lysate: indicates lysate pre-incubation with or without RNA. Discard lysate: indicates lysate post-precipitation.

### 3.3.4 Assessing importance of cellular origin in ZIKV infection

To investigate the replicative capabilities of insect versus mammalian derived ZIKV, the strain PE243 was propagated in either mammalian-derived A549 Npro cells or mosquito-derived C6/36 cells. The A549 Npro cell line are a subclone of A549 cells which are derived from human lung epithelial tissue – the Npro sub clone expresses the bovine viral diarrhoeal N protein to render the type I IFN system ineffective; thus, making it a suitable cell line for viral propagation. The invertebrate cell line C6/36 is derived from *Aedes albopictus*, a commonly used cell line in ZIKV propagation. Virus was produced using the same elite stock of ZIKV, generating progeny virus of the same passage number and strain, the only difference being the propagation cell line. The resultant viruses are herein referred to as PE243 A549 Npro, and PE243 C6/36.

Firstly, a plaque assay was performed to assess the plaque phenotype produced by PE243 A549 Npro and PE243 C6/36 viruses (Figure 3–12). There were no remarkable differences in the sizes of plaques produced between PE243 A549 Npro and PE243 C6/36 produced viruses.

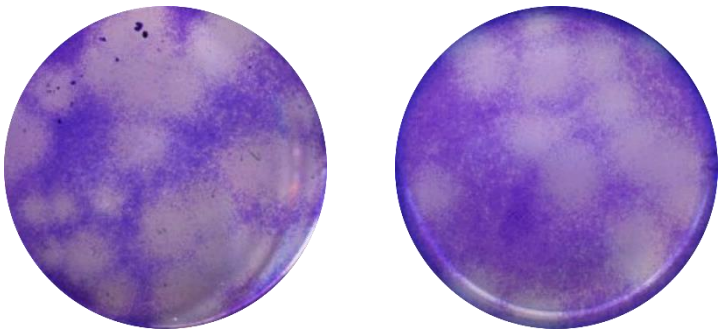


**Figure 3–12 Size comparison of plaques produced in A549 monolayer from PE243 A549 Npro and PE243 C6/36 viruses.**
Serial dilutions of PE243 A549 Npro and PE243 C6/36 viruses were made in 2% FBS/PBS. The serial dilutions were used to infect monolayers of A549 cells for 1 hour prior to removal of infection media and replacement with 2x MEM 4% FBS diluted 1:1 with 1.2% Avicel. At 5 days post infection, the cell monolayers were fixed in 8% formaldehyde for 1 hour prior to staining with toluidine blue.

PE243 A549 Npro and PE243 C6/36, in addition to MR766 (propagated in A549 Npro cells), were then used to infect central and peripheral nervous system (CNS and PNS respectively) mixed-cell co-cultures either WT or KO for the IFN α/β receptor (*Ifnar1*). CNS and PNS co-cultures are derived from embryonic day 13 mouse spinal cord (CNS) or dorsal root ganglion (PNS), and possess all the major cell types of their respective nervous system (generated by Verena Schultz and Jennifer Barrie; detailed further in Section 4.2.2). Cultures were infected with the respective virus at a MOI of 1 PFU/cell. Cell culture supernatant was harvested, and total cellular RNA was extracted at 24 and 72 h p.i. Infectious virus in the cell culture supernatant was determined by plaque assay. Plaque assay data can be found in the right-hand column of Figure 3–13. Total cellular RNA was reverse transcribed and subjected to analysis by qPCR using primer pairs specific to ZIKV. Primer pairs specific for the house keeping gene glyceraldehyde 3-phosphate dehydrogenase (GAPDH), were used as an internal control. The relative gene expression values for ZIKV RNA were determined using the $2^{-\Delta\Delta}C_T$ method. Gene expression values are relative to an uninfected control sample, and data can be found in the left-hand column of Figure 3–13.

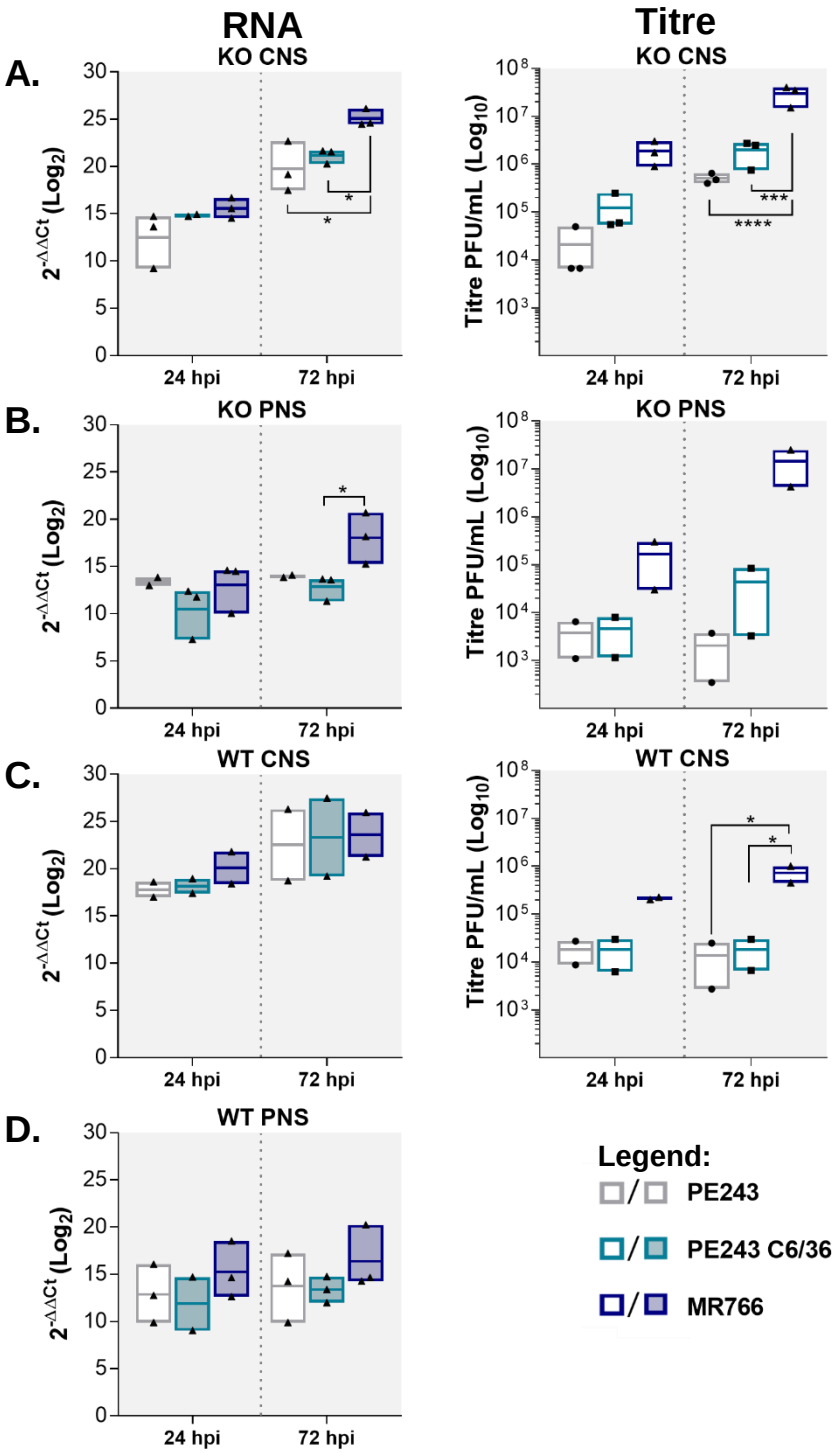


**Figure 3–13 Quantitative comparison of virus replication and production of different ZIKV strains as determined by relative qPCR and virus titration**

*Ifnar1* WT and KO CNS and PNS co-cultures were infected with ZIKV PE243 produced in either mammalian or invertebrate cells (PE243 A549 Npro, PE243 C6/36 respectively) or ZIKV strain MR766 (produced in A549 Npro cells), at a MOI of 1 PFU/cell. At 24 and 72 h p.i., culture supernatant and total cell RNA samples were harvested. **A.** KO CNS, **B.** KO PNS CNS, **C.** WT CNS, **D.** WT PNS. **Left column:** Total cellular RNA underwent analysis by qPCR using a ZIKV specific primer set using a two-step qPCR protocol. A primer pair specific to GAPDH was used as an internal control. Relative gene expression values were determined using the $2^{-\Delta\Delta}C_T$ method. Gene expression values shown are relative to an uninfected control sample. Biological replicates: n=2 for KO PNS PE243 24 & 72 h p.i., KO CNS & WT PNS PE243 C6/36 24 h p.i., WT CNS all samples. All other samples n=3. **Right column:** Infectious virus titres in plaque forming units per mL (PFU/mL) was determined by viral plaque assay of cell culture supernatant harvested at 24 and 72 h p.i.. Virus titres were undetermined for WT PNS culture samples, as no plaques were produced. Biological replicates: WT PNS/CNS n=2, KO CNS n=3. Statistics: * p<0.05 ***p 0.0001, **** p<0.0001, determined by 2way ANOVA.

In all *Ifnar1* KO and WT CNS and PNS cultures, it appeared that MR766 consistently has high relative expression of ZIKV RNA and achieved higher titres compared to either PE243 or PE243 C6/36 at both 24 and 72 h p.i. All three ZIKV strains produced higher virus titres in KO CNS co-cultures compared with their WT CNS counterpart and KO PNS cultures (when right panels of Figure 3–13 A are compared with C/D).

In *Ifnar1* KO CNS cultures, all three ZIKV strains replicate and produce infectious virions as determined by qPCR and plaque assay, respectively (Figure 3–13A). MR766 displayed higher relative expression of ZIKV RNA and produced more infectious particles than either PE243 or PE243 C6/36 at both 24 and 72 h p.i. At 72 h p.i., the difference in relative expression levels and virus titres between MR766 and either PE243 sample reached statistical significance as determined by 2way ANOVA. MR766 produced titres almost 1.5-2 logs higher than PE243 at 24 and 74 h p.i., compared with 1 log increase between MR766 and PE243 C6/36 at 24 and 72 h p.i. PE243 C6/36 produced higher virus titres than PE243 at 24 and 72 h p.i. (Figure 3–13A). At 24 h p.i., the mean virus titre was just under 1 log higher in PE243 C6/36 compared to PE243. At 72 h p.i. the difference in mean virus titre was around ½ a log. Differences in titres between PE243 and PE243 C6/36 did not reach statistical significance. The difference in virus titres between PE243 samples was not reflected in the relative expression of ZIKV RNA. At both 24 and 72 h p.i., the relative expression of ZIKV RNA between PE243 and PE243 C6/36 was similar, though at 72 h p.i. the average RNA expression level was slightly higher in PE243 C6/36 than PE243.

MR766 achieved high titres in KO PNS cultures, with a demonstrable increase in titre between 24 h p.i. and 72 h p.i. (right panel, Figure 3–13B). In contrast, PE243 did not appear to increase virus titre between 24 h p.i. and 72 h p.i. in KO PNS cultures (right panel, Figure 3–13B). Furthermore, the relative gene expression of ZIKV RNA in PE243 infected PNS KO cultures did not change between 24 and 72 h p.i. (left panel, Figure 3–13B). On the other hand, the virus titre of PE243 C6/36 appeared to increase slightly between 24 and 72 h p.i. (right hand, Figure 3–13B). The relative expression of ZIKV RNA does not corroborate the increase in virus titre when KO PNS cultures are infected with PE243 C6/36; the qPCR data indicated that neither PE243 or PE243 C6/36

replicates in KO PNS co-cultures. A further replicate of titration data could help resolve this discrepancy.

In WT CNS cultures, the virus titre at 24 h p.i. and 72 h p.i. did not change for either PE243 or PE243 C6/36 (right panel, Figure 3–13C). The titre of MR766 increased by less than half a log in WT CNS co-cultures between 24 and 72 h p.i. The relative RNA expression levels suggest that ZIKV RNA levels increase between 24 and 72 h p.i. for all three ZIKV strains. However, the large variation in data should be noted and further replicates will be required.

Titration data could not be obtained for ZIKV infection of WT PNS co-cultures, as no visible plaques were produced. PE243 and PE243 C6/36 did not appear to replicate well in WT PNS co-cultures, as the relative ZIKV RNA expression levels did not change between 24 and 72 h p.i; whereas the relative ZIKV RNA expression levels increased slightly in MR766-infected WT PNS cultures. However, this difference is only marginal, and owing to the variation within the datasets, it may not reflect a genuine increase in viral RNA replication.

In summary, *Ifnar1* KO CNS and PNS cultures are more susceptible to ZIKV infection compared to their WT counterparts. MR766 consistently achieved higher infection levels in *Ifnar1* KO and WT CNS and PNS cultures than either PE243 or PE243 C6/36 viruses as determined by qPCR, with exception of WT PNS co-cultures in which none of the sampled viruses demonstrated significant increases in viral replication. PE243 produced in mosquito cells (PE243 C6/36) achieved slightly higher infection levels in KO CNS co-cultures in comparison to PE243 produced in mammalian cells (PE243).

## 3.4 Discussion

Upon the commencement of this thesis, relatively few reagents were available to study ZIKV infection, and standardised laboratory protocols were yet to be established. The primary aim of this chapter was to identify suitable reagents and methodology for studying aspects of ZIKV infection and identify areas of investigation.

### 3.4.1 Antibodies

A range of uncharacterised antibodies were obtained from Aalto Bio Reagents, targeting either ZIKV envelope or NS1. These were subsequently tested using western blot and immunofluorescence analyses (Section 3.3.1).

All the antibodies targeting ZIKV envelope were used successfully to detect ZIKV-positive infected samples, with no detectable non-specific binding ZIKV-negative samples (both western blot and immunofluorescence) (Figure 3–2). One of the E antibodies (clone number 0402166) produced a discrete, single band at the correct approximate size (~50 kDa; E = 52 kDa). However, the other two clones produced two bands ~50 kDa and ~45 kDa. ZIKV E possesses an N-linked glycosylation motif (N-X-S/T) at amino acid position 154 (Haddow et al., 2012); the two bands observed by western blot may be attributable to alternate glycosylation statuses of E present in lysate samples. Detection of E in fixed cells by immunofluorescence techniques demonstrate no cross-reactivity in mock infected cells (Figure 3–2).

Antibodies targeting NS1 yielded differing results (Figure 3–3). Detection of ZIKV infection by western blot did not result in a singular discrete band; most of the NS1 antibodies detected multiple bands approximately ~62 kDa, ~45 kDa and <49 kDa (*Flavivirus* NS1 = 46-55 kDa). NS1 undergoes various post-translation modifications during the *Flavivirus* life cycle, resulting in distinct functional properties (Pryor and Wright, 1994). The multiple bands detected by western blot could reflect the range of glycosylation patterns of NS1. In most of the membranes probed with NS1 antibodies, a band ~55 kDa was present in ZIKV-negative samples. A band of this size was also present in ZIKV-positive samples,

but to differing intensities. Whether this reflected inherent cross-reactivity of the antibodies, or a lack of optimisation, would require further investigation.

Detection of NS1 in ZIKV-infected cells by immunofluorescence demonstrated no-cross reactivity in mock infected cells (Figure 3–3). One clone, 2901126, had speckles present in the uninfected sample, however these speckles did not adhere to the staining characteristic of ZIKV-positive samples (perinuclear), nor did they appear to be specific to a cell. Therefore, this could reflect an inadequate washing procedure during the staining protocol and the signal may pertain to residual fluorescent secondary antibodies. A control experiment in which cells were incubated with secondary antibody alone would determine if inadequate washing procedures would result in the non-specific signal observed. This control experiment was not performed initially as the secondary antibody in use (goat anti-mouse IgG Alexa Fluor ® 488) had been used extensively within the Kohl laboratory in combination with the cells in question (Vero E6) without issues of non-specific binding.

Downstream detection of ZIKV infection by western blot and immunofluorescence techniques will be performed using antibodies targeting E, specifically clone 0402166, given the target specificity of this antibody. Throughout the remainder of this thesis, this antibody clone shall only be referred to as ZIKV E.

### 3.4.2 Cells

The cell lines Vero E6 and A549/A549 Npro, commonly used in the study of other viruses, have been used to propagate and study ZIKV within the Kohl laboratory (Donald et al., 2016). The emergent neurological symptoms associated with ZIKV infection during the 2015/16 outbreak prompted study in a more biologically relevant cell line or primary cells. Other studies have focused on the role of ZIKV-mediated depletion of neural progenitors using neurospheres and organoid models of the developing brain; such studies highlighted differing region specific progenitor cells as a target for infection and contribute towards microcephaly (Bayless et al., 2016, Dang et al., 2016, Garcez et al., 2016, Onorati et al., 2016, Li et al., 2016a). Another study highlighted human foetal microglia as target for ZIKV infection, and a source of inflammation (Lum et al., 2017).

However, not all foetal ZIKV infections result in microcephaly, and the long-term effects of 'asymptomatic' foetal ZIKV infection are yet to be observed. It is therefore prudent to explore ZIKV infection in other cell types within the brain to determine populations which may contribute towards ambiguous pathologies (i.e. those which may not present until later-life), identify cells in which persistent infection may be established, and identify cells which contribute neuroprotective roles in ZIKV infection.

Astrocytes are one of the most abundant cell types within the brain, contributing to numerous supportive CNS functions including: blood-brain barrier maintenance, CNS homeostasis, synaptic pruning and immunological regulation (Miller, 2018). Astrogliosis has been demonstrated during infection with other neurotropic flaviviruses such as TBEV, JEV and WNV (German et al., 2006, van Marle et al., 2007, Gelpi et al., 2005). Astrogliosis refers to reactive astrocytes undergoing morphological, and probable molecular changes in response to CNS insult (Sofroniew, 2014); the nature of the insult influences such changes. Furthermore, it has been demonstrated that despite initial infection with flaviviruses such as TBEV, astrocytes are refractory to virus-induced cell death (Lindqvist et al., 2016). Instead, astrocytes contribute to *Flavivirus* restriction within the CNS via fast-acting type-I IFN responses (Lindqvist et al., 2016). Therefore, astrocytes represent an interesting cell population to study ZIKV interactions.

In this chapter, it has been demonstrated that ZIKV can establish productive infection within the transformed cell line SVGp12 (Figure 3–5), in addition to primary human astrocytes (Figure 3–7 and Figure 3–8). Owing to various culturing issues such as lack of expression of the astrocytic cell marker GFAP SVGp12 cells, and incompatibility of plasticware with NHA cells (to grow high quantity of cells), both these cell types were deemed unfit to pursue further study. It was instead decided that mouse-derived multi-cell type co-cultures which model the CNS and PNS, generated by a collaborating laboratory, would be a better suited model (Thomson et al., 2006). The brain is a complex organ with numerous cell types, all interacting with one another – with the expression of certain genes being dependent on such interactions. Therefore, pursuing a transcriptomic study using these co-cultures may be more indicative of what is occurring

globally with CNS during ZIKV infection. Chapter 4 explores initial studies conducted with CNS and PNS co-cultures and the results of transcriptomic analyses in CNS co-cultures can be found in Chapter 5.

### 3.4.3 ZIKV 3'UTR pulldown

The focus of this chapter was to produce methods to study ZIKV-host interactions. Few interactions have been described between 3'UTR and host proteins. Therefore, the aim of this line of research was to establish methodology to pursue research to delineate ZIKV 3'UTR interactions with host proteins, with the potential to expand to other members of the *Flaviviridae* family. Initial qPCR data demonstrate that like DENV, ZIKV sfRNA is produced in higher quantities than genomic RNA during infection.

Despite exhaustive efforts to adapt the protocol described by Chavali et al., 2017 (Section 3.3.3), there was insufficient data to suggest the successful use of biotinylated ZIKV 3'UTR as bait in a pulldown assay in the studies carried out in this chapter (Figure 3–11). Therefore, further proteomic analyses were not pursued. Numerous factors may have influenced this result. For example, Musashi-1 expression in A549 cells could be lower than in the U-251 cells used in Chavali et al., 2017 – which may influence the 'control' for pulldown efficiency in this dataset. Furthermore, Chavali et al., 2017 use a predetermined quantity of protein lysate in the pulldown assay, whereas data in this thesis the total protein concentration has not been quantified; cell count was used as a measure in place of protein concentration. This may mean that the amount of cell lysate used in the pulldown may have been insufficient to detect Musashi-1 within the 'control' pulldown.

Secondary structure formation is critical for some sfRNA functionality, such as XRN1 resistance. Whilst efforts were made to relax and refold biotinylated bait 3'UTR RNA, perhaps the RNA remained improperly folded – failing to bind Musashi-1. Additionally, incorporation of biotinylated UTP itself may alter secondary structure formation and hence influence the binding capacity of the bait 3'UTR RNA. However, this method was employed by Chavali et al 2017 and therefore may not be an influential factor in this study.

### 3.4.4 ZIKV strain comparison

The 2015/16 ZIKV outbreak lead to a rapid increase in ZIKV studies being published. The lack of established and standardised protocols resulted in an increase in varying methodologies being employed to study ZIKV. The use of differing viral strains and propagation methods could lead to the generation of artefactual data. The key difference in propagation method was the species origin of the employed cell line; many used an insect derived cell-line (C6/36), and others a mammalian (typically Vero E6, some used A549/A549 Npro). The primary difference in ZIKV strain was studies which used MR766 as a model ZIKV MR766 has an extensive passage history and is of African lineage, not Asian-lineage (the lineage of contemporary ZIKV outbreak isolates). One of the aims of this chapter was to determine if any of these confounding factors influence viral replication (determined by qPCR) and production (determined by viral plaque assay).

These data (Figure 3–13) showed that ZIKV PE243 propagated in insect cells (C6/36) may afford some reproductive advantage over PE243 propagated in mammalian cells (A549 Npro) within *Ifnar1* KO CNS co-cultures. ZIKV PE243 C6/36 produced higher titres of virus compared with ZIKV PE243 Npro, though this did not reach statistical significance. However, when examined by qPCR, both viruses produced similar quantities of viral RNA. Furthermore, in KO and WT PNS and WT CNS co-cultures, there was no significant difference between either PE243 virus. Overall, these results suggest that the species used to propagate PE243 virus does not affect virus replication in WT CNS and WT and KO PNS co-cultures.

In contrast, it is clear from these data that using MR766 produces markedly increased levels of infection within both WT and KO CNS and PNS co-cultures compared to either PE243 virus (Figure 3–12). MR766 historically has undergone just under 150 passages in the brains of suckling mice, in addition to various cell culture passages (Haddow et al., 2012). Whether the differences observed between MR766 and PE243 is a result of adaptation to mammalian cells or more specifically murine cells, neuro-adaptation or lineage-specific adaptation is unknown.

It has recently come to light that multiple variations of MR766 are in laboratory use, which differ in sequence (Carbaugh et al., 2019). Some variations possess the N154 glycosylation site, others have a single amino acid mutation which ablates the glycosylation site or a 4 amino acid deletion removing the glycosylation site altogether. Absent of N154 glycosylation, MR766 infection is attenuated in mice (Carbaugh et al., 2019). Many African-lineage ZIKV isolates lack N154 glycosylation, whereas all Asian-lineage ZIKV strains possess the N154 glycosylation signal. The N153/N154 glycosylation sequence is conserved amongst flaviviruses, contributing to pathogenicity and neuro-invasive properties in WNV (Shirato et al., 2004, Beasley et al., 2005). Interestingly, the MR766 isolate used in these studies does not have an intact N154 glycosylation site (GenBank accession number: AY632535). Absent N154 glycosylation, it may be that host adaption is the main contributor to the increased fitness of MR766 compared with either PE243 virus. However, this virus has not been re-sequenced since its acquisition. It would be intriguing to determine whether the inclusion of N154 glycosylation would be further advantageous to MR766 replication within the CNS and PNS co-cultures to corroborate findings of Carbaugh et al., 2019 which state that N154 glycosylation mediates ZIKV pathogenesis.

## 3.5 Summary

- The anti-ZIKV envelope antibody clone 0402166 from Aalto Biosciences can be used successfully in western blot and immunofluorescence protocols to detect ZIKV infection.

- ZIKV readily infects astrocytes. However, owing to a combination of functional and technical issues neither the astrocyte cell line SVGp12 or NHA will be used in downstream analyses in this thesis.

- The species origin of cell lines used to propagate ZIKV PE243 did not significantly affect viral replication in Ifnar1 KO and WT CNS and PNS co-cultures.

- ZIKV MR766 (GenBank accession number: AY632535) has significantly increased replicative capacity compared with ZIKV PE243 (produced in either mammalian or insect cells) in both *Ifnar1* KO/WT CNS and *Ifnar1* PNS co-cultures.

- CNS and PNS co-cultures represent a biologically relevant, complex model to investigate ZIKV interactions in the nervous system. Further characterisation of ZIKV infection in these systems can be found in Results Chapter 2.

# 4 Results chapter 2: ZIKV infection of the central and peripheral nervous systems

## 4.1 Chapter specific acknowledgements

Work undertaken in this chapter was conducted as part of an ongoing collaboration with members of neuroimmunology research groups at the University of Glasgow (Edgar, Barnett, and Willison labs). The author would like to thank and recognise each of the following for their valued contributions to these investigations:

Jennifer Barrie: culture generation, aid in immunofluorescence staining, contribution of cell counts

Verena Schultz: culture generation, image capture for quantification, contribution of cell counts

Madeleine Cunningham: contribution of PNS cell counts

Julia Edgar: aid in data consolidation

Julia Edgar, Hugh Willison, Sue Barnet and Alain Kohl: aid in data interpretation and experimental design

With thanks to Chris Linington for invaluable contributions to discussions surrounding this work.

Declaration: All images and graphs presented in this chapter were produced by S. Cumberworth (SC) unless otherwise stated. SC performed all infection procedures within this chapter, and contributed towards immunofluorescence staining of cultures, image capture for quantification purposes and representative images by confocal microscopy, contributed cell counts and contributed to experimental design.

## 4.2 Introduction

### 4.2.1 ZIKV and nervous system disorders

The 2015/16 ZIKV epidemic in South and Central America was characterised by an unprecedented rise in neurological disease complications affecting the central and peripheral nervous systems (CNS and PNS respectively) (Campos et al., 2015, Zanluca et al., 2015). Prior to this outbreak, documented symptoms of ZIKV included fever, maculopapular rash, myalgia, headache and arthralgia - symptoms also consistent with co-circulating arboviruses, DENV and chikungunya virus, also endemic in regions of ZIKV transmission (SIMPSON, 1964, Filipe et al., 1973, Dupont-Rouzeyrol et al., 2015, Villamil-Gómez et al., 2016).

Retrospective analyses of the 2013 outbreak of ZIKV in French Polynesia linked ZIKV infection with the increased incidence of GBS; a complication that has also been associated with the 2015/16 outbreak (Cao-Lormeau et al., 2016, Oehler et al., 2014). GBS is an acute paralysing neuropathy caused by aberrant immune responses targeting peripheral nerves, typically following infection. In addition to ZIKV, other infectious agents associated with GBS include bacteria such as *Campylobacter jejuni*, *Mycoplasma pneumoniae* and *Haemophilus influenzae*, and viruses such as cytomegalovirus, Epstein Barr virus, influenza A virus (Jacobs et al., 1998, Mori et al., 2000). A spectrum of pathological phenotypes exist, which are primarily dependent on nerve component involvement (reviewed in (Willison et al., 2016)). 'Acute inflammatory demyelinating polyneuropathy' denotes GBS syndromes where immune-related injury involves Schwann cells and the myelin sheath (see section 4.2.2.2 for description of nervous system cell types). Whereas, 'acute motor axonal neuropathy' describes GBS syndromes where the target of autoimmune injury are axons themselves (Willison et al., 2016). GBS is primarily managed by the administration of intravenous immunoglobulins. The aetiology of ZIKV-associated GBS remains to be determined; whether ZIKV-GBS reflects a post-infectious immune disorder or a consequence of direct viral infection of the PNS is currently unknown.

Novel sequelae of ZIKV infection affecting the CNS were a serious concern during the 2015/16 outbreak; this included an expanding spectrum of neurodevelopmental disorders predominantly affecting the CNS of neonates - now termed 'congenital ZIKV syndrome'. (Mlakar et al., 2016, Schuler-Faccini et al., 2016, Melo et al., 2016, Moura da Silva et al., 2016). A notable developmental disorder that arose during the 2015/16 outbreak is microcephaly (Section 1.3.4). Microcephaly is characteristically associated with a reduction in head circumference which is below the third percentile for age and sex (Mlakar et al., 2016). Pathological findings of ZIKV-infected infants report further malformations including extensive cerebral calcifications, ventriculomegaly (enlarged ventricles [fluid filled spaces] in the brain) and arthrogryposis (congenital joint contracture) (Chimelli et al., 2017). The spectrum of neurological manifestations associated with congenital ZIKV infection are collectively known as congenital ZIKV syndrome (CZS). Auditory and ocular impairments, fine motor delay, behavioural abnormalities, below average cognitive performance and expressive language delays have also been associated with congenital ZIKV infection (de Paula Freitas et al., 2016, Leal et al., 2016, Muller and Mulkey, 2019).

At the time of study, the pathobiology underlying the neurological manifestations of ZIKV were poorly characterised, and a comprehensive understanding of the cellular tropism within CNS and PNS tissue were lacking. Efforts were made to try and determine ZIKV entry receptors, highlighting Axl – a cell surface receptor tyrosine kinase - as a potential candidate; the importance of this molecule in facilitating virus entry is still debated (Nowakowski et al., 2016, Hastings et al., 2017, Li et al., 2017, Wang et al., 2017, Ojha et al., 2019). Studies involving neurospheres, organoids and induced pluripotent stem cells were used to investigate the potential causes of microcephaly, demonstrating that neural progenitor cells and radial glia were susceptible to ZIKV infection (Qian et al., 2017). Numerous studies involving mouse models were used to study ZIKV mediated birth defects and neuropathogenesis, amongst other effects such as testicular infection (Cugola et al., 2016, Li et al., 2016a, Fernandes et al., 2017, Govero et al., 2016). Previous studies in one-day-old Webster Swiss, AG129 and new-born Swiss mice, suggested that neurons and astrocytes may be

susceptible to ZIKV infection (Fernandes et al., 2017, Bell et al., 1971, Aliota et al., 2016).

Despite these findings, at the time of experimentation for this thesis no attempt had been made to examine the relative vulnerability of all the principle cell types within the CNS. Furthermore, no investigation of ZIKV infection within the PNS had been conducted.

## 4.2.2 Overview of CNS and PNS co-cultures

### 4.2.2.1 Co-culture generation

CNS and PNS co-cultures were kindly generated by J Barrie and V Schultz for downstream experimentation documented within this chapter, using techniques adapted from previous work (Thomson et al., 2006, Thomson et al., 2008).

CNS cultures were generated from the spinal cords of *Ifnar1* knockout (KO) and wildtype (WT) embryonic day 13 (E13) mouse embryos. The *Ifnar1* gene encodes IFN α/β receptor subunit 1; mice homozygous negative (-/-) for *Ifnar1* are rendered unable to respond to exogenous type I IFNs (IFN α/β) and typically have an increased susceptibility to viral infection (Müller et al., 1994). Briefly, a homogenous cell suspension of spinal cord tissue was generated and plated on top of coverslips and maintained until day 28 *in vitro* (DIV28). DIV28 CNS co-cultures are reflective of more mature CNS systems such as that of the adult brain, as axons are extended and fully myelinated (see Figure 4–12 for a schematic overview of neural developmental processes). CNS co-culture development can be tailored to reflect different stages of the developing brain, as described in section 4.3.4.

'Sister' peripheral nervous system cultures (PNS) were also generated from the same embryos, by harvesting dorsal root ganglia (DRG) and plating one DRG per coverslip. PNS cultures were maintained for the same length of time as CNS cultures.

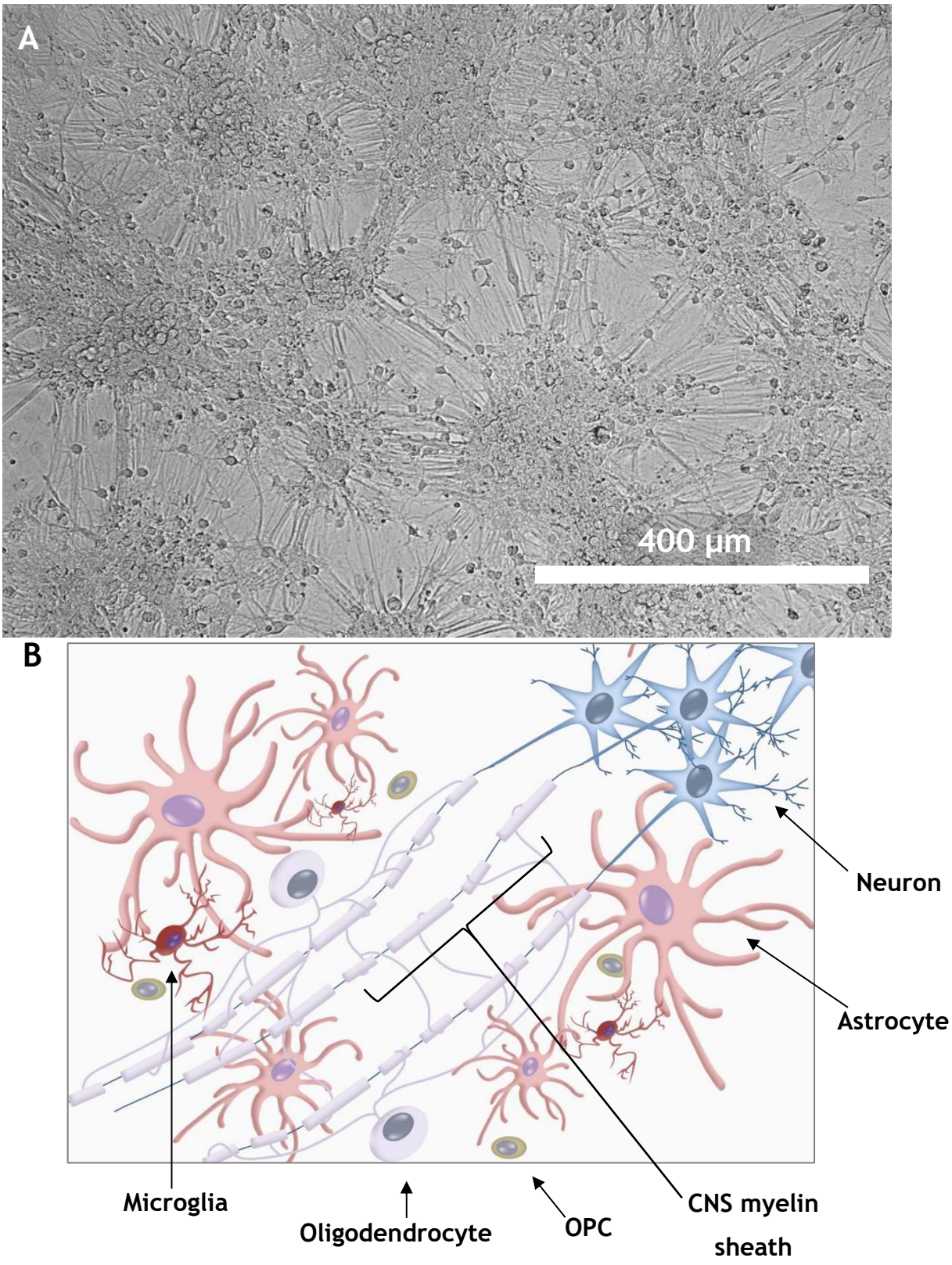


**Figure 4–1 Light microscope image and schematic of central nervous system (CNS).**
(**A**) Light microscope image of CNS co-culture imaged at DIV28. Neuronal cell bodies cluster to form nuclei, making connections with other nuclei via extensions (axons/dendrites). (**B**) Schematic representation of principle cell types present within CNS co-culture. Principle cell types include neurons, astrocytes, microglia, oligodendrocytes and oligodendrocyte precursors (OPCs). Oligodendrocytes are the myelin forming cell type of the CNS and wrap around the axons of neurons to enable saltatory conduction to take place. Myelinated axons form the white matter of the brain.

#### 4.2.2.2 **Co-culture composition**

To examine ZIKV tropism within the CNS and PNS, mixed cell co-cultures were employed in these studies. These co-cultures contain all principle cell types of their respective nervous system but lack secondary immune responses, for example those provided by T cells. Grown in semi-monolayer conditions atop of glass coverslips, they recapitulate complex cell-cell interactions of intact nervous systems – allowing for molecular studies of such interactions to be conducted.

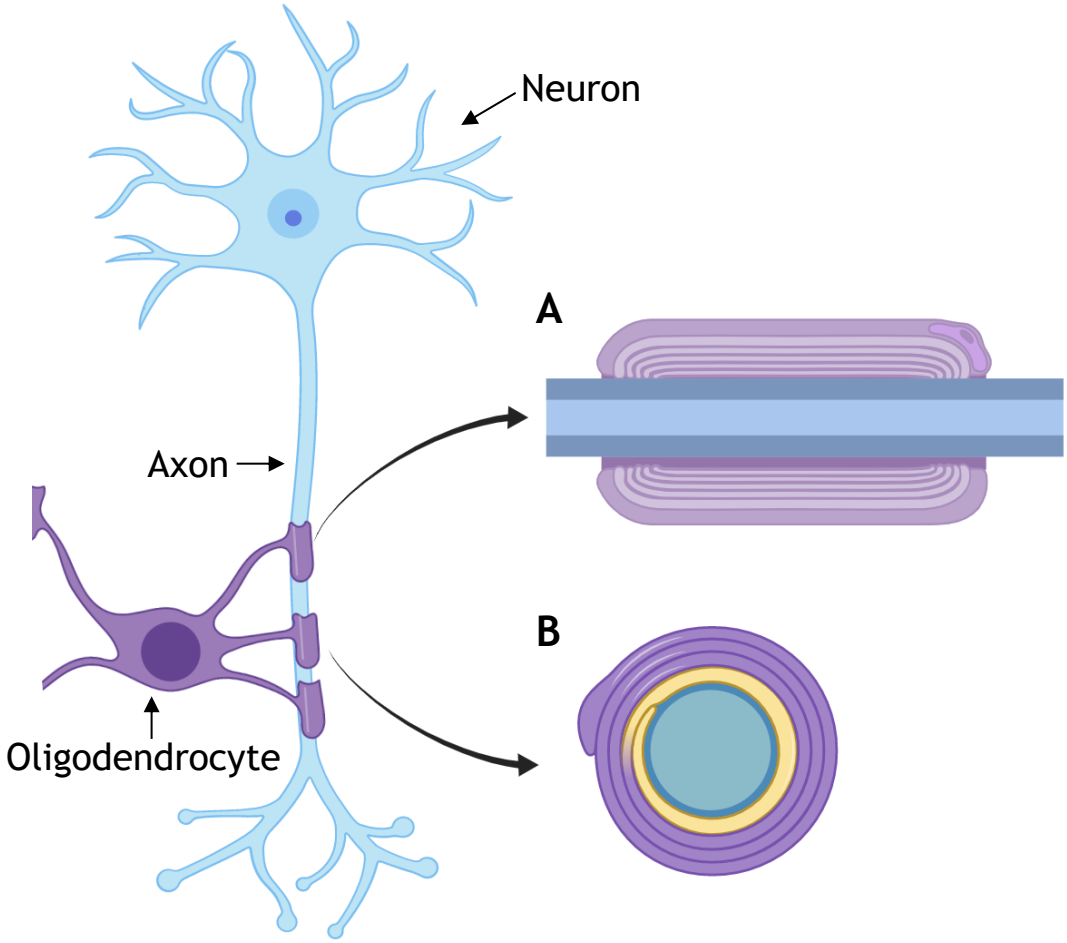


**Figure 4–2 Schematic representation of CNS myelin sheath produced by an oligodendrocyte**
Oligodendrocytes are the myelinating cell type of the central nervous system. One oligodendrocyte (purple) can form the myelin sheath for many axons. Oligodendrocytes extend processes which wrap a lipid-rich, specialised membrane around the axons of neurons (blue). (**A**) Transverse section of myelinated axon. (**B**) Longitudinal cross-section of myelinated axon. This image was produced using BioRender.

The CNS is composed of five principle cell types: neurons, astrocytes, microglia, oligodendrocytes and oligodendrocyte precursor cells (OPCs) (Figure 4–1). A brief overview of each cell type is summarised herein. Neurons communicate signals, via electrical impulses and neurotransmitters, from the CNS (and within) to the rest of the body to affect a response. Astrocytes are the most abundant cell type in the central nervous system and possess diverse functionality, reflected in the increased recognition of astroglia subpopulations (Miller, 2018). Astrocyte function includes but is not limited to the maintenance of CNS homeostasis, blood brain barrier function, neuron synaptogenesis, and immunological regulation (Miller, 2018). Oligodendrocytes are the myelin-producing cell type of the CNS. Myelin is a specialised cell membrane that wraps around axons, insulating them and enabling rapid conduction action potentials to take place; one oligodendrocyte can insulate multiple axons within the CNS (Figure 4–1B and Figure 4–2) (Snaidero and Simons, 2017). Oligodendrocyte precursor cells are a class of stem cell that can differentiate into mature oligodendrocytes. Microglia are the tissue resident macrophages of the CNS, implicated in the regulation of immune/inflammatory effects and CNS maintenance (Nayak et al., 2014).

The principle cell types of the PNS include neurons, macrophages and Schwann cells (Figure 4–3). Schwann cells are the cell type responsible for myelinating axons of the peripheral nervous system. The myelin sheath of the periphery differs to that of the CNS, as many Schwann cells are required to myelinate a singular axon in the PNS (Salzer, 2015). The cell body of the Schwann cell is in close proximity to PNS axons, whereas CNS oligodendrocyte cell bodies may reside in a distant location to a CNS axon (compare Figure 4–1B with Figure 4–3B).

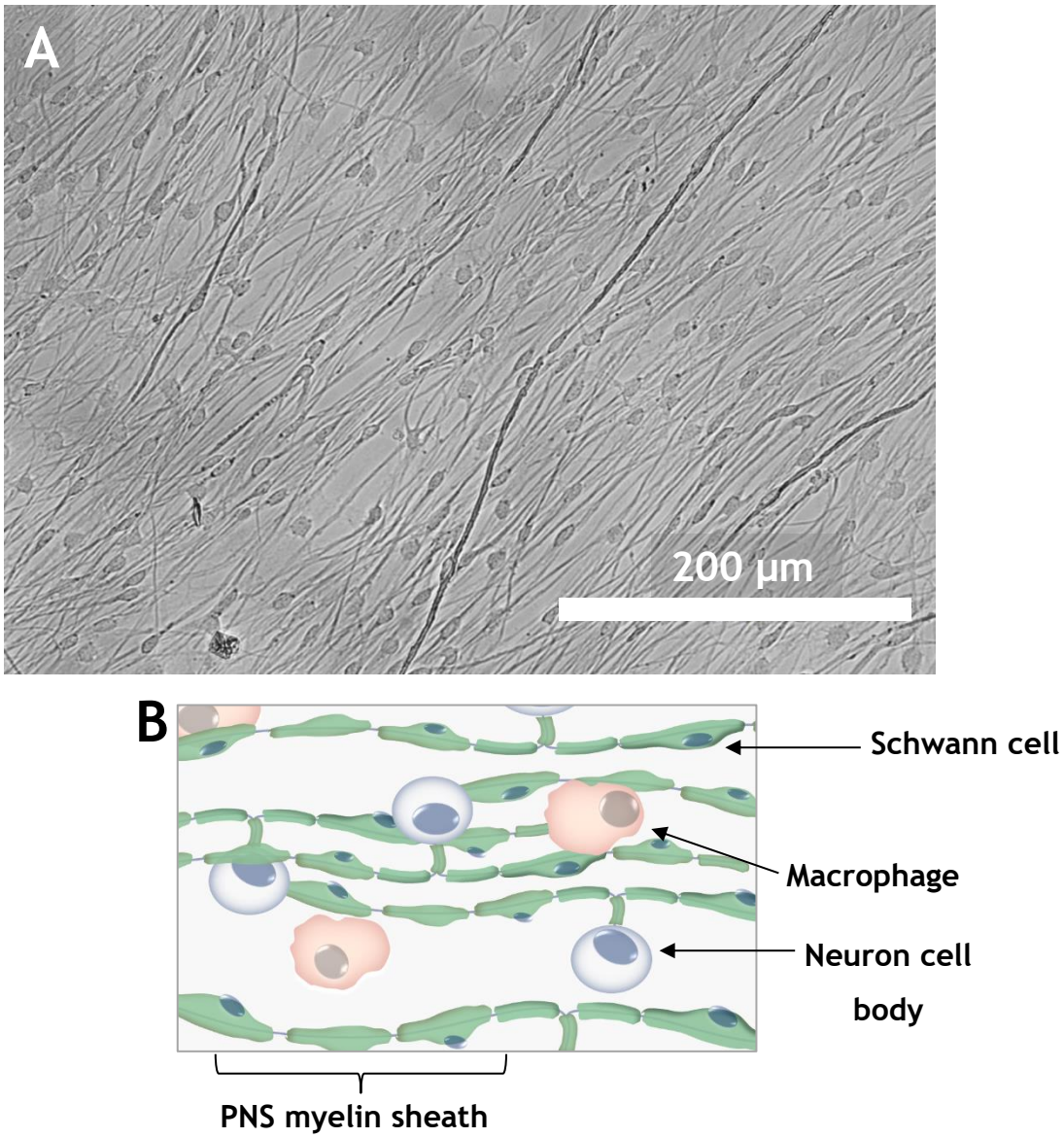


**Figure 4–3 Light microscope image and schematic of peripheral nervous system (PNS) cells.** (**A**) Light microscope image of PNS co-culture, imaged at DIV28. PNS neurons organise to form parallel bundles, extending out from DRGs (DRG not shown in this image). (**B**) Schematic representation of the principle cell types present within PNS co-culture. The principle cell types of the PNS include neurons, macrophages and Schwann cells. Schwann cells are the myelinating cell type of the PNS. Numerous Schwann cells are required to form the myelin sheath of a singular axon.

### 4.2.3 Chapter aims

Determining ZIKV tropism on a cell type specific level is essential in understanding ZIKV-associated neuro-pathologies. Therefore, the primary aim of this chapter was to determine the cellular targets and pathophysiological responses of ZIKV infection within the CNS and PNS using murine ‘myelinating’ co-cultures (see section 4.2.2.2 for co-culture composition and generation).

## 4.3 Results

### 4.3.1 CNS co-cultures are more susceptible to ZIKV infection than their PNS counterpart, even in the absence of type I IFN responses

To investigate ZIKV tropism within the CNS and PNS, *Ifnar1* KO and WT (herein referred to as KO and WT) co-cultures were infected with ZIKV for either 24 or 72 h p.i. at a MOI of 0.3 or 3.0 PFU/cell, respectively. The two differing MOIs and timepoints were used to examine different aspects of ZIKV tropism within the CNS and PNS co-cultures. The lower infectious dose coupled with the shorter timepoint (MOI 0.3/24 h p.i.) was used to investigate the initial infectious targets for ZIKV infection. Whereas the longer timepoint coupled with the higher infectious dose (MOI 3/72 h p.i.) was used to try to identify all possible infectious targets of ZIKV infection.

Cultures were fixed at the timepoints indicated, immunolabelled with an antibody targeting the ZIKV envelope protein (ZIKV E) and nuclei were counterstained with DAPI. ZIKV E positive and negative cells within an area of interest were quantified (rectangular area of interest [AOI] of 148,427 µm or 20,000 µm – see chapter Section 2.8.1 for details) (Figure 4–4 and Figure 4–7). ZIKV E positive cells were identified by observing characteristic staining patterns for the ZIKV E protein i.e. intense staining in cytoplasmic perinuclear distribution, or diffuse cytoplasmic staining with distinct association with a nucleus (Section 3.3.1, Figure 3–2)(Donald et al., 2016).

Overall, infection levels were lower in PNS cultures compared to CNS cultures, even in the absence of type I IFN responses (Figure 4–4). When infected at a MOI of 3.0 PFU/cell and fixed at 72 h p.i., 19% of the cells were infected in the KO CNS co-cultures, whereas the percentage of cells infected in the PNS equivalent for these conditions is only 1%. The lack of PNS infection is best exemplified visually when comparing KO cultures of CNS and PNS cultures (1$^{st}$ Column of data in Figure 4–4A/B).

At 24 h p.i., 4% of the cells in the KO CNS culture were infected as indicated by positive staining for ZIKV E, whereas only 2% of the cells were infected in the equivalent WT culture. The disparity in infection levels between WT and KO co-

cultures was most apparent when observing MOI 3.0/ 72 h p.i. co-cultures; KO cultures were 19% infected and WT, 4%. This demonstrates that the presence of type I IFN responses plays a protective role within CNS co-cultures during ZIKV infection. However, in PNS co-cultures overall infection levels were much lower than CNS co-cultures; infection levels with KO and WT co-cultures at either MOI/timepoint combination were around 1-2% (Figure 4-4B). This suggests that cells of the PNS co-cultures are intrinsically refractory to ZIKV infection; owing to such low levels of ZIKV infection, it is unclear from this study if type I IFN plays a critical protective role against ZIKV infection in PNS co-cultures, as it appears to do so in the CNS co-cultures.

Absent of type I IFN responses, high ZIKV infection levels can be achieved, and is advantageous for studying intrinsic cell type specific susceptibility to ZIKV infection. Therefore, the remainder of the studies in this chapter were subsequently performed using *Ifnar1* KO CNS co-cultures only.

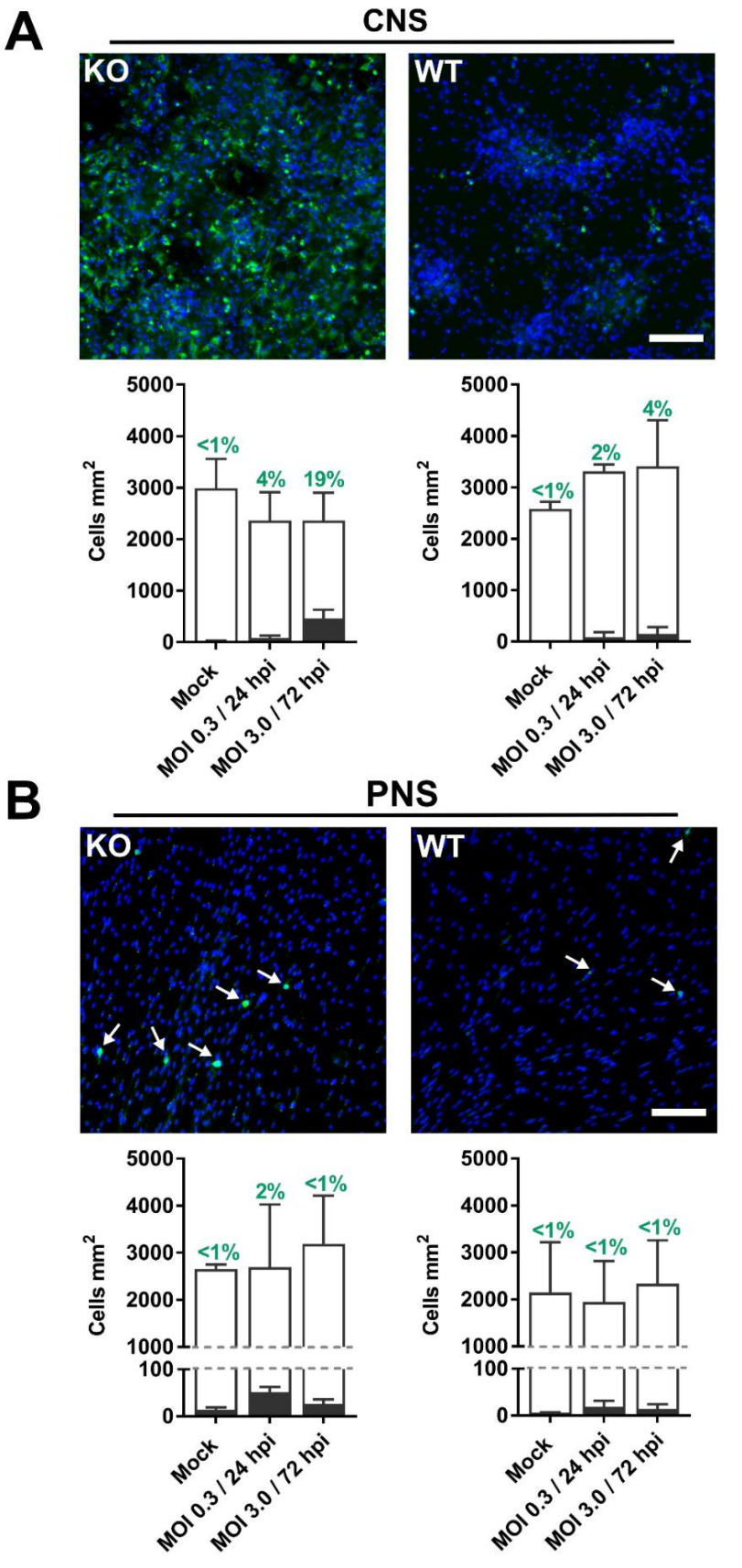


**Figure 4–4 Characterisation of ZIKV infection in *Ifnar1* KO and WT CNS and PNS co-cultures.** CNS and PNS co-cultures were infected with ZIKV with either MOI of 0.3 or 3 PFU/cell for and assayed at the time points indicated. ZIKV infection was quantified by a manual count of ZIKV envelope positive cells (using mouse anti-ZIKV E and goat anti-mouse IgG Alexa Fluor ® 488; green) vs total DAPI positive cells. Overview immunofluorescence images are displayed in the top panel. White bars represent total cell density whereas black bars indicate the infected cell density. The total percentage of infected cells (green) is displayed above the bars in the bottom panel.

#### 4.3.1.1 **PNS maintenance media does not inhibit ZIKV infection**

The maintenance media for CNS and PNS cultures differ in their composition. Notably, CNS media are serum-free whereas PNS media contain horse serum. To ensure that the apparent lack of ZIKV infection in PNS co-cultures is not an artefact of culture conditions, a series of infections were performed in a ZIKV permissible cell line to test PNS media components.

A549 cells, a cell line permissive to ZIKV infection (Donald et al., 2016), were infected with ZIKV at a MOI of 0.3 PFU/cell for 72 h. Cells were maintained in one of the following combinations of media post infection: DMEM supplemented with 10% FBS (normal A549 media), DMEM supplemented with 10% horse serum (HS), whole PNS maintenance media (10% HS), PNS maintenance media supplemented with 10% FBS. ZIKV infection was assessed qualitatively by immunostaining cells for ZIKV E and DAPI (representative images are shown in Figure 4–5).

Upon observation, infection levels remained consistent between the differing media conditions and it was decided that this qualitative assessment was sufficient in this investigation. Results show that horse serum does not inhibit ZIKV infection in either DMEM or PNS maintenance media. In fact, it seems that PNS maintenance media enhanced infection when supplemented with 10% FBS. In these conditions, it appeared that cells were clustered together with large blank spaces on coverslips and few cells remain uninfected, presumably as a result of enhanced cytopathic effect taking place (CPE).

Owing to the reduced infection within PNS co-cultures it appears unlikely that Guillain-Barré syndrome or other disorders affecting the periphery are a result of direct ZIKV infection of the PNS.

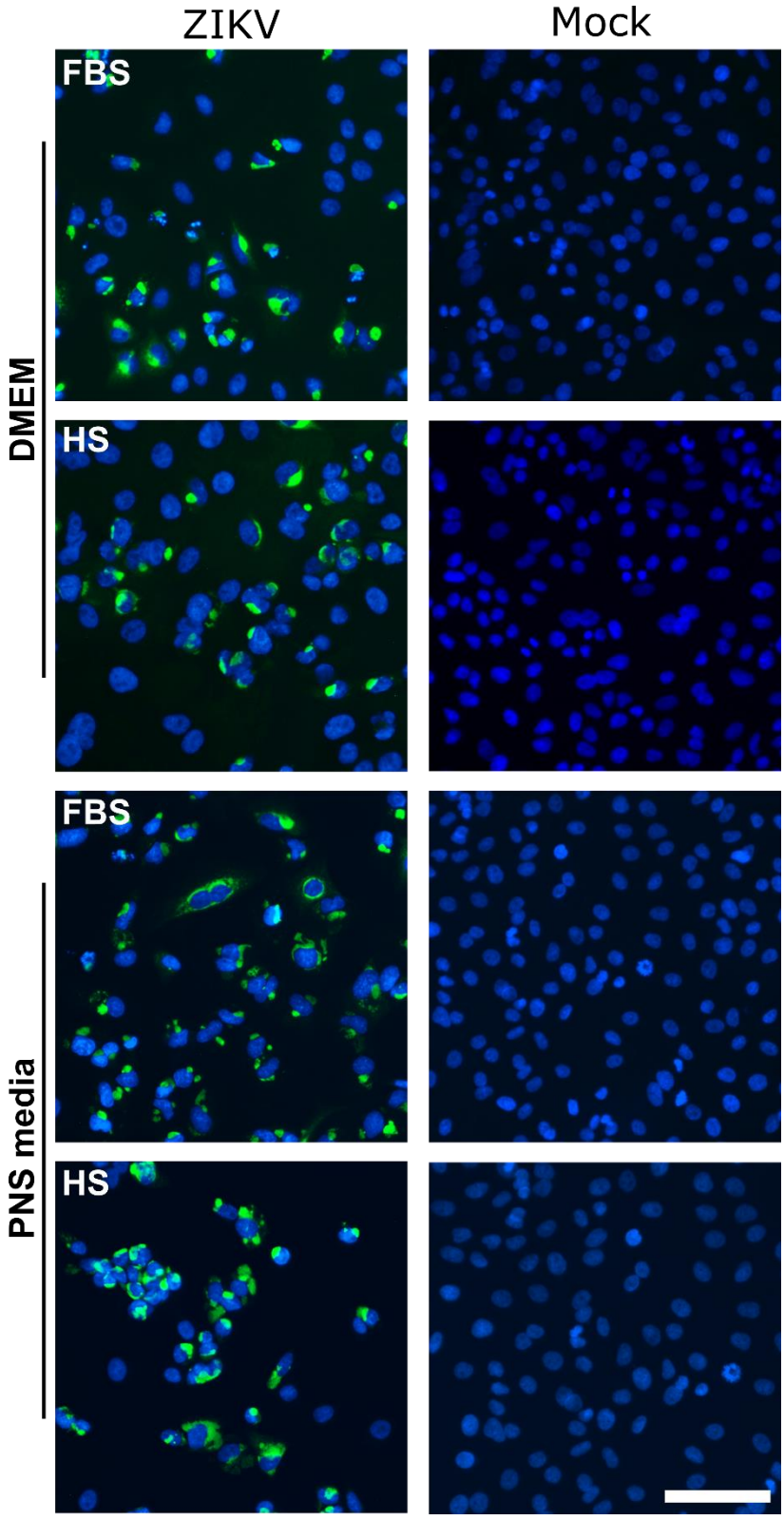


**Figure 4–5 PNS maintenance media do not inhibit ZIKV infection in A549 cells.**
A549 cells were infected with ZIKV at a MOI of 0.3 PFU/cell for 72 h. Following the adsorption period, cells were either maintained in complete PNS maintenance media (PNS 10% horse serum (HS)), PNS maintenance media supplemented with FBS (PNS 10% FBS), normal A549 maintenance media (DMEM 10% FBS) or A549 media supplemented with 10% horse serum (DMEM 10% HS). Scale bar: 100 µm Blue: DAPI Green: ZIKV envelope protein (mouse anti-ZIKV E [primary antibody], goat anti-rabbit IgG Alexa Fluor ® 488 [secondary antibody]).

### 4.3.2 Principle CNS cell types have varying susceptibility to infection with ZIKV

As ZIKV infection levels were greatest in *Ifnar1* KO CNS cultures, these cultures were used to investigate ZIKV tropism on a cell type specific level. As described previously in section 4.3.1, cultures were infected at MOI of 0.3 PFU/cell for 24 h or a MOI of 3.0 PFU/cell for 72 h to determine:

I) The initial cell types infected by ZIKV within the CNS

II) The range of cell types infected by ZIKV within the CNS

Post-fixation, cells were immunolabelled using cell type specific markers. Neurons were labelled with α-NeuN; NeuN is a transcription factor present in nucleus of neurons. Astrocytes were labelled with α-GFAP; GFAP - glial fibrillary acidic protein - is an intermediate filament. Oligodendrocytes were labelled with α-PLP/DM20; PLP (proteolipid protein) and DM20 are two abundant proteins found in myelin. Oligodendrocyte precursor cells (OPCs) were immunolabelled with α-NG2; NG2 is chondroitin sulphate proteoglycan and differentiates between OPCs and mature oligodendrocytes. Microglia were immunolabelled with α-F480; F480 is a surface glycoprotein found on macrophages. Cells were also immunolabelled with α-ZIKV E and nuclei were counterstained with DAPI. Cells that stained positive for a specific cell type marker were enumerated, in addition to cells with double positive staining (positive for cell type specific marker and ZIKV E). Representative images of each cell type can be found in Figure 4–6.

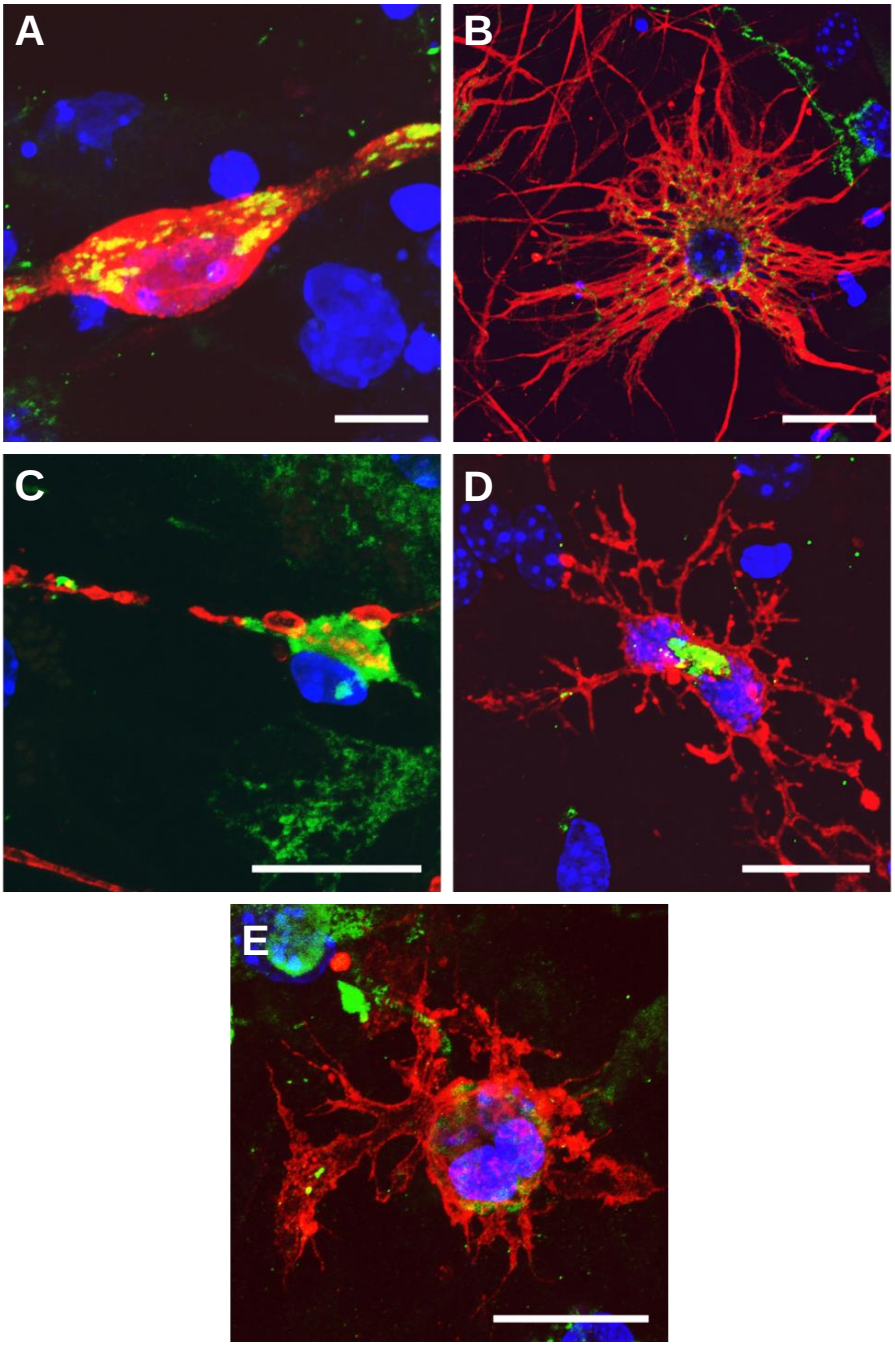


**Figure 4–6 Confocal microscopy of ZIKV infected CNS cells.**
Cell type specific immunofluorescence analysis of ZIKV infected cells in *Ifnar1* KO CNS co-cultures. (**A**) Neuron stained for NeuN, also known of Fox-3, a transcription factor which primarily resides in neuronal nuclei but can also exist within the cytoplasm of neurons. (**B**) Astrocyte stained for GFAP, an intermediate filament found within this star-shaped cell. (**C**) Oligodendrocyte stained for PLP/DM20, a component of myelin; this stain highlights oligodendrocyte cells bodies and myelin sheaths, which are long, thin, extensions of lipid-rich membranes that wrap around axons (**D**) Oligodendrocyte precursor cell (OPC) stained for NG2, which is an integral membrane proteoglycan. OPC's have several projections emanating from the cell body, which are immature myelin sheaths.(**E**) Microglial cell stained for F4/80, a macrophage-specific adhesion g-protein coupled receptor; projections from the cell body allow microglia to move and scavenge cellular debris and eliminate infected/damaged cells.Green: ZIKV envelope protein (mouse anti-ZIKV E [primary antibody], goat anti-rabbit IgG Alexa Fluor ® 488 [secondary antibody]), Blue: DAPI, red: cell- type specific marker (**A** Rabbit anti-NeuN [primary antibody]; **B** Rabbit anti-GFAP [primary antibody]; **C** Rat anti-PLP/DM20 [clone AA3; primary antibody]; **D** Rabbit anti-NG2 [primary antibody]; **E** - rat anti-F480 [primary antibody]). Secondary antibodies used to visualise cell specific markers were either goat anti-rabbit IgG or goat anti-rat IgG conjugated with Alexa Fluor ® 594. Scale bar: 10um.

The overall culture composition did not alter markedly between each of the infection conditions (MOI 0.3/24 h p.i., MOI 3/72 h p.i. and mock) when observing the profile of total cell type densities, measured in cells/mm$^2$ (compare white bars of Figure 4–7 A/B/C). This highlights the reproducible nature of co-culture generation, in addition to demonstrating that ZIKV infection, at least within these time frames, did not alter the proportions of cell-type specific populations in this culture. However, cultures infected at MOI 3/ 72 h p.i. showed a slight reduction in oligodendrocyte populations; the mean total cell density (cells/mm$^2$) was 90.1, 60.1 and 33.6 for mock, MOI 0.3/24 h p.i and MOI 3/72 h.p.i. respectively (Table 4–1,Table 4–2,Table 4–3).

| | ***Total cell density*** | | ***Infected cell density (MOI 0.3/24 h.p.i)*** | | ***% Infected considering the relative abundance of cell type*** |
|---|---|---|---|---|---|
| ***Cell Type*** | Mean (cells / mm$^2$) | SD | Mean (cells / mm$^2$) | SD | |
| ***Oligodendrocytes*** | 60.1 | 7.9 | 19.9 | 9.2 | **24%** |
| ***OPCs*** | 215.7 | 73.3 | 30.1 | 23.0 | **12%** |
| ***Microglia*** | 97.8 | 38.0 | 5.3 | 6.5 | **6%** |
| ***Astrocytes*** | 316.2 | 44.3 | 11.6 | 4.3 | **3%** |
| ***Neurons*** | 309.2 | 76.8 | 9.4 | 12.1 | **3%** |

**Table 4–1 Quantification cell-type specific ZIKV infection in CNS co-cultures: MOI 0.3**
*Ifnar1* CNS co-cultures were infected with ZIKV at a MOI of 0.3 and fixed with 4% formaldehyde at 24 h.p.i. Coverslips were immunostained for ZIKV in addition to cell-type specific markers. The number of infected and uninfected cells was enumerated, and percentage of infection calculated, taking into account the relative abundance of each cell type. SD: standard deviation.

The proportion of ZIKV-positive cell types are summarised in Table 4–1, Table 4–2 and Figure 4–7. Oligodendrocytes were the predominant cell type infected by ZIKV at both multiplicities of infection and time points. These data indicate that oligodendrocytes may be more permissive to ZIKV replication than other CNS cell types and may represent a key target during infection of the CNS with ZIKV.

| | *Total cell density* | | *Infected cell density (MOI 3/72 h.p.i)* | | *% Infected considering the relative abundance of cell type* |
|---|---|---|---|---|---|
| ***Cell Type*** | Mean (cells / $mm^2$) | SD | Mean (cells / $mm^2$) | SD | |
| ***Oligodendrocytes*** | 33.6 | 10.3 | 27.2 | 11.2 | **45%** |
| ***OPCs*** | 260.2 | 37.0 | 30.7 | 23.3 | **11%** |
| ***Microglia*** | 106.4 | 34.2 | 54.2 | 16.5 | **34%** |
| ***Astrocytes*** | 253.3 | 104.6 | 83.5 | 28.4 | **26%** |
| ***Neurons*** | 347.9 | 166.4 | 33.0 | 20.2 | **9%** |

**Table 4–2 Quantification cell-type specific ZIKV infection in CNS co-cultures: MOI 3**
*Ifnar1* CNS co-cultures were infected with ZIKV at a MOI of 3 and fixed with 4% formaldehyde at 72 h.p.i. Coverslips were immunostained for ZIKV in addition to cell-type specific markers. The number of infected and uninfected cells was enumerated, and percentage of infection calculated, taking into account the relative abundance of each cell type. SD: standard deviation.

Alternatively, neurons appeared less permissive to ZIKV infection, as evidenced by infection rates of 3 or 9% within the cell type population. In summary, these data demonstrate that each principle CNS cell type is susceptible to ZIKV infection, albeit to varying degrees of susceptibility; ranging from oligodendrocytes (most permissive) to neurons (least permissive).

| | *Total cell density* | | *Infected cell density (MOCK)* | | *% Infected (considering relative abundance of cell type)* |
|---|---|---|---|---|---|
| ***Cell Type*** | Mean (cells / $mm^2$) | SD | Mean (cells / $mm^2$) | SD | |
| ***Oligodendrocytes*** | 90.1 | 34.6 | 3.4 | 2.3 | **3%** |
| ***OPCs*** | 270.5 | 45.3 | 0.3 | 0.4 | **<1%** |
| ***Microglia*** | 85.6 | 29.6 | 1.1 | 1.4 | **2%** |
| ***Astrocytes*** | 346.6 | 69.1 | 8.5 | 10.2 | **4%** |
| ***Neurons*** | 372.0 | 114.8 | 3.0 | 4.0 | **<1%** |

**Table 4–3 Quantification cell-type specific ZIKV infection in CNS co-cultures: MOCK**
*Ifnar1* CNS co-cultures were mock infected with "% FBS/PBS and fixed with 4% formaldehyde at 72 h.p.i. Coverslips were immunostained for ZIKV in addition to cell-type specific markers. The number of infected and uninfected cells was enumerated and percentage of infection calculated, taking into account the relative abundance of each cell type. SD: standard deviation.

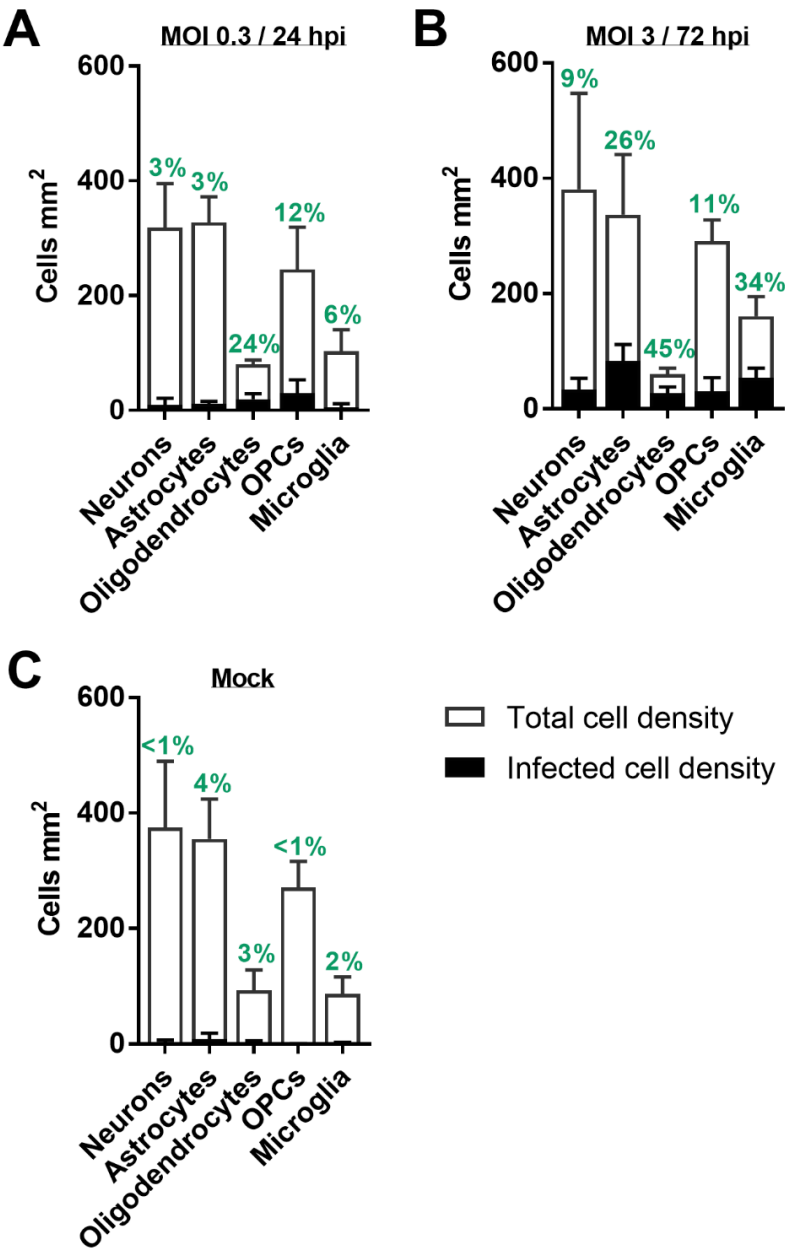


**Figure 4–7 Quantitation of cell type specific infection ZIKV within *Ifnar1*KO CNS co-cultures.** Cell type densities of CNS cultures were enumerated in the CNS cultures and presented as cells/mm$^2$ (white bars). The number of infected cells of each cell type is overlaid (black bars). The relative percentage of infection of each cell type is displayed above the corresponding bar. (**A**) Data from cultures infected at MOI 0.3 for 24 h p.i. (**B**) Data from cultures infect at a MOI of 3 PFU/cell for 72 h. **(C)** Enumeration of mock infected cultures. Bars represent mean ± SD; n=3.

### 4.3.3 ZIKV infection of the CNS and cell death

In addition to quantifying levels of ZIKV infection in different cell populations of the CNS, pyknotic nuclei were also counted as a marker for unhealthy and/or dying cells present in cultures (Figure 4–9). Pyknotic nuclei were distinguished from healthy nuclei based upon the intensity and homogeneity of DAPI labelling, and size. Pyknotic nuclei appeared very small and rounded with uniform, intense DAPI staining, whereas healthy nuclei varied in size and were heterogeneous in the uptake of DAPI stain - presenting intensely stained puncta within a lesser stained oval (Figure 4–8).

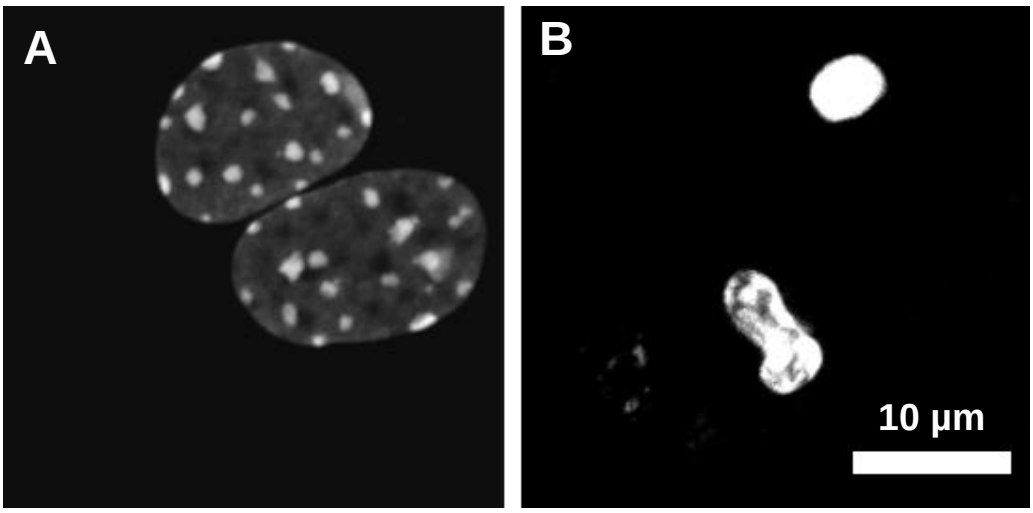


**Figure 4–8 Representative images of healthy and pyknotic nuclei**
CNS co-cultures (DIV28) were mock-infected by incubating with PBS supplemented with 2% FBS for one hour at 37 °C, prior to replacing with fresh CNS media. After 72 h p.i., cells were fixed in 4% formaldehyde. Nuclei within the CNS co-culture were stained using DAPI. (**A**) Image of healthy nuclei within a CNS co-culture (**B**) Image of unhealthy/pyknotic nuclei within a CNS co-culture. Images were taken at 20x magnification.

At 72 h p.i. (MOI 3), ZIKV infection appeared to cause injury to most cell types as determined by pyknotic nuclei counts - with exception of neurons. There was degree of variation in pyknotic nuclei counts across most cell types and conditions. However, this was most pronounced for data relating to oligodendrocytes. Oligodendrocyte cell bodies are quite small and may be easily confused for pyknotic nuclei in some cases, particularly given the resolution of some nuclei in images used to quantification. This is owed to the fact that CNS co-cultures are not true monolayer cultures, as such they have many different focal planes. Therefore, in any given image some nuclei were out of focus, should this be an oligodendrocyte nucleus it may appear pyknotic given its size. This might also account for the higher percentage of pyknotic oligodendrocyte

nuclei in mock infected cultures (Figure 4–9). Therefore, this large degree of variation in this dataset may be attributed to human error in addition to protocol methodology. Despite issues pertaining to variation, there was a significant increase in pyknotic nuclei belonging to astrocytes and microglia.

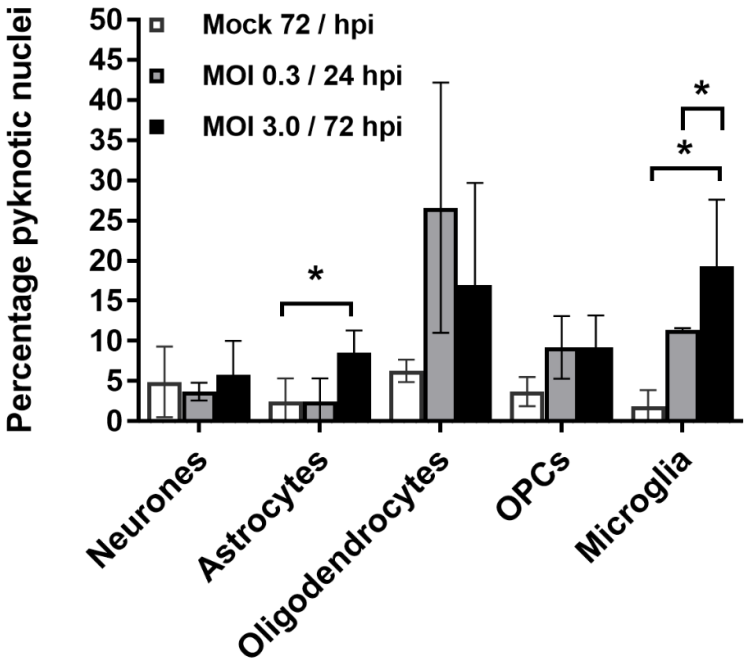


**Figure 4–9 Exploration of cell death within *Ifnar1* KO CNS co-cultures, as determined by pyknotic nuclei counts.**
Data from mock infected cultures are represented in white bars, MOI 0.3/24 h p.i. data are displayed in grey bars, and black bars represent data from MOI 3.0/72 h p.i. cultures. Bars represent mean ± SD; *p <0.05, n=3

To address the issues that arose due to the subjective nature of counting pyknotic nuclei, a chemical assay was employed to investigate the global health of infected CNS cultures. The ApoTox-Glo™ Triplex Assay (Promega) was used to assess cell viability, cytotoxicity and apoptosis. To perform this assay, CNS co-cultures were plated into 96 well plates instead of normal co-culture conditions. Cultures were infected with ZIKV at a MOI of 0.3 or 3 PFU/cell, and the assay was performed in accordance with manufacturer specifications at the time points indicated. Staurosporine, an inducer of apoptosis was used as a positive control of increasing cytotoxicity and apoptosis activation within this assay, and a negative control for cell viability. As staurosporine was solubilised in DMSO, DMSO was also used as a control and samples were assayed at 72 h post treatment.

The initial results (n=2) indicate there was relatively little change in cell viability between the different conditions (Figure 4–10A). Cultures at 24 h p.i. appeared to have a slight reduction in cell viability in comparison with 72 h p.i. and mock infected samples, with no considerable difference in GF-AFC intensity observed between cultures infected at the differing multiplicities of infection. When investigating cytotoxicity (Figure 4–10B), it appeared there was slightly more variation present between replicates 1 and 2, particularly at 72 h p.i. Overall, at 24 h p.i. cultures displayed similar levels of detected cytotoxicity to mock treated cultures. Whereas, at 72 h p.i. cultures displayed increased bis-AFF-R110 activity, with cultures infected at the higher MOI demonstrating the highest increase in cytotoxicity in comparison to the other cultures. When measuring apoptosis there was a slight increase in apoptosis in cells infected at a MOI of 3.0 PFU/cell at 72 h p.i. cultures in comparison to mock infected cultures (Figure 4–10C). However, this fold change is negligible and owing to high variability is not considered significant.

Overall, the initial observations of this experiment did not inspire further investigation, as the observed effects of ZIKV infection on global culture health at these timepoints were marginal. Therefore, further experimentation involving cell death using these conditions ceased.

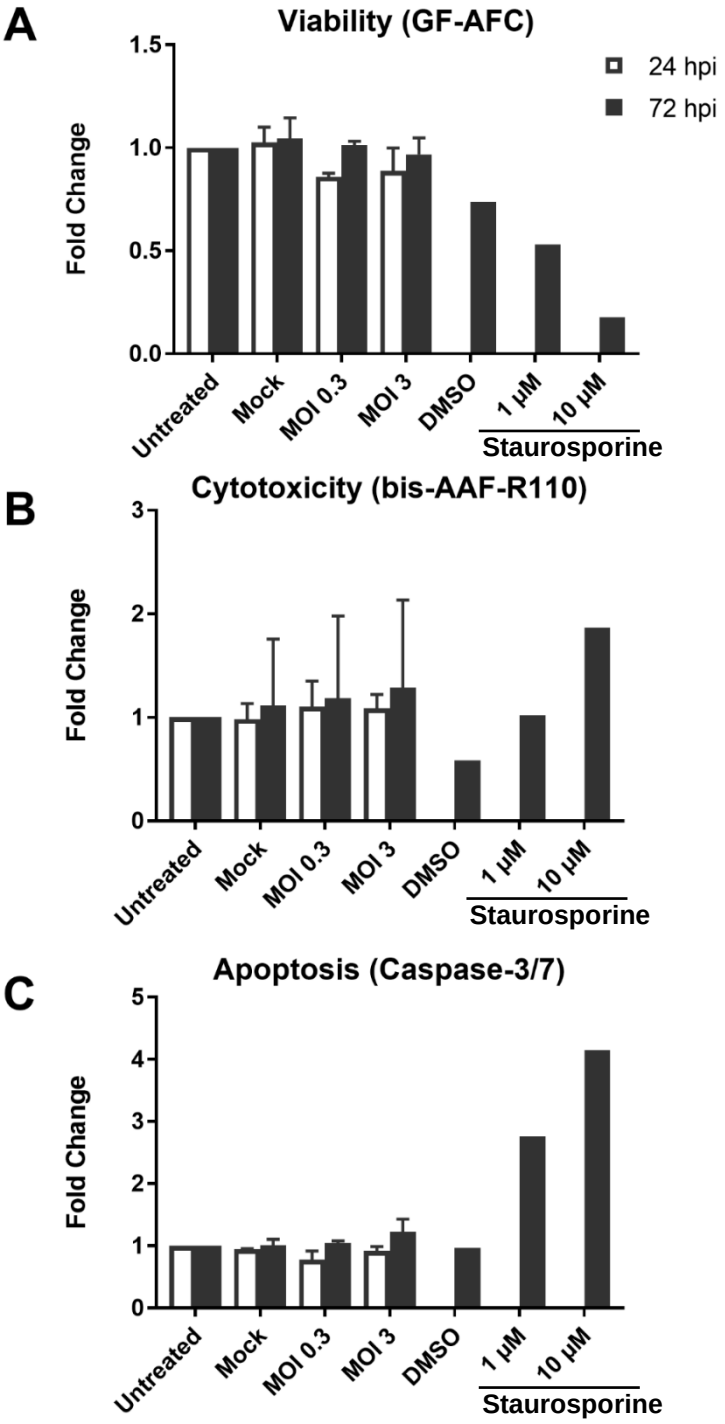


**Figure 4–10 Cell death analyses of IFN KO CNS co-cultures using ApoTox-Glo™ (Promega).** Ifnar-1 CNS co-cultures grown in wells of a 96 well-plate were infected in triplicate with ZIKV at a MOI of either 0.3 or 3 PFU/cell. Samples were assayed at 24 h p.i. (white bars) and 72 h p.i. (black bars) using the ApoTox-Glo™ Triplex Assay and measured using a GloMax® 20/20 Luminometer (Promega). (**A**) Cells were treated with a cell-permeable GF-AFC substrate, and viability was measured using a luminometer with a fluorescence filter (400 nm wavelength excitation/ 505 nm wavelength emission). (**B**) Cells were treated with a cell-impermeable bis-AAF substrate, and cytotoxicity was measured using a luminometer with a fluorescence filter (485 nm wavelength excitation/ 520 nm wavelength emission). (**C**) Cells were lysed with the Caspase-Glo® 3/7 reagent and markers of apoptosis (caspase 3/7 activation) were measured via luminescence using a luminometer. Staurosporine, a known inducer of apoptosis, was used as a positive control for cell death/apoptosis. Biological repeats n=2, drug controls n= 1.

### 4.3.4 ZIKV infection of CNS co-cultures induces injury to white matter structures

Oligodendrocytes were found to have the highest percentage of ZIKV infection of all principle CNS cell types present in our murine co-cultures (section 4.3.2). It became apparent during the quantification stages of earlier investigations of cell type specific levels of infection, that the PLP/DM20 (oligodendrocyte cell body and myelin) staining pattern in ZIKV infected cultures was slightly different compared to that of mock infected cultures. This was most pronounced in MOI 3/72 h p.i. infected cultures. Oligodendrocytes extend processes (extensions) which wrap axons within the CNS with layers of specialised cell membrane to form myelin sheaths (Snaidero and Simons, 2014). Myelin sheaths when stained with PLP/DM20 should appear as relatively smooth long strands, with some larger rounded patches (oligodendrocyte cell bodies); sometimes small bumps might appear on the surface of the long strands - however, this can vary between cultures (Thomson et al., 2008). In ZIKV infected samples, the myelin staining appears fragmented and strands appeared thinner, with a more 'bubbled' appearance in comparison to mock infected cultures (compare Figure 4–11A with Figure 4–11B). See Figure 4–11C for a closer, direct comparison of healthy (indicated by a smooth arrow and unhealthy (indicated by a dashed arrow) myelin.

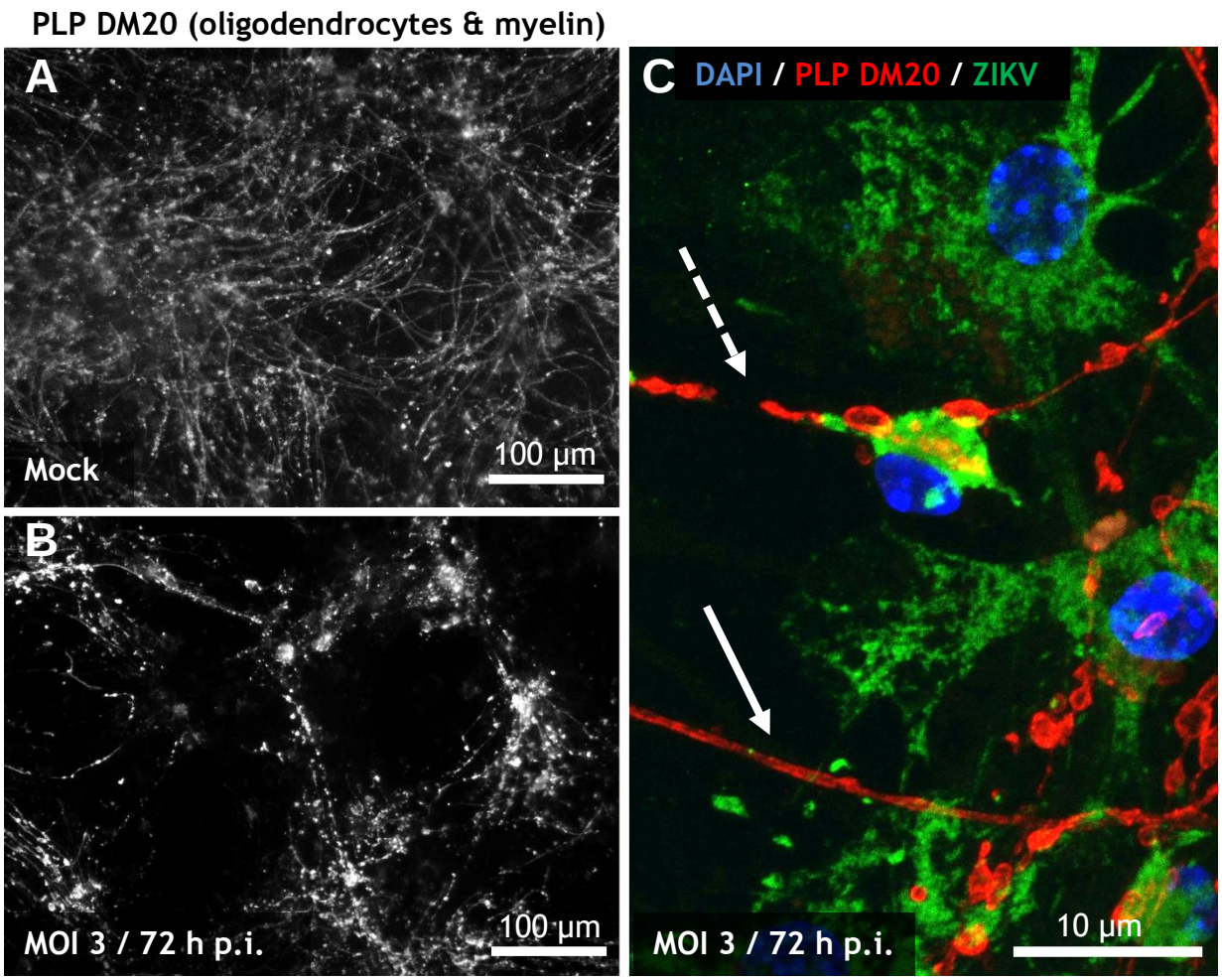


**Figure 4–11 Myelin damage during ZIKV infection.**
Cultures were infected with ZIKV at a MOI of 3.0 PFU/cell. At 72 h p.i. cells were fixed in 4% formaldehyde, stained for ZIKV E (mouse anti-ZIKV E [primary antibody], goat anti-rabbit IgG Alexa Fluor ® 488 [secondary antibody]; green), myelin (rabbit anti-PLP/DM20 [primary antibody], goat anti-rabbit IgG Alexa Fluor ® 594; red) and DAPI (blue) and analysed by confocal microscopy. (**A**) Mock-infected CNS co-culture stained for myelin. (**B**) ZIKV-infected CNS co-culture at 72 h p.i, stained for myelin (**C**) Close up of a ZIKV-infected oligodendrocyte, stained for ZIKV-E, myelin and DAPI. Dashed arrow points towards fragmented myelin sheath of an infected oligodendrocyte. The solid arrow points towards healthy myelin, which is smooth in appearance.

Myelination of neurons in the human brain occurs late in gestation and is not complete until early adulthood (a timeline of different neural development processes can be found in Figure 4–12) (Fields, 2008, Giedd, 2004). Previous experiments within this chapter utilised cultures which were relatively mature (DIV28) and are more reflective of an adult human brain (sections 4.3.1 to 4.3.3). This was because other studies at the time focused on predominantly immature CNS systems to model microcephaly as the highest risk for developing this condition was thought to be the first trimester. Our study aimed to understand ZIKV tropism in both the CNS and PNS; as GBS typically affects a more mature nervous system, and the effects of ZIKV infection within the CNS of

more mature brains e.g. infants remained unexplored. This led to using the later culture developmental time point to explore novel aspects of ZIKV infection. This was done in the knowledge that the stages of co-culture development were well established, and that we could tailor infection to reflect earlier time points of human foetal development (Thomson et al., 2006, Thomson et al., 2008).

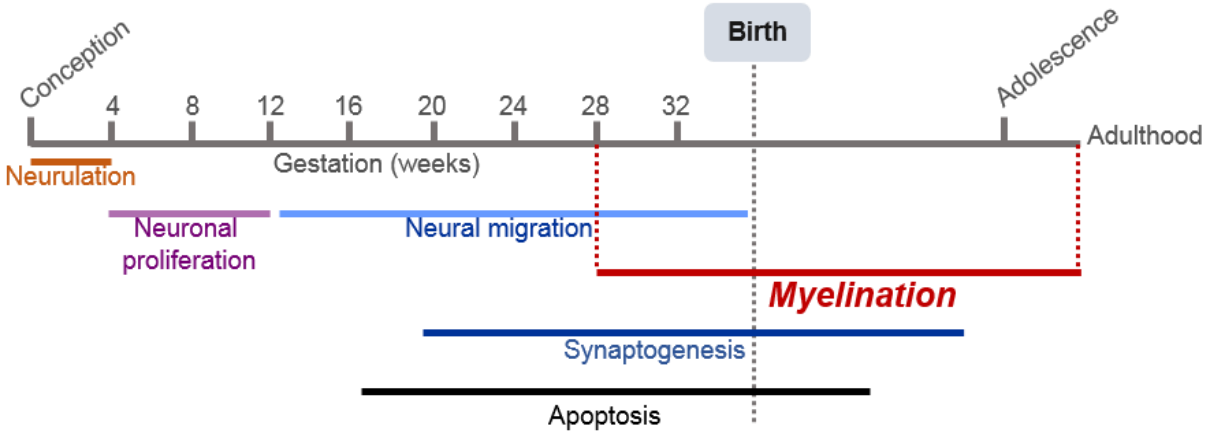


**Figure 4–12 Schematic representation of developmental processes within the human CNS from conception to adulthood.**
The grey bar indicates timepoints throughout life, with a large focus on the gestation period. Myelination occurs late in gestation period (red) and occurs throughout childhood into early adulthood. Figure adapted from (Tau and Peterson, 2010).

Therefore, to test if the process of myelination was affected by ZIKV infection, murine CNS co-cultures were infected at a developmental timepoint that reflected late foetal life when myelination was just starting to take place e.g. at 28 weeks post-conception (Figure 4–12 for overview of gestational timeline; top row Figure 4–13 for image co-culture equivalent, DIV18). Cultures were infected at a MOI of 0.3 PFU/cell in order to try and increase the longevity of the experiment, as myelination within CNS co-cultures was complete at DIV28 (reflective of post-natal life). The aim was to allow co-cultures to mature until DIV28 to observe if myelination was affected by infection with ZIKV from early stages of development. However, owing to culture deterioration in infected samples, experiments were halted at DIV24 (6 d p.i.). Cultures were maintained until DIV24 with media replenishments taking place 2 and 4 d p.i. (see Section 2.8.1 for details). Cultures were subsequently fixed and immunolabelled to depict white matter structures; myelin was immunolabelled with α-MBP (myelin basic protein) and axons with α-SMI31 (phosphorylated neurofilament). The

presence or absence of ZIKV infection was confirmed through separate immunostaining for ZIKV E (Figure 4–14).

In ZIKV-infected cultures, at DIV24 (6 d p.i.) there was a near complete loss of myelin (bottom row, first column -Figure 4–13), in comparison to mock cultures which had extensive myelin sheath formation (middle row, first column - Figure 4–13).

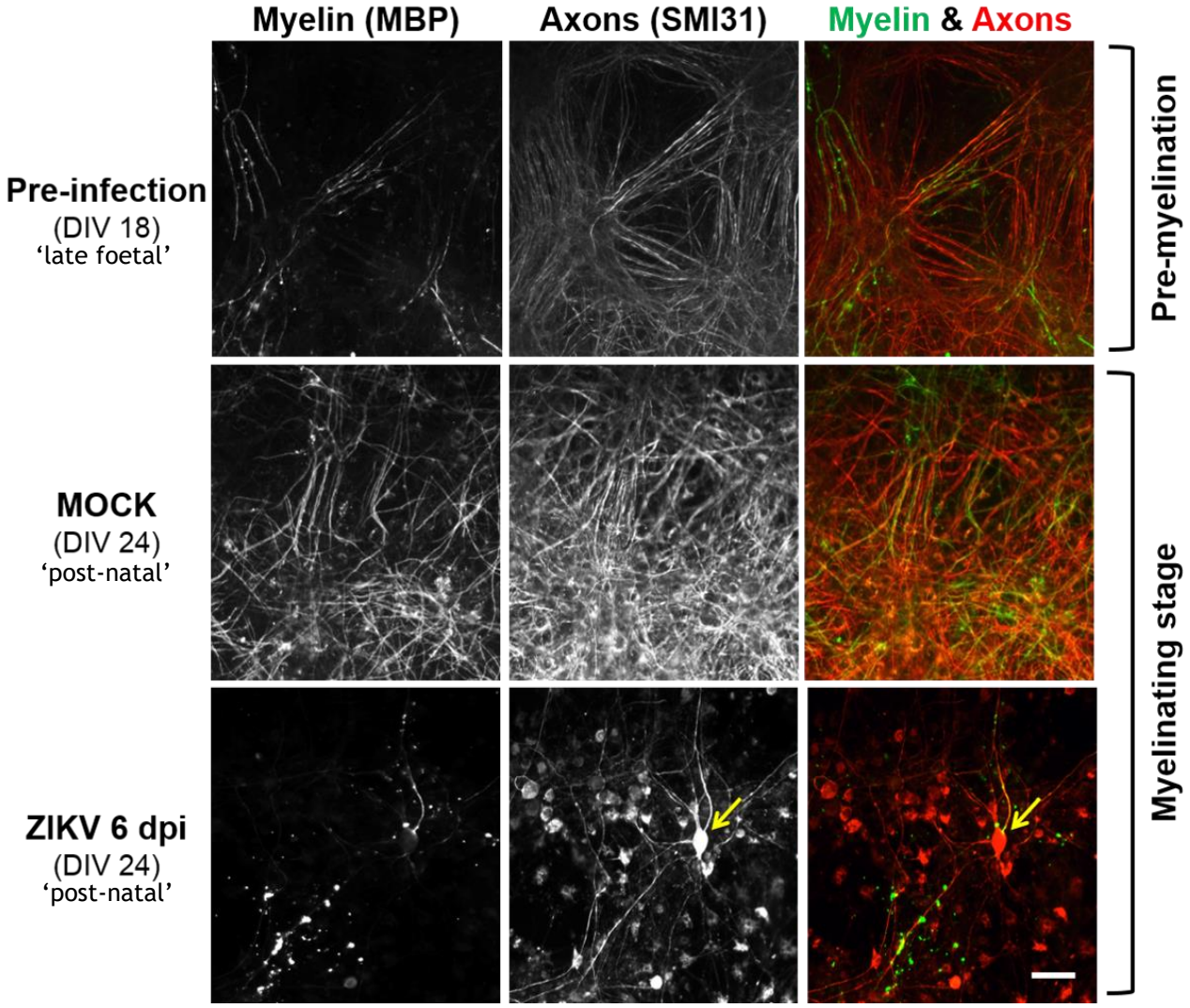


**Figure 4–13 Extensive loss of myelin and axons is observed during ZIKV infection of CNS co-cultures.**
Murine co-cultures were infected with ZIKV at a MOI of 0.3 PFU/cell. *Ifnar1* KO CNS co-cultures were infected when they reached DIV18, a developmental stage where myelination had just begun. Cells were maintained until DIV24 (6 d p.i.) when myelination should be extensive. Column 1: Myelin staining (rat anti-MBP [primary antibody], goat anti-rat IgG Alexa Fluor ® 594 [secondary antibody]); Column 2: Axons (mouse anti-SMI31 [primary antibody], goat anti-mouse IgG Alexa Fluor ® 488 [secondary antibody]); Column 3: merged image. myelin is shown in green, and axons are shown in red (false coloured for clarity). Arrows indicate prominent example of where phosphorylated neurofilament has retreated from the axons, to the neuron cell body – an indicator of axonal damage. Scale bar: 50 µm. Representative images from a minimum of three independent biological replicates, for which at least two coverslips were analysed.

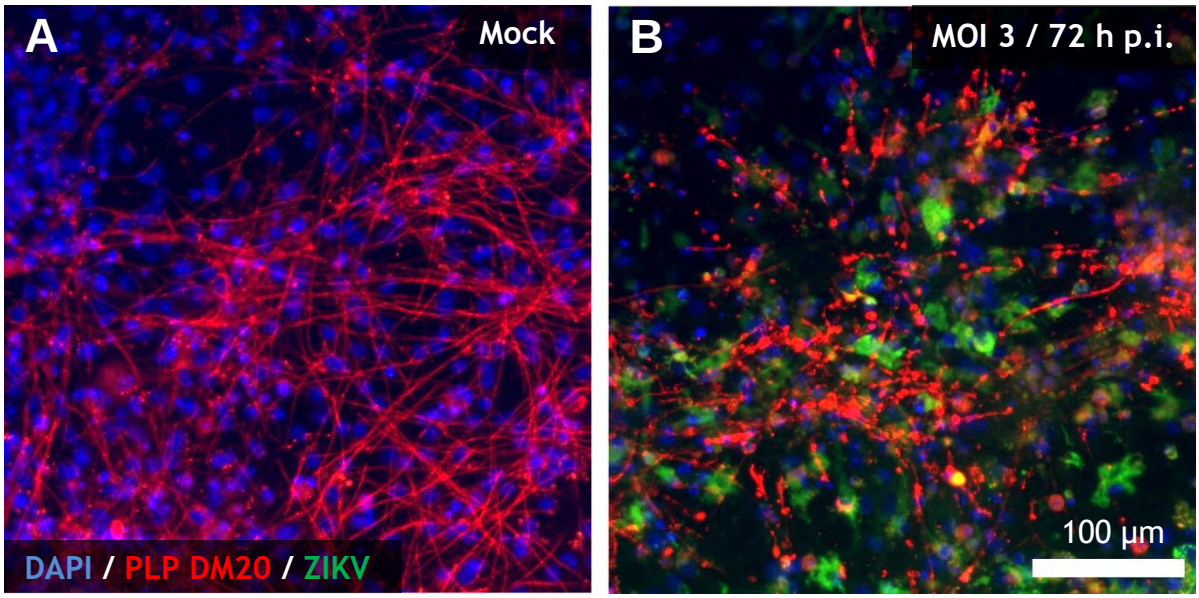


**Figure 4–14 ZIKV infection induces loss of myelin sheath in CNS co-cultures at 6 d p.i**
*Ifnar1* CNS co-cultures were infected on DIV18 with ZIKV at a MOI of 0.3 and maintained until 6 d p.i when cultures were fixed with 4% formaldehyde. Cells were immunolabelled with antibodies targeting ZIKV E (mouse anti-ZIKV E [primary antibody], goat anti-mouse IgG Alexa Fluor ® 488; green) and the myelin sheath/oligodendrocyte cell bodies (rabbit anti-PLP/DM20 [primary antibody], goat anti-rabbit IgG Alexa Fluor ® 594; red), and counterstained with DAPI (blue). (A) Mock-infected CNS co-culture with healthy myelin sheath development (red) absent of ZIKV-positive cells (green). (B) ZIKV-infected CNS co-culture with unhealthy, fragmented myelin sheaths (red), with many ZIKV-positive cells (green). Images taken by Dr Verena Schultz, a collaborator of the project. Representative images from a minimum of three independent biological replicates, for which at least two coverslips were analysed.

Additionally, axons appeared injured in ZIKV infected cultures at DIV24 (6 d p.i.) (Figure 4–13, second column). Immunolabelling with anti-SMI31 should reveal a dense network of axons in healthy samples (Figure 4–15A). However, during ZIKV infection SMI31 appeared to have retreated into neuron cell bodies – an indicator of axonal injury (Figure 4–15B). This axonal injury appeared to occur in absence of apparent neuronal injury, as indicated by the presence of relatively healthy neuronal nuclei (Figure 4–15Bi and Bii).

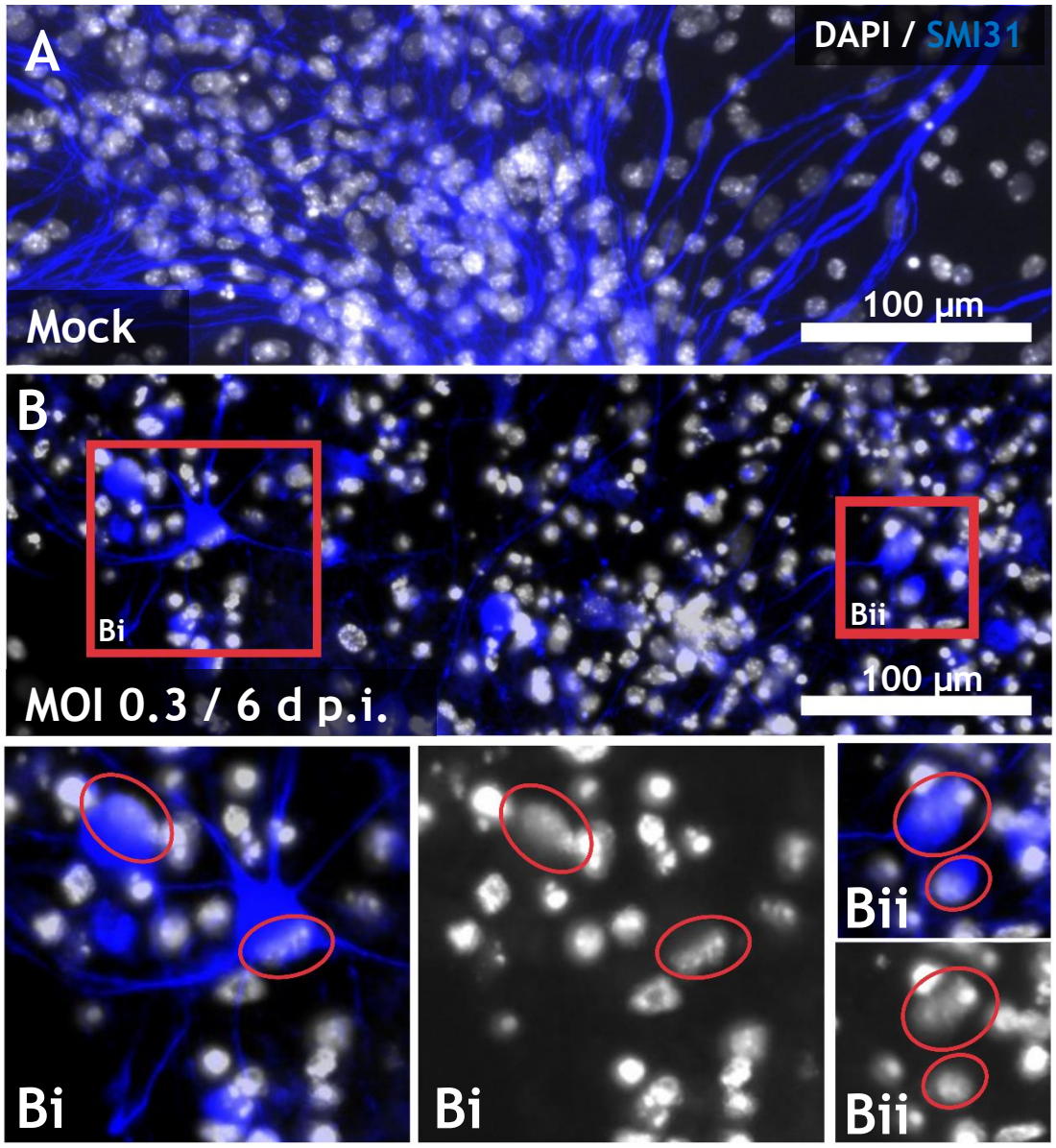


**Figure 4–15 Axonal injury occurs in absence of injury to neuronal cell bodies and nuclei.** Our data show that phosphorylated neurofilament retreats into the cell bodies of neurons in CNS co-cultures infected with ZIKV (MOI 0.3/6 d p.i.). (**A**) mock-infected CNS co-culture with typical SMI31 staining displaying a dense axonal network. (**B**) ZIKV-infected CNS co-culture demonstrating a loss of axonal network. Red boxes indicate neurons with abnormal SMI31 staining, which has retreated from the axons and in towards neuronal cell bodies. Images A and B were taken at 20x magnification. (**Bi/Bii**) Healthy neuronal nuclei belonging to neurons with axonal injury (enlarged from image B), displaying SMI31 staining within the cell body. Grey: DAPI stained nuclei, Blue (false coloured for clarity): SMI31 stained axons and/or neuronal cell body (mouse anti-SMI31 [primary antibody], goat anti-mouse IgG Alexa Fluor ® 488 [secondary antibody]. Representative images from a minimum of three independent biological replicates, for which at least two coverslips were analysed.

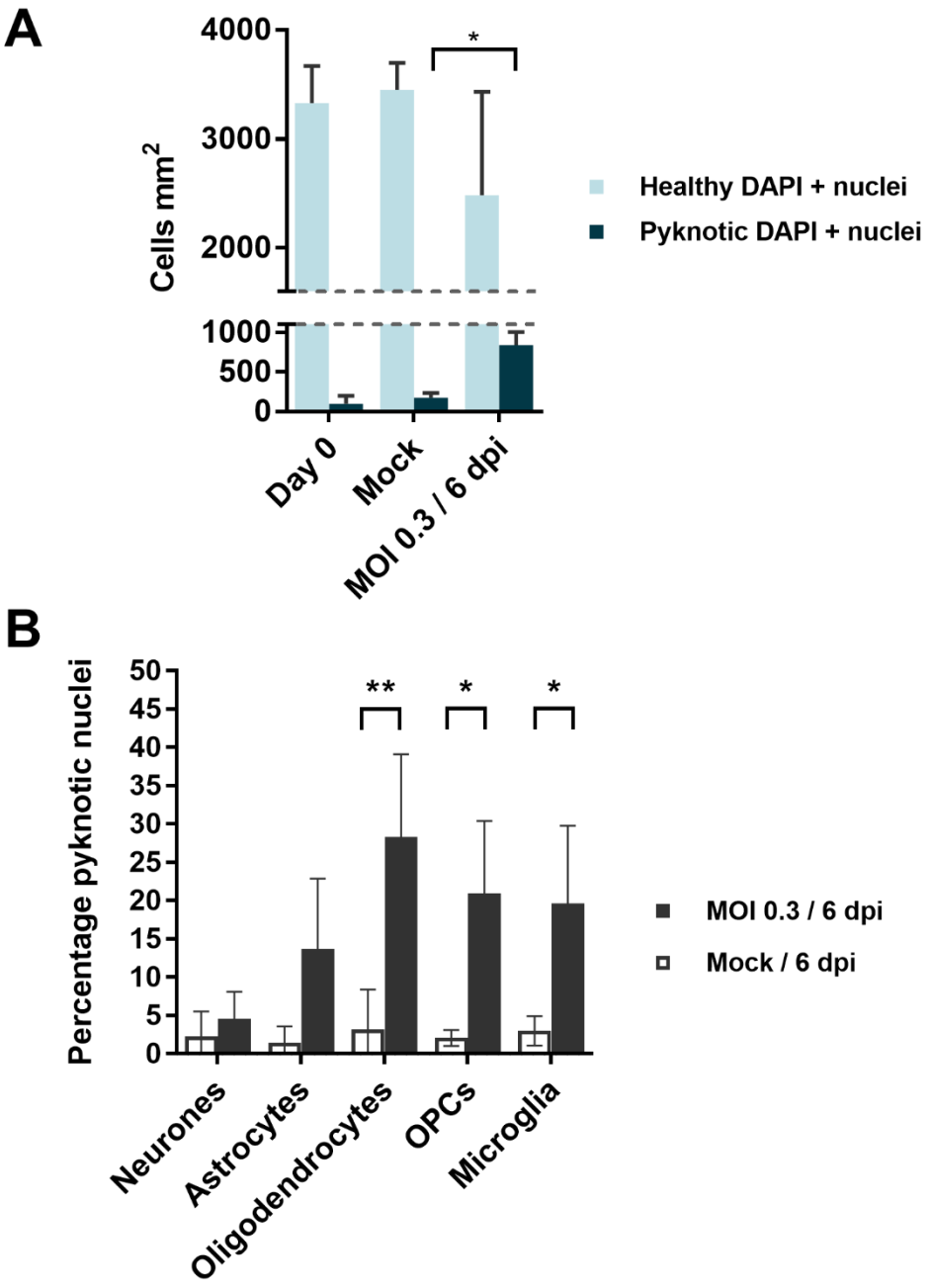


**Figure 4–16 Examining injury and cell death as determined by pyknotic nuclei count.**
*Ifnar1* KO CNS co-cultures were infected at DIV18 at a MOI of 0.3 and fixed with 4% formaldehyde at 6 d.p.i. Coverslips were immunolabelled against ZIKV-E (mouse anti-ZIKV E [primary antibody], goat anti-mouse IgG Alexa Fluor ® 488), a cell-type specific marker (neurons: rabbit anti-NeuN; astrocytes: rabbit anti-GFAP; oligodendrocytes: rat anti-PLP/DM20; OPCs: rabbit anti-NG2; microglia: rat anti-F4/80. Secondary antibodies: goat anti-rat IgG or goat anti-rabbit IgG conjugated with Alexa Fluor ® 594) and were counterstained with DAPI.Images were taken at 20x magnification and cells enumerated for total number of DAPI nuclei, and 'dying' DAPI nuclei (i.e. pyknotic nuclei) for each condition and per cell type. A) light blue bars are healthy DAPI nuclei in comparison to pyknotic nuclei in dark blue – this is measured in cells per $mm^2$ B) Percentage pyknotic nuclei per cell type. Black bars indicate MOI 0.3/d d.p.i and white bars indicate Mock infected cultures. * indicates $p< 0.05$ and ** $p< 0.005$ , bars represent mean ± SD. n=3

To investigate the possible causes of injury to myelin and axons, cell type specific pyknotic nuclei counts were performed. Cultures were infected at a MOI of 0.3 PFU/cell or mock infected and incubated at 37 $^{o}$C for 6 days until DIV24. There was a significant increase in the number of pyknotic nuclei per mm$^2$ at 6 d p.i. when cultures are infected with ZIKV at a MOI of 0.3, compared to mock infected cultures. Significant increases in the percentage of pyknotic nuclei pertaining to oligodendrocytes, OPCs and microglia were observed, with over 25% of total oligodendrocyte nuclei appearing pyknotic. As mentioned previously, oligodendrocyte nuclei can appear quite small and condensed in images taken for enumeration purposes. However, the rise in oligodendrocyte injury and/or cell death indicated by pyknotic nuclei counts may help explain the extensive myelin loss observed in ZIKV infected cultures at this timepoint. It is noteworthy that the percentage of pyknotic nuclei pertaining to neurons increased only slightly – suggesting that axonal injury occurs in absence of apparent neuronal cell death.

In summary, white matter structures are injured when CNS co-cultures are infected with ZIKV at a developmental stage reflective of late foetal/early post-natal life.

#### 4.3.4.1 Soluble factors alone are insufficient to induce injury to white matter components of the CNS

Results in section 4.3.4 (Figure 4–13) demonstrated that myelin was obliterated when co-cultures were infected with ZIKV at a MOI of 0.3 PFU/cell for 6 days. An increase in the percentage of pyknotic nuclei cell counts suggested that the loss of myelin could be a result of increased oligodendrocyte cell death. To rule out the possibility that myelin injury could be caused by inflammatory molecules produced by the culture during infection, culture media from infected and uninfected co-cultures were examined.

CNS co-cultures were infected with ZIKV at a MOI of 0.3 PFU/cell (or mock infected) and culture supernatants were harvested at 6 d p.i. The supernatant from infected and uninfected CNS co-cultures were exposed to a UV lamp to inactivate ZIKV virus (refer to Section 2.8.2.1 for full methodology). Conditioned media (UV inactivated supernatant) were mixed with fresh media to negate any

effects that might be observed due to nutrient deficits. The subsequent mixtures were transferred onto fresh DIV18 cultures (when myelination is starting to take place). These cultures were maintained until DIV 24 (when extensive myelin loss is observed in ZIKV infected cultures - Figure 4–14), with refeeds taking place every 48 h with 1:1 conditioned:fresh media. On DIV24, samples were fixed in formaldehyde and immunolabelled against SMI31 and MBP (axons and myelin, as in Figure 4–13- Figure 4–17A), in addition to PLP/DM20 (myelin) and ZIKV E protein (Figure 4–17B).

There was no apparent difference in overall myelin quality and axonal health between media which originated from infected or mock-infected cultures (Figure 4–17A). There was no positive staining for ZIKV E protein in Figure 4–17B, indicating that the UV inactivation of ZIKV was successful (see Figure 4–17B inset for staining pattern of supernatant which was not inactivated by UV). These results indicate that injury to white matter structures is unlikely the result of soluble factors alone.

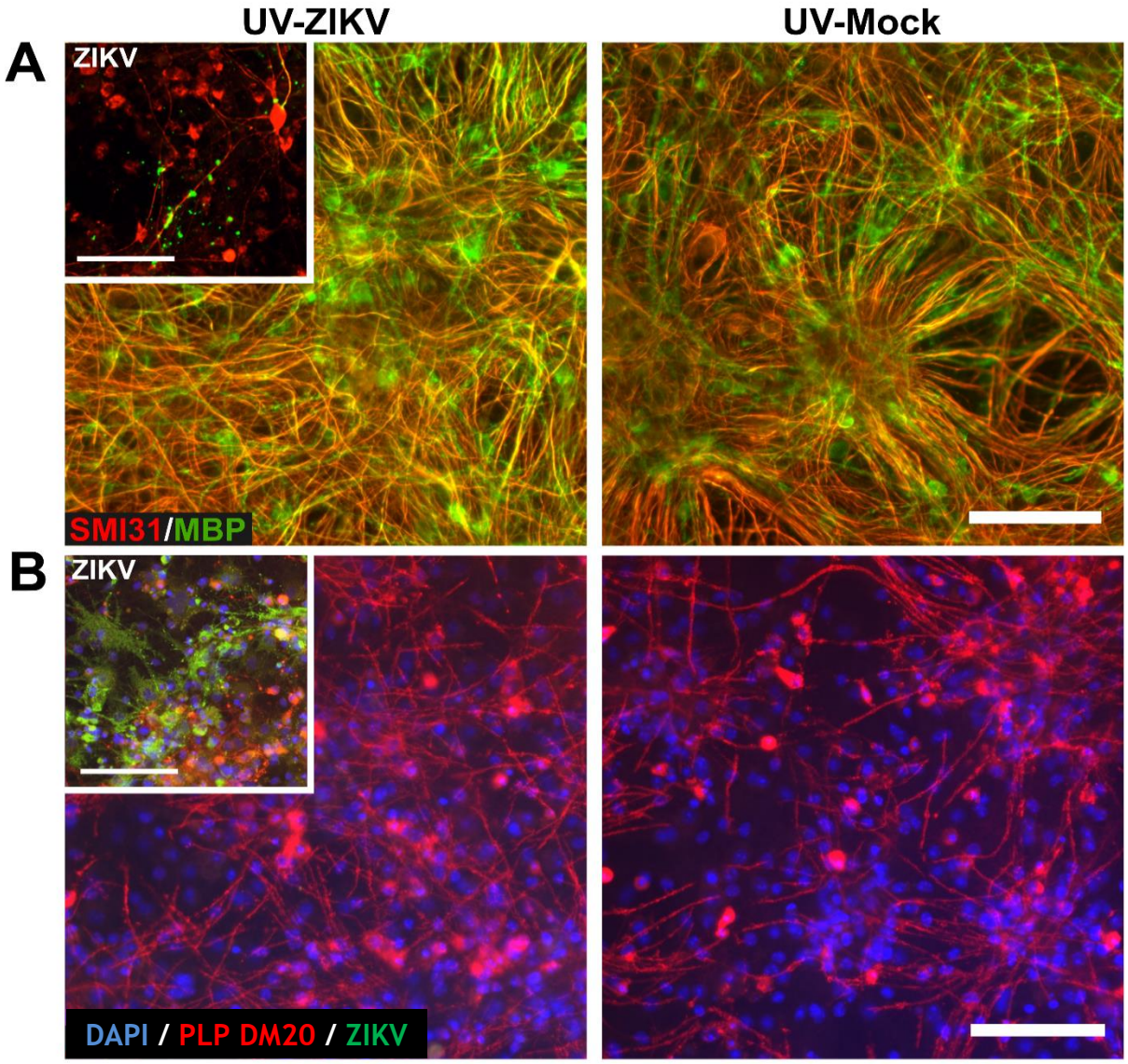


**Figure 4–17 UV inactivated, ZIKV infection conditioned media does not cause injury to white matter structures.**
CNS co-cultures were infected with ZIKV at a MOI of 0.3 PFU/cell and incubated at 37 $^{o}$C for 6 days. The supernatant was subjected to UV-inactivation before being transferred onto fresh DIV18 CNS co-cultures. These cultures were maintained until DIV24 (6 days post-transfer) and were subjected to immunofluorescence analyses. (**A**) CNS co-culture imaged at 6 days post-transfer, stained for axons (mouse anti-SMI31 [primary antibody], goat anti-mouse Alexa Fluor ® 488 [secondary antibody]; shown in red [false coloured]) and myelin (rat anti-MBP [primary antibody], goat anti-rat IgG Alexa Fluor ® 594 [secondary antibody]; shown in green [false coloured]). Inset image depicts MOI 0.3/ 6 d p.i. culture also stained for axons (red) and myelin (green) – demonstrating extensive myelin and axonal injury. (**B**) CNS co-culture images at 6 days post-transfer, stained for ZIKV-E (mouse anti-ZIKV E [primary antibody], goat anti-mouse IgG Alexa Fluor ® 488 [secondary antibody] green) and myelin (rabbit anti-PLP/DM20 [primary antibody], goat anti-rabbit IgG Alexa Fluor ® 594 [secondary antibody[; red) Inset image depicts MOI 0.3/ 6 d p.i. culture positive for ZIKV E staining (green) and abnormal myelin staining (red). Scale bar: 100 µm. Representative images are displayed from three individual biological replicates, for which a minimum of two coverslips were analysed per condition.

### 4.3.5 Supporting glial cells are required for ZIKV infection of mature neurons

Previous results in this chapter have established that neurons are less susceptible to ZIKV infection, compared with other principle CNS cell types, in *Ifnar1* KO CNS co-cultures (Section 4.3.2, Figure 4–7). However, axonal pathology is observed during prolonged ZIKV infection; a phenotype which appears to accompany myelin loss and cannot be recapitulated by the transference of UV inactivated ZIKV conditioned media (Section 4.3.4, Figure 4–13 and Figure 4–17). To determine if axonal injury is induced by direct ZIKV infection of neurons, 'pure' neuronal cultures were generated from spinal cord tissue. Two types of neuronal cultures were generated. One culture had been depleted of a moderate amount of contaminating glial cell types during preparation and was maintained only in neurobasal medium (NBM). The other culture had been supplemented with 5-Fluoro- 2'deoxyuridine (NBM + FUDR). FUDR is an anti-mitotic drug, which depletes the culture of proliferating cell types such as contaminating glial cells, whilst sparing mature post-mitotic neurons. The purity of neuronal cultures was assessed by V.Schultz prior to use and is demonstrated in Figure 4–18. Culture purity was assessed by taking cell type specific DAPI counts of principle CNS cell types, as previously described in section 4.3.2. Cultures maintained in NBM alone contain more contaminating glial cell types than those supplemented with FUDR. The predominant contaminating cell types were Olig2+ cells (Oligodendrocytes and OPCs).

Neuronal cultures were infected with ZIKV (MOI of 0.3 PFU/cell) and were fixed in 4% formaldehyde for 1 hour at 6 d p.i. Cultures were then immunolabelled against varying targets to examine: I) culture purity (Figure 4–19), II) axonal injury (Figure 4–20) and III) ZIKV infection (Figure 4–21, Figure 4–22). Under these conditions, whole CNS co-cultures possessed a decimated myelin sheath and axonal processes were injured (Cumberworth, Barrie et al. 2017). However, in both types of neuronal cultures (+/- FUDR), axonal networks remained intact (Figure 4–20). At 6 d p.i. neuronal cultures supplemented with FUDR did possess few contaminating glial cells, though this was a marked reduction in comparison to cultures maintained in NBM alone (Figure 4–19).

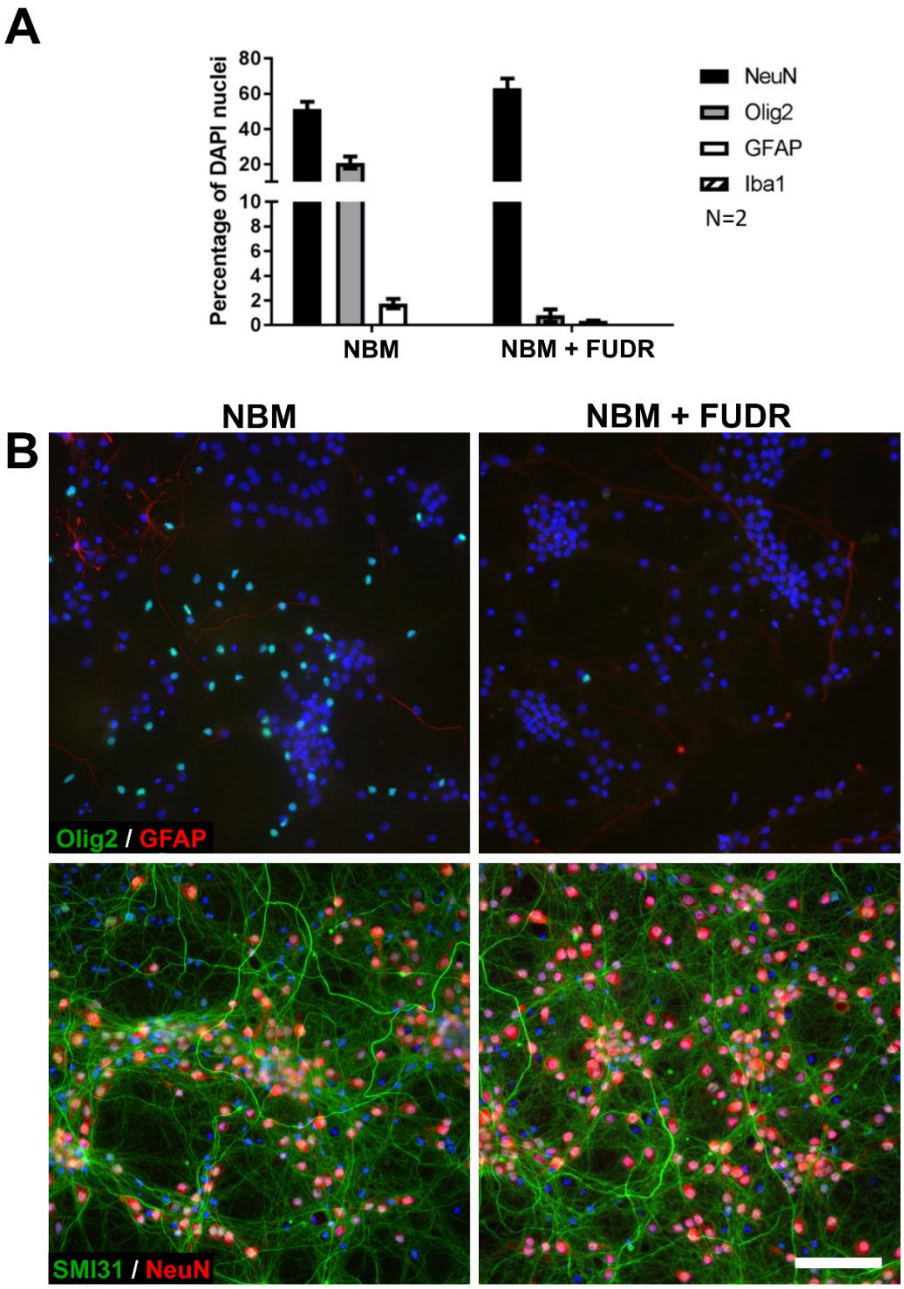


**Figure 4–18 Purity testing of neuronal cultures grown in the presence or absence of FUDR**
Culture generation, purity testing and figure components were kindly provided by V Schultz. Neuronal cultures were grown in neurobasal medium (NBM) in the presence or absence of mitotic inhibitor, FUDR (5-fluorodeoxyuridine). FUDR is used to curtail the growth of proliferative cell types within neuronal cultures (i.e. contaminating glial cell types) whilst sparing post-mitotic neurons (Oorschot, 1989). (**A**) A graph detailing the percentage of each cell type present in cultures grown in NBM alone or NBM+FUDR. NeuN: neurons, Olig2: oligodendroglia (oligodendrocytes and OPCs), GFAP: astrocytes, Iba1: microglia. Bars represent mean ± SD. (**B**) representative images of neuronal cultures grown in NBM or NBM+FUDR. Top row: cultures are immunolabelled against oligodendroglia (mouse anti-Olig2 [primary antibody], goat anti-mouse IgG Alexa Fluor ® 488 [secondary antibody]; green) and astrocytes (rabbit anti-GFAP [primary antibody], goat anti-rabbit IgG Alexa Fluor ® 594 [secondary antibody] ;red). Bottom row: cultures are immunolabelled against neuronal components – axons (mouse anti-SMI31, goat anti-mouse IgG Alexa Fluor ® 488 [secondary antibody]; green) and neuronal nuclei (rabbit anti-NeuN [primary antibody], goat anti-rabbit IgG Alexa Fluor ® 594 [secondary antibody];red). Nuclei were counterstained with DAPI (blue). Scale bar: 100 µm.

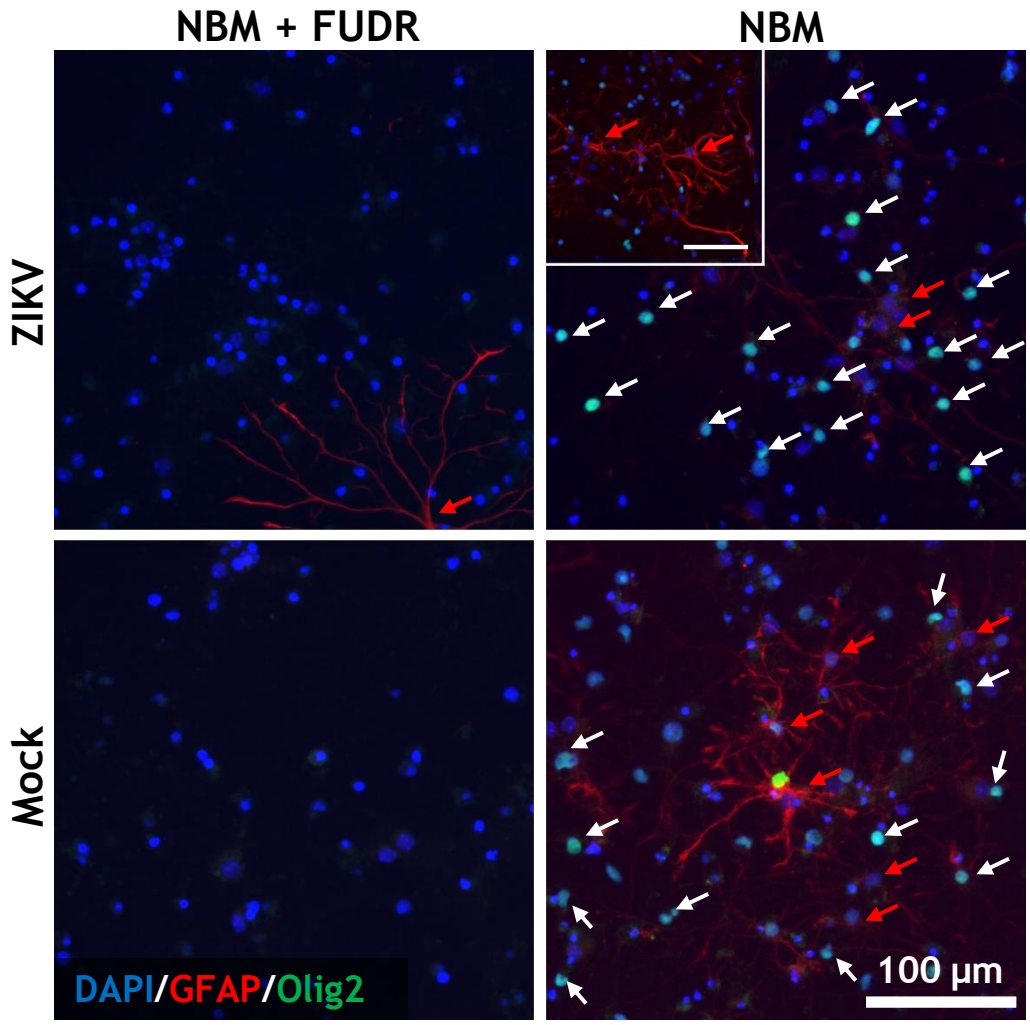


**Figure 4–19 Purity testing at 6 d p.i. of neuronal cultures maintained in neurobasal media alone or supplemented with FUDR.**
Neuronal cultures were grown in neurobasal medium (NBM) in the presence or absence of mitotic inhibitor, FUDR (5-fluorodeoxyuridine). Neuronal cultures were infected with ZIKV (MOI 0.3) or mock infected for 6 d p.i., with media replenishments taking place at 2 and 4 days post infection. At 6 d p.i. cultures were fixed and immunolabelled with antibodies raised against contaminating glial cell types; oligodendrocytes and OPCS (mouse anti-Olig2 [primary antibody], goat anti-mouse IgG Alexa Fluor ® 488 [secondary antibody]; green) and astrocytes (rabbit anti-GFAP [primary antibody], goat anti-rabbit IgG Alexa Fluor ® 594 [secondary antibody]; red).. Nuclei were counterstained with DAPI (blue). White arrows indicate oligodendroglia and red arrows indicate astrocytes.Inset image (NBM, top right), demonstrates astrocyte presence in ZIKV infected cultures in addition to Olig2+ cell types. Scale bar: 100 µm. Representative images are shown for 2 biological replicates, with 3 coverslips examined per replicate.

In the majority of cultures assayed by immunofluorescence analysis, there were no visible signs of ZIKV infection , except for one area of interest in neuronal cultures maintained in NBM only (n=2 biological replicates, 2 coverslips per condition per replicate) (Figure 4–21). The one focus of ZIKV infection occurred in a mixture of neuronal and non-neuronal cell types within this culture (Figure 4–22). It is therefore reasonable to suggest that for neurons to become infected, a high local concentration of virus is required, which may be provided by

infected non-neuronal cell types interacting with neuronal processes (Figure 4–22iii). Positive staining for the ZIKV envelope protein was also seen in neuronal processes emanating from NeuN positive cell bodies (Figure 4–22i/ii). It may be possible that neuronal infection is mediated by neuronal cell-cell contacts; if neurons were intrinsically susceptible to ZIKV infection, more neurons would appear positive for ZIKV E staining in distant regions.

The rarity of neuronal ZIKV infection within these cultures could be attributed in part to the type of neurons present in these cultures. Neuronal cultures are derived from murine *Ifnar1* KO spinal cords. These dissociated cell cultures lack region specific expression of genes that might typically be found *in vivo* (Cumberworth et al., 2017a). Additionally, a mixture of interneurons and 'motor' neurons are present within these cultures. The 'motor' neurons in these cultures do not innervate muscle – exemplifying alternative gene expression and subsequent functional phenotypes of culture vs *in vivo* cells. It has been demonstrated that cortical neurons can be infected with ZIKV (van den Pol et al., 2017, Olmo et al., 2017). It is therefore possible that ZIKV simply does not target the predominant neuronal cell type within this culture system.

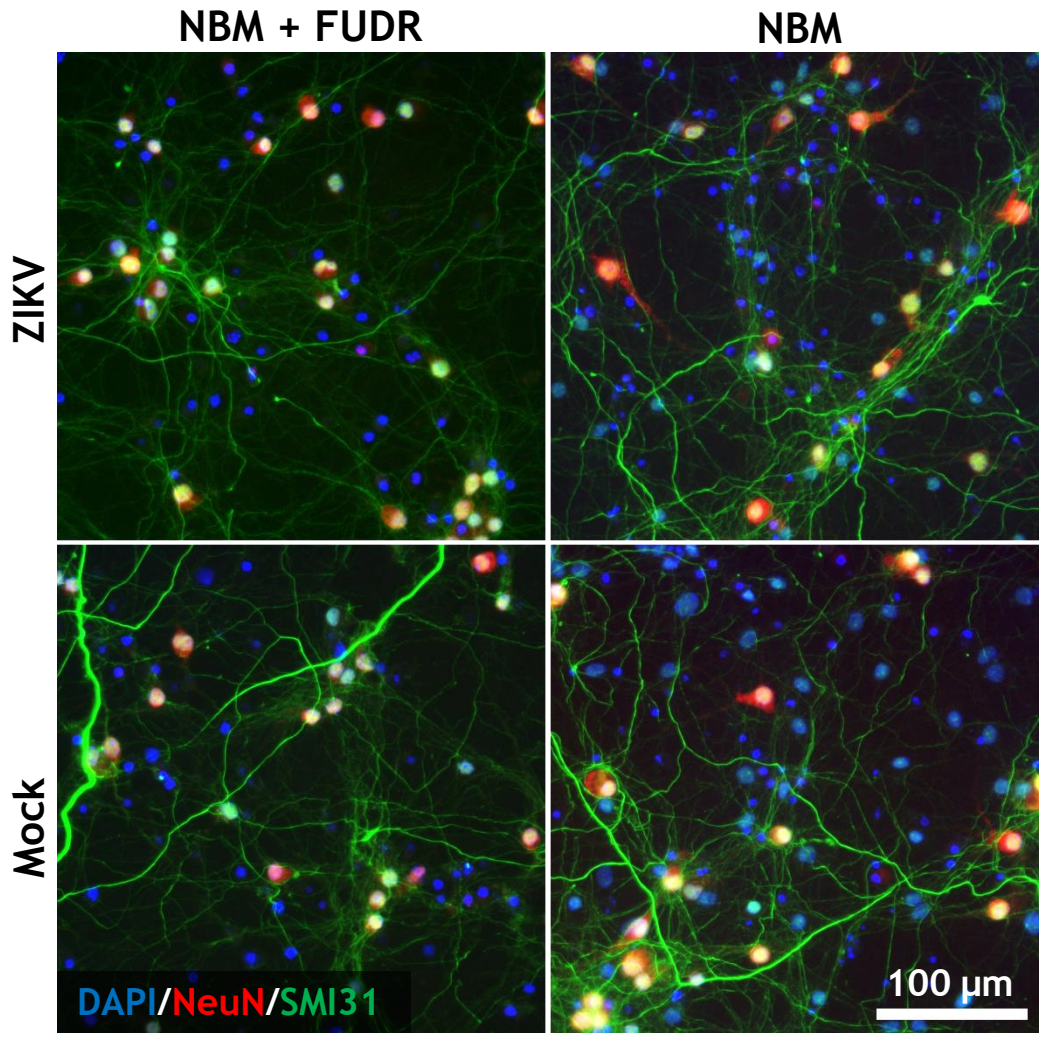


**Figure 4–20 ZIKV infection does not induced axonal damage in neuronal cultures maintained in the presence or absence FUDR.**
Neuronal cultures were grown in neurobasal medium either in the presence or absence of FUDR (5-fluorodeoxyuridine). Neuronal cultures were infected with ZIKV at a MOI of 0.3 PFU/cell for 6 days, with maintenance culture media replenishments taking place at 2 and 4 d p.i. Cultures were fixed at 6 d p.i. and immunolabelled with antibodies targeting a component of axons (mouse anti-SMI31, goat anti-mouse IgG Alexa Fluor ® 488 [secondary antibody]; green) and neuronal nuclei (rabbit anti-NeuN [primary antibody], goat anti-rabbit IgG Alexa Fluor ® 594 [secondary antibody];red). . Nuclei were counterstained with DAPI (blue). Scale bar: 100 µm. Representative images are shown for 2 biological replicates, with 3 coverslips examined per replicate.

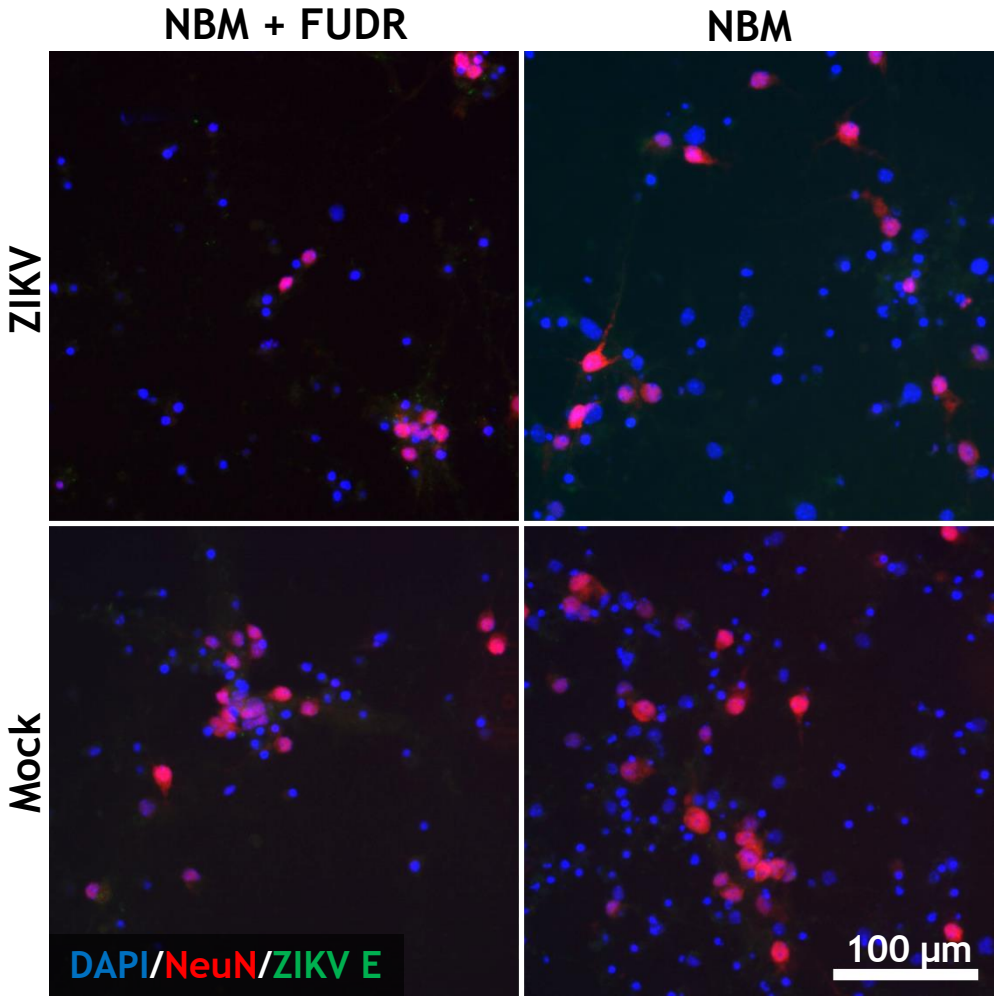


**Figure 4–21 'Pure' neuronal cultures are extremely resistant to ZIKV infection.**
Neuronal cultures were grown in neurobasal media (NBM) with or without FUDR (5-fluorodeoxyuridine). Neuronal cultures were infected with ZIKV at a MOI of 0.3 PFU/cell for 6 days, with maintenance culture media replenishments taking place at 2 and 4 d p.i. Cultures were fixed at 6 d p.i. and immunolabelled with antibodies against ZIKV E (mouse anti-ZIKV E [primary antibody], goat anti-mouse IgG Alexa Fluor ® 488 [secondary antibody]; green) and neuronal nuclei (rabbit anti-NeuN [primary antibody], goat anti-rabbit IgG Alexa Fluor ® 594 [secondary antibody]; red). Nuclei were counterstained with DAPI (blue). Representative images are shown for 2 biological replicates, with 3 coverslips examined per replicate.

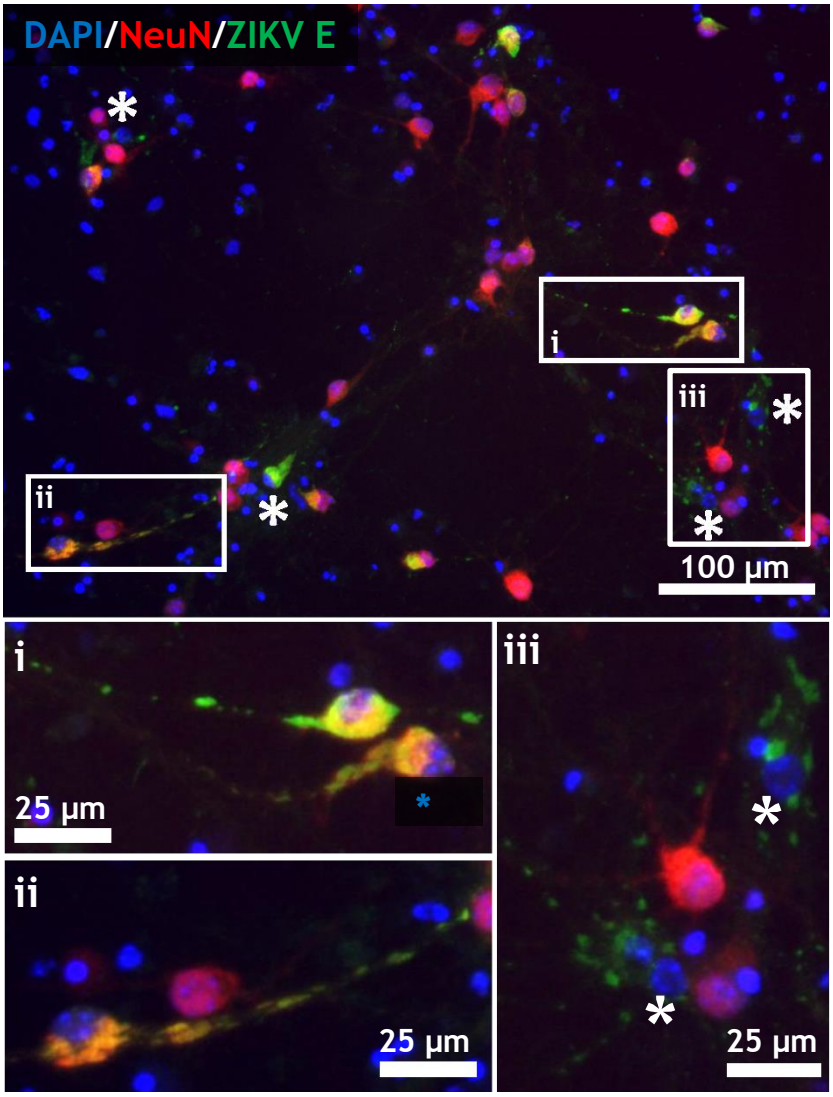


**Figure 4–22 Foci of ZIKV infected cells , including neruons, in 'impure' neuronal culture**
Neuronal cultures were maintained in neurobasal media alone, and were infected with ZIKV at a MOI of 0.3 PFU/cell for 6 days, with maintenance culture media replenishments taking place at 2 and 4 d p.i. Cultures were fixed at 6 d p.i. and immunolabelled with antibodies against ZIKV E ZIKV E (mouse anti-ZIKV E [primary antibody], goat anti-mouse IgG Alexa Fluor ® 488 [secondary antibody]; green) and neuronal nuclei (rabbit anti-NeuN [primary antibody], goat anti-rabbit IgG Alexa Fluor ® 594 [secondary antibody]; red). .Cell nuclei were counterstained with DAPI (blue). In the absence of the mitotic inhibitor FUDR, higher quantities of contaminating glial cells are present in neuronal cultures. This image represents the only focus of infection detected throughout experimentation using 'purified' neuronal cultures (biological replicates n=2, 3 coverslips per replicate). Neurons are indicated by the characteristic red stain for NeuN, found in the nuclei and cell bodies of neurons. Other glial cells are indicated by the presence of blue DAPI nuclei, which are not positive for NeuN staining. (*) Indicates an infected glial cell (i.e. perinuclear green staining, blue nucleus, no red NeuN stain), (I/II) Highlights infected neurons (i.e. perinuclear green staining, blue nucleus, red NeuN stain in nucleus/cell body). In this image, the green ZIKV E staining extends the length of the neuronal process (III) Demonstrates uninfected neurons in the presence of infected glial cell types.

## 4.4 Discussion

Identifying the infectious targets of ZIKV within the CNS and PNS is paramount in understanding the pathogenesis of ZIKV infection. The primary aim of this chapter was to determine the susceptibility of cells within the CNS and PNS to ZIKV infection and observe the consequences of ZIKV infection within these systems. Mixed mouse-embryo derived cell co-cultures which replicate several aspects of intact central and peripheral nervous systems were used in these studies (kindly generated by either J Barrie or V Schultz). Such cultures were generated from E13 embryonic mouse spinal cord or dorsal root ganglion to give rise to CNS and PNS cultures respectively (in the background of mouse strains A129, *Ifnar1* KO or WT).

### 4.4.1 PNS cells are highly resistant to ZIKV infection in comparison to CNS cells

The pathobiology surround ZIKV-associated GBS, a peripheral neuropathy, is unknown. Therefore, to determine whether ZIKV-GBS could be attributed to direct infection of the PNS, this study infected PNS co-cultures with ZIKV PE243 and quantified levels of ZIKV positive cells. These data demonstrate that PNS cells are less susceptible to ZIKV infection than their CNS counterpart generated from the same embryo, even if the absence of type I IFN responses (Figure 4–4). The apparent lack of infection within PNS cultures was found not to be a result of potential inhibitory factors within PNS maintenance media (Figure 4–5).

Contrary to these findings, is the work of Oh et al,. 2017 whereby A129 *Ifnar1* KO mice were infected with ZIKV (ZIKV strain SZ01 [GenBank accession:KU866423], propagated in C6/36 cells) by intraperitoneal injection and immunofluorescence analysis revealed infection of PNS DRG neurons (Oh et al., 2017). Furthermore, this study demonstrates infection and injury of peripheral neurons derived from human neural crest stem cells. However, Oh et al. made no efforts in the way of quantifying levels of ZIKV infection. The representative images shown are of very small area and display only 1-2 infected neurons in a given space. The study claims that ZIKV positive DRG neurons are also positive for cleaved caspase 3 – an indicator of apoptosis- and suggest ZIKV infection induces apoptosis in DRG neurons. Given the small sample area, it is not possible

to ascertain the extent of, nor the effect of, ZIKV infection within DRG neurons from this study alone.

Another study (Volpi et al., 2018) also claimed to contradict the findings within this chapter. However, upon further investigation it seems that they report similar findings as described here in terms of levels of infection within the PNS. Volpi et al., employs DRG explant cultures (aka PNS co-cultures – background strain C57BL/6 *Ifnar1* KO) to investigate ZIKV infection in the PNS, using ZIKV strains MR766 and PRVABC59 (a strain isolated during the 2015/16 outbreak). The study infects PNS co-cultures with 7 x $10^5$ PFU of MR766 or 1.2 x $10^6$ PFU of PRVABC59 with an infection time of 4 hours. This is in contrast to studies conducted in this chapter which utilises ZIKV PE243 infecting PNS co-cultures with the equivalent of 1.2 x $10^5$ PFU (MOI 0.3) or 1.2 x $10^6$ PFU (MOI 3) with a virus exposure time of 1 hour. Virus propagation methods were not disclosed in this paper.

Volpi *et al.*, 2018 also makes no attempt to quantify the level of infection within PNS cultures and refers only to qualitative immunofluorescence studies. The images displayed in this paper primarily focus in on the DRG cell body cluster when attempting to identify ZIKV infection, instead of neurons extending out-with the DRG. In MR766 infected cultures, higher levels of infection are present, a finding consistent with data reported in this thesis (Chapter 3 Section 3.3.4). MR766 is a ZIKV strain first isolated in Uganda but has since undergone over 100 passages in a mixture of the brains of suckling mice and cell culture. Therefore, MR766 could represent a highly adapted ZIKV strain to mammalian cells, and perhaps even cells of neural origin. As demonstrated in Section 3.3.4, MR766 displays higher levels of infection in *Ifnar1* KO CNS cultures in comparison to infection with ZIKV PE243 produced in either insect or mammalian cells. It is therefore unsurprising that there are higher levels of infection in the studies of the PNS conducted by Volpi et al which utilise a similar infection model system.

The infection levels of ZIKV strain PRVABC59 in the paper by Volpi *et al* are markedly less than that of MR766 samples. At 3 d p.i, the representative image displays only one cell infected with PRVABC59. Despite infecting cultures for a longer time period (1.2 x $10^6$ PFU/4 hours compared with 1.2 x $10^6$ PFU/1 hour) this finding does not appear too dissimilar to those in this chapter (ZIKV PE243

infection of *Ifnar1* KO PNS co-cultures at 72 h p.i. are 1%). Given that no attempts at quantification were made, it is difficult to ascertain any differences in infection levels without a direct comparison of data obtained by equivalent methods. However, the data presented by Volpi *et al.*, 2018 do not appear to demonstrate markedly increased infection levels despite differences in ZIKV strains, infection timeframe and mouse background strain to produce cultures.

Volpi *et al*. also demonstrate a slight visual decline in myelin staining at 10 d p.i. in PNS co-cultures infected with either MR766 or PRVABC59. This is not a line of investigation pursued in this chapter; PNS co-culture infections in this chapter only explore PNS infection up to 72 h p.i. (3 d p.i) with MOI 3 (equivalent of 1.2 x $10^6$ PFU). Despite low infection levels within PNS cultures in this chapter (section 4.3.1), cell type specific analyses revealed the myelinating cell type of the PNS, Schwann cells, can be infected with ZIKV (Cumberworth et al., 2017a). In Volpi *et al*. virus titre in culture supernatant of PNS cultures increases over time indicating active viral reproduction. This is a finding not replicated by our own studies which indicate that virus titres decrease over time in PNS culture supernatant. Perhaps the infection in the cultures described by Volpi *et al*. targeted Schwann cells. Follow up studies would need to confirm viral replication within PNS cultures, and the apparent loss of myelin observed in studies by Volpi *et al*. However, pathological findings demonstrate that the DRG is unaffected in case reports of ZIKV infected infants (Chimelli et al., 2017).

Further studies are required to clarify the infection status of PNS cells both by *in vitro* and *in vivo* methods. Given the apparent lack of infection *in vitro* and clinical findings and that GBS is typically regarded as a post infectious auto-antibody mediated disorder, it might seem more prudent to identify gangliosides implicated in PNS injury that may contribute to the development of GBS.

### 4.4.2 ZIKV infection in CNS injures white matter structures

In the most recent ZIKV outbreak, striking complications of the CNS were observed in neonates born to mothers infected with ZIKV during pregnancy. The underlying cause of the associated neurodevelopmental disorders, and the true extent of the damage is still relatively unknown. At the time of investigation, little was understood regarding the tropism of ZIKV within the CNS, or indeed if

the neurological complications of ZIKV were strain specific. Findings within this chapter indicate that all principle cell types within the CNS can be infected with a strain of ZIKV isolated from a patient with no reported neurological symptoms (ZIKV/H.sapiens/Brazil/PE243/2015 Genbank accession number KX197192 (Donald et al., 2016) – referred to as ZIKV or ZIKV PE243) (Figure 4–6 and Figure 4–7). Type I IFN responses play a protective role in ZIKV infection of CNS co-cultures, reducing infection levels from 19% to 4% in *Ifnar1* WT cultures (MOI 3/72 h p.i.). ZIKV infection of *Ifnar1* KO cultures lead to an increase in pyknotic nuclei, an indicator of injury and cell death (Figure 4–9). These data imply that this strain of ZIKV is capable of inflicting CNS injury, despite not being associated with a patient exhibiting neurological disease. This might indicate that infection of neural cell types is not strain specific and may be dependent on alternative factors such as the immunological status of the patient, amongst other factors.

Myelin damage in ZIKV infected *Ifnar1* KO CNS co-cultures was first observed at 72 h p.i. (MOI 3), when broken myelin sheaths were increasing in abundance (Figure 4–11). Axons and myelin were substantially depleted when challenging CNS co-cultures at a developmental stage reflective of late foetal development, when myelination was first beginning, and allowing cultures to progress to a stage when myelination should be nearing completion (post-natal life) (Figure 4–13). Whether the loss of myelin represents a de- or a dys-myelinating phenotype is unclear. Demyelination is the destruction of pre-existing myelin whereas dysmyelination describes impaired myelin development. Oligodendrocytes are the leading target for ZIKV infection in CNS co-cultures presenting the highest percentage level of infection at 24 (MOI 0.3) and 72 h p.i. (MOI 3) (Figure 4–7). The lower infectious dose and shorter timepoint was used to ascertain the initial infectious targets of ZIKV infection; these data reflect that oligodendrocytes are a particularly vulnerable cell type for ZIKV infection. Moreover, at 6 d p.i. (when myelin loss is observed), there was a significant increase in the percentage of pyknotic nuclei pertaining to oligodendrocytes (Figure 4–9). Therefore, this may be indicative of a demyelinating phenotype that is secondary to oligodendrocyte cell death as opposed to impaired myelin development. Though this does not explain the observed axonal injury (Figure 4–15).

Data presented in this chapter suggest neuronal infection within CNS co-cultures is relatively rare; neurons possessed the lowest percentage of infection at 72 h p.i. with ZIKV at MOI 3 (9%) (Figure 4–7). Furthermore, no infection was observed in 'pure' neuronal cultures derived from spinal cord - except for in the presence of contaminating glia (Figure 4–21 and Figure 4–22). However, this observation was only made in one area of a singular coverslip of one biological replicate (biological replicates n=2, 3 coverslips per biological replicate) (Figure 4–22). This suggests that neurons derived from the spinal cord may be intrinsically resistant to ZIKV infection, requiring supporting glial cells to become infected. It is unlikely that neurons in CNS co-cultures express the entire complement of gene products which are produced *in vivo*, as a result of absent or mis-localised CNS region-specific cell fate determinants (Cumberworth et al., 2017a). Neurons present in the CNS co-culture are a mixture of neuronal subtypes. Neurons derived from the cortex are susceptible to ZIKV infection (van den Pol et al., 2017, Azouz et al., 2019). Therefore, it may be interesting to conduct studies to determine the susceptibility of various neuronal types.

Complementary to the *in vitro* data presented in this chapter, it was shown that neuronal infection in a variety of CNS regions occurred secondary to infection of glial cells, primarily astrocytes, in the brains of mice infected with ZIKV on the day of birth by intraperitoneal injection (van den Pol et al., 2017). Whether these data implies neurons become infected via cell-cell spread or they just require a high local concentration of virus in order to become infected requires further investigation.

Axonal injury occurred in absence of substantial neuron infection and cell death (Figure 4–15). The transfer of UV inactivated ZIKV-conditioned media did not induce injury to myelin or axonal structures, suggesting that the damage incurred is not mediated by soluble factors alone (Figure 4–17). The only substance which causes demonstrable axonal injury *in vitro* is nitric oxide (Smith et al., 2001). Nitric oxide is important for synaptic plasticity in the CNS,and involved in neurotransmission; however, if nitric oxide is produced in excess it becomes noxious (Calabrese et al., 2007).Given the short half-life of nitric oxide, if present in UV-ZIKV conditioned media it is unlikely to have substantial effects unless replenished often (i.e. by a producer of nitric oxide) (Hakim et

al., 1996). Both astrocytes and microglia are producers of nitric oxide in the central nervous system; production of nitric oxide can be induced by viral infection. It would be interesting to know whether there is increased production of this molecule in ZIKV-infected co-cultures, and if this may be a cause of white matter injury in CNS co-cultures.

The injury to white matter structures (myelinated axons) observed in CNS co-cultures is consistent with pathological findings in clinical case studies, whereby a reduction in CNS white matter is demonstrated (Chimelli et al., 2017, Chimelli and Avvad-Portari, 2018). In these cases, the spinal cord was unharmed by ZIKV infection. In this chapter, white matter injury was modelled in cultures of spinal cord origin, these findings suggest that other determinants factor in the exclusion of spinal cord injury in these cases.

CNS co-cultures infected at a developmental timepoint reflective of late foetal life displayed extensive myelin loss when observed at a timepoint modelling infancy/childhood (Figure 4–13). Myelin is required for optimal cognitive function in addition to learning and memory. It is prudent that follow up studies be conducted with babies born with inapparent symptoms of ZIKV congenital syndrome, as more subtle neurodevelopmental defects may be present e.g. learning disorders (Fields, 2008, Stanelle-Bertram et al., 2018). This is exemplified by a report from a prospective cohort study completed with babies born to mothers who had PCR confirmed ZIKV infection during pregnancy during the 2015/16 ZIKV outbreak in Brazil (Nielsen-Saines et al., 2019). The study involved the clinical and neurological assessment of 216 infants with a median age of 18 months (range 7-32 months). Notably, 35% of infants in this study had below average for age language function, and 31.5% had other neurodevelopmental/ophthalmic/auditory impairments. Interestingly this follow-up study demonstrated that normal assessments at birth did not guarantee normal results in subsequent neurological assessments; 25% (17/68) of children with normal early assessments had below-average neurodevelopmental assessments at follow-up. Three infants in the cohort were diagnosed with autism spectrum disorder (ASD); further investigations are required to investigate this potential link between ZIKV and ASD (Vianna et al., 2018).

It is therefore essential that follow-up analyses of children born to mothers with confirmed ZIKV infection continue, in order to understand the full complement of neurodevelopmental sequalae.

## 4.5 Summary

- Type I IFN plays a protective role in ZIKV infection of CNS co-cultures.

- PNS cells are less susceptible to ZIKV infection than CNS cells, even in the absence of type I IFN. Given the lack of PNS infection, it is unlikely that ZIKV associated GBS is a result of direct viral infection of the PNS.

- Of the principle CNS cell types, oligodendroglia (oligodendrocytes and OPCs) are particularly vulnerable to ZIKV infection and injury.

- White matter structures are injured during ZIKV infection of *Ifnar1* KO CNS co-cultures, resulting in substantial myelin and axon loss– this injury is not caused by soluble factors alone but may be directly due to virus infection.

- CNS neurons derived from *Ifnar1* KO spinal cord are particularly resistant to ZIKV infection in the absence of supporting glial cells – suggesting that axonal injury is unlikely to be a result of direct neuronal infection and instead secondary to the production of inflammatory molecules by cells within inCNS co-cultures.

# 5 Results Chapter 3: Transcriptomic analysis of Zika virus infected Central Nervous System (CNS) co-cultures

## 5.1 Introduction

CNS co-cultures derived from embryonic mice possess all the principle cell types of the CNS: neurons, astrocytes, oligodendrocytes, oligodendrocyte precursor cells and microglia (see Chapter 4 Section 4.2.2 for further details of the roles of individual cell types). CNS co-cultures recapitulate many of the neuro-glial interactions observed in the CNS; furthermore, if matured until 28 days *in vitro*, neurons are fully extended and myelinated (white matter structures) (Thomson et al., 2006). This culture system can be manipulated to represent different developmental timeframes. Data presented in Chapter 4 demonstrated that when infected with ZIKV at a developmental timeframe which crossed late foetal/post-natal stages, much of the white matter structures in CNS co-cultures (*Ifnar1* KO) were destroyed (6 d p.i./144 h p.i.[Section 4.3.4]). Specifically, the myelin sheath is destroyed in addition to substantial axonal damage. Importantly, many neurons presenting axonal injury within the co-cultures did not show signs of infection with ZIKV and appeared to have intact, healthy nuclei, despite neuronal cell bodies swelling and becoming filled with phosphorylated neurofilament (an indicator of neuronal damage (Yuan et al., 2017)). Results in Chapter 4 (Section 4.3.4.1) indicated that this pathology was unlikely to be the result of the action of soluble factors alone. However, it is undetermined whether the loss of myelin associated with ZIKV infection is a result of the death of oligodendrocytes, or a distinct dys- or de-myelination process determined by altered mRNA transcript expression during infection. De-myelination refers to the deterioration of pre-established myelin, whereas dys-myelination is the impaired production of myelin. Therefore, we decided to investigate the transcriptomic profiles of ZIKV-infected CNS co-cultures.

## 5.2 Aims

The aim of this chapter is to compare the transcriptome of early and late stage infected CNS co-cultures in order to identify differentially expressed genes (DEGs) induced by ZIKV infection. These data may highlight candidate transcripts associated with ZIKV-induced white matter injury in CNS co-cultures.

## 5.3 Results

### 5.3.1 Preparation of samples for RNAseq

CNS co-cultures (*Ifnar1* KO) were prepared as previously described (Chapter 4, Section 4.2.2). The cultures were maintained until matured to DIV18 (+/- 2 days), at which time they were mock-infected (i.e. treated with 2% FBS diluted in PBS) or infected with ZIKV at a MOI of 0.3 PFU/cell. At 48 h p.i. and 96 h p.i. cell culture media were aspirated, cells washed once with PBS, and total cellular RNA was harvested from the co-cultures using TRIzol reagent. These timepoints were selected as they preceded the destruction of myelin. It was noted in Chapter 4 Section 4.3.1 that at 24 h p.i ZIKV infection of CNS co-cultures was limited, and at 72 h p.i infection was well established; therefore, 48 h p.i. was selected as the early infectious timepoint. The later timepoint, 96 h p.i., was selected as it appeared that cultures looked unhealthy, but many cell bodies remained when visualised under a light microscope (Figure 5–1). Therefore, this may be a suitable timepoint to highlight any potential damage associated transcripts.

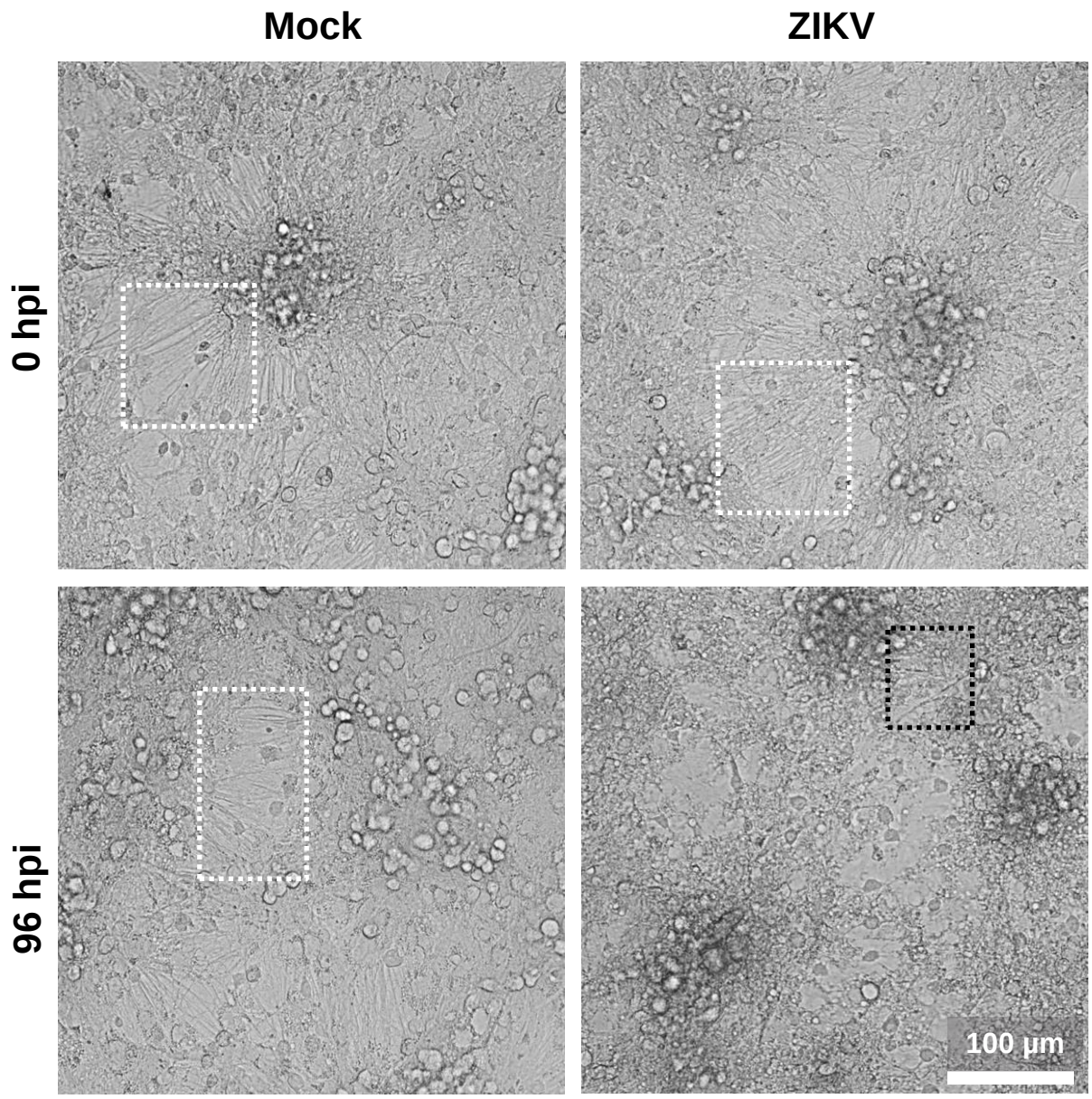


**Figure 5–1 Light microscopy images of CNS co-cultures infected with ZIKV.**
*Ifnar1* KO CNS co-cultures were infected with ZIKV at a MOI of 0.3 PFU/cell or were mock infected. Cultures were imaged using an EVOS FL microscope using the transmitted light setting at 0 h p.i. and 96 h p.i. Examples of fibrous strands, likely white matter structures (myelinated axons), are indicated by white boxes. The black box indicates injured fibrous structures at 96 h p.i.

The quality of extracted RNA was analysed using a High Sensitivity RNA ScreenTape® (Agilent; Table 5–1; performed by Natasha Johnson, MRC University of Glasgow Centre for Virus Research). RNA samples were initially assessed using RINe (RNA Integrity Number equivalent) score, in addition to appearance of 28S and 16S rRNA bands separated through gel electrophoresis. RINe scores above 8.5 are typically considered high enough quality for library preparation to take place (Schroeder et al., 2006, Agilent, 2012). RNA sequencing libraries were prepared by Natasha Johnson using the TruSeq stranded mRNA library prep workflow (illumina). Following the PCR stage of library preparation, a further quality control check of the RNA was performed by RNA screen tape analysis prior to sequencing. Next generation sequencing was performed using the NextSeq® Sequencing System using NextSeq® 500/550 High Output Kit v2 Cartridges.

| Sample | RIN$^{e}$ |
|---|---|
| R1_48h p.i. | 9.1 |
| R1_48h_mock | 8.8 |
| R1_96h p.i. | 9.2 |
| R1_96h_mock | 9.2 |
| R3_48h p.i. | 9.3 |
| R3_48h_mock | 9.1 |
| R3_96h p.i. | 9.5 |
| R3_96h_mock | 9.4 |
| R4_48h p.i. | 9.3 |
| R4_48h_mock | 9.4 |
| R4_96h p.i. | 9.6 |
| R4_96h_mock | 9.6 |

**Table 5–1 RNA integrity numbers of initial RNA samples used to generate libraries for RNAseq analyses.**
RNA quality control was performed using the High Sensitivity RNA ScreenTape®. R1,3,4 indicates to which biological replicate group the sample belonged to.

### 5.3.2 Assessing sample set variation

To assess biological replicate and sample set variation, data were analysed using a multidimensional scaling (MDS) plot (kindly generated by Dr Quan Gu, MRC University of Glasgow Centre for Virus Research) (Figure 5–2). MDS plots assess the degree of similarity between data. In this plot, the transcriptomic profile of a single biological replicate is represented by a sample set name (e.g. virus96h). Samples which are most similar, will cluster together closely, meanwhile dissimilar samples will be distanced further apart.

One biological replicate for all 4 sample sets (virus 96h, virus48h mock96h and mock48h; top half of the MDS plot, Figure 5–2) was disparate from the other 2 biological replicates, which cluster relatively close together with their corresponding sample set counterparts (bottom half of the MDS plot, Figure 5–2). Typically, it would be expected that biological replicates have slight dissimilarities but not to the extent observed in these data. However, RNA from these samples were taken from primary mixed cell cultures. Each biological replicate is representative of cultures taken from embryos pertaining to different litters. Whilst the generation of CNS co-cultures is reproducible and biological effects are robust and reproducible in previous experiments, expression data may vary depending upon the biological composition of cell types present in these cultures. As co-cultures were infected +/- two days, this may have had a greater effect on gene expression than anticipated. Further analyses of the expression data will reveal more information about this dissimilarity.

Samples mock48h, mock96h and virus48h cluster closely together (bottom right hand corner of MDS plot, Figure 5–2) indicating that these groups have similar RNA expression data. Meanwhile the sample set ‘virus96h’ groups further away from this cluster (bottom left hand corner of MDS plot, Figure 5–2) indicating gene expression at the later timepoint with ZIKV infected cells differs substantially from early and mock infected cultures.

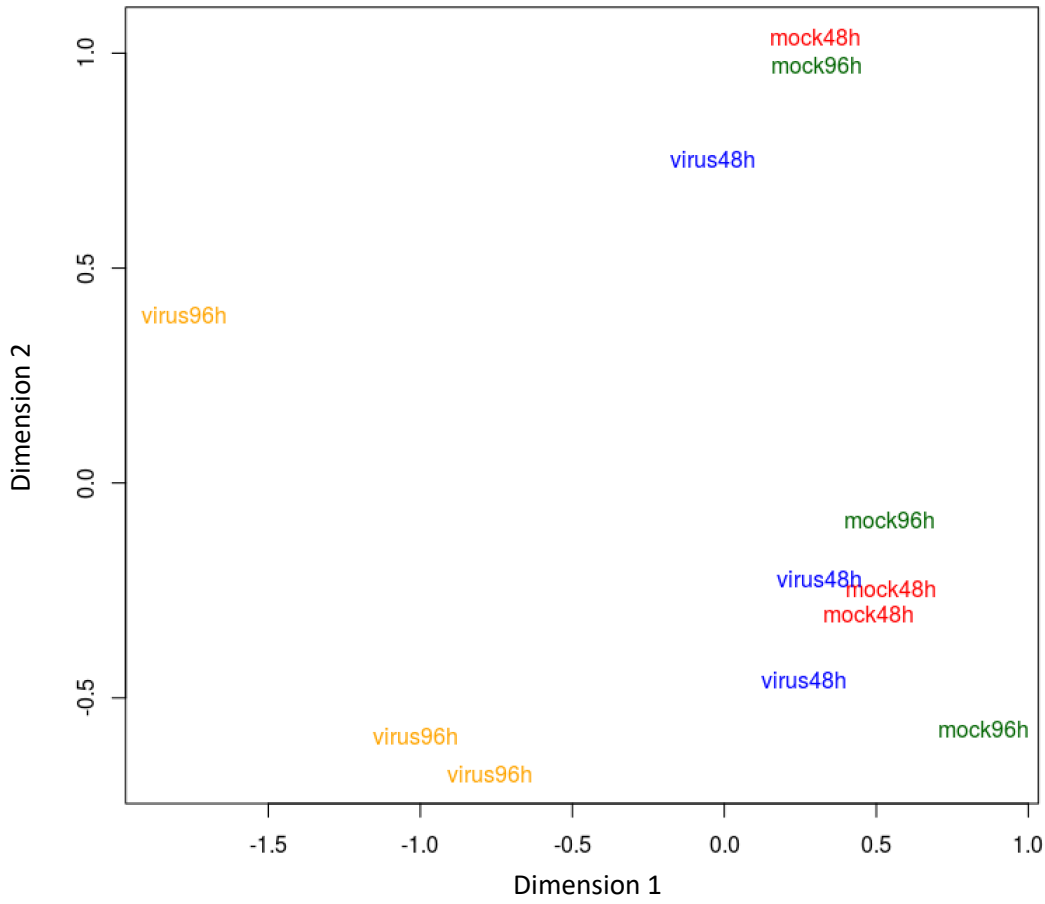


**Figure 5–2 Multidimensional scaling (MDS) plot comparing datasets obtained from mock or infected samples at 48 h p.i. and 96h p.i.**
Variation between timepoints, infected and uninfected samples and biological replicates were analysed using an MDS plot. This MDS plot was generated using the LogFC method; this method calculates distances between samples based on log2 fold changes (Log2FC). The x- and y- axes are representative of Euclidean distances between samples. The greater the distance between datapoints, the less related the datapoints are. CNS co-cultures were either infected with ZIKV at a MOI of 0.3 PFU/cell (virus- yellow/blue) or mock-infected (mock- red/green). RNA was harvested at either 48 h p.i. (48h – red/blue) or 96 h p.i. (96h – yellow/green). The MDS plot was kindly provided by Dr Quan Gu.

### 5.3.3 Differentially expressed gene comparison between grouped analyses

Differentially expressed genes (DEGs) were identified using RNAseq expression data. Only statistically significant DEGs with a Q value of <0.05 were included in these analyses. The q-value is an adjusted p-value which takes into account the false discovery rate (Storey and Tibshirani, 2003). DEGs were identified for the following datasets: 48 h p.i. V 48 h mock, 96 h p.i. V 96 h mock, and 48 h mock V 96 h mock. To assess the number of shared DEGs between different groups of paired analyses, a Venn diagram was produced (Figure 5–3).

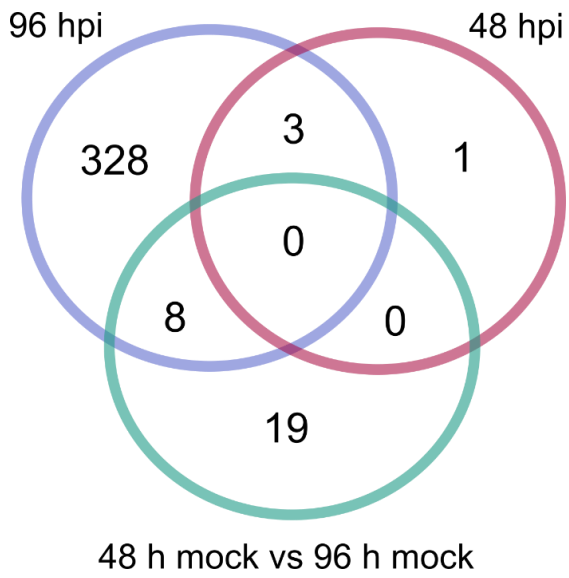


**Figure 5–3 Venn diagram displaying the number of shared differentially expressed genes (DEGs).**
DEG lists were obtained by comparing RNAseq data between ZIKV infected and mock infected samples from 48 and 96 h p.i., in addition to comparing RNAseq data between 48 h mock and 96 h mock samples. Only DEGs with a Q-value <0.05 were included in these analyses.

To determine differentially expressed genes which may be associated with normal culture function and/or development as opposed to virus infection, 48h mock V 96 mock DEGS were compared with data from other grouped analyses (Figure 5–3).

A total of 27 significant DEGs were identified between 48 h mock V 96 h mock datasets. Comparing this with DEGs from other analyses, 19 DEGs were unique to 48 h mock V 96h mock, and 8 hits were also found at 96 h p.i. (Figure 5–3). To determine whether these 8 DEGs were involved in normal culture development, or if they represent genes whose expression are altered by ZIKV infection, a heatmap was generated using the raw expression values for each DEG in the 48 h

mock, 96 h mock and 96 h p.i. dataset (Figure 5–4). As the expression of these 8 DEGs are altered between both mock and infected samples sets, it can be assumed that the expression of these genes may be altered by ZIKV infection and therefore do not represent genes implicated in normal culture function and development.

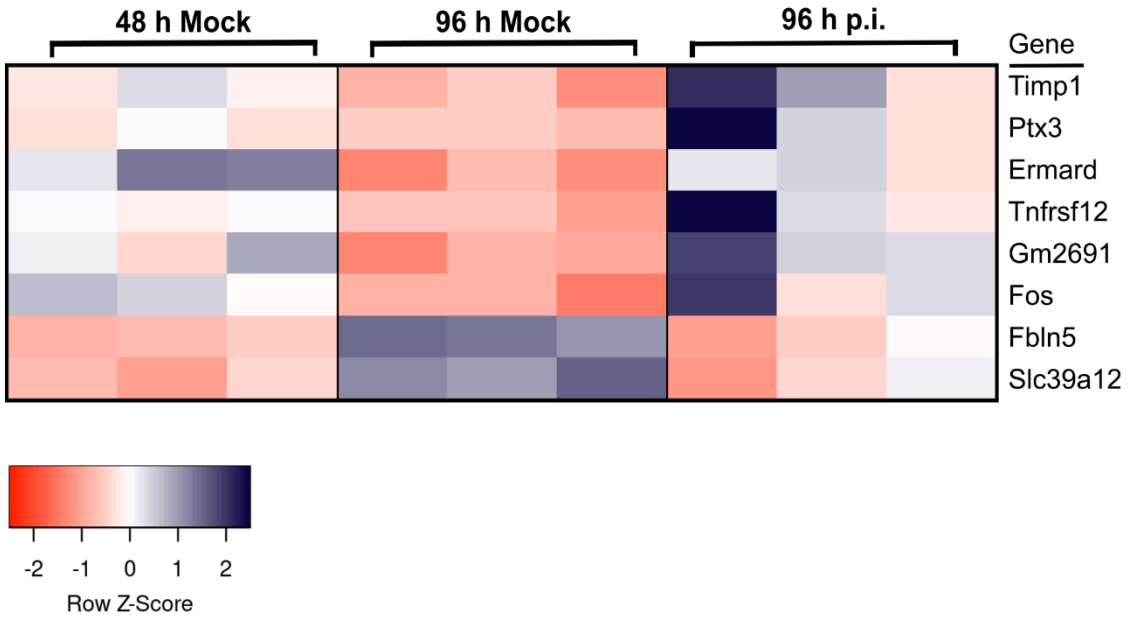


**Figure 5–4 A heatmap indicating DEGs which were shared between 48 h Mock V 96 h Mock, and 96 h Mock V 96 h p.i. dataset comparisons are not involved in normal CNS co-culture development.**
DEG lists were obtained by comparing RNAseq data between ZIKV infected and mock infected CNS co-culture samples from 48 and 96 h p.i., in addition to comparing RNAseq data between 48 h mock and 96 h mock samples. In total, 8 DEGs were found to be shared between 48 h Mock V 96 h Mock, and 96 h Mock V 96 h p.i. comparisons. Raw expression values for each condition (n=3; 48 h mock, 96 h mock, 96 h p.i.) were subsequently used to generate a heatmap. The row Z-score (the number of standard deviations an observation is from the mean) is indicated by a colour scale representing values from -2 to 2; this visually represents how different data are between comparator datasets.Each sub-column is representative of a single biological replicate. N=3 biological replicates per experimental condition underwent RNAseq and subsequent analyses to identify DEGs. Heatmap generated using Heatmapper (Babicki et al., 2016)

The 19 DEGs which are unique to the 48 h mock vs 96 h mock dataset are summarised in Table 5–2. As these DEGs differ between the mock cultures of differing timepoints (48 h p.i./DIV20, 96 h p.i./DIV22), they may be involved in culture function/development.

| Gene | Description | Log2FC | Q-value |
|---|---|---|---|
| **5430419D17Rik** | RIKEN cDNA 5430419D17 gene | 1.349822632 | 0.013727 |
| **Ptgds** | Prostaglandin D2 synthase which is highly expressed in mouse brain tissue | 1.159369699 | 6.11E-13 |
| **Dcd dopa decarboxylase** | Dcd dopa decarboxylase | 0.798480908 | 0.001119 |
| **Prdm16os** | Prdm16 opposite strand transcript | 0.783089832 | 0.047293 |
| **C1s1** | Complement component 1, subcomponent 1 | 0.781542798 | 0.032348 |
| **Sult1a1** | Sulfotransferase family 1A, phenol-preferring, member 1 | 0.735819031 | 0.039275 |
| **Lyz2** | Lysozyme C-2 precursor | 0.67208358 | 0.000261 |
| **Abca9** | ATP-binding cassette, sub-family A (ABC1), member 9 | 0.624110509 | 0.032074 |
| **Lrriq1** | Leucine-rich repeats and IQ motif containing 1 | 0.548544221 | 0.040768 |
| **Aldh6a1** | Aldehyde dehydrogenase family 6, subfamily A1 | 0.504553732 | 0.013727 |
| **Hacd4** | 3-hydroxyacyl-CoA dehydratase 4 | 0.479419852 | 0.040768 |
| **Prom1** | Prominin 1 | 0.47554711 | 0.042655 |
| **Ccdc3** | Coiled-coil domain containing 3 | 0.453373011 | 0.04515 |
| **Lims2** | LIM zinc finger domain containing 2 | -0.474966406 | 0.029954 |
| **Dbx2** | Developing brain homeobox 2 | -0.589232159 | 0.001985 |
| **Tubb6** | tubulin, beta 6 class V | -0.718924133 | 0.028927 |
| **Cited1** | Cbp/p300-interacting transactivator with Glu/Asp-rich carboxy-terminal domain 1 | -0.823628338 | 0.032684 |
| **Kif23** | Kinesin family member 23 | -0.961728063 | 0.040768 |
| **Gm35455** | Uncharacterised | -1.272445743 | 0.042655 |

**Table 5–2 Table summarising DEGs unique to 48 h mock V 96 h mock analysis.**
A brief summary of gene function and expression data (expressed as Log2 fold change [Log2FC]) are shown. Q-values <0.05 are considered significant.

### 5.3.4 DEGs associated with 'early' ZIKV infection

As indicated by the MDS plot (Figure 5–2), it is evident that the expression profiles of ZIKV infected samples at 48 h p.i. were not dissimilar to their mock counterparts. The ZIKV infected sample had only 4 DEGs that reached the significance value cut off (Q value <0.05). These genes were: Ifit1, Cxcl10, Ccl5 and Tpd52-ps. In contrast, the 96 h p.i. timepoint had 340 significant DEGs when compared to the 96h mock dataset; 3 DEGs of which are also differentially expressed at 48 h p. I (Ifit1, Cxcl10 and Ccl5). Despite sharing DEG hits, these 3 genes have disparate expression levels in both datasets. Details of which, including gene function, can be found in Table 5–3.

| Gene | Function | Log2FC 48 h p.i. V 48h mock | Log2FC 96 h p.i. V 96h mock |
|---|---|---|---|
| Ifit1 | Encodes a protein which has been demonstrated to have antiviral effects in response to type I IFN. May inhibit viral replication and translation initiation. | 2.19792935 | 5.1699853 |
| Cxcl10 | Immune modulatory role stimulation of monocytes, natural killer and T-cell migration, and modulation of adhesion molecule expression. | 2.15402709 | 6.7479685 |
| Ccl5 | Immunoregulatory molecule, acts as member of the CC subfamily, functions as a chemoattractant for blood monocytes, memory T helper cells and eosinophils. | 1.52118905 | 7.4386244 |

**Table 5–3 DEGs shared between datasets comparing 48 h p.i. V 48h mock data with that of 96 h p.i. V 96h mock data.**
A brief summary of gene function and expression data (expressed as Log2FC) are shown.

All the genes listed in Table 5–3 (Ifit1, Cxcl10 and Ccl5), have been described to coordinate the mammalian immune responses to viral infection (Trifilo et al., 2004, Hosking and Lane, 2010, Diamond, 2014). Ccxl10 and Ccl5 are typically secreted cytokines involved in chemotaxis of immune cells; expression of these cytokines has been associated with both neuroprotective and neuropathological roles in the CNS (Glass et al., 2004, Hosking and Lane, 2010). Whereas Ifit1 is an interferon stimulated gene (ISG) that exerts its function intracellularly within the cytoplasm, restricting foreign messenger RNA molecules, such as viral RNA genomes (Diamond, 2014). Given that the co-cultures had been infected with ZIKV, it is unsurprising that molecules with immunomodulatory roles were

upregulated at this timepoint, as it would be assumed that cells were starting to mount a response to virus infection. These CNS co-cultures are generated from embryonic mice which lack to type I IFN receptor (*Ifnar1*). Loss of this receptor renders cells incapable of responding to type I IFNs, though cells can still produce them. However, cells can produce antiviral transcripts via alternative routes such as NF-κB signalling, though should not necessarily be able to produce transcripts from the ISRE promoter. Furthermore, the expression values of all three genes increase between 48 h p.i and 96 h p. I (Ifit1 >2-fold, Cxcl10 >3-fold, Ccl5 >4-fold increase in Log2FC from 48 h to 96 h. p. i [Table 5–3]), indicating that these genes were being upregulated in response to ZIKV infection.

Despite 48 h p.i. being a relatively early stage of ZIKV infection within CNS co-cultures, the identification of only 4 significant DEGs is somewhat perplexing. ZIKV infection in *Ifnar1* CNS co-cultures was detected by qPCR, plaque assay and immunofluorescence staining as early as 24 h p.i.(Chapters 3 and 4, Sections 3.3.4 and 4.3.1). Furthermore, the upregulation of immune related transcripts, albeit a minor selection that reached statistical significance, indicated the presence of infection. Perhaps at this timepoint the level of infection is too low to incur a large shift in expression profile, and any transcripts that may be altered due to ZIKV infection were subsequently discounted from analyses due to restrictions of statistical significance (Q-value of <0.5).

Imposing a restriction of Q value <1 returned only an additional 2 DEGs compared to the original analysis: Eln (encodes the protein elastin which is a component of the extracellular matrix) and Rsad2 (in humans encodes the antiviral protein, viperin).Upon further investigation, discounting any Q-value restrictions, over 15,000 DEGs were identified at 48 h.p.i. The top 10 most up- and down-regulated genes (as determined by Log2FC values) are summarised in Table 5–4.

A mixture of gene functions can be found within the top 10 up and down regulated gene lists including genes implicated in immune regulation, cellular recruitment and trafficking, antiviral genes, undescribed genes and a few genes out width these categories. Lhx5, a gene implicated in neural cell differentiation and the development of several structures in the CNS, was downregulated at 48 h.p.i compared to mock (Zhao et al., 1999, Peng and Westerfield, 2006, Lui et

al., 2017). Lhx5 is not significantly differentially expressed at 96 h.p.i (Log2FC 0.01221; Q value 1). Whilst the downregulation of Lhx5 by ZIKV infection would be an interesting prospect, without further validation using methods such as qRT-PCR, no conclusion can be drawn yet from this finding.

Another gene of interest highlighted in this list is kazn; a gene with roles in cellular adhesion and cytoskeletal organisation. The dataset suggests at 48 h.p.i kazn is downregulated, which would imply cells are more motile, given that this gene is involved in cell adhesion. This wouldn't be unreasonable to suggest as phagocytic cells in the CNS culture will need to adopt a more motile phenotype in order to target infected cells and clear cellular debris generated as a result of any lytic ZIKV infection. Many of the DEGs identified at 96 h.p.i also have reported functions in chemotaxis and cellular migration and were upregulated following ZIKV infection (Section 5.3.5). However, Kazn was not significantly differentially expressed at 96 h.p.i, nor was it differentially expressed in absence of Q-value restrictions; further validation is required to determine if this gene is differentially expressed at 48 h.p.i.

| Gene | Log2FC | Q-value | Description |
|---|---|---|---|
| Ifit1 | 2.19793 | 7.29E-09 | Encodes a protein which has been demonstrated to have antiviral effects in response to type I IFN. |
| Cxcl10 | 2.15403 | 7.29E-09 | Immune modulatory role stimulation of monocytes, natural killer and T-cell migration, and modulation of adhesion molecule expression. |
| Ccl5 | 1.52119 | 0.0269 | Immunoregulatory molecule, acts as member of the CC subfamily, functions as a chemoattractant for blood monocytes, memory T helper cells and eosinophils. |
| Rsad2 | 1.130597 | 0.666863 | Encodes antiviral protein Viperin |
| Neurod1 | 0.98904 | 1 | Neurogenic differentiation 1 |
| Tpd2-ps | 0.96765 | 0.02662 | Tumor protein D52, pseudogene |
| Ccl2 | 0.92428 | 1 | Chemokine (C-C motif) ligand 2 - |
| ENSMUSG00000112795 | 0.92247 | 1 | Uncharacterised |
| Gm17066 | 0.89398 | 1 | Predicted gene 17066 |
| ENSMUSG00000116597 | 0.88127 | 1 | Uncharacterised |
| GM23935 | -0.6911 | 1 | Protein coding, implicated in TCA cycle in drosophila |
| Galntl6 | -0.70072 | 1 | UDP-N-acetyl-alpha-D-galactosamine:polypeptide N-acetylgalactosaminyltransferase-like 6 |
| Hnrnpu | -0.70346 | 1 | Heterogeneous nuclear ribonucleoprotein U - gene expression mRNA processing |
| Ntsr1 | -0.73996 | 1 | Neurotensin receptor 1 |
| Actn2 | -0.76273 | 1 | Actn alpha 2 |
| Cpne7 | -0.76902 | 1 | Copine VII - calcium dependent protein |
| Npy | -0.81905 | 1 | Neuropeptide y - many physiological functions such as food intake, energy homeostasis, circadian rhythm, and cognition |
| Lhx5 | -0.83744 | 1 | LIM homeobox 5 - neural cell differentiation/development, transcription factor activity forebrain development learning and motor function in adult mice |
| Gm12666 | -0.99276 | 1 | Predicted gene 12666 |
| Kazn | -1.80951 | 1 | Kazrin, periplakin interacting protein - cell adhesion, cytoskeletal organisation |

**Table 5–4 Top 10 up- and down-regulated DEGs at 48 h.p.i, minus Q value restrictions.**
A brief summary of gene function and expression data (expressed as Log2FC) are shown. The Q-value is also shown as an indicator of significance of expression data. Downregulated DEGs are shaded in grey.

To determine whether any other DEGs found in the unrestricted 48 h.p.i DEG list could be supported by differential expression at 96 h.p.i, a comparison between the two datasets was performed. Genes from the unrestricted list of DEGs identified at 48 h.p.i with a Log2FC value >0.5 (either up- or down-regulated) were extracted – this yielded a smaller list of 187 DEGs. This list was then compared with significant DEGs identified at 96 h p.i. (Q value <0.05) in order to identify shared molecules. A summary of the shared DEGs and their Log2FC values at 48 h p.i. and 96 h p.i. can be found in Table 5–5.

Again, the analysis returned genes which can primarily be connected to immune and inflammatory responses. One gene of interest consistently returned in the analyses is Rsad2; also known as viperin. This is one of the top 10 upregulated genes at 48 h p.i., possessing a Log2FC value of 1.1306 - though its Q- value does not reach the significance threshold of <0.05 (Q-value = 0.666863). Despite not reaching statistical significance at 48 h p.i., it is differentially expressed at 96 h p.i. At 96 h p.i., it becomes one of the top 25 upregulated DEGs, possessing a log2FC value of 4.979172, and reaches statistical significance with a Q-value of 8.02E-32. Recent studies suggest that viperin is important in the restriction of flaviviruses such as WNV, DENV, TBEV and HCV, with ZIKV being the most recent addition to this list (Lindqvist et al., 2018, Van der Hoek et al., 2017).Viperin exerts its antiviral activity using numerous mechanisms which can vary between members of the same family; in the case of ZIKV, data suggests viperin imposes restriction at the level of RNA replication (Van der Hoek et al., 2017).

| Gene | 48 h p.i. | | 96 h p.i. | |
|---|---|---|---|---|
| | **Log2FC** | **Q-value (unrestricted)** | **Log2FC** | **Q-value (<0.05)** |
| Ifit1 | 2.19792935 | 7.29E-09 | 5.169985341 | 1.86E-73 |
| Cxcl10 | 2.154027086 | 7.29E-09 | 6.747968503 | 3.44E-89 |
| Ccl5 | 1.521189045 | 0.0269 | 7.438624412 | 1.58E-41 |
| Rsad2 | 1.130599647 | 0.66686 | 4.979171573 | 8.02E-32 |
| Ccl2 | 0.924277083 | 0.92428 | 6.209304557 | 1.04E-69 |
| Tnfaip2 | 0.580833818 | 1 | 3.428105096 | 5.12E-28 |
| Steap4 | 0.578902358 | 1 | 3.796855457 | 1.18E-30 |
| Lcn2 | 0.570631425 | 1 | 3.5666967 | 1.12E-21 |
| Saa3 | 0.569793506 | 1 | 2.911601427 | 0.009854 |
| Gbp9 | 0.551932227 | 1 | 2.522424279 | 3.29E-12 |
| Ptx3 | 0.537151005 | 1 | 2.718479723 | 3.45E-06 |
| Mir6236 | -0.683920338 | 1 | 0.980588 | 0.006554 |
| Gm23935 | -0.691106922 | 1 | 1.082937375 | 0.000334 |

**Table 5–5 List of DEGs that appear at both 48 h p.i. and 96 h p.i. and their associated Log2FC expression values.**
Expression data (expressed as Log2FC) are shown for DEGs which appear at both 48 h p.i. and 96 h p.i. The Q-value is also shown as an indicator of significance of expression data; statistically significant Q value <0.05.

### 5.3.5 Initial analyses of 96 h p.i. vs mock dataset

Herein the DEG dataset in use is 96 h p.i. vs 96 h mock, as this provided the most significant DEGs (48 h p.i. vs 48 h p.i. had only 4 DEGs which were above the Q-value threshold of <0.5). In total 340 significant DEGs were identified at 96 h p.i. in comparison to the equivalent mock dataset; of which, 303 genes were up-regulated, and 37 genes were down-regulated. A summary of which can found in Figure 5–5.

Next, the top 10 most up- and down-regulated molecules were identified within the dataset (Table 5–6). The 10 most upregulated genes have a median Log2FC of 7.659 (range: 6.748 — 10.982) and their functions broadly categorise into genes involved in cell-cell signalling and recruitment, and type I IFN responses. The top 10 most up regulated genes, in descending order of expression include: IFNB1, OVOL1, HEATR9, OASL, Cxcl11, Cxcl2, Ccl5, IL6, GBP5 and CXCL10. IFNB1, which encodes IFN-β (a type I IFN), was the most up-regulated gene in response to ZIKV infection at 96 h p.i. Type I IFN plays a protective role in ZIKV infection, as demonstrated in Chapter 4 Section 4.3.1, whereby CNS co-cultures which possessed WT *Ifnar1* were less susceptible to ZIKV infection. A recent study highlights that astrocyte mount a rapid type I IFN response which protects cells against cytopathic effects of ZIKV infection (Lindqvist et al., 2016).

The 10 most downregulated genes have a median Log2FC of -0.817 (range: - 0.667 — -7.858). In descending order of expression, the 10 most downregulated genes include: PTGS1, SLCO2B1, ADAMTS16, PPP1R1B, TPRKβ, TP73, TLR8, TMEM52, MRC1, IL11RA (Table 5–6). IL11RA was the most downregulated gene in response to ZIKV infection at 96 h p.i.; IL11RA encodes the interleukin 11 receptor subunit alpha and is a member of the hematopoietic cytokine receptor family.

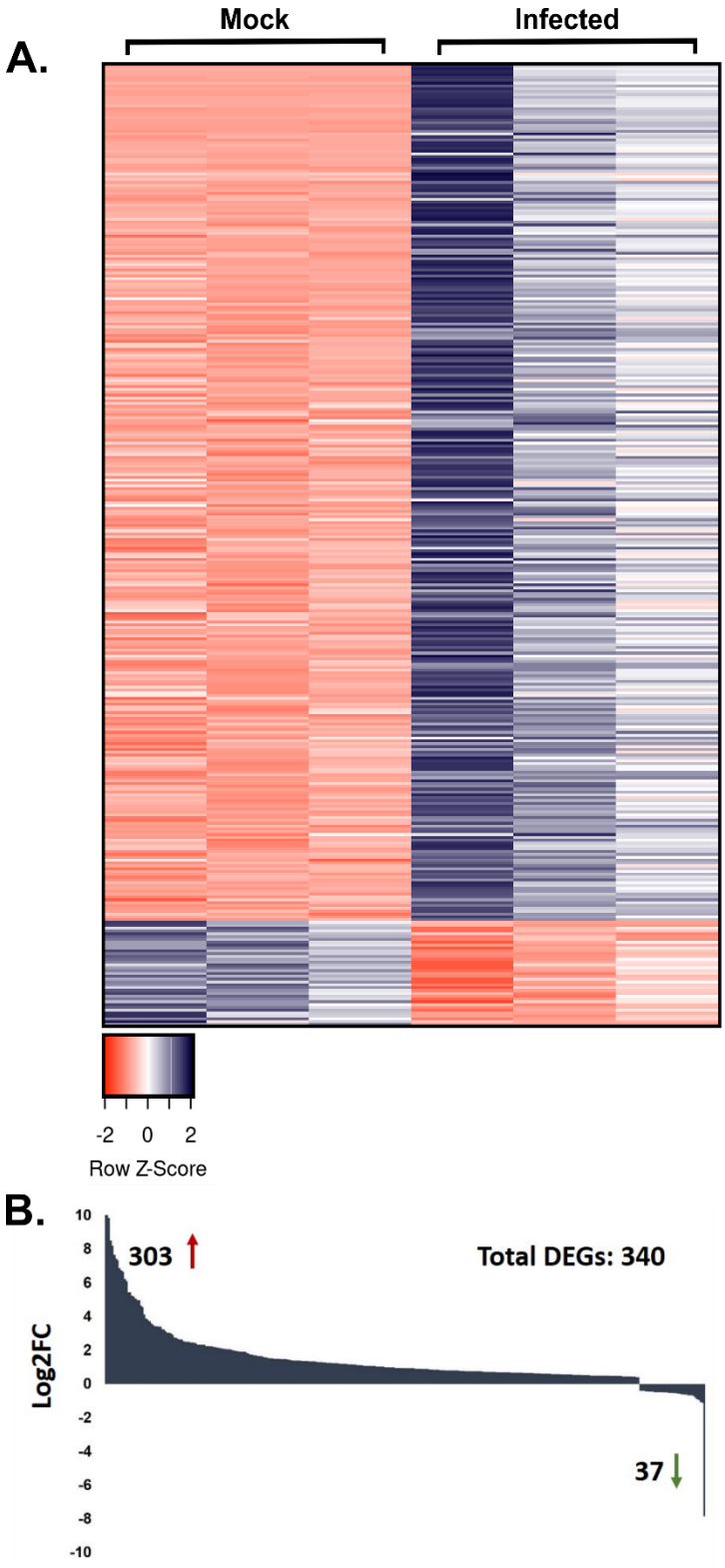


**Figure 5–5 DEGs between mock and infected samples at 96 h p.i.**
A total list of significant DEGs were identified by isolating expression data possessing a Q-value <0.05. (**A**) A heatmap representing DEGs across 3 independent experiments comparing mock and infected samples at 96 h p.i. Each column represents a biological replicate. Heatmap generated using Heatmapper (Babicki et al., 2016). (**B**) A plot representing the total number of DEGs up (red arrow) and downregulated (green arrow) at 96 h p.i.

| Gene | Description | Log2FC | Q-value |
|---|---|---|---|
| IFNB1 | Interferon beta 1 | 10.982 | 1.57E-48 |
| OVOL1 | Ovo like zink finger 1- transcription factor involved in the development and differentiation of numerous tissues.(Kagawa et al., 2019) | 10.006 | 2.20E-25 |
| HEATR9 | HEAT repeat containing 9 – uncharacterised function, suggested role in haematopeotic stem cell differentiation. Also upregulated in influenza infection of alveolar epithelial cells (Stairiker et al., 2018). | 9.840 | 1.57E-27 |
| OASL | 2'-5'-oligoadenylate synthetase like – IFN inducible enzyme which has antiviral activity. Senses exogenous nucleic acid and induces its degradation via RNase L. | 8.517 | 7.85E-42 |
| Cxcl11 | Chemokine which binds the CXCR3 receptor. | 8.202 | 7.24E-34 |
| CxCl2 | Produced by activated monocytes, expressed at sites of inflammation. | 7.659 | 6.30E-75 |
| CCL5 | Chemoattractant for blood monocytes, memory T helper cells and eosinophils | 7.439 | 1.58E-41 |
| IL6 | Interleukin 6 - involved in inflammatory response | 7.349 | 2.98E-29 |
| GBP5 | Guanylate binding protein 5 - Activator of NLRP3 inflammasome with roles in innate immunity and inflammation. | 6.880 | 9.54E-42 |
| CXCL10 | Immunoregulatory molecule - functions as a chemoattractant for blood monocytes, memory T helper cells and eosinophils. | 6.748 | 3.44E-89 |
| PTGS1 | Prostaglandin G/H synthase 1 precursor | -0.667 | 0.002376 |
| SLCO2B1 | Solute carrier organic anion transporter family member 2B1 – modules Na+ independent transport of organic anions e.g. prostaglandins | -0.679 | 0.014771 |
| ADAMTS16 | ADAM Metallopeptidase with thrombospondin type 1 motif 16 - | -0.683 | 0.033574 |
| PPP1R1B | Protein phosphatase 1 regulatory inhibitor subunit 1B – signal transduction molecule involved in dopaminergic and glutaminergic signalling. | -0.725 | 0.000103 |
| TPRKB | TP53RK binding protein | -0.817 | 0.000471 |
| TP73 | Tumour protein P73 – member of the p53 family of transcription factors. It is located on chromosome 1p36 in humans, that is frequently deleted in neuroblastoma and other tumours. | -0.885 | 0.02568 |
| TLR8 | Toll like receptor 8 | -0.962 | 0.011103 |
| TMEM52 | Transmembrane protein 52 | -1.059 | 0.029592 |
| MRC1 | Mannose receptor C-Type 1 – mediates endocytosis of glycoproteins by macrophages. Involved in antiviral immune responses to HIV-1 (Sukegawa et al., 2018) and DENV entry (Miller et al., 2008, Lo et al., 2016) | -1.114 | 0.003129 |
| IL11RA | Interleukin 11 receptor subunit alpha | -7.858 | 9.82E-17 |

**Table 5–6 Top 10 up- and down- regulated significant DEGs at 96 h p.i.**
Expression data (expressed as Log2FC) are shown for genes which are differentially expressed at 96 h p.i. compared to 96 h mock. The Q-value is also shown as an indicator of significance of expression data. Downregulated genes are highlighted in grey and upregulated genes are white.

It is noteworthy that Table 5-6 only details 20/340 DEGs found at 96 h p.i. with ZIKV; the remainder can be found in the Appendix. This is a microscopic view of the expression profile found at 96 h p.i., furthermore individual genes expressed in response to ZIKV infection in a mixed-cell co-culture provides little context as to what is occurring on a more global scale in the CNS. Therefore, further analyses using the Ingenuity Pathway Analysis (IPA) software was used to examine canonical signalling pathways affected in the dataset (section 5.3.6), in addition to disease and function analyses (section 5.3.7).

## 5.3.6 Top canonical signalling pathways affected at 96 h p.i.

DEGs identified at 96 h p.i. were imported into the ingenuity pathway analysis (IPA) tool. IPA was then used to predict biological functions associated with the DEG dataset. A summary of the top 20 canonical signalling pathways identified by IPA can be found in Figure 5-6.

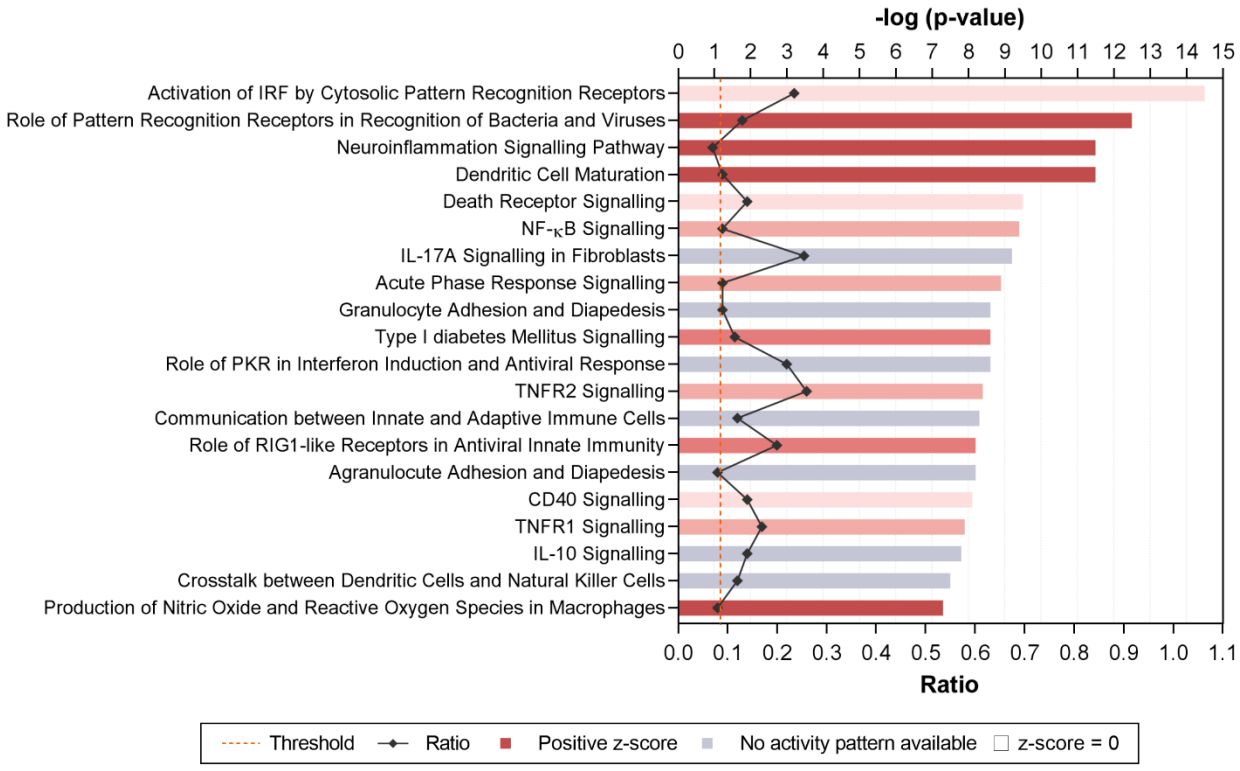


**Figure 5–6 Top 20 significant canonical pathways affected at 96 h p.i. vs mock infected CNS samples, determined by p-value, as identified by IPA.**
Bars are measured against -log(p-values). The bigger the bar, the smaller the p value, indicating that the activity in this pathway from the dataset is statistically significant. The intensity of the colour red correlates with z-score positivity. Positive z-scores indicate upregulated pathways, whereas negative z-scores are indicative of downregulation. Grey bars indicate that although a pathway is affected, the resulting activity (activation or repression) is unknown. The ratio reflects the number of molecules presented in the dataset that are involved in a given pathway, against the known total of pathway components.

Many of the top canonical pathways identified by IPA are implicated in immune and inflammatory responses. This is to be expected as infection of mammalian cells with any microbe elicits an immune response; viral infection of mammalian cells potentiates innate immune responses (Brubaker et al., 2015). At 96 h p.i. with ZIKV, the two most significantly affected canonical pathways involve the detection of pathogens by pattern recognition receptors (PRRs), including 'IRF activation by cytosolic PRRs and 'Role of PRRs in recognition of bacteria and viruses' (Figure 5–6). ZIKV replicates within the cytoplasm and possesses non-self motifs which can be detected by PRRs; examples of PRRs implicated in detecting ZIKV infection include RIG-I-like receptors (RLRs), MDA-5, cGMP-AMP synthase (cGAS) and TLR3.

Whilst canonical pathways involved in PRR activation are the most significantly affected pathways, other pathways correlate with stronger activation (as determined by z-score). The canonical pathways with the most positive z-scores include: 'role of PRRs of bacteria and viruses', 'neuroinflammation signalling pathway', 'dendritic cell maturation' and 'production of nitric oxide and reactive oxygen species in macrophages' (Figure 5–6). Genes implicated in neuroinflammation, and their associated expression levels are summarised in Figure 5–7.

For some pathways which were significantly affected by ZIKV infection at 96 h p.i., no activity patterns were available to assign a positive or negative z-score, these include: 'IL-17A signalling in fibroblasts', 'granulocyte adhesion and diapedesis', 'role of PKR in IFN induction and antiviral response', 'communications between innate and adaptive immune cells', 'agranulocyte adhesion and diapedesis', 'IL-10 signalling', and 'cross-talk between dendritic cells and natural killer cells'.

Another factor implicated in the assessment of canonical pathway activation is the number of molecules found to be differentially expressed which pertain to a particular pathway, expressed as a ratio (Figure 5–6). The higher the ratio, the more molecules in a pathway are differentially expressed in the dataset. At 96 h p.i. with ZIKV, the canonical pathways with the most DEGs involved include: 'IL-17A signalling in fibroblasts', 'TNFR2 signalling', 'role of RIG-I like receptors in antiviral immunity', and 'role of PKR in IFN induction and antiviral response'.

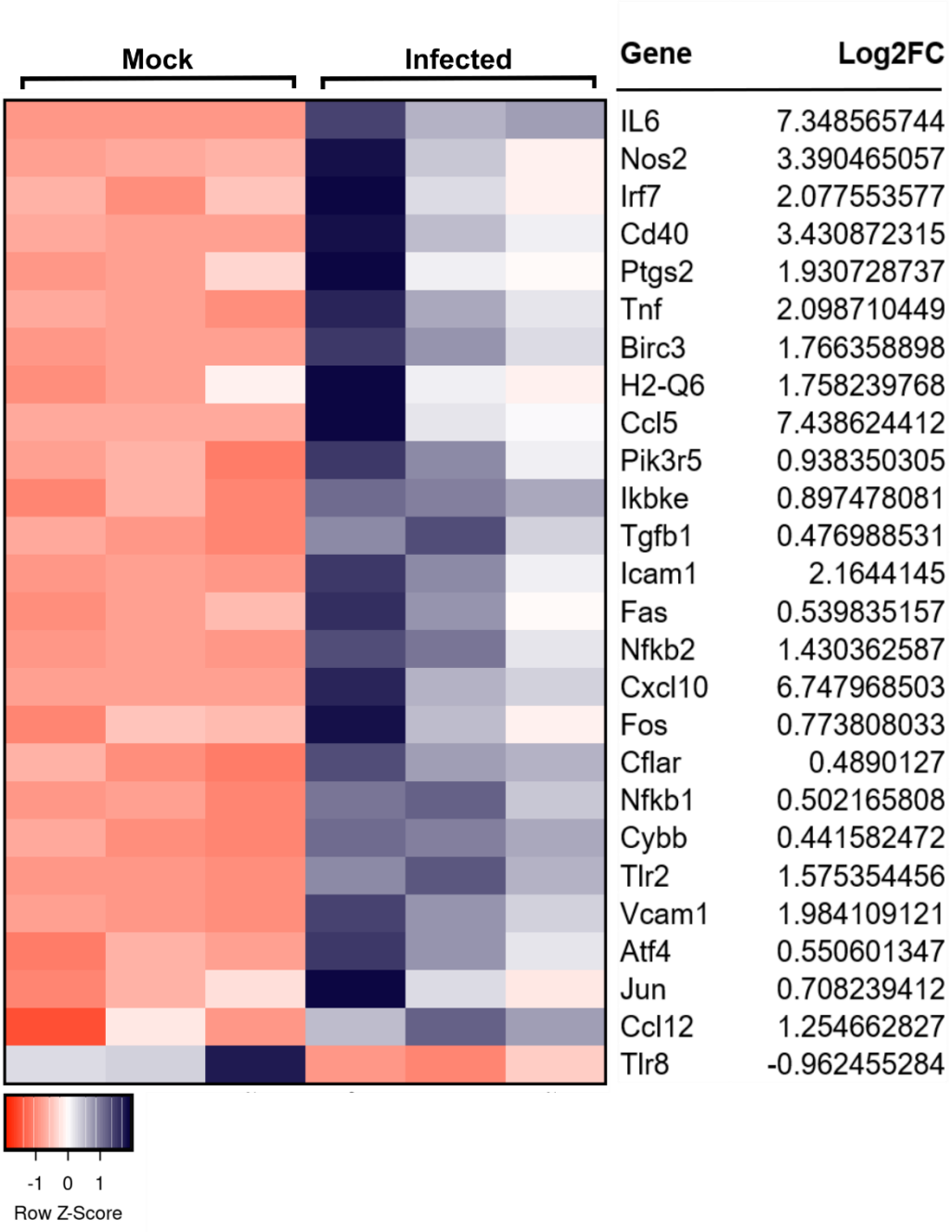


| Gene | Log2FC |
|---|---|
| IL6 | 7.348565744 |
| Nos2 | 3.390465057 |
| Irf7 | 2.077553577 |
| Cd40 | 3.430872315 |
| Ptgs2 | 1.930728737 |
| Tnf | 2.098710449 |
| Birc3 | 1.766358898 |
| H2-Q6 | 1.758239768 |
| Ccl5 | 7.438624412 |
| Pik3r5 | 0.938350305 |
| Ikbke | 0.897478081 |
| Tgfb1 | 0.476988531 |
| Icam1 | 2.1644145 |
| Fas | 0.539835157 |
| Nfkb2 | 1.430362587 |
| Cxcl10 | 6.747968503 |
| Fos | 0.773808033 |
| Cflar | 0.4890127 |
| Nfkb1 | 0.502165808 |
| Cybb | 0.441582472 |
| Tlr2 | 1.575354456 |
| Vcam1 | 1.984109121 |
| Atf4 | 0.550601347 |
| Jun | 0.708239412 |
| Ccl12 | 1.254662827 |
| Tlr8 | -0.962455284 |

**Figure 5–7 DEGs implicated in neuroinflammatory pathways.**
Expression analyses were performed using IPA (Ingenuity pathway analysis) and filtered to only include nervous system tissues, CNS cell lines and neuroblastoma cell lines. The displayed DEGS were grouped and categorised using the canonical pathways tool. The heatmap displays expression values from 3 independent experiments for mock and infected samples at 96 h p.i. Log2FC: Log2 Fold change expression value. Heatmap generated using Heatmapper (Babicki et al., 2016).

Only seven canonical pathways had a negative z-score, indicating that they are down regulated at 96 h p.i. following ZIKV infection. In order of increasing p-value, pathways with negative z-scores include: ‘Angiopoeitin signalling’, ‘LXR/RXR activation’, ‘Apoptosis signalling’, ‘PPAR signalling’, ‘PPARα/RXRα activation’, ‘antioxidant action of vitamin C’, and ‘PTEN signalling’. These pathways are broadly implicated in lipid metabolism, cell survival and proliferation, as well as angiogenesis.

### 5.3.7 Disease and Function analyses of CNS co-cultures at 96 h p.i. with ZIKV

The top 5 disease pathways related to ZIKV infection at 96 h p.i. identified using the disease and functions tools in IPA included: ‘inflammatory response’, ‘organismal injury and abnormalities’, ‘infectious disease’, ‘immunological disease’, and ‘gastrointestinal disease’. Upon further exploration of the dataset, it was found that 194 disease/function annotations were predicated to have increased activity with ZIKV infection at 96 h p.i. These broadly categorised into: cellular movement/recruitment (33.5%), cell survival/proliferation (25.3%), cell death (13.4%), activation of cells (7.2%), immune responses (7.2%), differentiation of cells (6.7%), and other functions (6.7%). Nine disease/function annotations were predicted to be decreased with ZIKV infection at 96 h p.i., including: replication of RNA virus, replication of virus, replication of *Herpesviridae*, infection of mammalia, atrophy of lymphoid organ, nephritis, weight loss, morbidity or mortalitiy, and organismal death. Upon further investigation, a number of molecules were upregulated at 96 h p.i. infection with ZIKV which were associated with the decrease in viral replication (

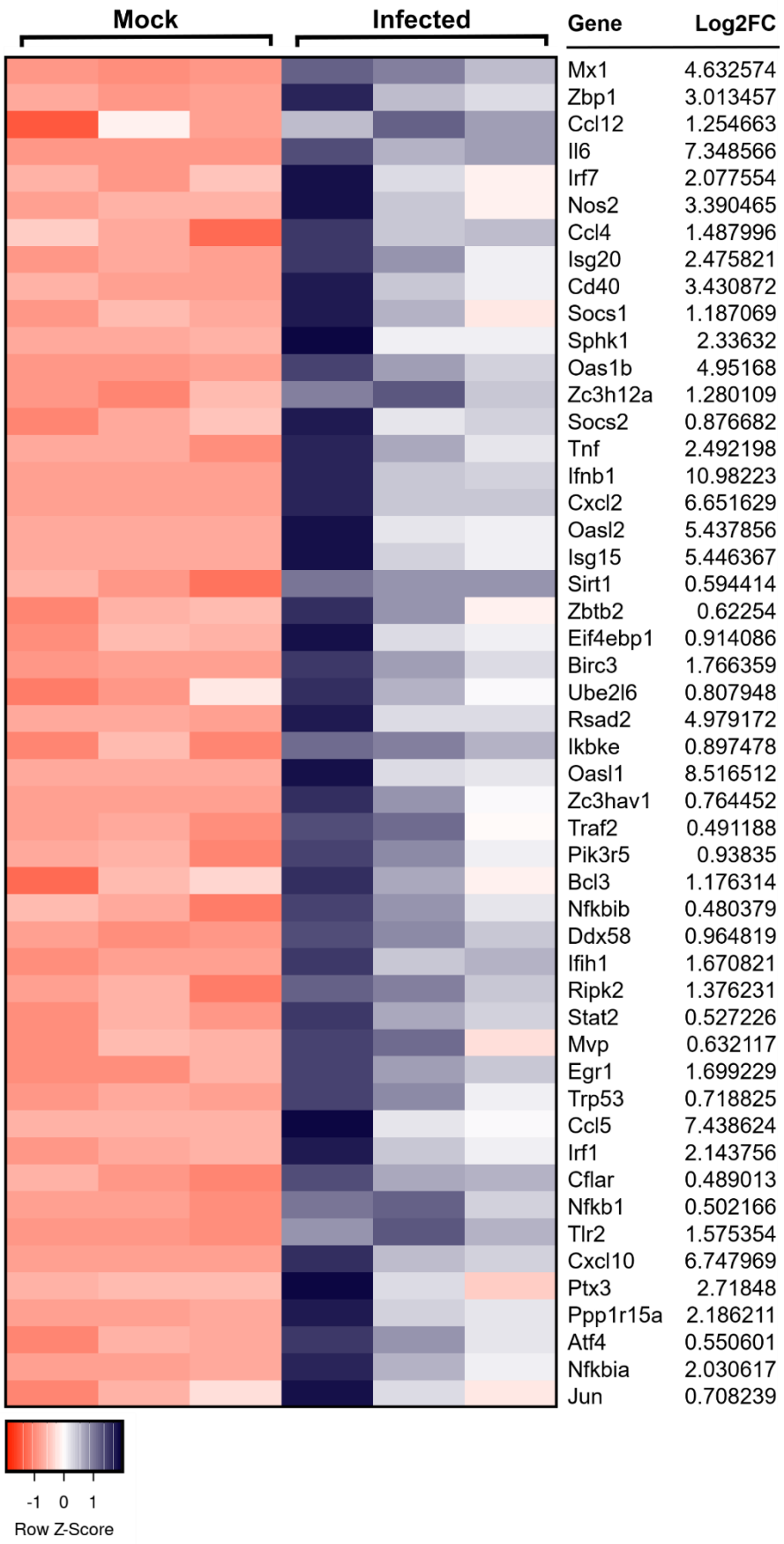


Figure 5-8). This is indicative of the elicitation of a potent anti-viral response within CNS co-cultures in response to infection with ZIKV.

These disease/function categories provide little insight into the injury observed in CNS co-cultures when infected with ZIKV, this could be due to the complex nature of using a multi-cell type model system. Therefore, subsequent disease/function analyses were performed with a filter to only include results pertaining to cells of neurological origin, in order to yield more specific disease/function categories.

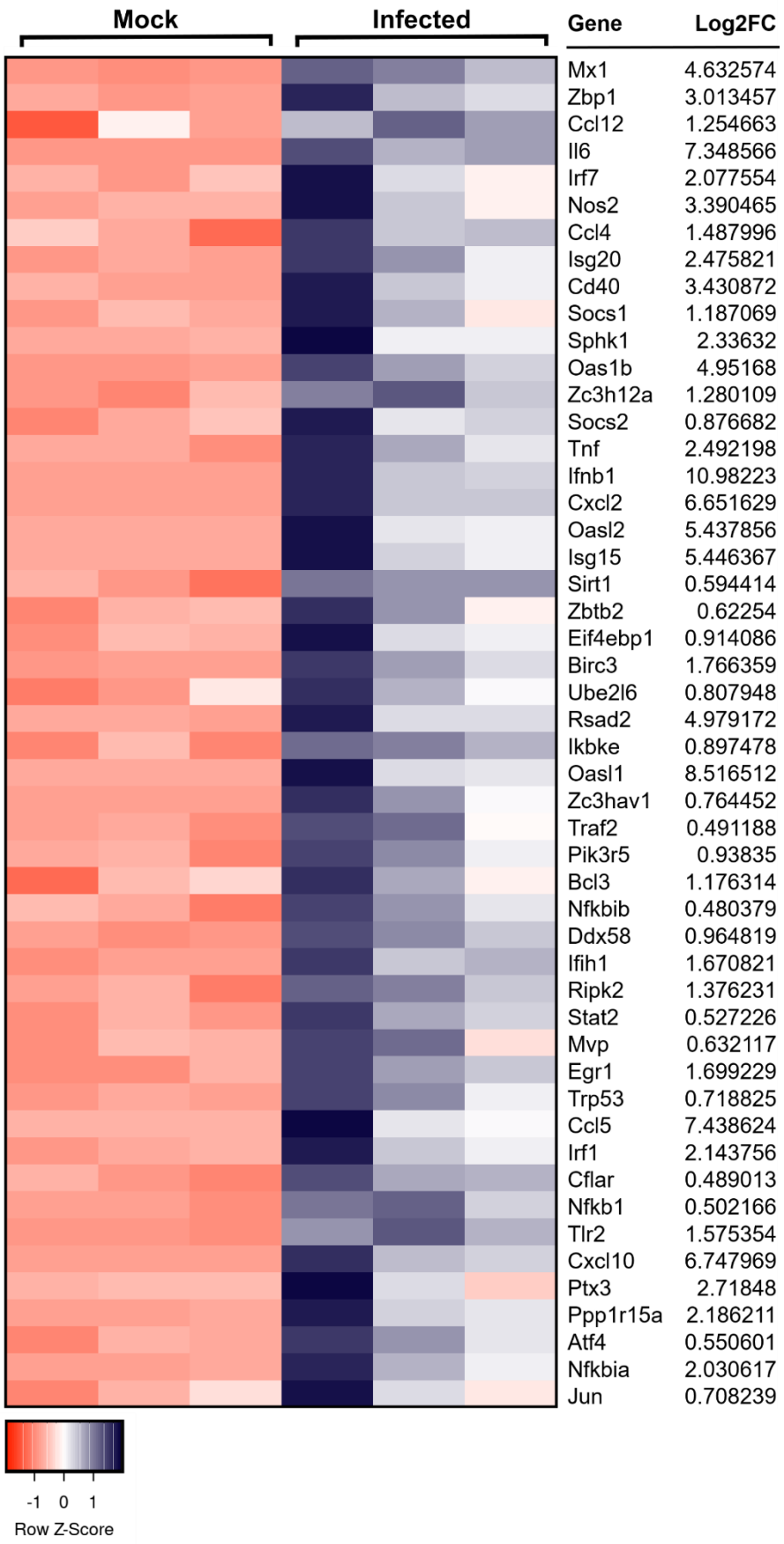


**Figure 5–8 DEGs implicated in the reduction of viral replication.**
Expression analyses were performed using IPA (Ingenuity pathway analysis); expression data was not filtered to exclude cell types in this analysis. The displayed DEGS were grouped and categorised using the disease and function tool. The heatmap displays expression values from 3 independent experiments for mock and infected samples at 96 h p.i. Log2FC: Log2 Fold change expression. Heatmap generated using Heatmapper (Babicki et al., 2016).

With a filter to exclude cell types which are not of neurological origin, the top 5 disease/functions were: neurological disease, organismal injury and abnormalities, inflammatory response, cardiovascular disease and psychological disorders. Further exploration of the disease and function analyses revealed groupings of molecules pertaining to disease/functions predicted to have increased activity at 96 h p.i. with ZIKV. The IPA tool highlighted these predictions as 'biased'; however, because the mixed cell co-culture used in this study is of CNS origin, these analyses were pursued. A list of the disease/function annotations, together with their p-value, activation score and associated molecules identified within the dataset can be found in Table 5–7. Positive activation z-scores indicate that the pathway is predicted to be activated; the closer the activation z-score is to 0, the less activated the pathway. The 22 annotations which are predicated to be activated at 96 h p.i. with ZIKV broadly categorise into one or more of the following functions: activation of cells (22.7%), cell movement/migration (31.8%), lipid metabolism (13.6%), neuron/neurite morphology (27.3%) and cell viability (4.5%).

| Annotation | p-value | Activation z-score | Molecules |
|---|---|---|---|
| **Activation of cells** | 3.21E-10 | 3.791 | C3,Ccl2,CCL5,CDKN1A,CEBPB,CXCL10,CYBB,FGF2,FOS,GJA5,IL6,LCN2,LIF,NOS2,PTGS2,SIRT1,TGFB1,TLR2,TNF,VSIR |
| **Cell movement** | 2.05E-07 | 3.36 | BTG2,C3,CCL2,Ccl2,CCL4,CCL5,CD44,CD74,CHL1,CXCL10,CXCL2,CXCL3,EGR1,EPHA2,FAS,FGF2,HBEGF,ICAM1,IL11RA,LCN2,SERPINE1,TGFB1,TIMP1,TLR2 |
| **Activation of leukocytes** | 1.04E-10 | 3.082 | C3,Ccl2,CCL5,CEBPB,CXCL10,CYBB,IL6,LCN2,NOS2,PTGS2,TGFB1,TLR2,TNF,VSIR |
| **Migration of cells** | 2.5E-07 | 2.994 | BTG2,C3,CCL2,Ccl2,CCL4,CCL5,CD44,CD74,CHL1,CXCL10,CXCL2,CXCL3,EGR1,EPHA2,FAS,FGF2,HBEGF,ICAM1,IL11RA,LCN2,SERPINE1,TLR2,TNF,TRPC1,V |
| **Activation of microglia** | 7.71E-10 | 2.915 | C3,Ccl2,CCL5,CEBPB,CXCL10,CYBB,IL6,LCN2,NOS2,PTGS2,TGFB1,TLR2,TNF |
| **Organisation of cytoskeleton** | 5.87E-10 | 2.847 | ATF3,BTG2,C3,CD44,CDKN1A,CHL1,CYBB,EGR1,EIF4EBP1,EPHA2,FGF2,FOS,GEM,ICAM1,IFRD1,IGSF9,IL11RA,IL6,JUN,LCN2,MICALL2,NFKB1,NFKBIA,PTGS |
| **Microtubule dynamics** | 0.000115 | 2.733 | ATF3,BTG2,C3,CD44,CDKN1A,CHL1,CYBB,EGR1,EIF4EBP1,EPHA2,FGF2,FOS,GEM,IFRD1,IGSF9,IL11RA,IL6,JUN,LCN2,MICALL2,NFKB1,NFKBIA,PTGS2,RALB |
| **Activation of neurons** | 0.00147 | 2.619 | FOS,GJA5,IL6,LIF,PTGS2,SIRT1,TNF |
| **Synthesis of lipid** | 0.000111 | 2.577 | EGR1,FOS,IL6,NOS2,PTGES,PTGS2,TNF |
| **Cell movement of CNS cells** | 0.0203 | 2.412 | BTG2,CCL2,CHL1,CXCL3,LCN2,TIMP1 |
| **Activation of CNS cells** | 0.000123 | 2.047 | CCL5,CDKN1A,CEBPB,IL6,LIF,PTGS2,TLR2 |

**Table 5–7 Predicated increased disease/functions as determined by IPA analysis at 96 h p.i., using a filter for neurological cell types. (1/2)**

Ordered in decreasing order of Activation Z-score, which is indicative of the level of activation of a pathway; scores above 0 are upregulated.

| Annotation | p-value | Activation z-score | Molecules |
|---|---|---|---|
| Synthesis of fatty acids | 3.39E-06 | 2.391 | EGR1,IL6,NOS2,PTGES,PTGS2,TNF |
| Shape change of neurites | 4.43E-05 | 2.386 | ATF3,C3,CDKN1A,CHL1,EIF4EBP1,FGF2,FOS,IGSF9,IL6,LCN2,NFKB1,PTGS2,RALB,RELB,RND1,TGFB1,TNF,TP53,TRPC1,VASP |
| Branching of Neurites | 9.41E05 | 2.386 | ATF3,C3,CDKN1A,EIF4EBP1,FGF2,FOS,IGSF9,IL6,LCN2,NFKB1,PTGS2,RALB,RELB,RND1,TGFB1,TNF,TP53,TRPC1,VASP |
| Cell viability | 9.36E-09 | 2.37 | CCL5,CXCL3,CYBB,EGR1,FGF2,FOS,HBEGF,HLA-A,IL11RA,IL6,JUN,LCN2,LIF,NFKBIA,NFKBIB,PTGS2,REL,RIPK2,SIRT1,SPHK1,TGFB1,TN |
| Development of neurons | 0.000846 | 2.215 | ATF3,BTG2,C3,CD44,CDKN1A,CHL1,CYBB,EGR1,EIF4EBP1,FGF2,FOS,GEM,ICAM1,IGSF9,IL11RA,IL6,JUN,LCN2,MICALL2,NFKB1,NFKBIA,PLXND1,PTGS2,RALB,RELB,RND1,T |
| Cell movement of mononuclear | 6.39E-09 | 2.203 | C3,CCL2,Ccl2,CCL4,CCL5,CD44,CXCL10,IL11RA,TNF |
| Synthesis of prostaglandin E2 | 3.26E-06 | 2.201 | IL6,NOS2,PTGES,PTGS2,TNF |
| Shape change of axons | 0.0105 | 2.183 | ATF3,CHL1,FGF2,FOS,TGFB1,TP53 |
| Branching of axons | 0.0226 | 2.183 | ATF3,FGF2,FOS,TGFB1,TP53 |
| Cell movement of leukocytes | 1.24E-08 | 2.18 | C3,CCL2,Ccl2,CCL4,CCL5,CD44,CXCL10,FAS,IL11RA,TNF,VCAM1 |
| Extension of neurites | 0.0153 | 2.157 | ATF3,CDKN1A,EPHA2,GEM,IFRD1,RRAD,SERPINE1,TNFRSF12A |

**Table 5-7 Continued - Predicated increased disease/functions as determined by IPA analysis at 96 h p.i., using a filter for neurological cell types. (2/2). Ordered in decreasing order of Activation Z-score, which is indicative of the level of activation of a pathway; scores above 0 are upregulated.**

## 5.4 Discussion

The aim of this chapter was to conduct a transcriptomic analysis of ZIKV-infected CNS co-cultures which were derived from the spinal cords of *Ifnar1* KO embryonic day 13 mice. CNS co-cultures possess all of the major cell types of the CNS, which include astrocytes, neurons, oligodendrocytes, oligodendrocyte precursors and microglia. Cultures were infected with ZIKV PE243 and RNAseq performed on RNA harvested at early and late infectious timepoints (48 and 96 h p.i, respectively) from co-cultures derived from three different litters (i.e. 3 independent biological replicates).

At 48 h p.i only 4 significant DEGs (Q value <0.05) were identified in ZIKV-infected co-cultures, comprising Ifit1, Cxcxl10, Ccl5 and Tpd52-ps – all of which were upregulated. Whereas at 96 h p.i 340 significant DEGs were identified; 303 DEGs were upregulated, and 37 downregulated. Numerous upregulated significant DEGs had immunomodulatory roles, the majority of which were involved in the recruitment of immune cells; this observation was made not only by examining individual upregulated transcripts, but also using the IPA gene function and pathway analysis tools.

An upregulated gene of note is Ovol1; it is the second most upregulated gene in cells infected with ZIKV at 96 h p.i, possessing a Log2FC value of 10.006. Interestingly, Ovol1 has also been found to be upregulated during influenza infection of mouse airway epithelial cells (Ioannidis et al., 2012), though its role in infection is unknown. Ovol1 is a transcription factor that acts downstream of Wnt/ß-catenin and TGF-ß signalling pathways. Ovol1 is expressed in a variety of tissues and is involved in the terminal differentiation of progenitor cells. A recent study of cellular programming in induced pluripotent stem cell production suggests that Ovol1 acts to repress the proliferation of cells that do not reprogram to acquire pluripotency i.e. transition into iPSCs (Kagawa et al., 2019). This study highlights that whilst Ovol1 is not directly involved in the acquisition of pluripotency it aids the reprogramming process in iPSC generation. Another molecule KLF4 (Kruppel-like factor 4), is implicated in reprogramming somatic cells into iPSCs (Qin and Zhang, 2012). Moreover, KLF4 was found to significantly upregulated during ZIKV infection at 96 h p.i. (Log2FC 1.023976, Q-value 0.004668). Oct3/4 Sox2 and c-Myc are also key contributors to iPSC

generation (Takahashi and Yamanaka, 2006). However, only Sox2 was found in the 96 h p.i. dataset, with marginal differential expression in ZIKV infected cultures (Log2fc 0.01341, Q-value 1). It is well documented that ZIKV replicates efficiently in iPSCs and progenitor cells (Dang et al., 2016, Russo et al., 2017, Tang et al., 2016) . It would be interesting to determine if ZIKV influences cell type populations within CNS co-cultures in order to render a favourable cellular niche, by increasing progenitor cell populations to confer a replicative advantage. In Chapter 4 Section 4.3.2, cell type specific populations of CNS co-cultures were quantified; however, oligodendrocyte progenitor cells were the only progenitor cell population analysed in this culture. Re-analysing these co-cultures using a stain for pluripotent cell types would be of interest. However, ZIKV also induces cytopathic responses within neural progenitor cells, therefore this may be difficult to determine by quantification of progenitor cell populations alone (Tang et al., 2016, Dang et al., 2016).To determine if Ovol1 and KLF4 aid viral replication, siRNA knockdown of these genes in cell lines or knockout cell lines could be generated.

Interestingly, aside from its roles in maintaining pluripotency, studies demonstrate the KLF4 is an regulator of axonal development; enhanced expression of KLF4 abolishes neurite outgrowth (processes extending from neurons) and impedes neuronal migration *in vitro* and *in vivo* (Moore et al., 2009, Qin and Zhang, 2012). Further roles of KLF4 as a transcription factor include cell cycle arrest and augmentation of pro-inflammatory responses; in particular, it has been demonstrated that KLF4 activates microglia, upregulating iNOS and pro-inflammatory cytokines such as TNF-a MCP-1 and IL-6 (Kaushik et al., 2010). iNOS is the only known agent that causes axonal injury *in vitro* (Smith et al., 2001, Kapoor et al., 2003). In Chapter 4 Section 4.3.4, it was found that CNS co-cultures infected with ZIKV are dramatically depleted of axons, whilst maintaining healthy neuron populations which consisted primarily of neuronal cell bodies possessing no neurite extensions. Whilst KLF4 expression may not contribute to axon loss, it may play roles in inhibiting axonal regeneration once damaged (Moore et al., 2009). Furthermore, KLF4 may indirectly exacerbate neuroinflammation which may drive axon loss in ZIKV-infected mixed-cell CNS co-cultures as a result of iNOS upregulation. Given the relatively low-level

upregulation of KLF4 (Log2FC 1.023976), it is likely several factors act cooperatively to cause the white matter pathology observed in CNS co-cultures.

A significantly downregulated gene of interested is the Mannose Receptor C Type 1 (MRC1; Log2FC -1.114). MRC1 is expressed on the surface of tissue macrophages and dendritic cells as well as some endothelial cells and can act as an entry receptor for numerous invading pathogens, including DENV (Taylor et al., 2005, Miller et al., 2008). Macrophage MRC1-mediated entry of HIV-1 results in non-productive infection. HIV-1 is processed by the antigen presentation pathway, resulting in the presentation of HIV-1 antigens by major histocompatibility complex-class II (MHCII) molecules, contributing to host innate immune responses (Trujillo et al., 2007, Sukegawa et al., 2018). A recent report demonstrates that MRC1 restricts HIV-1 release, and that HIV-1 counteracts this antiviral response via transcriptional silencing of MRC1 (Sukegawa et al., 2018). As MRC1 is downregulated during ZIKV infection, it may be that ZIKV has adapted mechanisms to overcome this innate immune response by reducing MRC1 expression. Though in this culture system, MRC downregulation is relatively low-level (Log2FC -1.114), this could be because expression is downregulated predominantly in microglia (CNS resident macrophages), which constitute a small portion of CNS co-cultures (microglia comprise approximately 7.3% of CNS co-cultures at DIV31 – Section 4.3.1).

In summary, this transcriptomic analysis of ZIKV-infected CNS co-cultures at early and late timepoints has provided an insight into the global CNS response to ZIKV infection. It is apparent from this dataset that ZIKV-infection induces an inflammatory response in CNS co-cultures, which is exacerbated over time both in the level of upregulation and number of pro-inflammatory molecules. Given the complex nature of this mixed-cell culture it is difficult to ascribe any given pathological phenotype, such as white matter structure injury, to specific molecules or cell-types. However, these analyses have provided a foundation for further study of candidate transcripts which may influence ZIKV infection of the CNS.

# 6 Concluding Remarks

The overarching aim of this thesis was to further knowledge surrounding ZIKV interactions within the CNS and PNS. Specific objectives included: the development/assessment of tools to study ZIKV infection *in vitro,* the identification of ZIKV permissive cell types in the CNS and PNS, and to analyse the transcriptome of a biologically relevant cell types infected with ZIKV.

In Chapter 3, an array of uncharacterised antibodies targeting either ZIKV NS1 or E protein were assessed by western blot and immunofluorescence analyses. This led to the identification of a highly specific monoclonal antibody which was used in downstream investigations (anti-ZIKV E clone 0402166, Aalto Biosciences). Using this antibody, it was found that astrocytes, the most prominent cell type in the CNS, are permissive to ZIKV infection. In this chapter a method for quantifying ZIKV genomic and subgenomic RNA was developed based upon a previously described protocol used in DENV research (Bidet et al., 2014); this qPCR methodology was subsequently used to determine that subgenomic RNA is produced in higher quantities than genomic RNA during ZIKV infection in A549 cells.

Mixed cell co-cultures containing the principle cell types of either the CNS or PNS were derived from mouse spinal cord or dorsal root ganglion, respectively; co-cultures were either WT or KO for the IFN α/ß receptor (*Ifnar1*). In Chapter 4, mixed-cell CNS and PNS cultures which contain all the principle cell types of their respective nervous system were identified as a biologically relevant, complex model to investigate ZIKV infection. It was found that both co-cultures are permissive to ZIKV infection, albeit to varying degrees. Furthermore, as determined by qPCR and plaque assay, it was found that the species origin of the cell line (mammalian vs invertebrate) used to propagate ZIKV affects virus replication in *Ifnar1* CNS co-cultures. ZIKV PE243 produced in invertebrate cells achieved higher titres and increased RNA levels in *Ifnar1* CNS co-cultures than its mammalian propagated counterpart (Section 3.3.4, Figure 3–13). It was also determined that the ZIKV strain MR766 has a significantly increased replicative capacity in both *Ifnar1* KO/WT CNS and *Ifnar1* PNS co-cultures compared with ZIKV strain PE243 of either mammalian or invertebrate cell origin (Section 3.3.4, Figure 3–13).

In Chapter 4, ZIKV infection of CNS and PNS co-culture was explored further. Using immunofluorescence techniques, it was found that CNS co-cultures are more susceptible to ZIKV infection than PNS co-cultures; PNS co-cultures were resistant to ZIKV infection. This indicates that the PNS disorder, Guillain-Barré syndrome, is unlikely to be a result of direct infection of cells of the PNS; rather ZIKV-associated GBS is likely to be a para- or post-infectious autoimmune disorder, as is predominantly the case with other infection related GBS aetiologies (Leonhard et al., 2018, Willison et al., 2016).

*Ifnar1* CNS co-cultures had the highest level of ZIKV infection and were used in all downstream investigations. Quantification of cell-type specific infection by manual counts of immunofluorescence images identified oligodendrocytes as the most vulnerable to infection with ZIKV. Whilst this method proved robust, a degree of variation may have been introduced into the experiment owing to human error when counting cells from complex images. It would therefore be interesting to develop a protocol which would enable the mixed-cell CNS co-culture to be analysed by cell type using flow cytometry in order to validate our cell-type specific quantification of ZIKV infection. This approach was considered during experimentation, though numerous factors prevented further exploration. The two main factors included 1) once the CNS co-culture is well established i.e. DIV28, trypsin does not effectively resuspend cells in this culture to allow it to be analysed by this method. 2) technical issues were faced when trying to locate a machine that would allow ZIKV-infected cells to be analysed. Another avenue that was explored was to develop a pipeline within ImageJ that would identify specific cell types, and therefore automate the process of quantifying cells. However, to generate and test this model robustly would have taken a significant amount of time; given that these data were time-critical upon commencement, it was not within the scope of this project.

Infection of CNS co-cultures at a timepoint reflective of late foetal development (approximating to the 3$^{rd}$ trimester, when myelination is starting to take place) caused injury to white matter structures leading to a remarkable loss of myelin, and axons. Curiously, the loss of axons was not accompanied by either injury to neuronal cell bodies, as indicated by healthy neuronal nuclei or marked increase in cell death within neuronal cell populations. The mechanism by which this

occurs remains to be determined. Given that these studies were performed *in vitro*, it would be prudent to perform the equivalent experiment *in vivo*. In order to make the experiment more authentic to real-life, it would be interesting to establish an infection model that uses mosquitoes to transmit ZIKV to the mammalian host. However, this would raise significant technical, practical and safety concerns and may be difficult to achieve unless in the appropriate facility. Instead, a method whereby mosquitoes could be allowed to bite the mammal, followed by subsequent injection of virus at the bite site, as established in (Pingen et al., 2016) would raise the degree of authenticity regarding virus spread and negate the associated biosafety concerns. Importantly, in this model the virus would need to be propagated in invertebrate cells prior to injection at the bite site, as the virus would need to mimic transmission from an invertebrate – as such it would require invertebrate glycosylation patterns. Generating a model system which is as close to real life as possible is important as it has been demonstrated that different routes of injection of virus can lead to altered cellular tropism. This was demonstrated in a model of Semliki Forest virus (SFV; an *Alphavirus*) infection, whereby intraperitoneal (IP) and intracranial (IC) injections yielded differing neurotropism; IP SFV displayed perivascular localisation in the brain, whereas IC SFV had tropism for white matter tracts in the corpus callosum (Fazakerley et al., 2006). Interestingly, SFV also infects oligodendrocytes, and has been demonstrated to induce a loss of CNS myelin (Mokhtarian et al., 2003, Fragkoudis et al., 2009). Using mouse models, adaptive immune responses are involved in the loss of myelin induced by SFV infection. This includes cytotoxic T-cell responses, B-cell activation, and cross-reactive antibody responses (Mokhtarian et al., 2003). The CNS co-culture model of ZIKV infection described in this thesis does not contain any lymphocytes, which means that the loss of myelin these cultures occurs via different mechanisms to SFV-induced myelin loss.

In this thesis, experiments demonstrating ZIKV-associated white matter injury were performed in CNS co-cultures which are reflective of late foetal/early post-natal staging of neurodevelopment. It would be interesting to determine if the loss of myelin can occur post-partum. Follow-up studies of human babies born to mothers who were ZIKV positive during pregnancy, suggest that the likelihood of neurodevelopmental issues decreases with advanced gestation. The

continued follow-up of these children will be required to determine if more subtle neurodevelopmental issues arise later in life (Nielsen-Saines et al., 2019).

In chapter 5, the transcriptomes of *Ifnar1* CNS co-cultures infected with ZIKV at 48 h.p.i and 96 h.p.i were analysed. It was found that ZIKV upregulated a number of transcripts involved in inflammatory pathways. Notably, ZIKV induced the upregulation of nitric oxide synthase (iNOS; produces NO) at 96 h p.i. Nitric oxide is the only known substance which is sufficient to cause axonal damage *in vitro (Smith et al., 2001, Hakim et al., 1996, Kapoor et al., 2003)*. This may contribute in part to ZIKV-induced white matter injury observed in CNS co-cultures in Chapter4.

The transcriptomic analysis presented in Chapter 5 highlighted several other candidate molecules worthy of further exploration to broaden the molecular biology of ZIKV-host interactions. It was found that MRC1, a receptor implicated in DENV entry of dermal macrophages and in HIV antiviral responses (Miller et al., 2008, Trujillo et al., 2007), was downregulated 96 h after infection with ZIKV. It would be interesting to know if MRC1 can act as an entry receptor for ZIKV, and if ZIKV actively downregulates MRC1 to evade antiviral defences. Another molecule of interest upregulated by ZIKV was Ovol1; at 96 h p.i Ovol1 was the second most upregulated transcript in CNS co-cultures. As discussed previously in Chapter 5 Section 5.4, Ovol1 has roles in regulating stem cell differentiation together with KLF4 (Kagawa et al., 2019, Nair et al., 2007). It would therefore be interesting to explore the roles of Ovol1 and KLF4 in ZIKV infection and its effects on CNS co-culture stem cell populations, via gene knockdown or knockout studies.

Wider concerns for ZIKV research are more clinically oriented. There are still no approved vaccines or antivirals against ZIKV. Numerous challenges face the successful development and deployment of a ZIKV vaccine. The target recipients are ideally pregnant women, which as a cohort are notoriously difficult to test medical interventions on given their disposition. Furthermore, socio-economic concerns would need to be considered; places were ZIKV are endemic have large impoverished regions – ensuring the necessary uptake of vaccines may be also be a challenge. Of course, vector control strategies would be favourable in such regions as there are also numerous co-circulating arboviruses transmitted by the

same mosquito. Again, impoverished regions, for example shanti-towns, are rife with mosquito breeding grounds therefore any vector control strategy would need to be able to penetrate these areas. Therefore, such outbreaks require diverse intervention strategies, which can include the identification of potential drug targets.

As mentioned previously, the follow-up of individuals born during ZIKV outbreaks to ZIKV-positive mothers is imperative. This will illuminate the extent of neurodevelopmental disorders associated with congenital ZIKV syndrome (CZS) and inform clinical practices to treat affected individuals. Continued efforts in basic and translational research are also essential in understanding and combating CZS.

# Appendices

Appendix 1: Differentially expressed genes at 96 h p.i with ZIKV in *Ifnar1* CNS co-cultures, arranged in decreasing Log2FC.

| Gene symbol | GeneID | Log2FC | Q-value |
|---|---|---|---|
| Ifnb1 | ENSMUSG00000048806 | 10.98223 | 1.57E-48 |
| Ovol1 | ENSMUSG00000024922 | 10.00622 | 2.20E-25 |
| Heatr9 | ENSMUSG00000018925 | 9.839729 | 1.57E-27 |
| Oasl1 | ENSMUSG00000041827 | 8.516512 | 7.85E-42 |
| Cxcl11 | ENSMUSG00000060183 | 8.20223 | 7.24E-34 |
| Cxcl1 | ENSMUSG00000029380 | 7.659263 | 6.30E-75 |
| Ccl5 | ENSMUSG00000035042 | 7.438624 | 1.58E-41 |
| Il6 | ENSMUSG00000025746 | 7.348566 | 2.98E-29 |
| Gbp5 | ENSMUSG00000105504 | 6.87963 | 9.54E-42 |
| Cxcl10 | ENSMUSG00000034855 | 6.747969 | 3.44E-89 |
| Cxcl2 | ENSMUSG00000058427 | 6.651629 | 8.67E-41 |
| Ccl2 | ENSMUSG00000035385 | 6.209305 | 1.04E-69 |
| Ccl7 | ENSMUSG00000035373 | 6.090213 | 1.13E-28 |
| Isg15 | ENSMUSG00000035692 | 5.446367 | 2.11E-27 |
| Oasl2 | ENSMUSG00000029561 | 5.437856 | 1.68E-23 |
| Gbp10 | ENSMUSG00000105096 | 5.246991 | 1.54E-17 |
| Ifit1 | ENSMUSG00000034459 | 5.169985 | 1.86E-73 |
| UNCHARACTERISED | ENSMUSG00000116657 | 5.044746 | 2.50E-15 |
| Rsad2 | ENSMUSG00000020641 | 4.979172 | 8.02E-32 |
| Oas1b | ENSMUSG00000029605 | 4.95168 | 4.25E-36 |
| Mx1 | ENSMUSG00000000386 | 4.632574 | 5.74E-15 |
| Ddx60 | ENSMUSG00000037921 | 4.555893 | 7.47E-27 |
| Stx11 | ENSMUSG00000039232 | 4.121373 | 3.53E-36 |
| Mir155hg | ENSMUSG00000097418 | 3.882976 | 4.16E-12 |
| Steap4 | ENSMUSG00000012428 | 3.796855 | 1.18E-30 |
| Mlkl | ENSMUSG00000012519 | 3.713876 | 6.70E-12 |
| Lcn2 | ENSMUSG00000026822 | 3.566697 | 1.12E-21 |
| Mx2 | ENSMUSG00000023341 | 3.518444 | 1.04E-26 |
| Cd40 | ENSMUSG00000017652 | 3.430872 | 6.09E-12 |
| Tnfaip2 | ENSMUSG00000021281 | 3.428105 | 5.12E-28 |
| Nos2 | ENSMUSG00000020826 | 3.390465 | 1.14E-08 |
| Cd69 | ENSMUSG00000030156 | 3.38975 | 5.46E-10 |
| H2-K2 | ENSMUSG00000067203 | 3.255757 | 2.99E-19 |
| Fosl1 | ENSMUSG00000024912 | 3.229966 | 1.54E-10 |
| Acod1 | ENSMUSG00000022126 | 3.122075 | 2.89E-10 |
| Gbp3 | ENSMUSG00000028268 | 3.030523 | 8.33E-29 |
| Casp4 | ENSMUSG00000033538 | 3.027949 | 7.49E-18 |
| Zbp1 | ENSMUSG00000027514 | 3.013457 | 3.65E-09 |
| Saa3 | ENSMUSG00000040026 | 2.911601 | 0.009854 |
| Ankrd33b | ENSMUSG00000022237 | 2.746735 | 2.24E-08 |
| Ptx3 | ENSMUSG00000027832 | 2.71848 | 3.45E-06 |
| Lipg | ENSMUSG00000053846 | 2.657271 | 7.62E-20 |
| Hes7 | ENSMUSG00000023781 | 2.638918 | 6.49E-08 |

| Gene symbol | GeneID | Log2FC | Q-value |
|---|---|---|---|
| Gbp2b | ENSMUSG00000040264 | 2.633292 | 6.91E-26 |
| Gbp9 | ENSMUSG00000029298 | 2.522424 | 3.29E-12 |
| Serpina3h | ENSMUSG00000041449 | 2.515369 | 2.89E-10 |
| Tnf | ENSMUSG00000024401 | 2.492198 | 3.71E-12 |
| A3galt2 | ENSMUSG00000028794 | 2.486541 | 8.69E-08 |
| Isg20 | ENSMUSG00000039236 | 2.475821 | 2.02E-10 |
| Maff | ENSMUSG00000042622 | 2.449069 | 4.68E-11 |
| Atp4a | ENSMUSG00000005553 | 2.436033 | 4.61E-09 |
| Upp1 | ENSMUSG00000020407 | 2.403246 | 1.31E-06 |
| Rtp4 | ENSMUSG00000033355 | 2.346549 | 1.93E-06 |
| Sphk1 | ENSMUSG00000061878 | 2.33632 | 3.48E-08 |
| Tgm1 | ENSMUSG00000022218 | 2.326612 | 0.001622 |
| Gbp6 | ENSMUSG00000104713 | 2.320043 | 9.44E-14 |
| Serpina3i | ENSMUSG00000079014 | 2.312569 | 1.12E-08 |
| Ifi204 | ENSMUSG00000073489 | 2.256098 | 6.01E-07 |
| Clec4e | ENSMUSG00000030142 | 2.251443 | 3.49E-05 |
| C2cd4b | ENSMUSG00000091956 | 2.234479 | 0.000107 |
| Ifi203 | ENSMUSG00000039997 | 2.230407 | 1.50E-06 |
| Ppp1r15a | ENSMUSG00000040435 | 2.186211 | 3.44E-19 |
| Nfkbie | ENSMUSG00000023947 | 2.185414 | 1.50E-19 |
| Icam1 | ENSMUSG00000037405 | 2.164415 | 7.24E-22 |
| Irf1 | ENSMUSG00000018899 | 2.143756 | 1.84E-13 |
| Chil1 | ENSMUSG00000064246 | 2.113351 | 6.26E-27 |
| Tnfsf18 | ENSMUSG00000066755 | 2.09871 | 9.09E-07 |
| Irf7 | ENSMUSG00000025498 | 2.077554 | 0.000541 |
| Tnip3 | ENSMUSG00000044162 | 2.072711 | 3.25E-10 |
| Ier3 | ENSMUSG00000003541 | 2.064412 | 1.44E-10 |
| H2-Q5 | ENSMUSG00000055413 | 2.050554 | 0.000442 |
| Nfkbia | ENSMUSG00000021025 | 2.030617 | 1.11E-16 |
| Vcam1 | ENSMUSG00000027962 | 1.984109 | 5.69E-26 |
| Ccrl2 | ENSMUSG00000043953 | 1.975259 | 5.12E-07 |
| Relb | ENSMUSG00000002983 | 1.953259 | 1.03E-21 |
| Ptgs2 | ENSMUSG00000032487 | 1.930729 | 0.002346 |
| Gch1 | ENSMUSG00000037580 | 1.922931 | 3.40E-09 |
| Arhgap28 | ENSMUSG00000024043 | 1.912509 | 2.93E-07 |
| Gbp7 | ENSMUSG00000040253 | 1.912279 | 4.41E-14 |
| Tnfaip3 | ENSMUSG00000019850 | 1.903277 | 2.41E-25 |
| Gbp2 | ENSMUSG00000028270 | 1.836212 | 7.09E-11 |
| Birc3 | ENSMUSG00000032000 | 1.766359 | 3.86E-13 |
| H2-Q6 | ENSMUSG00000073409 | 1.75824 | 0.041978 |
| Ifi202b | ENSMUSG00000026535 | 1.720967 | 3.01E-11 |
| Hspa1b | ENSMUSG00000090877 | 1.710083 | 5.89E-08 |
| Egr1 | ENSMUSG00000038418 | 1.699229 | 1.10E-17 |

| Gene symbol | GeneID | Log2FC | Q-value |
|---|---|---|---|
| Ifih1 | ENSMUSG00000026896 | 1.670821 | 2.11E-16 |
| Gm16465 | ENSMUSG00000083994 | 1.649543 | 0.001714 |
| Nfkbiz | ENSMUSG00000035356 | 1.647556 | 4.04E-18 |
| Timp1 | ENSMUSG00000001131 | 1.60703 | 0.00011 |
| Rnd1 | ENSMUSG00000054855 | 1.581276 | 2.62E-11 |
| Tlr2 | ENSMUSG00000027995 | 1.575354 | 1.11E-30 |
| Trib3 | ENSMUSG00000032715 | 1.528195 | 5.74E-05 |
| Stap2 | ENSMUSG00000038781 | 1.522349 | 0.000165 |
| AW112010 | ENSMUSG00000075010 | 1.520008 | 9.71E-06 |
| Pmaip1 | ENSMUSG00000024521 | 1.500973 | 4.95E-08 |
| Gpr84 | ENSMUSG00000063234 | 1.490917 | 2.80E-16 |
| Ccl4 | ENSMUSG00000018930 | 1.487996 | 0.001099 |
| Pappa | ENSMUSG00000028370 | 1.483866 | 0.00071 |
| Atf3 | ENSMUSG00000026628 | 1.478203 | 8.52E-06 |
| Has2 | ENSMUSG00000022367 | 1.47557 | 1.11E-08 |
| 1810032O08Rik | ENSMUSG00000020812 | 1.471084 | 1.00E-06 |
| Epha2 | ENSMUSG00000006445 | 1.46626 | 0.002563 |
| Cebpd | ENSMUSG00000071637 | 1.456389 | 8.32E-07 |
| Nfkb2 | ENSMUSG00000025225 | 1.430363 | 1.27E-15 |
| Ifit3 | ENSMUSG00000074896 | 1.402604 | 8.16E-07 |
| Junb | ENSMUSG00000052837 | 1.3934 | 9.71E-11 |
| Snhg15 | ENSMUSG00000085156 | 1.383603 | 1.09E-05 |
| Bid | ENSMUSG00000004446 | 1.379887 | 8.55E-08 |
| Ripk2 | ENSMUSG00000041135 | 1.376231 | 4.25E-12 |
| Gadd45b | ENSMUSG00000015312 | 1.374645 | 3.51E-08 |
| Cldn23 | ENSMUSG00000055976 | 1.369747 | 0.030078 |
| Plekha4 | ENSMUSG00000040428 | 1.36173 | 7.65E-05 |
| Il2rg | ENSMUSG00000031304 | 1.353359 | 8.82E-07 |
| Serpine1 | ENSMUSG00000037411 | 1.35277 | 0.015305 |
| Noct | ENSMUSG00000023087 | 1.349527 | 8.46E-11 |
| Gja5 | ENSMUSG00000057123 | 1.343735 | 0.001763 |
| Csrnp1 | ENSMUSG00000032515 | 1.339001 | 7.65E-05 |
| Ifrd1 | ENSMUSG00000001627 | 1.331742 | 4.09E-23 |
| Lif | ENSMUSG00000034394 | 1.315829 | 0.019062 |
| Adamts14 | ENSMUSG00000059901 | 1.301778 | 0.009153 |
| Ddit3 | ENSMUSG00000025408 | 1.296168 | 8.29E-09 |
| Gm20559 | ENSMUSG00000106734 | 1.291044 | 6.43E-05 |
| Ripk3 | ENSMUSG00000022221 | 1.283323 | 0.015958 |
| Zc3h12a | ENSMUSG00000042677 | 1.280109 | 1.04E-06 |
| Ccl12 | ENSMUSG00000035352 | 1.254663 | 0.020853 |
| Trim47 | ENSMUSG00000020773 | 1.254361 | 7.93E-06 |
| Samd9l | ENSMUSG00000047735 | 1.245596 | 3.05E-11 |
| Ptges | ENSMUSG00000050737 | 1.240614 | 2.58E-06 |

| Gene symbol | GeneID | Log2FC | Q-value |
|---|---|---|---|
| Gm13889 | ENSMUSG00000087006 | 1.236165 | 7.86E-06 |
| Hspa1a | ENSMUSG00000091971 | 1.233032 | 0.000807 |
| Cd274 | ENSMUSG00000016496 | 1.222071 | 1.04E-05 |
| Zmynd15 | ENSMUSG00000040829 | 1.199774 | 0.006932 |
| Dusp5 | ENSMUSG00000034765 | 1.193466 | 0.012799 |
| Ifit3b | ENSMUSG00000062488 | 1.187206 | 7.29E-07 |
| Socs1 | ENSMUSG00000038037 | 1.187069 | 0.007503 |
| Oas1c | ENSMUSG00000001166 | 1.182401 | 0.013967 |
| Bcl3 | ENSMUSG00000053175 | 1.176314 | 0.007688 |
| Grhl1 | ENSMUSG00000020656 | 1.171187 | 0.002275 |
| Gm45053 | ENSMUSG00000108368 | 1.158499 | 0.027982 |
| Rab20 | ENSMUSG00000031504 | 1.15442 | 0.000528 |
| Ocln | ENSMUSG00000021638 | 1.141036 | 3.39E-05 |
| Rhbdf2 | ENSMUSG00000020806 | 1.129858 | 2.17E-06 |
| Slc43a3 | ENSMUSG00000027074 | 1.117446 | 5.86E-09 |
| Pbld2 | ENSMUSG00000020072 | 1.105384 | 0.035792 |
| Rrad | ENSMUSG00000031880 | 1.095113 | 7.65E-05 |
| Cd74 | ENSMUSG00000024610 | 1.085794 | 0.013298 |
| Gm23935 | ENSMUSG00000076258 | 1.082937 | 0.000334 |
| Pim1 | ENSMUSG00000024014 | 1.077897 | 0.025362 |
| Micall2 | ENSMUSG00000036718 | 1.066716 | 2.27E-06 |
| Slc39a4 | ENSMUSG00000063354 | 1.055463 | 0.015565 |
| Parp14 | ENSMUSG00000034422 | 1.048938 | 3.51E-07 |
| Ier2 | ENSMUSG00000053560 | 1.04863 | 8.76E-07 |
| Slamf8 | ENSMUSG00000053318 | 1.039288 | 0.049214 |
| Klf4 | ENSMUSG00000003032 | 1.023976 | 0.004668 |
| H2-Q4 | ENSMUSG00000035929 | 1.016959 | 0.017643 |
| Gem | ENSMUSG00000028214 | 1.014068 | 0.000224 |
| Efcab8 | ENSMUSG00000044083 | 1.00994 | 0.024332 |
| Cp | ENSMUSG00000003617 | 1.000119 | 2.02E-06 |
| Taf4b | ENSMUSG00000054321 | 0.984892 | 0.000201 |
| Mir6236 | ENSMUSG00000098973 | 0.980588 | 0.006554 |
| Ddx58 | ENSMUSG00000040296 | 0.964819 | 9.22E-09 |
| Snhg1 | ENSMUSG00000108414 | 0.964428 | 2.82E-06 |
| Plekhf1 | ENSMUSG00000074170 | 0.961454 | 7.29E-07 |
| Shisa3 | ENSMUSG00000050010 | 0.955845 | 0.014802 |
| Nabp1 | ENSMUSG00000026107 | 0.953856 | 1.08E-05 |
| Nupr1 | ENSMUSG00000030717 | 0.950689 | 0.022489 |
| A630072M18Rik | ENSMUSG00000101013 | 0.939031 | 0.001406 |
| Gm26917 | ENSMUSG00000097971 | 0.938401 | 8.16E-07 |
| Pik3r5 | ENSMUSG00000020901 | 0.93835 | 8.48E-06 |
| Ddias | ENSMUSG00000030641 | 0.935409 | 0.016418 |
| Gtse1 | ENSMUSG00000022385 | 0.934641 | 0.001336 |

| Gene symbol | GeneID | Log2FC | Q-value |
|---|---|---|---|
| Tnfrsf12a | ENSMUSG00000023905 | 0.93304 | 0.001914 |
| Arid5a | ENSMUSG00000037447 | 0.931238 | 0.001342 |
| Clec5a | ENSMUSG00000029915 | 0.922174 | 0.001691 |
| Eif4ebp1 | ENSMUSG00000031490 | 0.914086 | 0.005184 |
| Trim17 | ENSMUSG00000036964 | 0.913327 | 0.002731 |
| Helz2 | ENSMUSG00000027580 | 0.902181 | 7.11E-06 |
| Ikbke | ENSMUSG00000042349 | 0.897478 | 8.32E-07 |
| Pvr | ENSMUSG00000040511 | 0.88012 | 0.000639 |
| Bbc3 | ENSMUSG00000002083 | 0.880104 | 0.003072 |
| Tnfrsf10b | ENSMUSG00000022074 | 0.876957 | 0.000664 |
| Socs2 | ENSMUSG00000020027 | 0.876682 | 0.009579 |
| C3 | ENSMUSG00000024164 | 0.872478 | 0.012903 |
| 2410006H16Rik | ENSMUSG00000086841 | 0.854823 | 4.79E-05 |
| Arl5c | ENSMUSG00000038352 | 0.849281 | 0.026559 |
| Map3k8 | ENSMUSG00000024235 | 0.84342 | 0.004593 |
| Tapbpl | ENSMUSG00000038213 | 0.839065 | 0.002825 |
| Cxcl16 | ENSMUSG00000018920 | 0.831651 | 6.00E-07 |
| Cebpb | ENSMUSG00000056501 | 0.826168 | 0.002758 |
| Neurl3 | ENSMUSG00000047180 | 0.819525 | 0.032931 |
| Cd44 | ENSMUSG00000005087 | 0.809505 | 0.017599 |
| Ube2l6 | ENSMUSG00000027078 | 0.807948 | 0.019849 |
| Phlda1 | ENSMUSG00000020205 | 0.807528 | 0.000222 |
| Slc16a10 | ENSMUSG00000019838 | 0.803474 | 0.004824 |
| Herc6 | ENSMUSG00000029798 | 0.802781 | 0.002913 |
| Rras | ENSMUSG00000038387 | 0.801473 | 0.00473 |
| 5430416N02Rik | ENSMUSG00000097772 | 0.798025 | 0.017763 |
| Arrdc4 | ENSMUSG00000042659 | 0.791839 | 0.003304 |
| Ctps | ENSMUSG00000028633 | 0.78739 | 1.46E-05 |
| Igsf9 | ENSMUSG00000037995 | 0.777398 | 0.012592 |
| Fos | ENSMUSG00000021250 | 0.773808 | 0.002837 |
| Snhg12 | ENSMUSG00000086290 | 0.770671 | 0.016492 |
| Zc3hav1 | ENSMUSG00000029826 | 0.764452 | 0.000569 |
| Tgif1 | ENSMUSG00000047407 | 0.764213 | 0.000155 |
| Zfp711 | ENSMUSG00000025529 | 0.761898 | 0.003507 |
| Btg2 | ENSMUSG00000020423 | 0.761751 | 0.000186 |
| Foxn2 | ENSMUSG00000034998 | 0.761473 | 4.37E-06 |
| Cdkn1a | ENSMUSG00000023067 | 0.758626 | 0.02053 |
| Slc4a7 | ENSMUSG00000021733 | 0.753568 | 2.11E-05 |
| Eda2r | ENSMUSG00000034457 | 0.752044 | 0.000425 |
| Dennd3 | ENSMUSG00000036661 | 0.746354 | 0.010778 |
| 2810474O19Rik | ENSMUSG00000032712 | 0.745389 | 7.43E-07 |
| Ets1 | ENSMUSG00000032035 | 0.743016 | 0.000732 |
| Chac1 | ENSMUSG00000027313 | 0.719942 | 0.034353 |

| Gene symbol | GeneID | Log2FC | Q-value |
|---|---|---|---|
| Trp53 | ENSMUSG00000059552 | 0.718825 | 3.49E-05 |
| Cd14 | ENSMUSG00000051439 | 0.71719 | 6.32E-05 |
| Tiparp | ENSMUSG00000034640 | 0.710561 | 1.76E-05 |
| Rnf19b | ENSMUSG00000028793 | 0.710034 | 1.43E-05 |
| Jun | ENSMUSG00000052684 | 0.708239 | 0.021571 |
| Slc7a1 | ENSMUSG00000041313 | 0.702388 | 3.40E-05 |
| Zfp36 | ENSMUSG00000044786 | 0.698112 | 0.045845 |
| Hbegf | ENSMUSG00000024486 | 0.694472 | 0.031739 |
| Apobr | ENSMUSG00000042759 | 0.693574 | 0.024366 |
| Slc25a25 | ENSMUSG00000026819 | 0.692594 | 7.65E-05 |
| Gnl3 | ENSMUSG00000042354 | 0.690501 | 3.96E-05 |
| Plxnd1 | ENSMUSG00000030123 | 0.687459 | 0.001631 |
| Thbs2 | ENSMUSG00000023885 | 0.680782 | 0.019062 |
| Itpkc | ENSMUSG00000003752 | 0.680026 | 0.009257 |
| Igsf6 | ENSMUSG00000035004 | 0.668832 | 0.01868 |
| Rnf213 | ENSMUSG00000070327 | 0.667909 | 1.13E-05 |
| Ptpn2 | ENSMUSG00000024539 | 0.666718 | 0.000224 |
| Pinx1 | ENSMUSG00000021958 | 0.662955 | 0.032312 |
| 1110008P14Rik | ENSMUSG00000039195 | 0.662885 | 0.000572 |
| Car13 | ENSMUSG00000027555 | 0.660341 | 0.007683 |
| Zfp948 | ENSMUSG00000067931 | 0.659014 | 0.02339 |
| Dok1 | ENSMUSG00000068335 | 0.655031 | 0.038499 |
| Fgf2 | ENSMUSG00000037225 | 0.644459 | 0.006132 |
| Ifit2 | ENSMUSG00000045932 | 0.644369 | 0.00113 |
| Snhg17 | ENSMUSG00000085385 | 0.641485 | 0.007567 |
| Itga5 | ENSMUSG00000000555 | 0.641108 | 0.004058 |
| Fam129a | ENSMUSG00000026483 | 0.63822 | 0.004668 |
| Mvp | ENSMUSG00000030681 | 0.632117 | 0.007355 |
| Zfas1 | ENSMUSG00000074578 | 0.625277 | 0.005164 |
| Smad3 | ENSMUSG00000032402 | 0.622829 | 0.006779 |
| Zbtb2 | ENSMUSG00000075327 | 0.62254 | 0.045379 |
| Mcc | ENSMUSG00000071856 | 0.608918 | 0.02388 |
| Ralb | ENSMUSG00000004451 | 0.605752 | 0.003832 |
| Aen | ENSMUSG00000030609 | 0.601381 | 0.006779 |
| Zbtb10 | ENSMUSG00000069114 | 0.596426 | 0.005168 |
| Sirt1 | ENSMUSG00000020063 | 0.594414 | 0.006454 |
| Rel | ENSMUSG00000020275 | 0.593104 | 0.012592 |
| Plk2 | ENSMUSG00000021701 | 0.583654 | 0.030078 |
| Baz1a | ENSMUSG00000035021 | 0.583246 | 0.016492 |
| Map3k14 | ENSMUSG00000020941 | 0.581162 | 0.033662 |
| Mapkapk3 | ENSMUSG00000032577 | 0.575067 | 0.046211 |
| Lacc1 | ENSMUSG00000044350 | 0.574281 | 0.00406 |
| Rassf1 | ENSMUSG00000010067 | 0.568801 | 0.039538 |

| Gene symbol | GeneID | Log2FC | Q-value |
|---|---|---|---|
| Rhbdf1 | ENSMUSG00000020282 | 0.56841 | 0.023155 |
| Parp9 | ENSMUSG00000022906 | 0.566044 | 0.025593 |
| Rai14 | ENSMUSG00000022246 | 0.561125 | 0.006313 |
| Sesn2 | ENSMUSG00000028893 | 0.552715 | 0.002115 |
| Atf4 | ENSMUSG00000042406 | 0.550601 | 0.002382 |
| Rnd3 | ENSMUSG00000017144 | 0.548773 | 0.00203 |
| Fas | ENSMUSG00000024778 | 0.539835 | 0.010607 |
| Ermard | ENSMUSG00000036552 | 0.535626 | 0.031739 |
| Nop58 | ENSMUSG00000026020 | 0.532125 | 0.001434 |
| Stat2 | ENSMUSG00000040033 | 0.527226 | 0.004381 |
| Insig1 | ENSMUSG00000045294 | 0.527043 | 0.000528 |
| Zfp131 | ENSMUSG00000094870 | 0.519264 | 0.004932 |
| Fam46a | ENSMUSG00000032265 | 0.516225 | 0.037385 |
| Chl1 | ENSMUSG00000030077 | 0.515374 | 0.038847 |
| Tmem39a | ENSMUSG00000002845 | 0.51519 | 0.027708 |
| Susd6 | ENSMUSG00000021133 | 0.507249 | 0.014771 |
| Klf6 | ENSMUSG00000000078 | 0.503998 | 0.012944 |
| Pde4b | ENSMUSG00000028525 | 0.50396 | 0.021258 |
| Mthfd2 | ENSMUSG00000005667 | 0.50225 | 0.041511 |
| Nfkb1 | ENSMUSG00000028163 | 0.502166 | 0.001962 |
| Sap30 | ENSMUSG00000031609 | 0.492761 | 0.049214 |
| Traf2 | ENSMUSG00000026942 | 0.491188 | 0.037139 |
| Gm8566 | ENSMUSG00000047905 | 0.490643 | 0.03747 |
| Cflar | ENSMUSG00000026031 | 0.489013 | 0.002913 |
| Vasp | ENSMUSG00000030403 | 0.488591 | 0.040214 |
| Slc2a6 | ENSMUSG00000036067 | 0.48606 | 0.019849 |
| Bcl10 | ENSMUSG00000028191 | 0.485127 | 0.020596 |
| Cebpg | ENSMUSG00000056216 | 0.481012 | 0.003383 |
| Nfkbib | ENSMUSG00000030595 | 0.480379 | 0.031895 |
| Tgfb1 | ENSMUSG00000002603 | 0.476989 | 0.027708 |
| Bach1 | ENSMUSG00000025612 | 0.471628 | 0.035792 |
| Pnrc1 | ENSMUSG00000040128 | 0.469079 | 0.020853 |
| Brd2 | ENSMUSG00000024335 | 0.466931 | 0.016492 |
| Mdm2 | ENSMUSG00000020184 | 0.465562 | 0.008314 |
| Trpc1 | ENSMUSG00000032839 | 0.460747 | 0.045182 |
| Ptpn12 | ENSMUSG00000028771 | 0.458711 | 0.013854 |
| Zc3h7a | ENSMUSG00000037965 | 0.458191 | 0.022685 |
| Tnip1 | ENSMUSG00000020400 | 0.443435 | 0.036386 |
| Cybb | ENSMUSG00000015340 | 0.441582 | 0.007688 |
| Anxa3 | ENSMUSG00000029484 | 0.433356 | 0.024315 |
| Slc25a37 | ENSMUSG00000034248 | 0.4199 | 0.038847 |
| Arhgef17 | ENSMUSG00000032875 | 0.41939 | 0.023332 |
| Ptpn23 | ENSMUSG00000036057 | 0.41599 | 0.049795 |
| Ascc3 | ENSMUSG00000038774 | 0.412092 | 0.040637 |

| Gene symbol | GeneID | Log2FC | Q-value |
|---|---|---|---|
| Crb2 | ENSMUSG00000035403 | -0.41195 | 0.040214 |
| Dhrs3 | ENSMUSG00000066026 | -0.41956 | 0.031895 |
| Psd2 | ENSMUSG00000024347 | -0.42121 | 0.049746 |
| Acot11 | ENSMUSG00000034853 | -0.42924 | 0.02636 |
| Ppp1r1a | ENSMUSG00000022490 | -0.43669 | 0.039538 |
| Spag6 | ENSMUSG00000022783 | -0.4538 | 0.027057 |
| Cfap52 | ENSMUSG00000020904 | -0.45551 | 0.016492 |
| Cfap46 | ENSMUSG00000049571 | -0.45863 | 0.049528 |
| Abhd1 | ENSMUSG00000006638 | -0.47371 | 0.033662 |
| Slc39a12 | ENSMUSG00000036949 | -0.47989 | 0.013874 |
| Ttc21a | ENSMUSG00000032514 | -0.48127 | 0.01682 |
| Cfap65 | ENSMUSG00000047021 | -0.49049 | 0.01329 |
| Drc3 | ENSMUSG00000056598 | -0.49113 | 0.017763 |
| Vsir | ENSMUSG00000020101 | -0.50713 | 0.012087 |
| Ak9 | ENSMUSG00000091415 | -0.50916 | 0.013388 |
| Sema6d | ENSMUSG00000027200 | -0.51389 | 0.02139 |
| Dnah6 | ENSMUSG00000052861 | -0.51425 | 0.026219 |
| Fbln5 | ENSMUSG00000021186 | -0.52889 | 0.001582 |
| Enho | ENSMUSG00000028445 | -0.53162 | 0.003507 |
| Nkain4 | ENSMUSG00000027574 | -0.5405 | 0.024315 |
| Map3k19 | ENSMUSG00000051590 | -0.54231 | 0.013967 |
| Fcgr3 | ENSMUSG00000059498 | -0.56318 | 0.026558 |
| Lcat | ENSMUSG00000035237 | -0.56365 | 0.029547 |
| Vstm4 | ENSMUSG00000050666 | -0.60156 | 0.012903 |
| Bbox1 | ENSMUSG00000041660 | -0.60195 | 0.007688 |
| Id4 | ENSMUSG00000021379 | -0.62854 | 0.000604 |
| Traf1 | ENSMUSG00000026875 | -0.63995 | 0.003507 |
| Ptgs1 | ENSMUSG00000047250 | -0.66685 | 0.002376 |
| Slco2b1 | ENSMUSG00000030737 | -0.67931 | 0.014771 |
| Adamts16 | ENSMUSG00000049538 | -0.68263 | 0.033574 |
| Ppp1r1b | ENSMUSG00000061718 | -0.72459 | 0.000103 |
| Tprkb | ENSMUSG00000054226 | -0.81679 | 0.000471 |
| Trp73 | ENSMUSG00000029026 | -0.88451 | 0.02568 |
| Tlr8 | ENSMUSG00000040522 | -0.96246 | 0.011103 |
| Tmem52 | ENSMUSG00000023153 | -1.05901 | 0.029592 |
| Mrc1 | ENSMUSG00000026712 | -1.11422 | 0.003129 |
| Il11ra2 | ENSMUSG00000095456 | -7.85813 | 9.82E-17 |

# List of References

ADAMS, N. J., PRESCOTT, L. E., JARVIS, L. M., LEWIS, J. C., MCCLURE, M. O., SMITH, D. B. & SIMMONDS, P. 1998. Detection in chimpanzees of a novel flavivirus related to GB virus-C/hepatitis G virus. *J Gen Virol,* 79 ( Pt 8), 1871-7.

ADAMS WALDORF, K. M., NELSON, B. R., STENCEL-BAERENWALD, J. E., STUDHOLME, C., KAPUR, R. P., ARMISTEAD, B., WALKER, C. L., MERILLAT, S., VORNHAGEN, J., TISONCIK-GO, J., BALDESSARI, A., COLEMAN, M., DIGHE, M. K., SHAW, D. W. W., ROBY, J. A., SANTANA-UFRET, V., BOLDENOW, E., LI, J., GAO, X., DAVIS, M. A., SWANSTROM, J. A., JENSEN, K., WIDMAN, D. G., BARIC, R. S., MEDWID, J. T., HANLEY, K. A., OGLE, J., GOUGH, G. M., LEE, W., ENGLISH, C., DURNING, W. M., THIEL, J., GATENBY, C., DEWEY, E. C., FAIRGRIEVE, M. R., HODGE, R. D., GRANT, R. F., KULLER, L., DOBYNS, W. B., HEVNER, R. F., GALE, M. & RAJAGOPAL, L. 2018. Congenital Zika virus infection as a silent pathology with loss of neurogenic output in the fetal brain. *Nat Med,* 24, 368-374.

ADEBANJO, T., GODFRED-CATO, S., VIENS, L., FISCHER, M., STAPLES, J. E., KUHNERT-TALLMAN, W., WALKE, H., ODUYEBO, T., POLEN, K., PEACOCK, G., MEANEY-DELMAN, D., HONEIN, M. A., RASMUSSEN, S. A., MOORE, C. A. & CONTRIBUTORS 2017. Update: Interim Guidance for the Diagnosis, Evaluation, and Management of Infants with Possible Congenital Zika Virus Infection - United States, October 2017. *MMWR Morb Mortal Wkly Rep,* 66, 1089-1099.

AGILENT 2012. RNA quality control using the Agilent 2200 TapeStation system – Assessment of the RINe quality metric. *Publication number 59911-0023EN.*

AKTEPE, T. E., LIEBSCHER, S., PRIER, J. E., SIMMONS, C. P. & MACKENZIE, J. M. 2017. The Host Protein Reticulon 3.1A Is Utilized by Flaviviruses to Facilitate Membrane Remodelling. *Cell Rep,* 21, 1639-1654.

ALEN, M. M., DALLMEIER, K., BALZARINI, J., NEYTS, J. & SCHOLS, D. 2012. Crucial role of the N-glycans on the viral E-envelope glycoprotein in DC-SIGN-mediated dengue virus infection. *Antiviral Res,* 96, 280-7.

ALIOTA, M. T., CAINE, E. A., WALKER, E. C., LARKIN, K. E., CAMACHO, E. & OSORIO, J. E. 2016. Characterization of Lethal Zika Virus Infection in AG129 Mice. *PLoS Negl Trop Dis,* 10, e0004682.

ALLISON, S. L., SCHALICH, J., STIASNY, K., MANDL, C. W. & HEINZ, F. X. 2001. Mutational evidence for an internal fusion peptide in flavivirus envelope protein E. *J Virol,* 75, 4268-75.

ARAGAO, M. F. V. V., HOLANDA, A. C., BRAINER-LIMA, A. M., PETRIBU, N. C. L., CASTILLO, M., VAN DER LINDEN, V., SERPA, S. C., TENÓRIO, A. G., TRAVASSOS, P. T. C., CORDEIRO, M. T., SARTESCHI, C., VALENCA, M. M. & COSTELLO, A. 2017. Nonmicrocephalic Infants with Congenital Zika Syndrome Suspected Only after Neuroimaging Evaluation Compared with Those with Microcephaly at Birth and Postnatally: How Large Is the Zika Virus "Iceberg"? *AJNR Am J Neuroradiol,* 38, 1427-1434.

AZOUZ, F., ARORA, K., KRAUSE, K., NERURKAR, V. R. & KUMAR, M. 2019. Integrated MicroRNA and mRNA Profiling in Zika Virus-Infected Neurons. *Viruses,* 11.

BABICKI, S., ARNDT, D., MARCU, A., LIANG, Y., GRANT, J. R., MACIEJEWSKI, A. & WISHART, D. S. 2016. Heatmapper: web-enabled heat mapping for all. *Nucleic Acids Res,* 44, W147-53.

BARKOVICH, A. J. & LINDAN, C. E. 1994. Congenital cytomegalovirus infection of the brain: imaging analysis and embryologic considerations. *AJNR Am J Neuroradiol,* 15**,** 703-15.

BAYLESS, N. L., GREENBERG, R. S., SWIGUT, T., WYSOCKA, J. & BLISH, C. A. 2016. Zika Virus Infection Induces Cranial Neural Crest Cells to Produce Cytokines at Levels Detrimental for Neurogenesis. *Cell Host Microbe,* 20**,** 423-428.

BEASLEY, D. W., WHITEMAN, M. C., ZHANG, S., HUANG, C. Y., SCHNEIDER, B. S., SMITH, D. R., GROMOWSKI, G. D., HIGGS, S., KINNEY, R. M. & BARRETT, A. D. 2005. Envelope protein glycosylation status influences mouse neuroinvasion phenotype of genetic lineage 1 West Nile virus strains. *J Virol,* 79**,** 8339-47.

BELL, T. M., FIELD, E. J. & NARANG, H. K. 1971. Zika virus infection of the central nervous system of mice. *Arch Gesamte Virusforsch,* 35**,** 183-93.

BESNARD, M., LASTERE, S., TEISSIER, A., CAO-LORMEAU, V. & MUSSO, D. 2014. Evidence of perinatal transmission of Zika virus, French Polynesia, December 2013 and February 2014. *Euro Surveill,* 19.

BEST, S. M. 2017. The Many Faces of the Flavivirus NS5 Protein in Antagonism of Type I Interferon Signaling. *J Virol,* 91.

BHUVANAKANTHAM, R., CHEONG, Y. K. & NG, M. L. 2010. West Nile virus capsid protein interaction with importin and HDM2 protein is regulated by protein kinase C-mediated phosphorylation. *Microbes Infect,* 12**,** 615-25.

BIDET, K., DADLANI, D. & GARCIA-BLANCO, M. A. 2014. G3BP1, G3BP2 and CAPRIN1 are required for translation of interferon stimulated mRNAs and are targeted by a dengue virus non-coding RNA. *PLoS Pathog,* 10**,** e1004242.

BRESSANELLI, S., STIASNY, K., ALLISON, S. L., STURA, E. A., DUQUERROY, S., LESCAR, J., HEINZ, F. X. & REY, F. A. 2004. Structure of a flavivirus envelope glycoprotein in its low-pH-induced membrane fusion conformation. *EMBO J,* 23**,** 728-38.

BRUBAKER, S. W., BONHAM, K. S., ZANONI, I. & KAGAN, J. C. 2015. Innate immune pattern recognition: a cell biological perspective. *Annu Rev Immunol,* 33**,** 257-90.

CALABRESE, V., MANCUSO, C., CALVANI, M., RIZZARELLI, E., BUTTERFIELD, D. A. & STELLA, A. M. 2007. Nitric oxide in the central nervous system: neuroprotection versus neurotoxicity. *Nat Rev Neurosci,* 8**,** 766-75.

CAMINADE, C., MEDLOCK, J. M., DUCHEYNE, E., MCINTYRE, K. M., LEACH, S., BAYLIS, M. & MORSE, A. P. 2012. Suitability of European climate for the Asian tiger mosquito Aedes albopictus: recent trends and future scenarios. *J R Soc Interface,* 9**,** 2708-17.

CAMPOS, G. S., BANDEIRA, A. C. & SARDI, S. I. 2015. Zika Virus Outbreak, Bahia, Brazil. *Emerg Infect Dis,* 21**,** 1885-6.

CAO-LORMEAU, V. M., BLAKE, A., MONS, S., LASTERE, S., ROCHE, C., VANHOMWEGEN, J., DUB, T., BAUDOUIN, L., TEISSIER, A., LARRE, P., VIAL, A. L., DECAM, C., CHOUMET, V., HALSTEAD, S. K., WILLISON, H. J., MUSSET, L., MANUGUERRA, J. C., DESPRES, P., FOURNIER, E., MALLET, H. P., MUSSO, D., FONTANET, A., NEIL, J. & GHAWCHÉ, F. 2016. Guillain-Barré Syndrome outbreak associated with Zika virus infection in French Polynesia: a case-control study. *Lancet,* 387**,** 1531-1539.

CAO-LORMEAU, V. M., ROCHE, C., TEISSIER, A., ROBIN, E., BERRY, A. L., MALLET, H. P., SALL, A. A. & MUSSO, D. 2014. Zika virus, French polynesia, South pacific, 2013. *Emerg Infect Dis,* 20**,** 1085-6.

CARBAUGH, D. L., BARIC, R. S. & LAZEAR, H. M. 2019. Envelope protein glycosylation mediates Zika virus pathogenesis. *J Virol*.

CDC. 2019. *Congenital Zika Syndrome & Other Birth Defects* [Online]. Centres for Disease Control and Prevention, Zika and Pregnancy: CDC. Available: https://www.cdc.gov/pregnancy/zika/testing-follow-up/zika-syndrome-birth-defects.html [Accessed 17 June 2019].

CHAMBERS, T. J., NESTOROWICZ, A., AMBERG, S. M. & RICE, C. M. 1993. Mutagenesis of the yellow fever virus NS2B protein: effects on proteolytic processing, NS2B-NS3 complex formation, and viral replication. *J Virol,* 67**,** 6797-807.

CHANDRIANI, S., SKEWES-COX, P., ZHONG, W., GANEM, D. E., DIVERS, T. J., VAN BLARICUM, A. J., TENNANT, B. C. & KISTLER, A. L. 2013. Identification of a previously undescribed divergent virus from the Flaviviridae family in an outbreak of equine serum hepatitis. *Proc Natl Acad Sci U S A,* 110**,** E1407-15.

CHANG, R. Y., HSU, T. W., CHEN, Y. L., LIU, S. F., TSAI, Y. J., LIN, Y. T., CHEN, Y. S. & FAN, Y. H. 2013. Japanese encephalitis virus non-coding RNA inhibits activation of interferon by blocking nuclear translocation of interferon regulatory factor 3. *Vet Microbiol,* 166**,** 11-21.

CHAPMAN, E. G., COSTANTINO, D. A., RABE, J. L., MOON, S. L., WILUSZ, J., NIX, J. C. & KIEFT, J. S. 2014a. The structural basis of pathogenic subgenomic flavivirus RNA (sfRNA) production. *Science,* 344**,** 307-10.

CHAPMAN, E. G., MOON, S. L., WILUSZ, J. & KIEFT, J. S. 2014b. RNA structures that resist degradation by Xrn1 produce a pathogenic Dengue virus RNA. *Elife,* 3**,** e01892.

CHAVALI, P. L., STOJIC, L., MEREDITH, L. W., JOSEPH, N., NAHORSKI, M. S., SANFORD, T. J., SWEENEY, T. R., KRISHNA, B. A., HOSMILLO, M., FIRTH, A. E., BAYLISS, R., MARCELIS, C. L., LINDSAY, S., GOODFELLOW, I., WOODS, C. G. & GERGELY, F. 2017. Neurodevelopmental protein Musashi-1 interacts with the Zika genome and promotes viral replication. *Science,* 357**,** 83-88.

CHIMELLI, L. & AVVAD-PORTARI, E. 2018. Congenital Zika virus infection: a neuropathological review. *Childs Nerv Syst,* 34**,** 95-99.

CHIMELLI, L., MELO, A. S. O., AVVAD-PORTARI, E., WILEY, C. A., CAMACHO, A. H. S., LOPES, V. S., MACHADO, H. N., ANDRADE, C. V., DOCK, D. C. A., MOREIRA, M. E., TOVAR-MOLL, F., OLIVEIRA-SZEJNFELD, P. S., CARVALHO, A. C. G., UGARTE, O. N., BATISTA, A. G. M., AMORIM, M. M. R., MELO, F. O., FERREIRA, T. A., MARINHO, J. R. L., AZEVEDO, G. S., LEAL, J. I. B. F., DA COSTA, R. F. M., REHEN, S., ARRUDA, M. B., BRINDEIRO, R. M., DELVECHIO, R., AGUIAR, R. S. & TANURI, A. 2017. The spectrum of neuropathological changes associated with congenital Zika virus infection. *Acta Neuropathol,* 133**,** 983-999.

CHRISTOPHERS, S. R. 1960. *Aedes aegypti (L.), the yellow fever mosquito: its life history, bionomics and structure,* Cambridge, MA, Cambridge University Press.

CHU, J. J. & NG, M. L. 2004a. Infectious entry of West Nile virus occurs through a clathrin-mediated endocytic pathway. *J Virol,* 78**,** 10543-55.

CHU, J. J. & NG, M. L. 2004b. Interaction of West Nile virus with alpha v beta 3 integrin mediates virus entry into cells. *J Biol Chem,* 279**,** 54533-41.

COLPITTS, T. M., BARTHEL, S., WANG, P. & FIKRIG, E. 2011. Dengue virus capsid protein binds core histones and inhibits nucleosome formation in human liver cells. *PLoS One,* 6**,** e24365.

CUGOLA, F. R., FERNANDES, I. R., RUSSO, F. B., FREITAS, B. C., DIAS, J. L., GUIMARÃES, K. P., BENAZZATO, C., ALMEIDA, N., PIGNATARI, G. C., ROMERO, S., POLONIO, C. M., CUNHA, I., FREITAS, C. L., BRANDÃO, W. N., ROSSATO, C., ANDRADE, D. G., FARIA, D. E. P., GARCEZ, A. T., BUCHPIGEL, C. A., BRACONI, C. T., MENDES, E., SALL, A. A., ZANOTTO, P. M., PERON, J. P., MUOTRI, A. R. & BELTRÃO-BRAGA, P. C. 2016. The Brazilian Zika virus strain causes birth defects in experimental models. *Nature,* 534**,** 267-71.

CUI, T., SUGRUE, R. J., XU, Q., LEE, A. K., CHAN, Y. C. & FU, J. 1998. Recombinant dengue virus type 1 NS3 protein exhibits specific viral RNA binding and NTPase activity regulated by the NS5 protein. *Virology,* 246**,** 409-17.

CULJAT, M., DARLING, S. E., NERURKAR, V. R., CHING, N., KUMAR, M., MIN, S. K., WONG, R., GRANT, L. & MELISH, M. E. 2016. Clinical and Imaging Findings in an Infant With Zika Embryopathy. *Clin Infect Dis,* 63**,** 805-11.

CUMBERWORTH, S. L., BARRIE, J. A., CUNNINGHAM, M. E., DE FIGUEIREDO, D. P. G., SCHULTZ, V., WILDER-SMITH, A. J., BRENNAN, B., PENA, L. J., FREITAS DE OLIVEIRA FRANCA, R., LININGTON, C., BARNETT, S. C., WILLISON, H. J., KOHL, A. & EDGAR, J. M. 2017a. Zika virus tropism and interactions in myelinating neural cell cultures: CNS cells and myelin are preferentially affected. *Acta Neuropathol Commun,* 5**,** 50.

CUMBERWORTH, S. L., CLARK, J. J., KOHL, A. & DONALD, C. L. 2017b. Inhibition of type I interferon induction and signalling by mosquito-borne flaviviruses. *Cell Microbiol,* 19.

DAGLEISH, M. P., CLARK, J. J., ROBSON, C., TUCKER, M., ORTON, R. J. & ROCCHI, M. S. 2018. A Fatal Case of Louping-ill in a Dog: Immunolocalization and Full Genome Sequencing of the Virus. *J Comp Pathol,* 165**,** 23-32.

DALRYMPLE, N. A., CIMICA, V. & MACKOW, E. R. 2015. Dengue Virus NS Proteins Inhibit RIG-I/MAVS Signaling by Blocking TBK1/IRF3 Phosphorylation: Dengue Virus Serotype 1 NS4A Is a Unique Interferon-Regulating Virulence Determinant. *MBio,* 6**,** e00553-15.

DANG, J., TIWARI, S. K., LICHINCHI, G., QIN, Y., PATIL, V. S., EROSHKIN, A. M. & RANA, T. M. 2016. Zika Virus Depletes Neural Progenitors in Human Cerebral Organoids through Activation of the Innate Immune Receptor TLR3. *Cell Stem Cell,* 19**,** 258-265.

DARWISH, M. A., HOOGSTRAAL, H., ROBERTS, T. J., AHMED, I. P. & OMAR, F. 1983. A sero-epidemiological survey for certain arboviruses (Togaviridae) in Pakistan. *Trans R Soc Trop Med Hyg,* 77**,** 442-5.

DAVIS, C. W., NGUYEN, H. Y., HANNA, S. L., SÁNCHEZ, M. D., DOMS, R. W. & PIERSON, T. C. 2006. West Nile virus discriminates between DC-SIGN and DC-SIGNR for cellular attachment and infection. *J Virol,* 80**,** 1290-301.

DAVISON, A. J., DOLAN, A., AKTER, P., ADDISON, C., DARGAN, D. J., ALCENDOR, D. J., MCGEOCH, D. J. & HAYWARD, G. S. 2003. The human cytomegalovirus genome revisited: comparison with the chimpanzee cytomegalovirus genome. *J Gen Virol,* 84**,** 17-28.

DE FATIMA VASCO ARAGAO, M., VAN DER LINDEN, V., BRAINER-LIMA, A. M., COELI, R. R., ROCHA, M. A., SOBRAL DA SILVA, P., DURCE COSTA GOMES DE CARVALHO, M., VAN DER LINDEN, A., CESARIO DE HOLANDA, A. & VALENCA, M. M. 2016. Clinical features and neuroimaging (CT and MRI) findings in presumed Zika virus related congenital infection and microcephaly: retrospective case series study. *BMJ,* 353**,** i1901.

DE PAULA FREITAS, B., DE OLIVEIRA DIAS, J. R., PRAZERES, J., SACRAMENTO, G. A., KO, A. I., MAIA, M. & BELFORT, R. 2016. Ocular Findings in Infants With Microcephaly Associated With Presumed Zika Virus Congenital Infection in Salvador, Brazil. *JAMA Ophthalmol*.

DIAMOND, M. S. 2014. IFIT1: A dual sensor and effector molecule that detects non-2'-O methylated viral RNA and inhibits its translation. *Cytokine Growth Factor Rev,* 25, 543-50.

DICK, G. W., KITCHEN, S. F. & HADDOW, A. J. 1952. Zika virus. I. Isolations and serological specificity. *Trans R Soc Trop Med Hyg,* 46, 509-20.

DING, F., FU, J., JIANG, D., HAO, M. & LIN, G. 2018. Mapping the spatial distribution of Aedes aegypti and Aedes albopictus. *Acta Trop,* 178, 155-162.

DOLLARD, S. C., GROSSE, S. D. & ROSS, D. S. 2007. New estimates of the prevalence of neurological and sensory sequelae and mortality associated with congenital cytomegalovirus infection. *Rev Med Virol,* 17, 355-63.

DONALD, C. L., BRENNAN, B., CUMBERWORTH, S. L., REZELJ, V. V., CLARK, J. J., CORDEIRO, M. T., FREITAS DE OLIVEIRA FRANCA, R., PENA, L. J., WILKIE, G. S., DA SILVA FILIPE, A., DAVIS, C., HUGHES, J., VARJAK, M., SELINGER, M., ZUVANOV, L., OWSIANKA, A. M., PATEL, A. H., MCLAUCHLAN, J., LINDENBACH, B. D., FALL, G., SALL, A. A., BIEK, R., REHWINKEL, J., SCHNETTLER, E. & KOHL, A. 2016. Full Genome Sequence and sfRNA Interferon Antagonist Activity of Zika Virus from Recife, Brazil. *PLoS Negl Trop Dis,* 10, e0005048.

DRIGGERS, R. W., HO, C. Y., KORHONEN, E. M., KUIVANEN, S., JÄÄSKELÄINEN, A. J., SMURA, T., ROSENBERG, A., HILL, D. A., DEBIASI, R. L., VEZINA, G., TIMOFEEV, J., RODRIGUEZ, F. J., LEVANOV, L., RAZAK, J., IYENGAR, P., HENNENFENT, A., KENNEDY, R., LANCIOTTI, R., DU PLESSIS, A. & VAPALAHTI, O. 2016. Zika Virus Infection with Prolonged Maternal Viremia and Fetal Brain Abnormalities. *N Engl J Med,* 374, 2142-51.

DUFFY, M. R., CHEN, T. H., HANCOCK, W. T., POWERS, A. M., KOOL, J. L., LANCIOTTI, R. S., PRETRICK, M., MARFEL, M., HOLZBAUER, S., DUBRAY, C., GUILLAUMOT, L., GRIGGS, A., BEL, M., LAMBERT, A. J., LAVEN, J., KOSOY, O., PANELLA, A., BIGGERSTAFF, B. J., FISCHER, M. & HAYES, E. B. 2009. Zika virus outbreak on Yap Island, Federated States of Micronesia. *N Engl J Med,* 360, 2536-43.

DUPONT-ROUZEYROL, M., BIRON, A., O'CONNOR, O., HUGUON, E. & DESCLOUX, E. 2016. Infectious Zika viral particles in breastmilk. *Lancet,* 387, 1051.

DUPONT-ROUZEYROL, M., O'CONNOR, O., CALVEZ, E., DAURÈS, M., JOHN, M., GRANGEON, J. P. & GOURINAT, A. C. 2015. Co-infection with Zika and dengue viruses in 2 patients, New Caledonia, 2014. *Emerg Infect Dis,* 21, 381-2.

ECDC. 2016. *Aedes albopictus - Factsheet for experts* [Online]. Available: https://www.ecdc.europa.eu/en/disease-vectors/facts/mosquito-factsheets/aedes-albopictus [Accessed 28 December 2019].

ECDC 2017. Rapid risk assessment: Zika virus disease epidemic, tenth update, 4 April 2017.

EGLOFF, M. P., BENARROCH, D., SELISKO, B., ROMETTE, J. L. & CANARD, B. 2002. An RNA cap (nucleoside-2'-O-)-methyltransferase in the flavivirus RNA polymerase NS5: crystal structure and functional characterization. *EMBO J,* 21, 2757-68.

EL COSTA, H., GOUILLY, J., MANSUY, J. M., CHEN, Q., LEVY, C., CARTRON, G., VEAS, F., AL-DACCAK, R., IZOPET, J. & JABRANE-FERRAT, N. 2016. ZIKA

virus reveals broad tissue and cell tropism during the first trimester of pregnancy. *Sci Rep,* 6**,** 35296.

ENG, L. F., GHIRNIKAR, R. S. & LEE, Y. L. 2000. Glial fibrillary acidic protein: GFAP-thirty-one years (1969-2000). *Neurochem Res,* 25**,** 1439-51.

FAGBAMI, A. H. 1979. Zika virus infections in Nigeria: virological and seroepidemiological investigations in Oyo State. *J Hyg (Lond),* 83**,** 213-9.

FAGERBERG, L., HALLSTROM, B. M., OKSVOLD, P., KAMPF, C., DJUREINOVIC, D., ODEBERG, J., HABUKA, M., TAHMASEBPOOR, S., DANIELSSON, A., EDLUND, K., ASPLUND, A., SJOSTEDT, E., LUNDBERG, E., SZIGYARTO, C. A., SKOGS, M., TAKANEN, J. O., BERLING, H., TEGEL, H., MULDER, J., NILSSON, P., SCHWENK, J. M., LINDSKOG, C., DANIELSSON, F., MARDINOGLU, A., SIVERTSSON, A., VON FEILITZEN, K., FORSBERG, M., ZWAHLEN, M., OLSSON, I., NAVANI, S., HUSS, M., NIELSEN, J., PONTEN, F. & UHLEN, M. 2014. Analysis of the human tissue-specific expression by genome-wide integration of transcriptomics and antibody-based proteomics. *Mol Cell Proteomics,* 13**,** 397-406.

FALGOUT, B., MILLER, R. H. & LAI, C. J. 1993. Deletion analysis of dengue virus type 4 nonstructural protein NS2B: identification of a domain required for NS2B-NS3 protease activity. *J Virol,* 67**,** 2034-42.

FARIA, N. R., AZEVEDO, R. D. S. D., KRAEMER, M. U. G., SOUZA, R., CUNHA, M. S., HILL, S. C., THÉZÉ, J., BONSALL, M. B., BOWDEN, T. A., RISSANEN, I., ROCCO, I. M., NOGUEIRA, J. S., MAEDA, A. Y., VASAMI, F. G. D. S., MACEDO, F. L. L., SUZUKI, A., RODRIGUES, S. G., CRUZ, A. C. R., NUNES, B. T., MEDEIROS, D. B. A., RODRIGUES, D. S. G., QUEIROZ, A. L. N., DA SILVA, E. V. P., HENRIQUES, D. F., DA ROSA, E. S. T., DE OLIVEIRA, C. S., MARTINS, L. C., VASCONCELOS, H. B., CASSEB, L. M. N., SIMITH, D. B., MESSINA, J. P., ABADE, L., LOURENÇO, J., ALCANTARA, L. C. J., DE LIMA, M. M., GIOVANETTI, M., HAY, S. I., DE OLIVEIRA, R. S., LEMOS, P. D. S., DE OLIVEIRA, L. F., DE LIMA, C. P. S., DA SILVA, S. P., DE VASCONCELOS, J. M., FRANCO, L., CARDOSO, J. F., VIANEZ-JÚNIOR, J. L. D. S., MIR, D., BELLO, G., DELATORRE, E., KHAN, K., CREATORE, M., COELHO, G. E., DE OLIVEIRA, W. K., TESH, R., PYBUS, O. G., NUNES, M. R. T. & VASCONCELOS, P. F. C. 2016. Zika virus in the Americas: Early epidemiological and genetic findings. *Science,* 352**,** 345-349.

FAYE, O., FREIRE, C. C., IAMARINO, A., DE OLIVEIRA, J. V., DIALLO, M., ZANOTTO, P. M. & SALL, A. A. 2014. Molecular evolution of Zika virus during its emergence in the 20(th) century. *PLoS Negl Trop Dis,* 8**,** e2636.

FAZAKERLEY, J. K., COTTERILL, C. L., LEE, G. & GRAHAM, A. 2006. Virus tropism, distribution, persistence and pathology in the corpus callosum of the Semliki Forest virus-infected mouse brain: a novel system to study virus-oligodendrocyte interactions. *Neuropathol Appl Neurobiol,* 32**,** 397-409.

FERNANDES, N. C., NOGUEIRA, J. S., RÉSSIO, R. A., CIRQUEIRA, C. S., KIMURA, L. M., FERNANDES, K. R., CUNHA, M. S., SOUZA, R. P. & GUERRA, J. M. 2017. Experimental Zika virus infection induces spinal cord injury and encephalitis in newborn Swiss mice. *Exp Toxicol Pathol,* 69**,** 63-71.

FIELDS, R. D. 2008. White matter in learning, cognition and psychiatric disorders. *Trends Neurosci,* 31**,** 361-70.

FILIPE, A. R., MARTINS, C. M. & ROCHA, H. 1973. Laboratory infection with Zika virus after vaccination against yellow fever. *Arch Gesamte Virusforsch,* 43**,** 315-9.

FOX, R. G., PARK, F. D., KOECHLEIN, C. S., KRITZIK, M. & REYA, T. 2015. Musashi signaling in stem cells and cancer. *Annu Rev Cell Dev Biol,* 31**,** 249-67.

FRAGKOUDIS, R., TAMBERG, N., SIU, R., KIIVER, K., KOHL, A., MERITS, A. & FAZAKERLEY, J. K. 2009. Neurons and oligodendrocytes in the mouse brain differ in their ability to replicate Semliki Forest virus. *J Neurovirol,* 15**,** 57-70.

FUNK, A., TRUONG, K., NAGASAKI, T., TORRES, S., FLODEN, N., BALMORI MELIAN, E., EDMONDS, J., DONG, H., SHI, P. Y. & KHROMYKH, A. A. 2010. RNA structures required for production of subgenomic flavivirus RNA. *J Virol,* 84**,** 11407-17.

GARCEZ, P. P., LOIOLA, E. C., MADEIRO DA COSTA, R., HIGA, L. M., TRINDADE, P., DELVECCHIO, R., NASCIMENTO, J. M., BRINDEIRO, R., TANURI, A. & REHEN, S. K. 2016. Zika virus impairs growth in human neurospheres and brain organoids. *Science,* 352**,** 816-8.

GELPI, E., PREUSSER, M., GARZULY, F., HOLZMANN, H., HEINZ, F. X. & BUDKA, H. 2005. Visualization of Central European tick-borne encephalitis infection in fatal human cases. *J Neuropathol Exp Neurol,* 64**,** 506-12.

GERMAN, A. C., MYINT, K. S., MAI, N. T., POMEROY, I., PHU, N. H., TZARTOS, J., WINTER, P., COLLETT, J., FARRAR, J., BARRETT, A., KIPAR, A., ESIRI, M. M. & SOLOMON, T. 2006. A preliminary neuropathological study of Japanese encephalitis in humans and a mouse model. *Trans R Soc Trop Med Hyg,* 100**,** 1135-45.

GIEDD, J. N. 2004. Structural magnetic resonance imaging of the adolescent brain. *Ann N Y Acad Sci,* 1021**,** 77-85.

GIRON, S., FRANKE, F., DECOPPET, A., CADIOU, B., TRAVAGLINI, T., THIRION, L., DURAND, G., JEANNIN, C., L'AMBERT, G., GRARD, G., NOËL, H., FOURNET, N., AUZET-CAILLAUD, M., ZANDOTTI, C., ABOUKAÏS, S., CHAUD, P., GUEDJ, S., HAMOUDA, L., NAUDOT, X., OVIZE, A., LAZARUS, C., DE VALK, H., PATY, M. C. & LEPARC-GOFFART, I. 2019. Vector-borne transmission of Zika virus in Europe, southern France, August 2019. *Euro Surveill,* 24.

GLASS, W. G., HICKEY, M. J., HARDISON, J. L., LIU, M. T., MANNING, J. E. & LANE, T. E. 2004. Antibody targeting of the CC chemokine ligand 5 results in diminished leukocyte infiltration into the central nervous system and reduced neurologic disease in a viral model of multiple sclerosis. *J Immunol,* 172**,** 4018-25.

GÖERTZ, G. P., ABBO, S. R., FROS, J. J. & PIJLMAN, G. P. 2018. Functional RNA during Zika virus infection. *Virus Res,* 254**,** 41-53.

GONÇALVES, J. T., SCHAFER, S. T. & GAGE, F. H. 2016. Adult Neurogenesis in the Hippocampus: From Stem Cells to Behavior. *Cell,* 167**,** 897-914.

GOURINAT, A. C., O'CONNOR, O., CALVEZ, E., GOARANT, C. & DUPONT-ROUZEYROL, M. 2015. Detection of Zika virus in urine. *Emerg Infect Dis,* 21**,** 84-6.

GOVERO, J., ESAKKY, P., SCHEAFFER, S. M., FERNANDEZ, E., DRURY, A., PLATT, D. J., GORMAN, M. J., RICHNER, J. M., CAINE, E. A., SALAZAR, V., MOLEY, K. H. & DIAMOND, M. S. 2016. Zika virus infection damages the testes in mice. *Nature,* 540**,** 438-442.

GRISCHOTT, F., PUHAN, M., HATZ, C. & SCHLAGENHAUF, P. 2016. Non-vector-borne transmission of Zika virus: A systematic review. *Travel Med Infect Dis,* 14**,** 313-30.

GRUBAUGH, N. D., SARAF, S., GANGAVARAPU, K., WATTS, A., TAN, A. L., OIDTMAN, R. J., LADNER, J. T., OLIVEIRA, G., MATTESON, N. L., KRAEMER, M. U. G., VOGELS, C. B. F., HENTOFF, A., BHATIA, D., STANEK, D., SCOTT,

B., LANDIS, V., STRYKER, I., CONE, M. R., KOPP, E. W., CANNONS, A. C., HEBERLEIN-LARSON, L., WHITE, S., GILLIS, L. D., RICCIARDI, M. J., KWAL, J., LICHTENBERGER, P. K., MAGNANI, D. M., WATKINS, D. I., PALACIOS, G., HAMER, D. H., GARDNER, L. M., PERKINS, T. A., BAELE, G., KHAN, K., MORRISON, A., ISERN, S., MICHAEL, S. F., ANDERSEN, K. G. & NETWORK, G. S. 2019. Travel Surveillance and Genomics Uncover a Hidden Zika Outbreak during the Waning Epidemic. *Cell,* 178**,** 1057-1071.e11.

GRUN, J. B. & BRINTON, M. A. 1987. Dissociation of NS5 from cell fractions containing West Nile virus-specific polymerase activity. *J Virol,* 61**,** 3641-4.

GUTSCHE, I., COULIBALY, F., VOSS, J. E., SALMON, J., D'ALAYER, J., ERMONVAL, M., LARQUET, E., CHARNEAU, P., KREY, T., MÉGRET, F., GUITTET, E., REY, F. A. & FLAMAND, M. 2011. Secreted dengue virus nonstructural protein NS1 is an atypical barrel-shaped high-density lipoprotein. *Proc Natl Acad Sci U S A,* 108**,** 8003-8.

HADDOW, A. D., SCHUH, A. J., YASUDA, C. Y., KASPER, M. R., HEANG, V., HUY, R., GUZMAN, H., TESH, R. B. & WEAVER, S. C. 2012. Genetic characterization of Zika virus strains: geographic expansion of the Asian lineage. *PLoS Negl Trop Dis,* 6**,** e1477.

HADDOW, A. J., WILLIAMS, M. C., WOODALL, J. P., SIMPSON, D. I. & GOMA, L. K. 1964. TWELVE ISOLATIONS OF ZIKA VIRUS FROM AEDES (STEGOMYIA) AFRICANUS (THEOBALD) TAKEN IN AND ABOVE A UGANDA FOREST. *Bull World Health Organ,* 31**,** 57-69.

HAGE, E., WILKIE, G. S., LINNENWEBER-HELD, S., DHINGRA, A., SUÁREZ, N. M., SCHMIDT, J. J., KAY-FEDOROV, P. C., MISCHAK-WEISSINGER, E., HEIM, A., SCHWARZ, A., SCHULZ, T. F., DAVISON, A. J. & GANZENMUELLER, T. 2017. Characterization of Human Cytomegalovirus Genome Diversity in Immunocompromised Hosts by Whole-Genome Sequencing Directly From Clinical Specimens. *J Infect Dis,* 215**,** 1673-1683.

HAKIM, T. S., SUGIMORI, K., CAMPORESI, E. M. & ANDERSON, G. 1996. Half-life of nitric oxide in aqueous solutions with and without haemoglobin. *Physiol Meas,* 17**,** 267-77.

HASTINGS, A. K., YOCKEY, L. J., JAGGER, B. W., HWANG, J., URAKI, R., GAITSCH, H. F., PARNELL, L. A., CAO, B., MYSOREKAR, I. U., ROTHLIN, C. V., FIKRIG, E., DIAMOND, M. S. & IWASAKI, A. 2017. TAM Receptors Are Not Required for Zika Virus Infection in Mice. *Cell Rep,* 19**,** 558-568.

HEANG, V., YASUDA, C. Y., SOVANN, L., HADDOW, A. D., TRAVASSOS DA ROSA, A. P., TESH, R. B. & KASPER, M. R. 2012. Zika virus infection, Cambodia, 2010. *Emerg Infect Dis,* 18**,** 349-51.

HEINZ, F. X. & STIASNY, K. 2017. The Antigenic Structure of Zika Virus and Its Relation to Other Flaviviruses: Implications for Infection and Immunoprophylaxis. *Microbiol Mol Biol Rev,* 81.

HEINZ, F. X., STIASNY, K., PÜSCHNER-AUER, G., HOLZMANN, H., ALLISON, S. L., MANDL, C. W. & KUNZ, C. 1994. Structural changes and functional control of the tick-borne encephalitis virus glycoprotein E by the heterodimeric association with protein prM. *Virology,* 198**,** 109-17.

HILTON, L., MOGANERADJ, K., ZHANG, G., CHEN, Y. H., RANDALL, R. E., MCCAULEY, J. W. & GOODBOURN, S. 2006. The NPro product of bovine viral diarrhea virus inhibits DNA binding by interferon regulatory factor 3 and targets it for proteasomal degradation. *J Virol,* 80**,** 11723-32.

HOSKING, M. P. & LANE, T. E. 2010. The role of chemokines during viral infection of the CNS. *PLoS Pathog,* 6**,** e1000937.

HOU, S., KUMAR, A., XU, Z., AIRO, A. M., STRYAPUNINA, I., WONG, C. P., BRANTON, W., TCHESNOKOV, E., GÖTTE, M., POWER, C. & HOBMAN, T. C. 2017. Zika Virus Hijacks Stress Granule Proteins and Modulates the Host Stress Response. *J Virol,* 91.

HSIEH, P. & ROBBINS, P. W. 1984. Regulation of asparagine-linked oligosaccharide processing. Oligosaccharide processing in Aedes albopictus mosquito cells. *J Biol Chem,* 259, 2375-82.

HUNG, Y. F., SCHWARTEN, M., HOFFMANN, S., WILLBOLD, D., SKLAN, E. H. & KOENIG, B. 2015. Amino Terminal Region of Dengue Virus NS4A Cytosolic Domain Binds to Highly Curved Liposomes. *Viruses,* 7, 4119-30.

IOANNIDIS, I., MCNALLY, B., WILLETTE, M., PEEPLES, M. E., CHAUSSABEL, D., DURBIN, J. E., RAMILO, O., MEJIAS, A. & FLAÑO, E. 2012. Plasticity and virus specificity of the airway epithelial cell immune response during respiratory virus infection. *J Virol,* 86, 5422-36.

ISSUR, M., GEISS, B. J., BOUGIE, I., PICARD-JEAN, F., DESPINS, S., MAYETTE, J., HOBDEY, S. E. & BISAILLON, M. 2009. The flavivirus NS5 protein is a true RNA guanylyltransferase that catalyzes a two-step reaction to form the RNA cap structure. *RNA,* 15, 2340-50.

JACOBS, B. C., ROTHBARTH, P. H., VAN DER MECHÉ, F. G., HERBRINK, P., SCHMITZ, P. I., DE KLERK, M. A. & VAN DOORN, P. A. 1998. The spectrum of antecedent infections in Guillain-Barré syndrome: a case-control study. *Neurology,* 51, 1110-5.

JAN, C., LANGUILLAT, G., RENAUDET, J. & ROBIN, Y. 1978. [A serological survey of arboviruses in Gabon]. *Bull Soc Pathol Exot Filiales,* 71, 140-6.

JOHNSON, A. J., GUIRAKHOO, F. & ROEHRIG, J. T. 1994. The envelope glycoproteins of dengue 1 and dengue 2 viruses grown in mosquito cells differ in their utilization of potential glycosylation sites. *Virology,* 203, 241-9.

KAGAWA, H., SHIMAMOTO, R., KIM, S. I., OCEGUERA-YANEZ, F., YAMAMOTO, T., SCHROEDER, T. & WOLTJEN, K. 2019. OVOL1 Influences the Determination and Expansion of iPSC Reprogramming Intermediates. *Stem Cell Reports,* 12, 319-332.

KAMPHUIS, W., MAMBER, C., MOETON, M., KOOIJMAN, L., SLUIJS, J. A., JANSEN, A. H., VERVEER, M., DE GROOT, L. R., SMITH, V. D., RANGARAJAN, S., RODRÍGUEZ, J. J., ORRE, M. & HOL, E. M. 2012. GFAP isoforms in adult mouse brain with a focus on neurogenic astrocytes and reactive astrogliosis in mouse models of Alzheimer disease. *PLoS One,* 7, e42823.

KAPOOR, R., DAVIES, M., BLAKER, P. A., HALL, S. M. & SMITH, K. J. 2003. Blockers of sodium and calcium entry protect axons from nitric oxide-mediated degeneration. *Ann Neurol,* 53, 174-80.

KAUSHIK, D. K., GUPTA, M., DAS, S. & BASU, A. 2010. Krüppel-like factor 4, a novel transcription factor regulates microglial activation and subsequent neuroinflammation. *J Neuroinflammation,* 7, 68.

KEARSE, M., MOIR, R., WILSON, A., STONES-HAVAS, S., CHEUNG, M., STURROCK, S., BUXTON, S., COOPER, A., MARKOWITZ, S., DURAN, C., THIERER, T., ASHTON, B., MEINTJES, P. & DRUMMOND, A. 2012. Geneious Basic: an integrated and extendable desktop software platform for the organization and analysis of sequence data. *Bioinformatics,* 28, 1647-9.

KHROMYKH, A. A., MEKA, H., GUYATT, K. J. & WESTAWAY, E. G. 2001. Essential role of cyclization sequences in flavivirus RNA replication. *J Virol,* 75, 6719-28.

KHROMYKH, A. A. & WESTAWAY, E. G. 1996. RNA binding properties of core protein of the flavivirus Kunjin. *Arch Virol,* 141**,** 685-99.

KIERMAYR, S., KOFLER, R. M., MANDL, C. W., MESSNER, P. & HEINZ, F. X. 2004. Isolation of capsid protein dimers from the tick-borne encephalitis flavivirus and in vitro assembly of capsid-like particles. *J Virol,* 78**,** 8078-84.

KINDHAUSER, M. K., ALLEN, T., FRANK, V., SANTHANA, R. S. & DYE, C. 2016. Zika: the origin and spread of a mosquito-borne virus. *Bull World Health Organ,* 94**,** 675-686C.

KOFLER, R. M., HEINZ, F. X. & MANDL, C. W. 2002. Capsid protein C of tick-borne encephalitis virus tolerates large internal deletions and is a favorable target for attenuation of virulence. *J Virol,* 76**,** 3534-43.

KONISHI, E. & MASON, P. W. 1993. Proper maturation of the Japanese encephalitis virus envelope glycoprotein requires cosynthesis with the premembrane protein. *J Virol,* 67**,** 1672-5.

KUHN, R. J., ZHANG, W., ROSSMANN, M. G., PLETNEV, S. V., CORVER, J., LENCHES, E., JONES, C. T., MUKHOPADHYAY, S., CHIPMAN, P. R., STRAUSS, E. G., BAKER, T. S. & STRAUSS, J. H. 2002. Structure of dengue virus: implications for flavivirus organization, maturation, and fusion. *Cell,* 108**,** 717-25.

KÜMMERER, B. M. & RICE, C. M. 2002. Mutations in the yellow fever virus nonstructural protein NS2A selectively block production of infectious particles. *J Virol,* 76**,** 4773-84.

LANCIOTTI, R. S., KOSOY, O. L., LAVEN, J. J., VELEZ, J. O., LAMBERT, A. J., JOHNSON, A. J., STANFIELD, S. M. & DUFFY, M. R. 2008. Genetic and serologic properties of Zika virus associated with an epidemic, Yap State, Micronesia, 2007. *Emerg Infect Dis,* 14**,** 1232-9.

LANZIERI, T. M., CHUNG, W., FLORES, M., BLUM, P., CAVINESS, A. C., BIALEK, S. R., GROSSE, S. D., MILLER, J. A., DEMMLER-HARRISON, G. & GROUP, C. C. L. S. 2017. Hearing Loss in Children With Asymptomatic Congenital Cytomegalovirus Infection. *Pediatrics,* 139.

LANZIERI, T. M., DOLLARD, S. C., BIALEK, S. R. & GROSSE, S. D. 2014. Systematic review of the birth prevalence of congenital cytomegalovirus infection in developing countries. *Int J Infect Dis,* 22**,** 44-8.

LAURETI, M., NARAYANAN, D., RODRIGUEZ-ANDRES, J., FAZAKERLEY, J. K. & KEDZIERSKI, L. 2018. Flavivirus Receptors: Diversity, Identity, and Cell Entry. *Front Immunol,* 9**,** 2180.

LEAL, M. C., MUNIZ, L. F., FERREIRA, T. S., SANTOS, C. M., ALMEIDA, L. C., VAN DER LINDEN, V., RAMOS, R. C., RODRIGUES, L. C. & NETO, S. S. 2016. Hearing Loss in Infants with Microcephaly and Evidence of Congenital Zika Virus Infection - Brazil, November 2015-May 2016. *MMWR Morb Mortal Wkly Rep,* 65**,** 917-9.

LEE, C. M., XIE, X., ZOU, J., LI, S. H., LEE, M. Y., DONG, H., QIN, C. F., KANG, C. & SHI, P. Y. 2015. Determinants of Dengue Virus NS4A Protein Oligomerization. *J Virol,* 89**,** 6171-83.

LEE, E., LEANG, S. K., DAVIDSON, A. & LOBIGS, M. 2010. Both E protein glycans adversely affect dengue virus infectivity but are beneficial for virion release. *J Virol,* 84**,** 5171-80.

LEE, K. M., CHIU, K. B., SANSING, H. A., DIDIER, P. J., LACKNER, A. A. & MACLEAN, A. G. 2016. The flavivirus dengue induces hypertrophy of white matter astrocytes. *J Neurovirol,* 22**,** 831-839.

LEI, Y., YU, H., DONG, Y., YANG, J., YE, W., WANG, Y., CHEN, W., JIA, Z., XU, Z., LI, Z. & ZHANG, F. 2015. Characterization of N-Glycan Structures on the Surface of Mature Dengue 2 Virus Derived from Insect Cells. *PLoS One,* 10, e0132122.

LEONHARD, S. E., LANT, S., JACOBS, B. C., WILDER-SMITH, A., FERREIRA, M. L. B., SOLOMON, T. & WILLISON, H. J. 2018. Zika virus infection in the returning traveller: what every neurologist should know. *Pract Neurol,* 18, 271-277.

LEUNG, J. Y., PIJLMAN, G. P., KONDRATIEVA, N., HYDE, J., MACKENZIE, J. M. & KHROMYKH, A. A. 2008. Role of nonstructural protein NS2A in flavivirus assembly. *J Virol,* 82, 4731-41.

LI, C., XU, D., YE, Q., HONG, S., JIANG, Y., LIU, X., ZHANG, N., SHI, L., QIN, C. F. & XU, Z. 2016a. Zika Virus Disrupts Neural Progenitor Development and Leads to Microcephaly in Mice. *Cell Stem Cell,* 19, 672.

LI, F., WANG, P. R., QU, L. B., YI, C. H., ZHANG, F. C., TANG, X. P., ZHANG, L. G. & CHEN, L. 2017. AXL is not essential for Zika virus infection in the mouse brain. *Emerg Microbes Infect,* 6, e16.

LI, H., CLUM, S., YOU, S., EBNER, K. E. & PADMANABHAN, R. 1999. The serine protease and RNA-stimulated nucleoside triphosphatase and RNA helicase functional domains of dengue virus type 2 NS3 converge within a region of 20 amino acids. *J Virol,* 73, 3108-16.

LI, X. D., DENG, C. L., YE, H. Q., ZHANG, H. L., ZHANG, Q. Y., CHEN, D. D., ZHANG, P. T., SHI, P. Y., YUAN, Z. M. & ZHANG, B. 2016b. Transmembrane Domains of NS2B Contribute to both Viral RNA Replication and Particle Formation in Japanese Encephalitis Virus. *J Virol,* 90, 5735-5749.

LI, X. D., LI, X. F., YE, H. Q., DENG, C. L., YE, Q., SHAN, C., SHANG, B. D., XU, L. L., LI, S. H., CAO, S. B., YUAN, Z. M., SHI, P. Y., QIN, C. F. & ZHANG, B. 2014. Recovery of a chemically synthesized Japanese encephalitis virus reveals two critical adaptive mutations in NS2B and NS4A. *J Gen Virol,* 95, 806-15.

LI, Y., LEE, M. Y., LOH, Y. R. & KANG, C. 2018. Secondary structure and membrane topology of dengue virus NS4A protein in micelles. *Biochim Biophys Acta Biomembr,* 1860, 442-450.

LIN, C., AMBERG, S. M., CHAMBERS, T. J. & RICE, C. M. 1993. Cleavage at a novel site in the NS4A region by the yellow fever virus NS2B-3 proteinase is a prerequisite for processing at the downstream 4A/4B signalase site. *J Virol,* 67, 2327-35.

LINDQVIST, R., KURHADE, C., GILTHORPE, J. D. & ÖVERBY, A. K. 2018. Cell-type- and region-specific restriction of neurotropic flavivirus infection by viperin. *J Neuroinflammation,* 15, 80.

LINDQVIST, R., MUNDT, F., GILTHORPE, J. D., WÖLFEL, S., GEKARA, N. O., KRÖGER, A. & ÖVERBY, A. K. 2016. Fast type I interferon response protects astrocytes from flavivirus infection and virus-induced cytopathic effects. *J Neuroinflammation,* 13, 277.

LIU, R., YUE, L., LI, X., YU, X., ZHAO, H., JIANG, Z., QIN, E. & QIN, C. 2010. Identification and characterization of small sub-genomic RNAs in dengue 1-4 virus-infected cell cultures and tissues. *Biochem Biophys Res Commun,* 391, 1099-103.

LIU, W. J., CHEN, H. B. & KHROMYKH, A. A. 2003. Molecular and functional analyses of Kunjin virus infectious cDNA clones demonstrate the essential

roles for NS2A in virus assembly and for a nonconservative residue in NS3 in RNA replication. *J Virol,* 77**,** 7804-13.

LIU, W. J., WANG, X. J., MOKHONOV, V. V., SHI, P. Y., RANDALL, R. & KHROMYKH, A. A. 2005. Inhibition of interferon signaling by the New York 99 strain and Kunjin subtype of West Nile virus involves blockage of STAT1 and STAT2 activation by nonstructural proteins. *J Virol,* 79**,** 1934-42.

LO, Y. L., LIOU, G. G., LYU, J. H., HSIAO, M., HSU, T. L. & WONG, C. H. 2016. Dengue Virus Infection Is through a Cooperative Interaction between a Mannose Receptor and CLEC5A on Macrophage as a Multivalent Hetero-Complex. *PLoS One,* 11**,** e0166474.

LOBIGS, M., LEE, E., NG, M. L., PAVY, M. & LOBIGS, P. 2010. A flavivirus signal peptide balances the catalytic activity of two proteases and thereby facilitates virus morphogenesis. *Virology,* 401**,** 80-9.

LORENZ, I. C., ALLISON, S. L., HEINZ, F. X. & HELENIUS, A. 2002. Folding and dimerization of tick-borne encephalitis virus envelope proteins prM and E in the endoplasmic reticulum. *J Virol,* 76**,** 5480-91.

LUCIGNANI, G., ROSSI ESPAGNET, M. C., NAPOLITANO, A., FIGÀ TALAMANCA, L., CALÒ CARDUCCI, F. I., AURITI, C. & LONGO, D. 2019. A new MRI severity score to predict long-term adverse neurologic outcomes in children with congenital Cytomegalovirus infection. *J Matern Fetal Neonatal Med***,** 1-8.

LUI, N. C., TAM, W. Y., GAO, C., HUANG, J. D., WANG, C. C., JIANG, L., YUNG, W. H. & KWAN, K. M. 2017. Lhx1/5 control dendritogenesis and spine morphogenesis of Purkinje cells via regulation of Espin. *Nat Commun,* 8**,** 15079.

LUM, F. M., LOW, D. K., FAN, Y., TAN, J. J., LEE, B., CHAN, J. K., RÉNIA, L., GINHOUX, F. & NG, L. F. 2017. Zika Virus Infects Human Fetal Brain Microglia and Induces Inflammation. *Clin Infect Dis,* 64**,** 914-920.

MA, J., KETKAR, H., GENG, T., LO, E., WANG, L., XI, J., SUN, Q., ZHU, Z., CUI, Y., YANG, L. & WANG, P. 2018a. Zika Virus Non-structural Protein 4A Blocks the RLR-MAVS Signaling. *Front Microbiol,* 9**,** 1350.

MA, L., JONES, C. T., GROESCH, T. D., KUHN, R. J. & POST, C. B. 2004. Solution structure of dengue virus capsid protein reveals another fold. *Proc Natl Acad Sci U S A,* 101**,** 3414-9.

MA, L., LI, F., ZHANG, J. W., LI, W., ZHAO, D. M., WANG, H., HUA, R. H. & BU, Z. G. 2018b. Host Factor SPCS1 Regulates the Replication of Japanese Encephalitis Virus through Interactions with Transmembrane Domains of NS2B. *J Virol,* 92.

MACFADDEN, A., O'DONOGHUE, Z., SILVA, P., CHAPMAN, E. G., OLSTHOORN, R. C., STERKEN, M. G., PIJLMAN, G. P., BREDENBEEK, P. J. & KIEFT, J. S. 2018. Mechanism and structural diversity of exoribonuclease-resistant RNA structures in flaviviral RNAs. *Nat Commun,* 9**,** 119.

MACKENZIE, J. M., KHROMYKH, A. A., JONES, M. K. & WESTAWAY, E. G. 1998. Subcellular localization and some biochemical properties of the flavivirus Kunjin nonstructural proteins NS2A and NS4A. *Virology,* 245**,** 203-15.

MACNAMARA, F. N. 1954. Zika virus: a report on three cases of human infection during an epidemic of jaundice in Nigeria. *Trans R Soc Trop Med Hyg,* 48**,** 139-45.

MALET, H., EGLOFF, M. P., SELISKO, B., BUTCHER, R. E., WRIGHT, P. J., ROBERTS, M., GRUEZ, A., SULZENBACHER, G., VONRHEIN, C., BRICOGNE, G., MACKENZIE, J. M., KHROMYKH, A. A., DAVIDSON, A. D. & CANARD, B. 2007. Crystal structure of the RNA polymerase domain of the West Nile virus non-structural protein 5. *J Biol Chem,* 282**,** 10678-89.

MARCHETTE, N. J., GARCIA, R. & RUDNICK, A. 1969. Isolation of Zika virus from Aedes aegypti mosquitoes in Malaysia. *Am J Trop Med Hyg,* 18**,** 411-5.

MARKOFF, L., FALGOUT, B. & CHANG, A. 1997. A conserved internal hydrophobic domain mediates the stable membrane integration of the dengue virus capsid protein. *Virology,* 233**,** 105-17.

MÁRQUEZ-JURADO, S., NOGALES, A., ÁVILA-PÉREZ, G., IBORRA, F. J., MARTÍNEZ-SOBRIDO, L. & ALMAZÁN, F. 2018. An Alanine-to-Valine Substitution in the Residue 175 of Zika Virus NS2A Protein Affects Viral RNA Synthesis and Attenuates the Virus In Vivo. *Viruses,* 10.

MARTINES, R. B., BHATNAGAR, J., KEATING, M. K., SILVA-FLANNERY, L., MUEHLENBACHS, A., GARY, J., GOLDSMITH, C., HALE, G., RITTER, J., ROLLIN, D., SHIEH, W. J., LUZ, K. G., RAMOS, A. M., DAVI, H. P., KLEBER DE OLIVERIA, W., LANCIOTTI, R., LAMBERT, A. & ZAKI, S. 2016. Notes from the Field: Evidence of Zika Virus Infection in Brain and Placental Tissues from Two Congenitally Infected Newborns and Two Fetal Losses--Brazil, 2015. *MMWR Morb Mortal Wkly Rep,* 65**,** 159-60.

MAXIMOVA, O. A. & PLETNEV, A. G. 2018. Flaviviruses and the Central Nervous System: Revisiting Neuropathological Concepts. *Annu Rev Virol,* 5**,** 255-272.

MCCRAE, A. W. & KIRYA, B. G. 1982. Yellow fever and Zika virus epizootics and enzootics in Uganda. *Trans R Soc Trop Med Hyg,* 76**,** 552-62.

MCLEAN, J. E., WUDZINSKA, A., DATAN, E., QUAGLINO, D. & ZAKERI, Z. 2011. Flavivirus NS4A-induced autophagy protects cells against death and enhances virus replication. *J Biol Chem,* 286**,** 22147-59.

MEERTENS, L., CARNEC, X., LECOIN, M. P., RAMDASI, R., GUIVEL-BENHASSINE, F., LEW, E., LEMKE, G., SCHWARTZ, O. & AMARA, A. 2012. The TIM and TAM families of phosphatidylserine receptors mediate dengue virus entry. *Cell Host Microbe,* 12**,** 544-57.

MELO, A. S., AGUIAR, R. S., AMORIM, M. M., ARRUDA, M. B., MELO, F. O., RIBEIRO, S. T., BATISTA, A. G., FERREIRA, T., DOS SANTOS, M. P., SAMPAIO, V. V., MOURA, S. R., RABELLO, L. P., GONZAGA, C. E., MALINGER, G., XIMENES, R., DE OLIVEIRA-SZEJNFELD, P. S., TOVAR-MOLL, F., CHIMELLI, L., SILVEIRA, P. P., DELVECHIO, R., HIGA, L., CAMPANATI, L., NOGUEIRA, R. M., FILIPPIS, A. M., SZEJNFELD, J., VOLOCH, C. M., FERREIRA, O. C., BRINDEIRO, R. M. & TANURI, A. 2016. Congenital Zika Virus Infection: Beyond Neonatal Microcephaly. *JAMA Neurol,* 73**,** 1407-1416.

MILLER, J. L., DE WET, B. J., DEWET, B. J., MARTINEZ-POMARES, L., RADCLIFFE, C. M., DWEK, R. A., RUDD, P. M. & GORDON, S. 2008. The mannose receptor mediates dengue virus infection of macrophages. *PLoS Pathog,* 4**,** e17.

MILLER, S., KASTNER, S., KRIJNSE-LOCKER, J., BÜHLER, S. & BARTENSCHLAGER, R. 2007. The non-structural protein 4A of dengue virus is an integral membrane protein inducing membrane alterations in a 2K-regulated manner. *J Biol Chem,* 282**,** 8873-82.

MILLER, S., SPARACIO, S. & BARTENSCHLAGER, R. 2006. Subcellular localization and membrane topology of the Dengue virus type 2 Non-structural protein 4B. *J Biol Chem,* 281**,** 8854-63.

MILLER, S. J. 2018. Astrocyte Heterogeneity in the Adult Central Nervous System. *Front Cell Neurosci,* 12**,** 401.

MINER, J. J. & DIAMOND, M. S. 2017. Zika Virus Pathogenesis and Tissue Tropism. *Cell Host Microbe,* 21**,** 134-142.

MLAKAR, J., KORVA, M., TUL, N., POPOVIĆ, M., POLJŠAK-PRIJATELJ, M., MRAZ, J., KOLENC, M., RESMAN RUS, K., VESNAVER VIPOTNIK, T., FABJAN VODUŠEK, V., VIZJAK, A., PIŽEM, J., PETROVEC, M. & AVŠIČ ŽUPANC, T. 2016. Zika Virus Associated with Microcephaly. *N Engl J Med,* 374**,** 951-8.

MODIS, Y., OGATA, S., CLEMENTS, D. & HARRISON, S. C. 2004. Structure of the dengue virus envelope protein after membrane fusion. *Nature,* 427**,** 313-9.

MOKHTARIAN, F., HUAN, C. M., ROMAN, C. & RAINE, C. S. 2003. Semliki Forest virus-induced demyelination and remyelination--involvement of B cells and anti-myelin antibodies. *J Neuroimmunol,* 137**,** 19-31.

MONLUN, E., ZELLER, H., LE GUENNO, B., TRAORÉ-LAMIZANA, M., HERVY, J. P., ADAM, F., FERRARA, L., FONTENILLE, D., SYLLA, R. & MONDO, M. 1993. [Surveillance of the circulation of arbovirus of medical interest in the region of eastern Senegal]. *Bull Soc Pathol Exot,* 86**,** 21-8.

MOORE, C. A., STAPLES, J. E., DOBYNS, W. B., PESSOA, A., VENTURA, C. V., FONSECA, E. B., RIBEIRO, E. M., VENTURA, L. O., NETO, N. N., ARENA, J. F. & RASMUSSEN, S. A. 2017. Characterizing the Pattern of Anomalies in Congenital Zika Syndrome for Pediatric Clinicians. *JAMA Pediatr,* 171**,** 288-295.

MOORE, D. L., BLACKMORE, M. G., HU, Y., KAESTNER, K. H., BIXBY, J. L., LEMMON, V. P. & GOLDBERG, J. L. 2009. KLF family members regulate intrinsic axon regeneration ability. *Science,* 326**,** 298-301.

MORI, M., KUWABARA, S., MIYAKE, M., NODA, M., KUROKI, H., KANNO, H., OGAWARA, K. & HATTORI, T. 2000. Haemophilus influenzae infection and Guillain-Barré syndrome. *Brain,* 123 ( Pt 10)**,** 2171-8.

MORI, Y., OKABAYASHI, T., YAMASHITA, T., ZHAO, Z., WAKITA, T., YASUI, K., HASEBE, F., TADANO, M., KONISHI, E., MORIISHI, K. & MATSUURA, Y. 2005. Nuclear localization of Japanese encephalitis virus core protein enhances viral replication. *J Virol,* 79**,** 3448-58.

MOURA DA SILVA, A. A., GANZ, J. S., SOUSA, P. D., DORIQUI, M. J., RIBEIRO, M. R., BRANCO, M. D., QUEIROZ, R. C., PACHECO, M. J., VIEIRA DA COSTA, F. R., SILVA, F. S., SIMÕES, V. M., PACHECO, M. A., LAMY-FILHO, F., LAMY, Z. C. & SOARES DE BRITTO E ALVES, M. T. 2016. Early Growth and Neurologic Outcomes of Infants with Probable Congenital Zika Virus Syndrome. *Emerg Infect Dis,* 22**,** 1953-1956.

MUKHOPADHYAY, S., KIM, B. S., CHIPMAN, P. R., ROSSMANN, M. G. & KUHN, R. J. 2003. Structure of West Nile virus. *Science,* 302**,** 248.

MÜLLER, U., STEINHOFF, U., REIS, L. F., HEMMI, S., PAVLOVIC, J., ZINKERNAGEL, R. M. & AGUET, M. 1994. Functional role of type I and type II interferons in antiviral defense. *Science,* 264**,** 1918-21.

MULLER, W. J. & MULKEY, S. B. 2019. Lessons about early neurodevelopment in children exposed to ZIKV in utero. *Nat Med,* 25**,** 1192-1193.

MUÑOZ-JORDÁN, J. L., LAURENT-ROLLE, M., ASHOUR, J., MARTÍNEZ-SOBRIDO, L., ASHOK, M., LIPKIN, W. I. & GARCÍA-SASTRE, A. 2005. Inhibition of alpha/beta interferon signaling by the NS4B protein of flaviviruses. *J Virol,* 79**,** 8004-13.

MUÑOZ-JORDAN, J. L., SÁNCHEZ-BURGOS, G. G., LAURENT-ROLLE, M. & GARCÍA-SASTRE, A. 2003. Inhibition of interferon signaling by dengue virus. *Proc Natl Acad Sci U S A,* 100**,** 14333-8.

MUSSO, D., ROCHE, C., NHAN, T. X., ROBIN, E., TEISSIER, A. & CAO-LORMEAU, V. M. 2015a. Detection of Zika virus in saliva. *J Clin Virol,* 68**,** 53-5.

MUSSO, D., ROCHE, C., ROBIN, E., NHAN, T., TEISSIER, A. & CAO-LORMEAU, V. M. 2015b. Potential sexual transmission of Zika virus. *Emerg Infect Dis,* 21**,** 359-61.

NAIR, M., BILANCHONE, V., ORTT, K., SINHA, S. & DAI, X. 2007. Ovol1 represses its own transcription by competing with transcription activator c-Myb and by recruiting histone deacetylase activity. *Nucleic Acids Res,* 35**,** 1687-97.

NAYAK, D., ROTH, T. L. & MCGAVERN, D. B. 2014. Microglia development and function. *Annu Rev Immunol,* 32**,** 367-402.

NEUFELDT, C. J., CORTESE, M., ACOSTA, E. G. & BARTENSCHLAGER, R. 2018. Rewiring cellular networks by members of the Flaviviridae family. *Nat Rev Microbiol,* 16**,** 125-142.

NIELSEN-SAINES, K., BRASIL, P., KERIN, T., VASCONCELOS, Z., GABAGLIA, C. R., DAMASCENO, L., PONE, M., ABREU DE CARVALHO, L. M., PONE, S. M., ZIN, A. A., TSUI, I., SALLES, T. R. S., DA CUNHA, D. C., COSTA, R. P., MALACARNE, J., REIS, A. B., HASUE, R. H., AIZAWA, C. Y. P., GENOVESI, F. F., EINSPIELER, C., MARSCHIK, P. B., PEREIRA, J. P., GAW, S. L., ADACHI, K., CHERRY, J. D., XU, Z., CHENG, G. & MOREIRA, M. E. 2019. Delayed childhood neurodevelopment and neurosensory alterations in the second year of life in a prospective cohort of ZIKV-exposed children. *Nat Med,* 25**,** 1213-1217.

NOTOMI, T., MORI, Y., TOMITA, N. & KANDA, H. 2015. Loop-mediated isothermal amplification (LAMP): principle, features, and future prospects. *J Microbiol,* 53**,** 1-5.

NOWAKOWSKI, T. J., POLLEN, A. A., DI LULLO, E., SANDOVAL-ESPINOSA, C., BERSHTEYN, M. & KRIEGSTEIN, A. R. 2016. Expression Analysis Highlights AXL as a Candidate Zika Virus Entry Receptor in Neural Stem Cells. *Cell Stem Cell,* 18**,** 591-6.

OEHLER, E., WATRIN, L., LARRE, P., LEPARC-GOFFART, I., LASTERE, S., VALOUR, F., BAUDOUIN, L., MALLET, H., MUSSO, D. & GHAWCHE, F. 2014. Zika virus infection complicated by Guillain-Barre syndrome--case report, French Polynesia, December 2013. *Euro Surveill,* 19.

OH, Y., ZHANG, F., WANG, Y., LEE, E. M., CHOI, I. Y., LIM, H., MIRAKHORI, F., LI, R., HUANG, L., XU, T., WU, H., LI, C., QIN, C. F., WEN, Z., WU, Q. F., TANG, H., XU, Z., JIN, P., SONG, H., MING, G. L. & LEE, G. 2017. Zika virus directly infects peripheral neurons and induces cell death. *Nat Neurosci,* 20**,** 1209-1212.

OJHA, C. R., RODRIGUEZ, M., KARUPPAN, M. K. M., LAPIERRE, J., KASHANCHI, F. & EL-HAGE, N. 2019. Toll-like receptor 3 regulates Zika virus infection and associated host inflammatory response in primary human astrocytes. *PLoS One,* 14**,** e0208543.

OLMO, I. G., CARVALHO, T. G., COSTA, V. V., ALVES-SILVA, J., FERRARI, C. Z., IZIDORO-TOLEDO, T. C., DA SILVA, J. F., TEIXEIRA, A. L., SOUZA, D. G., MARQUES, J. T., TEIXEIRA, M. M., VIEIRA, L. B. & RIBEIRO, F. M. 2017. Zika Virus Promotes Neuronal Cell Death in a Non-Cell Autonomous Manner by Triggering the Release of Neurotoxic Factors. *Front Immunol,* 8**,** 1016.

OLSON, J. G., KSIAZEK, T. G., SUHANDIMAN & TRIWIBOWO 1981. Zika virus, a cause of fever in Central Java, Indonesia. *Trans R Soc Trop Med Hyg,* 75**,** 389-93.

ONORATI, M., LI, Z., LIU, F., SOUSA, A. M. M., NAKAGAWA, N., LI, M., DELL'ANNO, M. T., GULDEN, F. O., POCHAREDDY, S., TEBBENKAMP, A. T. N., HAN, W., PLETIKOS, M., GAO, T., ZHU, Y., BICHSEL, C., VARELA, L., SZIGETI-BUCK, K., LISGO, S., ZHANG, Y., TESTEN, A., GAO, X. B., MLAKAR,

J., POPOVIC, M., FLAMAND, M., STRITTMATTER, S. M., KACZMAREK, L. K., ANTON, E. S., HORVATH, T. L., LINDENBACH, B. D. & SESTAN, N. 2016. Zika Virus Disrupts Phospho-TBK1 Localization and Mitosis in Human Neuroepithelial Stem Cells and Radial Glia. *Cell Rep,* 16**,** 2576-2592.

OORSCHOT, D. E. 1989. Effect of fluorodeoxyuridine on neurons and non-neuronal cells in cerebral explants. *Exp Brain Res,* 78**,** 132-8.

PARRA, B., LIZARAZO, J., JIMÉNEZ-ARANGO, J. A., ZEA-VERA, A. F., GONZÁLEZ-MANRIQUE, G., VARGAS, J., ANGARITA, J. A., ZUÑIGA, G., LOPEZ-GONZALEZ, R., BELTRAN, C. L., RIZCALA, K. H., MORALES, M. T., PACHECO, O., OSPINA, M. L., KUMAR, A., CORNBLATH, D. R., MUÑOZ, L. S., OSORIO, L., BARRERAS, P. & PARDO, C. A. 2016. Guillain-Barré Syndrome Associated with Zika Virus Infection in Colombia. *N Engl J Med,* 375**,** 1513-1523.

PENG, G. & WESTERFIELD, M. 2006. Lhx5 promotes forebrain development and activates transcription of secreted Wnt antagonists. *Development,* 133**,** 3191-200.

PEREIRA, L. 2018. Congenital Viral Infection: Traversing the Uterine-Placental Interface. *Annu Rev Virol,* 5**,** 273-299.

PESSOA, A., VAN DER LINDEN, V., YEARGIN-ALLSOPP, M., CARVALHO, M. D. C. G., RIBEIRO, E. M., VAN NAARDEN BRAUN, K., DURKIN, M. S., PASTULA, D. M., MOORE, J. T. & MOORE, C. A. 2018. Motor Abnormalities and Epilepsy in Infants and Children With Evidence of Congenital Zika Virus Infection. *Pediatrics,* 141**,** S167-S179.

PIJLMAN, G. P., FUNK, A., KONDRATIEVA, N., LEUNG, J., TORRES, S., VAN DER AA, L., LIU, W. J., PALMENBERG, A. C., SHI, P. Y., HALL, R. A. & KHROMYKH, A. A. 2008. A highly structured, nuclease-resistant, noncoding RNA produced by flaviviruses is required for pathogenicity. *Cell Host Microbe,* 4**,** 579-91.

PINGEN, M., BRYDEN, S. R., PONDEVILLE, E., SCHNETTLER, E., KOHL, A., MERITS, A., FAZAKERLEY, J. K., GRAHAM, G. J. & MCKIMMIE, C. S. 2016. Host Inflammatory Response to Mosquito Bites Enhances the Severity of Arbovirus Infection. *Immunity,* 44**,** 1455-69.

PLEVKA, P., BATTISTI, A. J., SHENG, J. & ROSSMANN, M. G. 2014. Mechanism for maturation-related reorganization of flavivirus glycoproteins. *J Struct Biol,* 185**,** 27-31.

PRASAD, V. M., MILLER, A. S., KLOSE, T., SIROHI, D., BUDA, G., JIANG, W., KUHN, R. J. & ROSSMANN, M. G. 2017. Structure of the immature Zika virus at 9 Å resolution. *Nat Struct Mol Biol,* 24**,** 184-186.

PRYOR, M. J. & WRIGHT, P. J. 1994. Glycosylation mutants of dengue virus NS1 protein. *J Gen Virol,* 75 ( Pt 5)**,** 1183-7.

PYKE, A. T., DALY, M. T., CAMERON, J. N., MOORE, P. R., TAYLOR, C. T., HEWITSON, G. R., HUMPHREYS, J. L. & GAIR, R. 2014. Imported zika virus infection from the cook islands into australia, 2014. *PLoS Curr,* 6.

QIAN, X., NGUYEN, H. N., JACOB, F., SONG, H. & MING, G. L. 2017. Using brain organoids to understand Zika virus-induced microcephaly. *Development,* 144**,** 952-957.

QIN, S. & ZHANG, C. L. 2012. Role of Kruppel-like factor 4 in neurogenesis and radial neuronal migration in the developing cerebral cortex. *Mol Cell Biol,* 32**,** 4297-305.

RASTOGI, M., SHARMA, N. & SINGH, S. K. 2016. Flavivirus NS1: a multifaceted enigmatic viral protein. *Virol J,* 13**,** 131.

RATHER, I. A., LONE, J. B., BAJPAI, V. K., PAEK, W. K. & LIM, J. 2017. Zika Virus: An Emerging Worldwide Threat. *Front Microbiol,* 8**,** 1417.

RAY, D., SHAH, A., TILGNER, M., GUO, Y., ZHAO, Y., DONG, H., DEAS, T. S., ZHOU, Y., LI, H. & SHI, P. Y. 2006. West Nile virus 5'-cap structure is formed by sequential guanine N-7 and ribose 2'-O methylations by nonstructural protein 5. *J Virol,* 80**,** 8362-70.

REY, F. A., STIASNY, K., VANEY, M. C., DELLAROLE, M. & HEINZ, F. X. 2018. The bright and the dark side of human antibody responses to flaviviruses: lessons for vaccine design. *EMBO Rep,* 19**,** 206-224.

REZELJ, V. V., LI, P., CHAUDHARY, V., ELLIOTT, R. M., JIN, D. Y. & BRENNAN, B. 2017. Differential Antagonism of Human Innate Immune Responses by Tick-Borne. *mSphere,* 2.

ROBIN, Y. & MOUCHET, J. 1975. [Serological and entomological study on yellow fever in Sierra Leone]. *Bull Soc Pathol Exot Filiales,* 68**,** 249-58.

ROBY, J. A., PIJLMAN, G. P., WILUSZ, J. & KHROMYKH, A. A. 2014. Noncoding subgenomic flavivirus RNA: multiple functions in West Nile virus pathogenesis and modulation of host responses. *Viruses,* 6**,** 404-27.

ROBY, J. A., SETOH, Y. X., HALL, R. A. & KHROMYKH, A. A. 2015. Post-translational regulation and modifications of flavivirus structural proteins. *J Gen Virol,* 96**,** 1551-69.

RUSSO, F. B., JUNGMANN, P. & BELTRÃO-BRAGA, P. C. B. 2017. Zika infection and the development of neurological defects. *Cell Microbiol,* 19.

SAKAKIBARA, S., IMAI, T., HAMAGUCHI, K., OKABE, M., ARUGA, J., NAKAJIMA, K., YASUTOMI, D., NAGATA, T., KURIHARA, Y., UESUGI, S., MIYATA, T., OGAWA, M., MIKOSHIBA, K. & OKANO, H. 1996. Mouse-Musashi-1, a neural RNA-binding protein highly enriched in the mammalian CNS stem cell. *Dev Biol,* 176**,** 230-42.

SALUZZO, J. F., GONZALEZ, J. P., HERVÉ, J. P. & GEORGES, A. J. 1981. [Serological survey for the prevalence of certain arboviruses in the human population of the south-east area of Central African Republic (author's transl)]. *Bull Soc Pathol Exot Filiales,* 74**,** 490-9.

SALZER, J. L. 2015. Schwann cell myelination. *Cold Spring Harb Perspect Biol,* 7**,** a020529.

SAMUEL, G. H., WILEY, M. R., BADAWI, A., ADELMAN, Z. N. & MYLES, K. M. 2016. Yellow fever virus capsid protein is a potent suppressor of RNA silencing that binds double-stranded RNA. *Proc Natl Acad Sci U S A,* 113**,** 13863-13868.

SCHAFFNER, F., MEDLOCK, J. M. & VAN BORTEL, W. 2013. Public health significance of invasive mosquitoes in Europe. *Clin Microbiol Infect,* 19**,** 685-92.

SCHLICK, P., TAUCHER, C., SCHITTL, B., TRAN, J. L., KOFLER, R. M., SCHUELER, W., VON GABAIN, A., MEINKE, A. & MANDL, C. W. 2009. Helices alpha2 and alpha3 of West Nile virus capsid protein are dispensable for assembly of infectious virions. *J Virol,* 83**,** 5581-91.

SCHROEDER, A., MUELLER, O., STOCKER, S., SALOWSKY, R., LEIBER, M., GASSMANN, M., LIGHTFOOT, S., MENZEL, W., GRANZOW, M. & RAGG, T. 2006. The RIN: an RNA integrity number for assigning integrity values to RNA measurements. *BMC Mol Biol,* 7**,** 3.

SCHULER-FACCINI, L., RIBEIRO, E. M., FEITOSA, I. M., HOROVITZ, D. D., CAVALCANTI, D. P., PESSOA, A., DORIQUI, M. J., NERI, J. I., NETO, J. M., WANDERLEY, H. Y., CERNACH, M., EL-HUSNY, A. S., PONE, M. V., SERAO, C. L., SANSEVERINO, M. T. & FORCE, B. M. G. S. Z. E. T. 2016. Possible

Association Between Zika Virus Infection and Microcephaly - Brazil, 2015. *MMWR Morb Mortal Wkly Rep,* 65**,** 59-62.

SHAN, C., XIE, X., REN, P., LOEFFELHOLZ, M. J., YANG, Y., FURUYA, A., DUPUIS, A. P., KRAMER, L. D., WONG, S. J. & SHI, P. Y. 2017. A Rapid Zika Diagnostic Assay to Measure Neutralizing Antibodies in Patients. *EBioMedicine,* 17**,** 157-162.

SHANG, Z., SONG, H., SHI, Y., QI, J. & GAO, G. F. 2018. Crystal Structure of the Capsid Protein from Zika Virus. *J Mol Biol,* 430**,** 948-962.

SHIRATO, K., MIYOSHI, H., GOTO, A., AKO, Y., UEKI, T., KARIWA, H. & TAKASHIMA, I. 2004. Viral envelope protein glycosylation is a molecular determinant of the neuroinvasiveness of the New York strain of West Nile virus. *J Gen Virol,* 85**,** 3637-45.

SILVA, S. J. R. D., PAIVA, M. H. S., GUEDES, D. R. D., KROKOVSKY, L., MELO, F. L., SILVA, M. A. L. D., SILVA, A. D., AYRES, C. F. J. & PENA, L. J. 2019. Development and Validation of Reverse Transcription Loop-Mediated Isothermal Amplification (RT-LAMP) for Rapid Detection of ZIKV in Mosquito Samples from Brazil. *Sci Rep,* 9**,** 4494.

SIMMONDS, P., BECHER, P., BUKH, J., GOULD, E. A., MEYERS, G., MONATH, T., MUERHOFF, S., PLETNEV, A., RICO-HESSE, R., SMITH, D. B., STAPLETON, J. T. & ICTV REPORT CONSORTIUM 2017. ICTV Virus Taxonomy Profile: Flaviviridae. *J Gen Virol,* 98**,** 2-3.

SIMPSON, D. I. 1964. ZIKA VIRUS INFECTION IN MAN. *Trans R Soc Trop Med Hyg,* 58**,** 335-8.

SINGH, R. K., DHAMA, K., KARTHIK, K., TIWARI, R., KHANDIA, R., MUNJAL, A., IQBAL, H. M. N., MALIK, Y. S. & BUENO-MARÍ, R. 2017. Advances in Diagnosis, Surveillance, and Monitoring of Zika Virus: An Update. *Front Microbiol,* 8**,** 2677.

SLONCHAK, A. & KHROMYKH, A. A. 2018. Subgenomic flaviviral RNAs: What do we know after the first decade of research. *Antiviral Res,* 159**,** 13-25.

SMITH, D. B., BECHER, P., BUKH, J., GOULD, E. A., MEYERS, G., MONATH, T., MUERHOFF, A. S., PLETNEV, A., RICO-HESSE, R., STAPLETON, J. T. & SIMMONDS, P. 2016. Proposed update to the taxonomy of the genera Hepacivirus and Pegivirus within the Flaviviridae family. *J Gen Virol,* 97**,** 2894-2907.

SMITH, D. B., MEYERS, G., BUKH, J., GOULD, E. A., MONATH, T., SCOTT MUERHOFF, A., PLETNEV, A., RICO-HESSE, R., STAPLETON, J. T., SIMMONDS, P. & BECHER, P. 2017. Proposed revision to the taxonomy of the genus Pestivirus, family Flaviviridae. *J Gen Virol,* 98**,** 2106-2112.

SMITH, K. J., KAPOOR, R., HALL, S. M. & DAVIES, M. 2001. Electrically active axons degenerate when exposed to nitric oxide. *Ann Neurol,* 49**,** 470-6.

SNAIDERO, N. & SIMONS, M. 2014. Myelination at a glance. *J Cell Sci,* 127**,** 2999-3004.

SNAIDERO, N. & SIMONS, M. 2017. The logistics of myelin biogenesis in the central nervous system. *Glia,* 65**,** 1021-1031.

SOFRONIEW, M. V. 2014. Astrogliosis. *Cold Spring Harb Perspect Biol,* 7**,** a020420.

SOMNUKE, P., HAUHART, R. E., ATKINSON, J. P., DIAMOND, M. S. & AVIRUTNAN, P. 2011. N-linked glycosylation of dengue virus NS1 protein modulates secretion, cell-surface expression, hexamer stability, and interactions with human complement. *Virology,* 413**,** 253-64.

STADLER, K., ALLISON, S. L., SCHALICH, J. & HEINZ, F. X. 1997. Proteolytic activation of tick-borne encephalitis virus by furin. *J Virol,* 71**,** 8475-81.

STAIRIKER, C., MUELLER, Y., VAN MEURS, M., BROUWERS-HASPELS, I., ERKELAND, S. & KATSIKIS, P. D. 2018. Heatr9 is upregulated during influenza virus infection in lung alveolar epithelial cells. *The Journal of Immunology,* 200**,** 109.16-109.16.

STANELLE-BERTRAM, S., WALENDY-GNIRß, K., SPEISEDER, T., THIELE, S., ASANTE, I. A., DREIER, C., KOUASSI, N. M., PREUß, A., PILNITZ-STOLZE, G., MÜLLER, U., THANISCH, S., RICHTER, M., SCHARRENBERG, R., KRAUS, V., DÖRK, R., SCHAU, L., HERDER, V., GERHAUSER, I., PFANKUCHE, V. M., KÄUFER, C., WALTL, I., MORAES, T., SELLAU, J., HOENOW, S., SCHMIDT-CHANASIT, J., JANSEN, S., SCHATTLING, B., ITTRICH, H., BARTSCH, U., RENNÉ, T., BARTENSCHLAGER, R., ARCK, P., CADAR, D., FRIESE, M. A., VAPALAHTI, O., LOTTER, H., BENITES, S., ROLLING, L., GABRIEL, M., BAUMGÄRTNER, W., MORELLINI, F., HÖLTER, S. M., AMARIE, O., FUCHS, H., HRABE DE ANGELIS, M., LÖSCHER, W., CALDERON DE ANDA, F. & GABRIEL, G. 2018. Male offspring born to mildly ZIKV-infected mice are at risk of developing neurocognitive disorders in adulthood. *Nat Microbiol,* 3**,** 1161-1174.

STERN, O., HUNG, Y. F., VALDAU, O., YAFFE, Y., HARRIS, E., HOFFMANN, S., WILLBOLD, D. & SKLAN, E. H. 2013. An N-terminal amphipathic helix in dengue virus nonstructural protein 4A mediates oligomerization and is essential for replication. *J Virol,* 87**,** 4080-5.

STOREY, J. D. & TIBSHIRANI, R. 2003. Statistical significance for genomewide studies. *Proc Natl Acad Sci U S A,* 100**,** 9440-5.

SUKEGAWA, S., MIYAGI, E., BOUAMR, F., FARKAŠOVÁ, H. & STREBEL, K. 2018. Mannose Receptor 1 Restricts HIV Particle Release from Infected Macrophages. *Cell Rep,* 22**,** 786-795.

TAKAHASHI, K. & YAMANAKA, S. 2006. Induction of pluripotent stem cells from mouse embryonic and adult fibroblast cultures by defined factors. *Cell,* 126**,** 663-76.

TANG, H., HAMMACK, C., OGDEN, S. C., WEN, Z., QIAN, X., LI, Y., YAO, B., SHIN, J., ZHANG, F., LEE, E. M., CHRISTIAN, K. M., DIDIER, R. A., JIN, P., SONG, H. & MING, G. L. 2016. Zika Virus Infects Human Cortical Neural Progenitors and Attenuates Their Growth. *Cell Stem Cell,* 18**,** 587-90.

TAU, G. Z. & PETERSON, B. S. 2010. Normal development of brain circuits. *Neuropsychopharmacology,* 35**,** 147-68.

TAYLOR, P. R., GORDON, S. & MARTINEZ-POMARES, L. 2005. The mannose receptor: linking homeostasis and immunity through sugar recognition. *Trends Immunol,* 26**,** 104-10.

TEO, C. S. & CHU, J. J. 2014. Cellular vimentin regulates construction of dengue virus replication complexes through interaction with NS4A protein. *J Virol,* 88**,** 1897-913.

THOMSON, C. E., HUNTER, A. M., GRIFFITHS, I. R., EDGAR, J. M. & MCCULLOCH, M. C. 2006. Murine spinal cord explants: a model for evaluating axonal growth and myelination in vitro. *J Neurosci Res,* 84**,** 1703-15.

THOMSON, C. E., MCCULLOCH, M., SORENSON, A., BARNETT, S. C., SEED, B. V., GRIFFITHS, I. R. & MCLAUGHLIN, M. 2008. Myelinated, synapsing cultures of murine spinal cord--validation as an in vitro model of the central nervous system. *Eur J Neurosci,* 28**,** 1518-35.

TOGNARELLI, J., ULLOA, S., VILLAGRA, E., LAGOS, J., AGUAYO, C., FASCE, R., PARRA, B., MORA, J., BECERRA, N., LAGOS, N., VERA, L., OLIVARES, B., VILCHES, M. & FERNÁNDEZ, J. 2016. A report on the outbreak of Zika virus on Easter Island, South Pacific, 2014. *Arch Virol,* 161**,** 665-8.

TRIFILO, M. J., MONTALTO-MORRISON, C., STILES, L. N., HURST, K. R., HARDISON, J. L., MANNING, J. E., MASTERS, P. S. & LANE, T. E. 2004. CXC chemokine ligand 10 controls viral infection in the central nervous system: evidence for a role in innate immune response through recruitment and activation of natural killer cells. *J Virol,* 78**,** 585-94.

TRUJILLO, J. R., ROGERS, R., MOLINA, R. M., DANGOND, F., MCLANE, M. F., ESSEX, M. & BRAIN, J. D. 2007. Noninfectious entry of HIV-1 into peripheral and brain macrophages mediated by the mannose receptor. *Proc Natl Acad Sci U S A,* 104**,** 5097-102.

TU, Y. C., YU, C. Y., LIANG, J. J., LIN, E., LIAO, C. L. & LIN, Y. L. 2012. Blocking double-stranded RNA-activated protein kinase PKR by Japanese encephalitis virus nonstructural protein 2A. *J Virol,* 86**,** 10347-58.

UMAREDDY, I., CHAO, A., SAMPATH, A., GU, F. & VASUDEVAN, S. G. 2006. Dengue virus NS4B interacts with NS3 and dissociates it from single-stranded RNA. *J Gen Virol,* 87**,** 2605-14.

VAN DEN POL, A. N., MAO, G., YANG, Y., ORNAGHI, S. & DAVIS, J. N. 2017. Zika Virus Targeting in the Developing Brain. *J Neurosci,* 37**,** 2161-2175.

VAN DER HOEK, K. H., EYRE, N. S., SHUE, B., KHANTISITTHIPORN, O., GLAB-AMPI, K., CARR, J. M., GARTNER, M. J., JOLLY, L. A., THOMAS, P. Q., ADIKUSUMA, F., JANKOVIC-KARASOULOS, T., ROBERTS, C. T., HELBIG, K. J. & BEARD, M. R. 2017. Viperin is an important host restriction factor in control of Zika virus infection. *Sci Rep,* 7**,** 4475.

VAN MARLE, G., ANTONY, J., OSTERMANN, H., DUNHAM, C., HUNT, T., HALLIDAY, W., MAINGAT, F., URBANOWSKI, M. D., HOBMAN, T., PEELING, J. & POWER, C. 2007. West Nile virus-induced neuroinflammation: glial infection and capsid protein-mediated neurovirulence. *J Virol,* 81**,** 10933-49.

VIANNA, P., GOMES, J. D. A., BOQUETT, J. A., FRAGA, L. R., SCHUCH, J. B., VIANNA, F. S. L. & SCHULER-FACCINI, L. 2018. Zika Virus as a Possible Risk Factor for Autism Spectrum Disorder: Neuroimmunological Aspects. *Neuroimmunomodulation,* 25**,** 320-327.

VILLAMIL-GÓMEZ, W. E., GONZÁLEZ-CAMARGO, O., RODRIGUEZ-AYUBI, J., ZAPATA-SERPA, D. & RODRIGUEZ-MORALES, A. J. 2016. Dengue, chikungunya and Zika co-infection in a patient from Colombia. *J Infect Public Health,* 9**,** 684-6.

VOLPI, V. G., PAGANI, I., GHEZZI, S., IANNACONE, M., D'ANTONIO, M. & VICENZI, E. 2018. Zika Virus Replication in Dorsal Root Ganglia Explants from Interferon Receptor1 Knockout Mice Causes Myelin Degeneration. *Sci Rep,* 8**,** 10166.

WALKER, C. L., LITTLE, M. E., ROBY, J. A., ARMISTEAD, B., GALE, M., RAJAGOPAL, L., NELSON, B. R., EHINGER, N., MASON, B., NAYERI, U., CURRY, C. L. & ADAMS WALDORF, K. M. 2019. Zika virus and the nonmicrocephalic fetus: why we should still worry. *Am J Obstet Gynecol,* 220**,** 45-56.

WANG, Z. Y., WANG, Z., ZHEN, Z. D., FENG, K. H., GUO, J., GAO, N., FAN, D. Y., HAN, D. S., WANG, P. G. & AN, J. 2017. Axl is not an indispensable factor for Zika virus infection in mice. *J Gen Virol,* 98**,** 2061-2068.

WEAVER, S. C. & REISEN, W. K. 2010. Present and future arboviral threats. *Antiviral Res,* 85**,** 328-45.

WEBER, F., WAGNER, V., RASMUSSEN, S. B., HARTMANN, R. & PALUDAN, S. R. 2006. Double-stranded RNA is produced by positive-strand RNA viruses and

DNA viruses but not in detectable amounts by negative-strand RNA viruses. *J Virol,* 80, 5059-64.
WELSCH, S., MILLER, S., ROMERO-BREY, I., MERZ, A., BLECK, C. K., WALTHER, P., FULLER, S. D., ANTONY, C., KRIJNSE-LOCKER, J. & BARTENSCHLAGER, R. 2009. Composition and three-dimensional architecture of the dengue virus replication and assembly sites. *Cell Host Microbe,* 5, 365-75.
WENGLER, G. 1991. The carboxy-terminal part of the NS 3 protein of the West Nile flavivirus can be isolated as a soluble protein after proteolytic cleavage and represents an RNA-stimulated NTPase. *Virology,* 184, 707-15.
WESTAWAY, E. G., KHROMYKH, A. A., KENNEY, M. T., MACKENZIE, J. M. & JONES, M. K. 1997. Proteins C and NS4B of the flavivirus Kunjin translocate independently into the nucleus. *Virology,* 234, 31-41.
WHO. 2015. *Zika Situation Report* [Online]. World Health Organisation. Available: https://apps.who.int/iris/bitstream/handle/10665/204348/zikasitrep_5Feb2016_eng.pdf?sequence=1 [Accessed 2019].
WHO 2016. Laboratory testing for Zika virus infection: Interim Guidance.
WHO. 2017. *Zika virus Situation Report* [Online]. Available: https://apps.who.int/iris/bitstream/handle/10665/254714/zikasitrep10Mar17-eng.pdf [Accessed 2019].
WICKER, J. A., WHITEMAN, M. C., BEASLEY, D. W., DAVIS, C. T., MCGEE, C. E., LEE, J. C., HIGGS, S., KINNEY, R. M., HUANG, C. Y. & BARRETT, A. D. 2012. Mutational analysis of the West Nile virus NS4B protein. *Virology,* 426, 22-33.
WILLISON, H. J., JACOBS, B. C. & VAN DOORN, P. A. 2016. Guillain-Barré syndrome. *Lancet,* 388, 717-27.
XIE, X., GAYEN, S., KANG, C., YUAN, Z. & SHI, P. Y. 2013. Membrane topology and function of dengue virus NS2A protein. *J Virol,* 87, 4609-22.
XU, S., CI, Y., WANG, L., YANG, Y., ZHANG, L., XU, C., QIN, C. & SHI, L. 2019. Zika virus NS3 is a canonical RNA helicase stimulated by NS5 RNA polymerase. *Nucleic Acids Res.*
YAP, T. L., XU, T., CHEN, Y. L., MALET, H., EGLOFF, M. P., CANARD, B., VASUDEVAN, S. G. & LESCAR, J. 2007. Crystal structure of the dengue virus RNA-dependent RNA polymerase catalytic domain at 1.85-angstrom resolution. *J Virol,* 81, 4753-65.
YOUN, S., LI, T., MCCUNE, B. T., EDELING, M. A., FREMONT, D. H., CRISTEA, I. M. & DIAMOND, M. S. 2012. Evidence for a genetic and physical interaction between nonstructural proteins NS1 and NS4B that modulates replication of West Nile virus. *J Virol,* 86, 7360-71.
YOUNG, P. R., HILDITCH, P. A., BLETCHLY, C. & HALLORAN, W. 2000. An antigen capture enzyme-linked immunosorbent assay reveals high levels of the dengue virus protein NS1 in the sera of infected patients. *J Clin Microbiol,* 38, 1053-7.
YU, I. M., HOLDAWAY, H. A., CHIPMAN, P. R., KUHN, R. J., ROSSMANN, M. G. & CHEN, J. 2009. Association of the pr peptides with dengue virus at acidic pH blocks membrane fusion. *J Virol,* 83, 12101-7.
YU, I. M., ZHANG, W., HOLDAWAY, H. A., LI, L., KOSTYUCHENKO, V. A., CHIPMAN, P. R., KUHN, R. J., ROSSMANN, M. G. & CHEN, J. 2008. Structure of the immature dengue virus at low pH primes proteolytic maturation. *Science,* 319, 1834-7.

YU, L., TAKEDA, K. & MARKOFF, L. 2013. Protein-protein interactions among West Nile non-structural proteins and transmembrane complex formation in mammalian cells. *Virology,* 446**,** 365-77.

YUAN, A., RAO, M. V., VEERANNA & NIXON, R. A. 2017. Neurofilaments and Neurofilament Proteins in Health and Disease. *Cold Spring Harb Perspect Biol,* 9.

YUKI, N., SUSUKI, K., KOGA, M., NISHIMOTO, Y., ODAKA, M., HIRATA, K., TAGUCHI, K., MIYATAKE, T., FURUKAWA, K., KOBATA, T. & YAMADA, M. 2004. Carbohydrate mimicry between human ganglioside GM1 and Campylobacter jejuni lipooligosaccharide causes Guillain-Barre syndrome. *Proc Natl Acad Sci U S A,* 101**,** 11404-9.

ZANLUCA, C., MELO, V. C., MOSIMANN, A. L., SANTOS, G. I., SANTOS, C. N. & LUZ, K. 2015. First report of autochthonous transmission of Zika virus in Brazil. *Mem Inst Oswaldo Cruz,* 110**,** 569-72.

ZHANG, Q., HUNKE, C., YAU, Y. H., SEOW, V., LEE, S., TANNER, L. B., GUAN, X. L., WENK, M. R., FIBRIANSAH, G., CHEW, P. L., KUKKARO, P., BIUKOVIC, G., SHI, P. Y., SHOCHAT, S. G., GRÜBER, G. & LOK, S. M. 2012. The stem region of premembrane protein plays an important role in the virus surface protein rearrangement during dengue maturation. *J Biol Chem,* 287**,** 40525-34.

ZHANG, R., MINER, J. J., GORMAN, M. J., RAUSCH, K., RAMAGE, H., WHITE, J. P., ZUIANI, A., ZHANG, P., FERNANDEZ, E., ZHANG, Q., DOWD, K. A., PIERSON, T. C., CHERRY, S. & DIAMOND, M. S. 2016. A CRISPR screen defines a signal peptide processing pathway required by flaviviruses. *Nature,* 535**,** 164-8.

ZHANG, W., CHEN, S., MAHALINGAM, S., WANG, M. & CHENG, A. 2017. An updated review of avian-origin Tembusu virus: a newly emerging avian Flavivirus. *J Gen Virol,* 98**,** 2413-2420.

ZHANG, X., GE, P., YU, X., BRANNAN, J. M., BI, G., ZHANG, Q., SCHEIN, S. & ZHOU, Z. H. 2013. Cryo-EM structure of the mature dengue virus at 3.5-Å resolution. *Nat Struct Mol Biol,* 20**,** 105-10.

ZHANG, Y., CORVER, J., CHIPMAN, P. R., ZHANG, W., PLETNEV, S. V., SEDLAK, D., BAKER, T. S., STRAUSS, J. H., KUHN, R. J. & ROSSMANN, M. G. 2003. Structures of immature flavivirus particles. *EMBO J,* 22**,** 2604-13.

ZHANG, Y., ZHANG, W., OGATA, S., CLEMENTS, D., STRAUSS, J. H., BAKER, T. S., KUHN, R. J. & ROSSMANN, M. G. 2004. Conformational changes of the flavivirus E glycoprotein. *Structure,* 12**,** 1607-18.

ZHAO, Y., SHENG, H. Z., AMINI, R., GRINBERG, A., LEE, E., HUANG, S., TAIRA, M. & WESTPHAL, H. 1999. Control of hippocampal morphogenesis and neuronal differentiation by the LIM homeobox gene Lhx5. *Science,* 284**,** 1155-8.

ZHOU, Y., RAY, D., ZHAO, Y., DONG, H., REN, S., LI, Z., GUO, Y., BERNARD, K. A., SHI, P. Y. & LI, H. 2007. Structure and function of flavivirus NS5 methyltransferase. *J Virol,* 81**,** 3891-903.

ZOU, J., LEE, L. T., WANG, Q. Y., XIE, X., LU, S., YAU, Y. H., YUAN, Z., GEIFMAN SHOCHAT, S., KANG, C., LESCAR, J. & SHI, P. Y. 2015a. Mapping the Interactions between the NS4B and NS3 proteins of dengue virus. *J Virol,* 89**,** 3471-83.

ZOU, J., XIE, X., WANG, Q. Y., DONG, H., LEE, M. Y., KANG, C., YUAN, Z. & SHI, P. Y. 2015b. Characterization of dengue virus NS4A and NS4B protein interaction. *J Virol,* 89**,** 3455-70.